Fluidised-MCPCM Glazed Energy Storage System

By Pruitipong Thaicham, BEng, MSc

Thesis submitted to the University of Nottingham

For the degree of Doctor of Philosophy

March 2004

Contents

Abstract

The thesis presents an experimental investigation into the feasibility of using a slurry containing a micro encapsulated phase change material (MCPCM), n-eicosane, as a heat transfer fluid for enhanced latent heat transport. Increasing the convective heat transfer coefficient would permit the use of a smaller volumetric flow rate and reduce pumping power. The primary parameters investigated are the volumetric concentrations and flow rates. Measurements of thermal capacity of the novel slurries were performed using two techniques, standard differential scanning calorimeter (DSC) and thermal analysis (TA). Pumping power consumption, viscosity and pressure loss of the flowing slurries were investigated in order to determine the most suitable concentration of MCPCM used in the slurry, over the range 5-40%. The effects of repeated use of liquid-solid phase change particles upon melting and solidifying were studied using a small-scale rig of a closed loop circuit. The research work further involved the design, construction and tests the proposed system based on incorporating microencapsulated phase change material (MCPCM) within a fluidised and sealed double glazed panel, which could be integrated into building fabric.

The use of a MCPCM slurry can improve the performance of a working fluid by as much as 52% compared to a single phase fluid. A concentration of 20-30% was the most suitable mixture for the working fluid due to the associated heat capacity and reasonable pressure drop. Measurement showed that a saving in pumping power of 12% could be obtained. The performance of the fluidised glazed energy storage system can be improved by up to 18% with the use of MCPCM slurry as a working fluid.

Acknowledgement

I would like to express my thanks and gratitude to Professor S.B. Riffat for his invaluable support and backing over the years. I would extend my sincere thanks to Dr. M.B. Gadi, whom without his constant encouragement and enthusiasm I would not have been able to complete this work.

Further thanks are due to the technicians at the Institute of Building Technology for their tireless, uncomplaining help and to my work colleagues who have made working at IBT a pleasurable experience. I also acknowledge EPSRC, School of Built Environment and International Office for their financial support for this project. My special thanks to my parents, my brothers and my girlfriend who encourage and support me to finish this research.

List of Figures

List of Tables

Nomenclature

Symbol	Term	Unit
A	Surface area	m^2
A_A	Collector surface area	m^2
A_a	Divided area	m^2
B	Bias error	
C_{pl}	Heat capacity at constant pressure of liquid phases	kJ/kg·K
C_{ps}	Heat capacity at constant pressure of solid phases	kJ/kg·K
C_p	Heat capacity,	kJ/kg·K
D	Circular diameter	m
E_{cv}	Internal energy in control volume	kJ
ΔE_{cv}	Internal energy change	kJ
f	Friction factor	
h	Heat transfer coefficient	$W/m^2 \cdot °C$
H	Enthalpy	kJ
ΔH	Enthalpy change	kJ
ΔH_f	Enthalpy of fusion	kJ
ΔH_v	Enthalpy of vaporisation	kJ
i	Current	A
I	Irradiance	W/m^2
I_{av}	Average irradiance	W/m^2
I_i	Instrument reading	
I_t	True value	
L	Pipe length	m

m	Mass	kg
$\dot{m}$	Mass flow rate	kg/sec
n	Quantity of the material	moles
η	Efficiency	
P	Pressure	Pa
ΔP	Pressure drop	Pa
ρ	Density	kg/m^3
Q	Heat	W
Q_{in}	Heat input	W
Q_{out}	Heat output	W
Q_{loss}	Heat loss	W
Re	Reynolds number	
S	Entropy	kJ
ΔS	Entropy change	kJ
t	Time	sec
Δt	Time change	sec
T	Temperature	°C
T_b	Temperature of boiling	°C
T_f	Temperature of fusion	°C
T_i	Inlet temperature	°C
T_o	Outlet temperature	°C
T_s	Substance temperature	°C
v	Voltage	V
V	Volume	m^3
ΔV	Volume change	m^3

V_m	Free mean fluid velocity	m/s
υ	Kinematic viscosity	m^2/s
W	Work	W

Chapter 1 Introduction

1.1 Background

Modern societies are now totally dependent upon the use of large quantities of energy, most of it in the form of fossil fuels (oil, coal and natural gas). The amount of this energy use and its concentration by the modern societies (mostly for the operation of the physical infrastructure, for the production of food, clothing, shelter, transportation, communication, and other essential human services) has caused the environmental degradation of air-, water- and land-dependent ecosystems on a local and regional scale. Of all environmental effects of fossil fuel usage, global warming, including its concomitant climate change, is the most perplexing, potentially most threatening, and arguably most intractable. Recent scientific studies have forecast potentially adverse global climate changes that would result from the accumulation of gaseous emissions to the atmosphere, principally carbon dioxide which is released when fossil fuels are burned. In 1996 the use of fossil energy produced 23.8 billion tonnes of carbon dioxide (CO_2) with oil and gas contributing about 60% to this figure (Kessel, 1999). It is estimated that continued use of fossil energy will lead to an increase of the average global temperature by 1.0-3.5°C in the coming 50-100 years. This warming would increase the natural convection currents (winds) which will have a number of effects including increasing the chances of severe hurricanes and tornados, lead to heavier rainfalls and greater chances of flooding and also increase the average sea level causing flooding of low lying areas.

Global warming can be ameliorated by reducing the emission of CO_2 and other greenhouse gases into the atmosphere. Limiting the growth rate of atmospheric carbon dioxide requires either (a) reducing the amount of fossil fuel burned or (b) sequestering the carbon dioxide below the earth's or ocean's surface. To maintain or increase the availability of energy while fossil fuel consumption is lowered, renewable energy must be used. Most renewable energy sources are derived from solar radiation, including the direct use of solar energy for heating or electricity generation, and indirect forms such as energy from the wind, waves and running water, and from plants and animals. Tidal sources of energy result from the gravitational pull of the moon and sun, and geothermal energy comes from the heat generated within the earth. The amount of energy coming from the sun is phenomenal and it has been estimated that the amount of solar energy incident on the earth every year is equivalent to 160 times the energy stored in the world's annual use of fossil fuels (Alexander, 1998).

One sector where the use of solar energy is likely to be significant is the building sector. In the UK, about half of all energy consumed is associated with buildings. It is estimated that about 50% of CO_2 emissions is a result of energy use in houses and other buildings (Amer, 2003). The UK has an ongoing commitment to reducing CO_2 emission as highlighted by its agreement at the Rio and Kyoto Summits, and one effective route to achieving emission targets would be to develop alternative energy sources for major energy demanding sectors. A significant proportion of the energy demand of buildings could be met by utilising renewable energy sources. The average solar irradiation reaching a south facing facade in the UK is about 2.0kWh/m^2/day. This energy could be collected and transferred into the building where it could be stored by an appropriate medium, e.g., a phase change material (PCM), for subsequent release and use.

Thermal storage components, such as Tromb walls, solar chimneys, water walls, solariums, and roof ponds may be integrated into passively heated or cooled buildings. Although these systems are still widely used, owing to their cheap construction and simple technology, their performance is dependent on the availability of solar energy. Unfortunately, in northern climates such as the UK, the intermittent and limited availability of solar energy may not be sufficient to justify the capital cost of these components. If solar energy is to be exploited in less sunny climates, a method providing more efficient absorption, storage and transfer of solar energy is required.

Most thermal stores used in conventional heating or cooling systems accept or reject heat without a change of phase. Such sensible heat storage media normally have a large storage volume per unit MJ. If advantage is made by taking of the latent heat of fusion for instance, much larger energy densities (MJ/m^3) could be accommodated, which would reduce both the volume and weight of the thermal store. Paraffin wax has a latent heat storage capacity of $196MJ/m^3$, compared to $3.8MJ/m^3$ sensible heat storage for a 2°C temperature difference in concrete (Abhat, 1982) When heated, a solid phase change material (PCM) melts and consequently takes heat from the surroundings. If the material is then passed through a cooler medium, it gives up its latent heat to its surroundings and solidifies.

For conventional systems using sensible materials (e.g. water) for heat transport, large diameter pipes/emitters (i.e., high capital cost) and high pumping power are required. Ice-water slurry was one of the first solid-liquid PCMs used in industrial applications. It has been reported that 25% ice slurry has a thermal capacity higher than chilled water by two to four times (Cleary, 1990). A suspended fluid using PCMs is similar to the ice slurry,

since ice is one kind of PCM. Choi (1994) stated that if a PCM could be suspended in a heat transfer fluid as small solid particles and transported through a heat exchanger, the heat transfer coefficient and thermal capacity of the working fluid could be improved. Two-component slurry combines the functions of both thermal energy storage and heat transportation and could be used as a secondary heat transfer medium in many applications (e.g., ammonia chillers for cooling food products in supermarkets, transfer of heat from solar collectors and underflow heating).

1.2 Objectives

The aim of this project is to investigate the integration into a building envelope of micro encapsulated phase change material (MCPCM) held within a fluidised double glazed panel. The panel is designed to be incorporated into the building fabric for storage and transfer of solar energy to the occupied space. Specific objectives of the project are as following:

- Investigate the performance of the MCPCM slurry regarding heat transfer and pressure loss by laboratory testing.
- Optimise the heat transfer performance by determining the appropriate MCPCM mixture.
- Assess the performance of the proposed system under the specific operating conditions by design, construction and testing a prototype system in the laboratory.
- Economic analysis of the proposed system.

Chapter 2 Sensible heat storage

2.1 Introduction

Solar energy has many attractive features. It is available anywhere on Earth, virtually inexhaustible, and can be collected easily with portable devices. Solar radiation can be effectively used within buildings to provide energy for space heating, hot water supply, electricity and lighting. However, the main problem is that the direct sunlight is the inconsistent energy source. Not only night but clouds and seasonal changes affect the rate at which direct sunlight can be collected. Furthermore it is a rather dilute energy source which requires a large area for collecting the solar energy. Erratic sunlight creates the need for methods of storing the energy collected until it is needed. This chapter describes how the solar energy can be stored within buildings to provide energy for space and water heating by using thermal energy storage system. Firstly, it is to look at the traditional forms of sensible heat storages in brief details in order to clarify the issues.

2.2 Thermal energy storage (TES)

The use of TES for thermal applications such as water and space heating or cooling etc. has received much attention. Many types of energy storage play an important role in energy conservation. In processes which yield waste heat that can be recovered, energy storage can result in savings of premium fuels. TES generally involves a temporary storage of high or low temperature thermal energy for later use. Examples of TES are storage of solar energy for overnight heating, of summer heat for winter use, of winter ice for space cooling in summer, and of heat or coolness generated electrically during of-peak hours for use during subsequent peak demand hours. Solar energy, unlike energy from fossil fuels, is

not available all the time. Cooling loads, which nearly coincide with maximum levels of solar radiation, are often present after sunset. TES can help offset this mismatch of availability and demand. The benefits achieved by TES can be seen by the following purposes.

a) To increase generation capacity: the excess generation available during low-demand periods can be used to charge a TES in order to increase the effective generation capacity during high demand periods.
b) To shift energy purchases to low cost periods: allows energy consumers subject to time of day pricing to shift energy purchases from high to low cost periods.
c) To enable better operation of cogeneration of plants: by incorporating TES, the plant need not be operated to follow a load.
d) To act as a reserve unit: to store energy from waste heat recovery systems or solar collectors.
e) To integrate with other functions: the efficiency of energy conversion for some systems may be improved by TES (i.e., no part-load operation: reduction of start-up and shut-down losses by buffer storage).

Typically, there are two types of TES systems, sensible (e.g. rock, water) and latent (e.g., water/ice, paraffin wax). Sensible storage systems commonly use rocks or water as the storage medium, the thermal energy stored by increasing the storage medium temperature. Latent heat storage systems store energy in phase change materials, with the thermal energy stored when the material changes phase, usually from a solid to a liquid. The basic principle of TES is the same in all applications. Energy is supplied to a storage system for removal and use at a later time. What mainly varies is the scale of the storage and the

storage method use. TES storage processes at least three steps, charging, storing and discharging as illustrated in Figure 2.1 (Dincer, 2002). In practical systems, some of the steps may occur simultaneously, for instance, charging and storing.

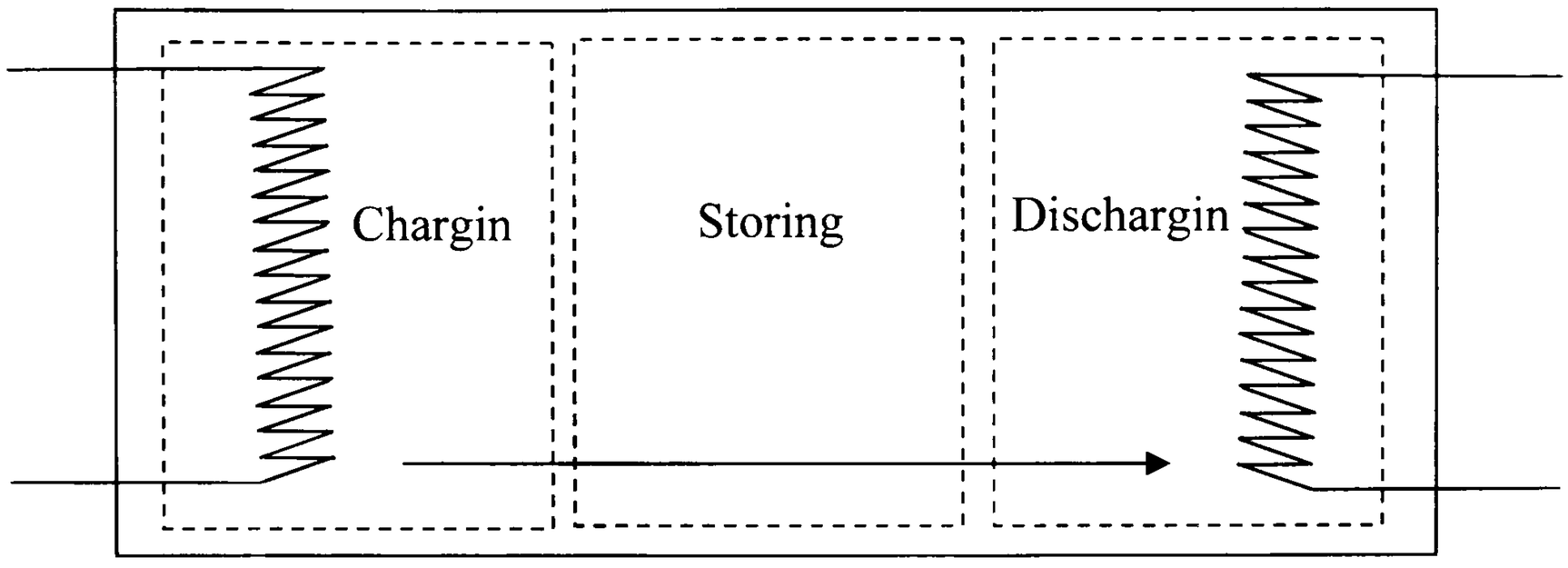

Figure 2.1: The three process in a TES system; charging, storing and discharging

In heating mode of TES, for example, heaters are operated at night to produce heating capacity for use during the day. The production of heat at night takes advantage of electric off-peak rates, which are sometime 30-70% less expensive than peak rates. Heat produced by the heaters at night is stored in storage media such as water, earth materials or ceramic bricks in insulated containers. When heat demand rises (i.e. for space heating), heat is recovered from the storage unit and transferred into the room.

In cooling mode, TES systems can be designed to shift the peak operating period of electric air conditioning systems to the less expensive night period. Cool TES based air conditioning systems operate by removing heat from an intermediate substance when the building does not need cooling, producing a cool reservoir that is stored until there is a need for cooling. The storage media is normally water, ice or eutectic salt solutions.

TES is important to the success of any intermittent energy source in meeting demand. The problem is especially severe for solar energy because it is usually needed most when solar availability is lowest. TES should be large enough to permit the system to operate over periods of inadequate sunshine. Because TES is the primary collecting system, it must be sufficiently large to build the supply of stored energy during periods of adequate insolation. The ability to store thermal energy is important for effective use of solar energy in buildings. Today, much interest is focused on passive systems for space heating and active systems for water heating. For building heating or cooling, conventional sensible TES stored energy by changing the temperature of a storage medium such as water, rocks and concrete. A more interesting approach is to use phase change materials in TES systems. This is because the heat capacity of latent heat is usually much higher than the sensible heat when a substance changes from one phase to another.

2.3 Sensible heat storage

Substance stores heat as its temperature rises and releases this heat later as it cools. This is called sensible heat storage if there is no phase change accompanied. A material is not considered good for sensible heat storage if it discharges heat quickly. Thus, it is desirable for the storage medium to have high specific heat capacity, long term stability under thermal cycling, compatibility with its containment and, most importantly, low cost (Hasnain, 1998). Furthermore, it should be convenient to add or withdraw heat from a sensible heat storage material. This requirement can be accomplished by either having the material possessing good heat conductivity (such as metals) or it should be easy to establish a heat transfer surface between the suitable medium and the material. Several materials satisfy the requirements for a sensible heat storage material like concrete, steel, adobe, stone, bricks, oil and water. Sensible heat storage can be divided on the basis of the

heat storage media as two categories, solid (i.e. rocks, metals etc.) and liquid storage (i.e. water, oil base fluids, molten salts etc.).

2.3.1 Solid sensible heat storage

Solid materials such as rocks, metals, concrete, sand, bricks etc., can be used for low and high temperature energy storage. The main advantage of the solid materials over liquid materials is that heat can be stored since these materials will not freeze or boil. The difficulties of high vapour pressure of water can be avoided by using solid sensible heat storage. Solid materials can act as both a storage medium and a heat exchanger, hence saving the cost of separate heat exchanger. Furthermore, solids do not leak from their containers. Cast iron has high density and specific heat, which nearly approaches the energy density of water. However, it is far more expensive than stone or brick resulting in a longer payback period. Due to the low cost, the most common and often used materials are rock pebbles.

Pebble rock heat storage

The pebble rock storage system consists of a bed of loosely packed rock materials in insulated vessels through which the flow of hot fluid can be passed. To store the thermal energy in the packed bed, hot air is forced through the bed and it loses its energy to the pebble rocks. To utilize the stored heat, the airflow is reversed in order to extract heat from the bed until the bed is fully discharged. Figure 2.2 shows a typical vertical pebble bed storage unit. Hasnain (1998) notices that the energy stored in a packed bed storage system depends on several parameters, for instance, rock size and shape, packing density and heat transfer fluid. Pebble rocks usually occupy 50-60% of the storage volume and the rest is

void fraction. As a consequence, heat transfer coefficient between the air and the solids is high, which means the hot air can lose its energy quickly to the pebble rocks (Hariri, 1988).

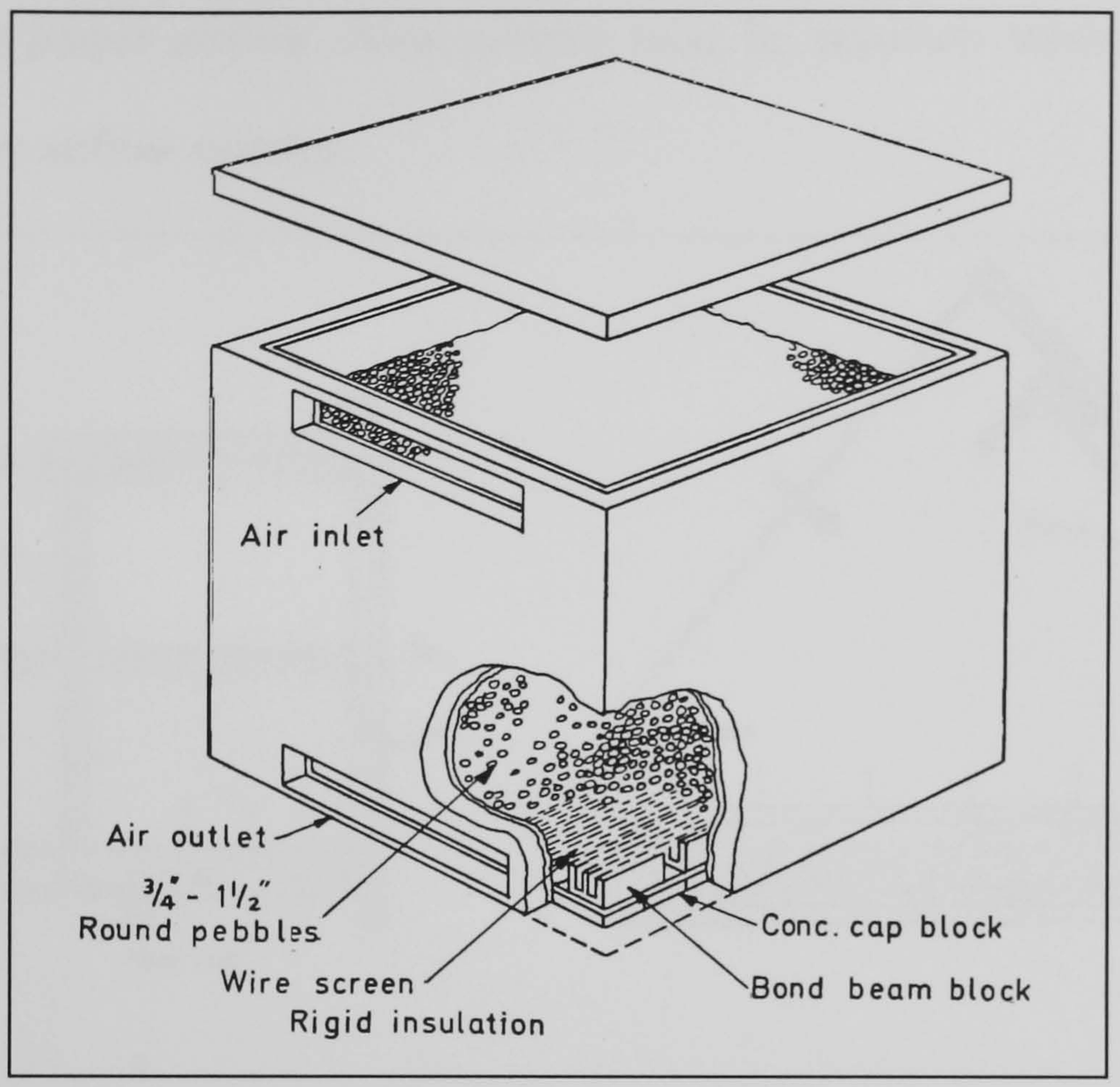

Figure 2.2: Rock bed heat storage unit (Burns, 1981)

An active solar heating system that stores heat in rocks or pebbles is convenient for use in buildings as illustrated in Figure 2.3. The storage is used very often for temperatures up to 100°C in combination with solar air heaters (King, 1981). Usually for space heating applications, the characteristic size of the pebble rocks varies from 1-5cm with the total weight of 300-500 kg/m^2 of solar collector area. For a temperature change of 50°C, rocks will store heat around 36kJ/kg (Hasnain, 1998). However, it can be used for temperature up to 1,000°C. The depth of the pebble bed is an important parameter. A shallow bed is desirable, as it requires a small fan to heat the bed. However, it takes a large floor area. Hariri (1988) suggests a compromise has to be made between a large shallow storage bed with low pressure drop and a tall storage bed with high temperature stratification. He found

that the optimum size for the bed ranged from 0.013-0.152m. A small rock diameter is recommended since this will enhance heat transfer but caution should be observed not to increase the bed pressure drop. The rocks should be as uniform in size and as spherical as possible to allow proper airflow. Also pebbles must be regularly washed to minimize clogging by dust in airflow systems.

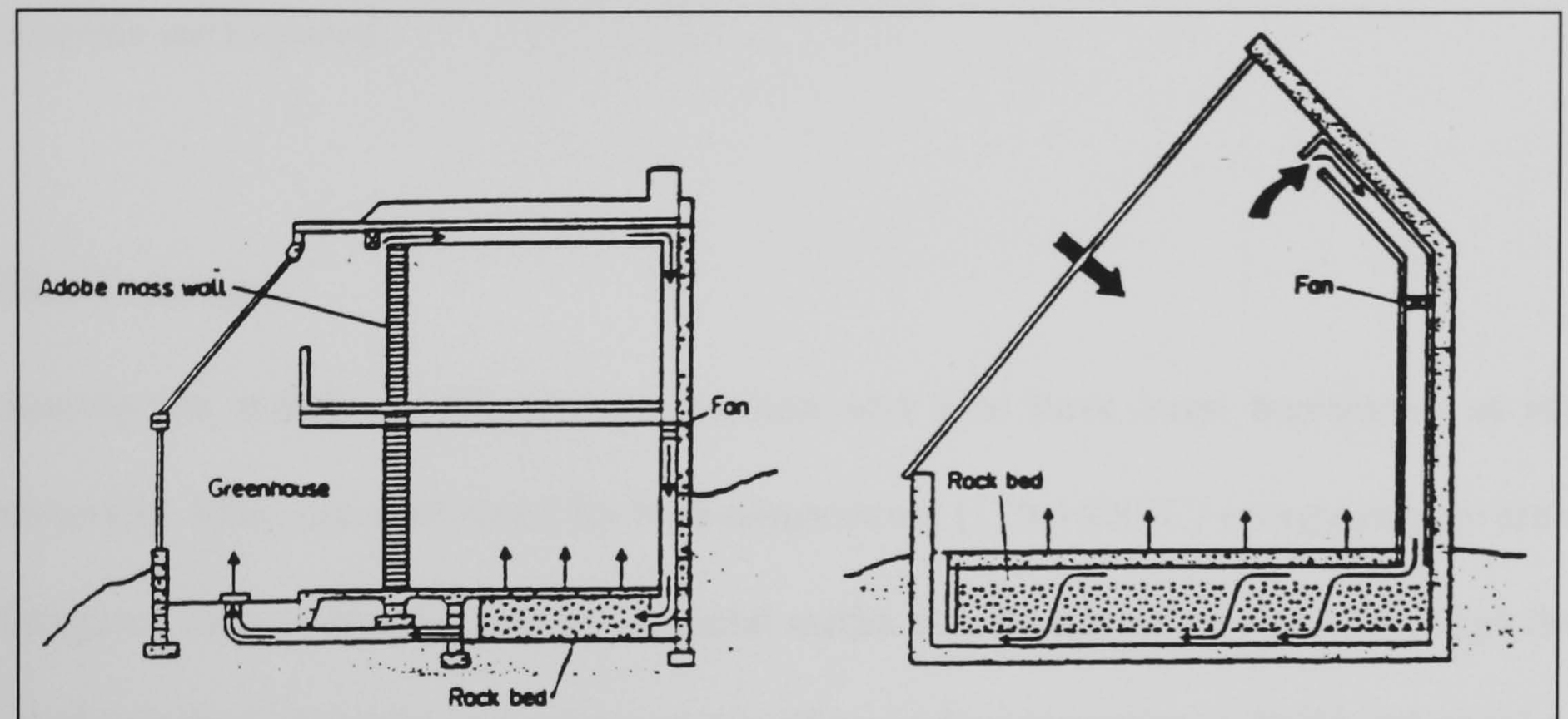

Figure 2.3: Cross section of the solar house with a shallow rock bed, (Clark,1982).

Building fabric storage

Building fabric can be used with active and passive storage designs. Heat storage is applicable to both new and existing buildings and can be integrated with both air and water distribution systems. The most prevalent storage material is ceramic brick. The common configuration using building mass for thermal storage is floor warming. The floor can be heated by a heat transfer fluid such as water, with direct electric resistance wiring or with air ducts. As a result, the floor becomes a large low temperature radiating surface with the concrete acting as the heat storage medium. Water is the most common heat transfer medium. Many buildings with floor warming do not utilize off peak electricity to charge

the storage, although they could be retrofitted with a control system to operate off peak heating. Other two categories of building fabric storage are hollow core construction and building inertia. The hollow core ventilation system is accomplished by that the supply air is distributed through the floor slabs, coupling it to the building mass. The technique to use inertia in building mass is where no additional HVAC equipment is installed but special controls are required.

Metal storage

Among the metals, aluminum, magnesium and zinc have been mentioned as suitable materials. Most materials used for high temperature (120-1400°C) energy storage are either inorganic salts or metals. The use of metal media may be advantageous where high thermal conductivity is required and where cost is of secondary importance. Solid industrial wastes like copper slag, iron slag, cast iron slag, aluminum slag and copper chips could be used as storage material for energy storage.

2.3.2 Liquid sensible heat storage

Water heat storage

At low and medium temperature water is the most commonly used liquid medium for sensible storage systems. In general, it can be used as a storage for short periods, e.g. from several hours to one or two days. The main advantage is that water has high specific heat and density. It is abundant, cheap and neither toxic nor combustible. Thus, water is widely used for solar heating applications. Using water as a heat storage medium eliminates the need for heat exchanger because transport fluid and storage medium are one. However, due to its high vapor pressure, it needs costly insulation and pressure withstanding containment

for high temperature applications. Water storages can be made from materials like aluminum, steel, reinforced concrete and fiber glass. The tanks are insulated with mineral wool, glass wool, or polyurethane. The sizes of the tanks used very from a few liters to thousands cubic meters.

Water can be used over a wide range of temperature i.e. from 10 to 90°C. For a 50°C temperature change, one kilogram of water stores 210 kJ of heat. Hot water is required for bathing and washing and commonly employed in radiators for space heating. In most liquid sensible storage, it is important that mixing of hot and cold liquids should be avoided as to minimize degradation of energy and to achieve optimum utilization of the stored energy. Thermal stratification or thermocline in solar water storage can be established due to the buoyancy forces, which ensure the highest temperature at the top and the lowest temperature at the bottom of the tank. Stratification is achieved through the elimination of mixing during storage, whereby a two-fold advantage is gained (Duffie, 1989). However, there have been attempts to use separate tanks or removable or collapsible membranes, for separating the hot fluid from the cold fluid.

Salt water heat storage

Salt water in solar ponds provides a simple technique for collecting and storing large amounts of solar energy in the form of low temperature thermal energy, between 50-95°C. This application has potential in space heating and cooling. Solar ponds can be classified as four basic factors; convecting or non-convecting, partitioned (multi-layered) or non-partitioned, gelled or non-gelled and separate collector and storage or in-pond storage (Hasnain, 1998). The most commonly used is the non-convecting salt gradient solar pond. A density gradient is created by using sea water or salt water (chloride and magnesium

chloride) and its concentration increases with depth from the surface. The salt gradient pond has a black or dark bottom which absorbs solar radiation. One of the largest ponds is in El Paso, Texas, with a 3,355m^2 surface area and has been operational since 1986. The pond has achieved temperatures over 90°C in its heating zone, equivalently generating more than 100kWe during peak power output and provides more than 80,000 gallons of potable water in a 24h period (Lodhi, 1996).

Other fluid heat storage

Other important fluids used for heat storage are petroleum-based oil and molten salts. The specific heat capacities of these fluids are about 25-40% of water. However, because of having lower vapor pressure than water, these substitutes are capable of operating at high temperatures (over 300°C). The oils are limited to less than 350°C due to safety reasons and can be quite expensive. Some other oils are such as Therminol and Caloria-HT (Duffie, 1989). A few molten mixtures of inorganic salts have been considered for very high temperatures and one of which is sodium hydroxide with a melting point of 320°C, which could be used for temperatures up to 800°C (Hasnain, 1995). However, the drawbacks are highly corrosive and difficulty in containment. Liquid metals are possible to be used as a heat storage media. The most benefit is their higher thermal conductivity. Stainless steel (type 304) is the most common material used for containment of oils and liquid metals with special attention given to the maintenance of an oxide free environment to prevent corrosion (Sorour, 1988).

2.4 Conclusions

A thermal energy storage system is one example of a simple solution for correcting the mismatch between the supply and demand of energy. Today the use of thermal energy storage has attracted interest in several thermal applications such as active and passive solar heating, cooling and air conditioning. The use of thermal energy storage is essential for solar energy applications because of fluctuations in the nature of solar energy. The ability to store solar energy is also important for effective utilisation of thermal energy in buildings. Most solar energy applications used in buildings require energy storage to supply hot water and space heating during the night and overcast periods. Sensible heat storage can be used for such the purposes and may be categorized by the basis of the heat storage media as two groups of solid (i.e. rocks, metals etc.) and liquid storage (i.e. water, oil base fluids, molten salts etc.). Examples of sensible heat storage are such as an active solar heating system that stores heat in pebble rocks for space heating and solar ponds that provide a simple technique for storing large amounts of solar energy for hot water supply. It is desirable for the sensible storage medium to have high specific heat capacity, long term stability under thermal cycling, compatibility with its containment and low cost.

Chapter 3 Latent heat storage

3.1 Introduction

In the previous chapter, we see that thermal energy storage is one of the key technologies for energy conservation and is of great practical important which can contribute significantly to meeting society's needs for more efficient, environmentally benign energy use in building heating and cooling. Sensible heat storage is presently in an advanced stage of development meanwhile latent heat storage is a developing technology that has been found to be very promising in recent times. This chapter outlines the development of new technology latent heat storage systems. It will look at the choice of the phase change material (PCM) which plays an important role in addition to heat transfer mechanisms in the thermal heat storage system. Technical problems of PCM have been addressed. Basic thermodynamics of latent heat storage and case studies on PCM applications have been reviewed.

3.2 Latent heat storage

Latent heat storage systems are a very attractive technique. It offers high energy density and has the potential to store heat as latent heat of fusion[1] at the constant temperature corresponding to the phase transition temperature of the phase change materials (PCMs). Table 3.1 shows a comparison between solid and liquid sensible heat storage using a rock bed, water and latent heat storage using organic and non-organic compounds. The advantage of latent heat storage over sensible heat storage is clearly shown in term of

---

[1] The amount of heat energy associated with solid-liquid-solid phase change is called the latent heat of fusion.

space saving of the storage unit required for storing a certain amount of heat. For instance, the use of an inorganic PCM in a heat storage system requires a space of only $2.7m^3$ to store 10^6J of heat, comparing to $30m^3$ of a rock bed heat storage.

Property	Rock	Water	Organic PCM	Inorganic PCM
Density, kg/m^3	2,240	1,000	800	1,600
Specific heat, kJ/kg	1.0	4.2	2.0	2.0
Latent heat, kJ/kg	-	-	190	230
Storage mass for 10^6 J, kg	67,000	16,000	5,300	4350
Storage volume for 10^6 J,m^3	30	16	6.6	2.7
Relative storage mass	15	4	1.25	1.0
Relative storage volume	11	6	2.5	1.0

Table 3.1: Comparison of sensible and latent heat storage materials

Latent energy storage involves the following changes of phase, solid to solid, solid to liquid, solid to gas and liquid to gas. Solid to solid PCMs absorb and release heat in the same manner as solid-liquid PCMs. These materials are such as polyhydric alcohols and some inorganic salts. Basically, they do not change into a liquid state under normal conditions. They merely soften or harden and have been identified that have heat of fusion and transition temperatures suitable for thermal storage applications. The phase change of liquid to gaseous material involves the largest latent heat. However, volumetric storage capacity of the vapor phase is rather low. Therefore, this type of latent heat storage has not been popularly used. The most commonly used materials are solid to liquid PCMs and back again with the former requiring less energy than the latter. Solid to liquid PCMs are very attractive because they store and release large amount of energy over a narrow temperature range without a corresponding large volume change. The temperature remains constant because all the available energy is being used to change phases.

Latent heat storage application possesses with the following three components, a heat storage substance, containment and heat exchanger. For typical latent heat storage

applications, a phase change substance is put in a container such as a small tube piled up in a large container. During a heating cycle, hot fluid collects heat from a heat source and is circulated through spaces between the tubes and melts the substance by storing the heat as both sensible and latent heat. During a heat recovery cycle, the circulation of low temperature fluid is reversed to pick up the stored energy from the material and released the energy to a heat sink. Then the heat storage material begins to cool and solidifies. The cycle then starts again. A development of latent heat storage involves an essential knowledge of two areas, heat storage materials and heat exchangers. Abhat (1982) gives an overview of different stages involved in the development and problems needed to be tackled as shown in Figure 3.1.

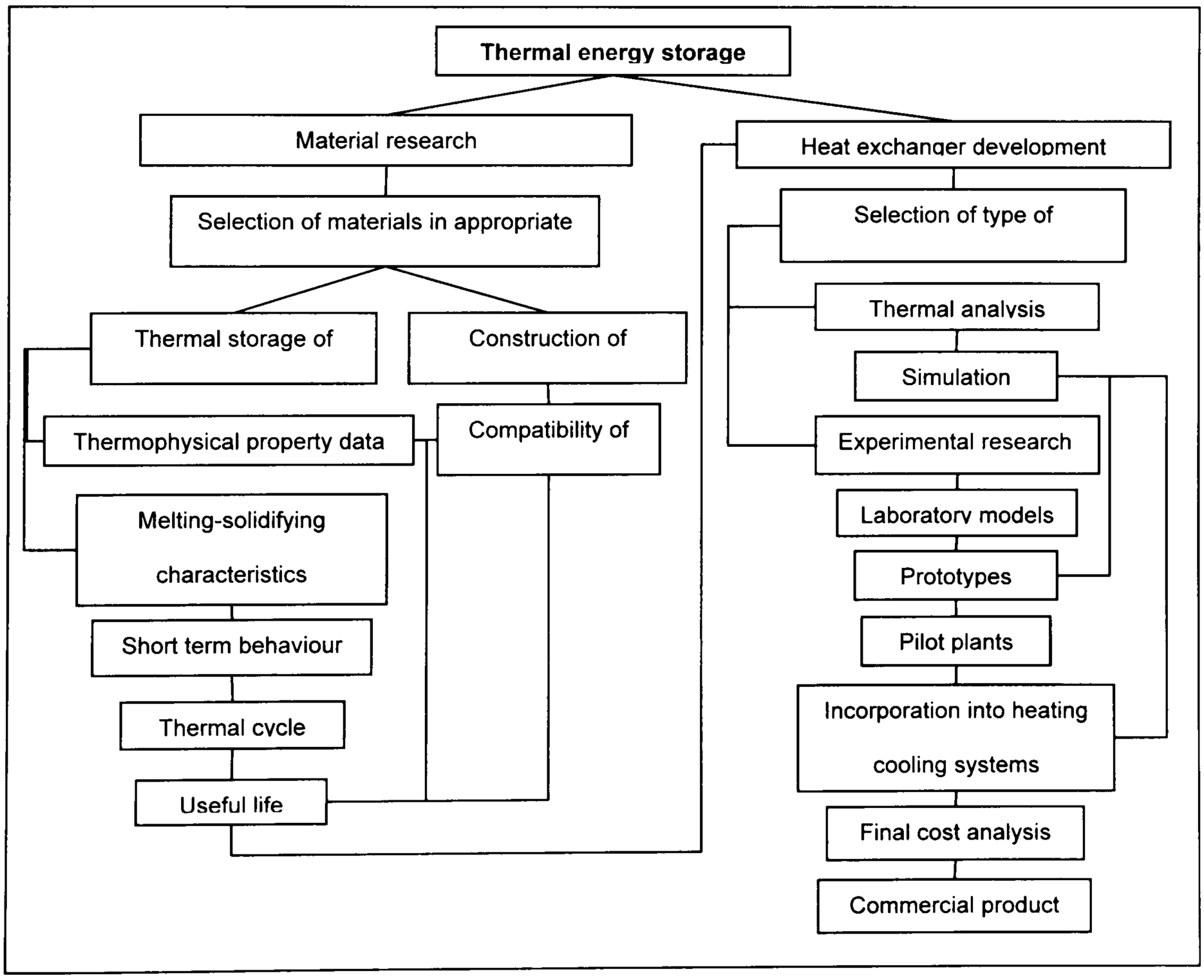

Figure 3.1: Flowchart of an overview of the development of latent heat storage system (Abhat, 1982)

3.3 Phase change material (PCM)

Ice is a very well known PCM which has been used for thousands of years and it is very widely used nowadays. Use of PCMs has been extended to space heating in a transport sector for railway and road vehicles since 19th century (Monegon, 1980). Towards the end of 19th century, PCM's shows were as an alternative means of space heating by using fire-heated bricks or stones. An example of a clever application is to use salt hydrates for keeping wagons warm in winter by storing the heat of the vapour produced by the locomotive as a by-product (Kurklu, 1998). Other interesting applications involve the use of PCMs in the protection of heat-sensitive parts of missiles and spacecraft, temperature stabilization in telephone boxes and computer rooms and the integration of PCMs into building materials.

For employment of latent heat storage materials, PCMs must exhibit certain desirable thermodynamic, kinetic and chemical properties. A summary of the various criteria governing a selection of PCM is shown in Table 3.2.

Criteria	Desired properties
Thermodynamic	The phase change material should exhibit ▪ A melting point in the desired operating temperature range ▪ High latent heat of fusion per unit mass, so that a lesser amount of material stores a given amount of energy ▪ High density, so that a smaller container volume holds the material ▪ High specific heat to provide for additional significant sensible heat storage effects ▪ High thermal conductivity, so that the temperature gradients required for changing and discharging the storage material are small ▪ Congruent melting: the material should melt completely so that the liquid and sold phases are identical in composition. Otherwise, the difference in densities between sold and liquid case segregation resulting in changes in the chemical composition of the material ▪ Small volume changes during phase transition, so that a simple containment and heat exchanger geometry can be used.
Kinetic	The phase change material should possess ▪ Little or no supercooling during freezing. The melt should crystallize at its thermodynamic freezing point. This is achieved through a high rate of nucleation and growth rate of the crystal. At times, the supercooling may be suppressed by introducing nucleating agent or a "cold finger" in the storage material.
Chemical	The phase change material should be ▪ Chemical stability ▪ No chemical decomposition, so that a high LTES system life is assured ▪ Non-corrosiveness to construction materials ▪ The material should be non-poisonous, non-flammable and non-explosive
Economic	The phase change material should show ▪ Available in large quantities ▪ Inexpensive

Table 3.2: Desired properties of phase change heat storage materials

(Abhat, 1982)

A classification of the substances used for latent heat storage system can be summarised as illustrated in Figure 3.2. PCMs can be classified into the following major categories, organic compounds, inorganic compounds and their eutectics. Organic compounds comprise of paraffin and non-paraffin whereas inorganic compounds involve salt hydrates, salts, metals and alloys.

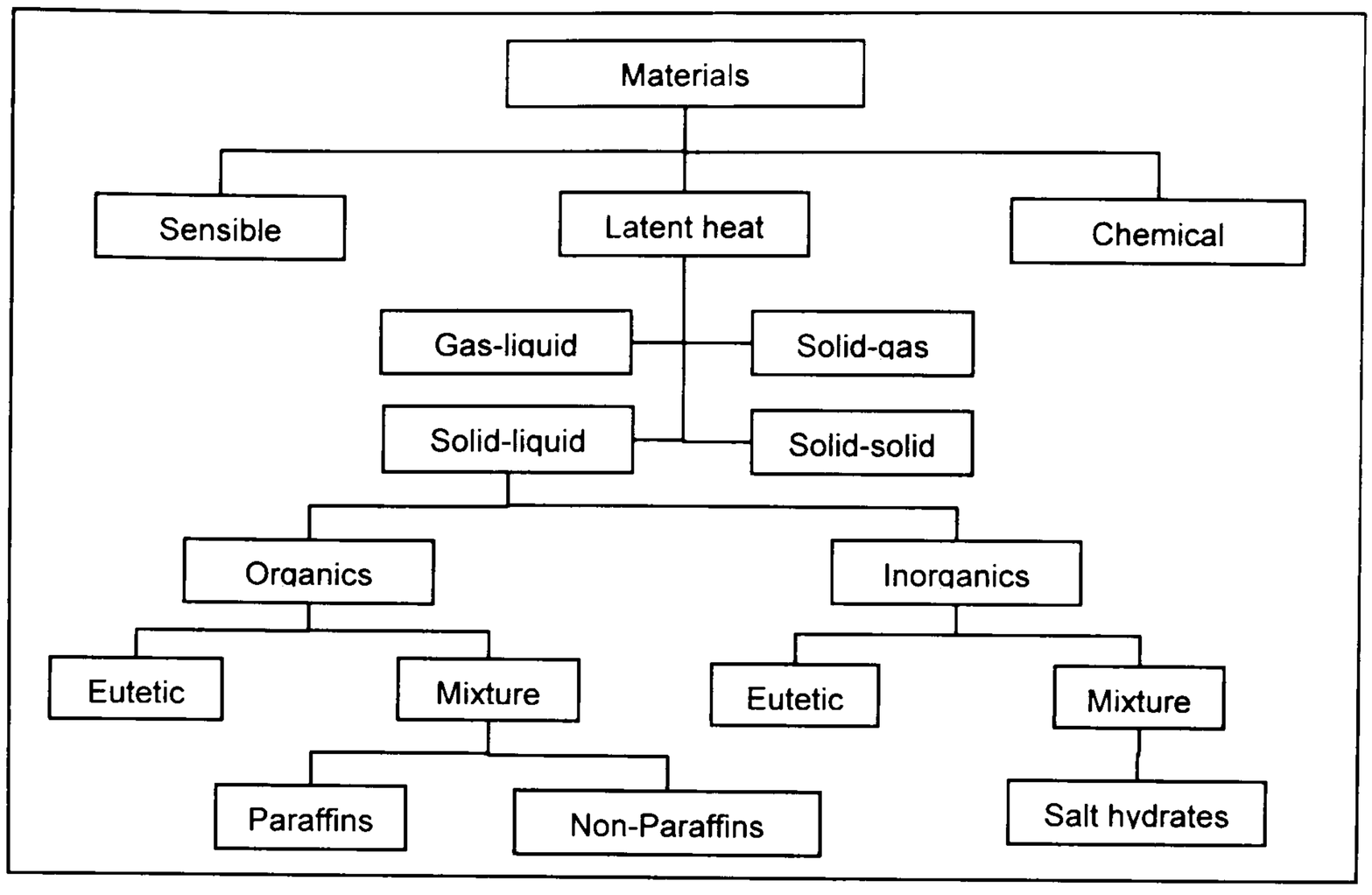

Figure 3.2: Classification of thermal energy storage materials (Abhat, 1982)

3.3.1 Paraffins

Paraffins are substances that have a waxy consistency at room temperature. They contain a major component called alkanes characterized by C_nH_{2n+2}; the *n*-alkane content in paraffin waxes usually exceeds 75% and may reach 100%. Another primary component of paraffin waxes is straight-chain hydrocarbons with only a small amount of branching, such as 2-methyl groups, near the end of the chain. Pure paraffins consist of only alkanes, for instance, paraffin octadecane, $C_{18}H_{38}$. The melting point of alkanes increases as the number of carbon increases. Alkanes with 14-40 C-atoms posses melting points between 6°C and 80°C (EPST, 1971). Two allotropic modifications that differ in their physical properties and crystal structure are generally found in solid phase of paraffins. The first medication existing at higher temperature is soft and plastic and the individual crystals are needle-shaped. The second modification existing at lower temperature is hard and brittle, and the crystals are disc-shaped (Abhat, 1982).

Some of the paraffin waxes investigated for heat storage applications include commercial waxes, *n*-eicosane and *n*-octadecane. Paraffin is found to exhibit many desirable characteristics as phase change substance for storage application including high heat of fusion, negligible supercooling, low vapor pressure in the melt, chemically inert and stable, self nucleating, no phase segregation and commercial availability at reasonable cost. However, they have some undesirable properties such as low thermal conductivity and large volume change during phase transition. Finned tube, metal matrix structure, metallic fillers and aluminum shavings are used to enhance their thermal conductivity. Table 3.3 lists some technical grade paraffins, which are essentially paraffin mixtures and are not completely refined of oil.

Compound	Melting temperature (˚C)	Heat of fusion (kJ/kg)	Thermal conductivity (W/m K)	Density (kg/m^3)
Paraffin C_{14}	4.5	165	n.a.	n.a.
Paraffin C_{15}-C_{16}	8	153	n.a.	n.a.
Polyglycol E400	8	99.6	0.187 (liquid,38.6˚C) 0.185 (liquid,69.9˚C)	1125 (liquid, 25˚C) 1228 (solid, 3˚C)
Dimethyl-sulfoxide (DMS)	16.5	85.7	n.a.	1009 (solid and liquid)
Paraffin C_{16}-$_{18}$	20-22	152	n.a.	n.a.
Polyglycol E600	22	127.2	0.189 (liquid,38.6˚C) 0.187 (liquid,67.0˚C)	1126 (liquid, 25˚C) 1232 (solid, 4˚C)
Paraffin C_{13}-C_{24}	22-24	189	0.21 (solid)	0.760 (liquid, 70˚C) 0.900 (solid, 20˚C)
1-Dodecanol	26	200	n.a.	n.a.
Paraffin C_{18}	28	244	0.148 (liquid, 40˚C)	0.774 (liquid, 70˚C)
	27.5	243.5	0.15 (solid) 0.358 (solid, 25˚C)	0.814 (solid, 20˚C)
1-Tetradecanol	38	205		
Paraffin C_{16}-C_{28}	42-44	189	0.21 (solid)	0.765 (liquid, 70˚C) 0.910 (solid, 20˚C)
Paraffin C_{29}-C_{33}	48-50	189	0.21 (solid)	0.769 (liquid, 70˚C) 0.912 (solid, 20˚C)
Paraffin C_{22}-C_{45}	58-60	189	0.21 (solid)	0.795 (liquid, 70˚C) 0.920 (solid, 20˚C)
Paraffin wax	64	173.6 266	0.167 (liquid,63.5˚C) 0.346 (solid,33.6˚C) 0.339 (solid,45.7˚C)	790 (liquid, 65˚C) 916 (solid, 24˚C)
Polyglycol E600	66	190.0	n.a.	1085 (liquid, 70˚C) 1212 (solid, 25˚C)
Paraffin C_{21}-C_{50}	66-68	189	0.21 (solid)	0.830 (liquid, 70˚C) 0.930 (solid, 20˚C)
Biphenyl	71	119.2	n.a.	991 (liquid, 73˚C) 1166 (solid, 24˚C)
Propionamide	79	168.2	n.a.	n.a.
Naphthalene	80	147.7	0.132 (liquid, 83.8˚C) 0.341 (solid, 49.9˚C) 0.310 (solid,66.6˚C)	976 (liquid, 84˚C) 1145 (solid, 20˚C)
Erythritol	118.0	339.8	0.326 (liquid, 140˚C) 0.733 (solid, 20˚C)	1300 (liquid, 140˚C) 1480 (solid, 20˚C)
HDPE	100-150	200	n.a.	n.a.
Trans-1,4-polybuta-diene (TPB)	145	144	n.a.	n.a.

n.a. : not available

Table 3.3: Physical properties data of paraffin waxes (Zalba, 2003)

3.3.2 Non-paraffin

Non-paraffin organics involve a wide variety of organic materials for instance fatty acids, esters, alcohols and glycols. They are basically characterized by $CH_3(CH_2)_{2n}COOH$ with heat of fusion values comparable to that of paraffin (EPST, 1971). Hale (1971) shows that about 70 non-paraffin organics have melting points in the range of 7°C to 187°C and heats of fusion in the range of 42kJ/kg to 250kJ/kg. Some fatty acids used in low temperature thermal applications are presented in Table 3.4. A study by Hasnain (1998) shows that

fatty acids have melting points suitable for heating applications and they exhibit excellent melting and freezing cycles without any supercooling. Their major drawback, however, is their cost which is about three times greater than that of paraffins.

Compound	Melting temperature (˚C)	Heat of fusion (kJ/kg)	Thermal conductivity (W/m K)	Density (kg/m^3)
Propyl palmiate	10	186	n.a.	n.a.
Isopropyl palmiate	11	95-100	n.a.	n.a.
Capric-lauric acid + pentadeeane (90:10)	13.3	142.2	n.a.	n.a.
Isopropyl stearate	14-18	140-142	n.a	n.a.
Caprylic acid	16	148.5	0.149 (liquid, 38.6˚C)	901 (liquid, 30˚C)
	16.3	149	0.145 (liquid, 67.7˚C)	862 (liquid, 80˚C)
			0.148 (liquid, 20˚C)	981 (solid, 13˚C)
				1033 (solid, 10˚C)
Capric-lauric acid (65 mol%-35 mol%)	18.0	148	n.a.	n.a.
Butyl stearate	19	140	n.a.	n.a.
		123-200		
Capric-lauric acid (45-55%)	21	143	n.a.	n.a.
Dimenthyl sabacate	21	120-135	n.a.	n.a.
34% Mistiric acid + 66% Capric acid	24	147.7	0.164 (liquid,39.1˚C)	888 (liquid, 25˚C)
			0.154 (liquid, 61.2˚C)	1018 (solid, 1˚C)
Vinyl stearate	27-29	122	n.a.	n.a.
Capric acid	32	152.7	0.153 (liquid, 38.5˚C)	878 (liquid, 45˚C)
	31.5	153	0.152 (liquid, 55.5˚C)	886 (liquid, 40˚C)
			0.149 (liquid, 40˚C)	1004 (solid, 24˚C)
Methyl-12 hydroxy-stearate	42-43	120-126	n.a.	n.a.
Lauric acid	42-44	178	0.147 (liquid, 50˚C)	862 (liquid, 60˚C)
	44	177.4		870 (liquid, 50˚C)
				1007 (solid,24˚C)
Myristic acid	49-51	204.5	n.a.	861 (liquid, 55˚C)
	54	187		844 (liquid, 80˚C)
	58	186.6		990 (solid, 24˚C)
Palmitic acid	64	185.4	0.162 (liquid, 68.4˚C)	850 (liquid, 65˚C)
	61	203.4	0.159 (liquid, 80.1˚C)	847 (liquid, 80˚C)
	63	187	0.165 (liquid, 80˚C)	989 (solid, 24˚C)
Stearic acid	69	202.5	0.172 (liquid, 70˚C)	848 (liquid, 70˚C)
	60-61	186.5		965 (solid, 24˚C)
	70	203		

% in weight; n.a.: not available.

Table 3.4: Physical properties of fatty acids (Zalba, 2003)

3.3.3 Salt hydrates (salts bound to water).

The use of salt hydrates has been propagated since early 1940s. Salt hydrates, characterized by $M.nH_2O$ (where M represents an inorganic compound) form an important class of heat storage substances due to their high volumetric latent storage density. Glauber's salt ($Na_2SO_4H_2O$) containing 44% Na_2SO_4 and 56% H_2O by weight has been

studied since 1950s (Abhat, 1982). It has a melting temperature of about 32.4°C, a high latent heat of 254kJ/kg, and is one of the cheapest materials that can be used for thermal energy storage. Some other salt hydrates are calcium chloride hexahydrate, sodium thiosulphate pentahydrate, barium hydroxide octahydrate and etc. Table 3.5 shows a list of some slat hydrates melting in the temperature range of 0-900°C along with their thermophysical properties. A main advantage of salt hydrates is that they have high heat of fusion in comparison with organic compounds. For instance, the organic materials have latent heat storage in the range of 125-200 kJ/m^3, whereas salt hydrates is almost twice as much, between 250-400 kJ/m^3.

However, a major drawback is that most of them melt incongruently. They melt to a solid phase and a saturated aqueous phase, which is generally a lower hydrate of the same salt. Because of differences in density, the solid phase sink to bottom of a container, so called decomposition phenomenon. This phenomenon is irreversible because during solidify cycle the solid particles cannot combine with the saturated solution to form the original salt hydrate. Another problem with salt hydrate is poor nucleating properties resulting in supercooling of the liquid salt hydrate prior to freezing. Biswas (1977) suggests using an extra water principle to prevent formation of the heavy anhydrous salt. Although this makes a system stable with cycling, it reduces a storage density and requires the system to be operated with a large temperature swing.

Table 3.5: Physical properties data of salt hydrates (Zalba, 2003)

Compound	Melting temperature (˚C)	Heat of fusion (kJ/kg)	Thermal conductivity (W/m K)	Density (kg/m3)
H_2O	0	333	0.612 (liquid, 20˚C)	998 (liquid, 20˚C)
		334	0.61 (30˚C)	996 (30˚C)
				917 (solid, 0˚C)
$LiClO_3 - 3H_2O$	8.1	253	n.a.	1720
$ZnCl_2 - 3H_2O$	10	n.a.	n.a.	n.a.
$K2HPO_2 - 6H_2O$	13	n.a.	n.a.	n.a.
$NaOH - 3\ ½\ H_20$	15	n.a.	n.a.	n.a.
	15.4			
$Na2CrO_4 - 10H_2O$	18	n.a.	n.a.	n.a.
$KF - 4H_2O$	18.5	23.1	n.a.	1447 (liquid, 20˚C)
				1455 (solid, 18˚C)
				1480
$Mn(No3)_2 - 6H_2O$	25.8	125.9	n.a.	1738 (liquid, 20˚C)
				1728 (liquid, 18˚C)
				1795 (solid, 5˚C)
$CaCl_2 - 6H_2O$	29	190.8	0.540 (liquid, 38.7˚C)	1562 (liquid, 32˚C)
	29.2	171	0.561 (liquid, 61.2˚C)	1496 (liquid)
	29.6	174.4	1.088 (solid, 23˚C)	1802 (solid, 24˚C)
	29.7	192		1710 (solid, 25˚C)
	30			1634
	29-39			1620
$LiNO_3 - 3H_2O$	30	296	n.a.	n.a.
$Na_2SO_4 - 10H_2O$	32.4	254	0.544	1485 (solid)
	32	251.1		1458
	31-32			
$Na_2CO_3 - 10H_2O$	32-36	246.5	n.a.	1442
	33	247		
$CaBr_2 - 6H_2O$	34	115.5	n.a.	1956 (liquid, 35˚C)
				2194 (solid, 24˚C)
$Na2HPO2 - 12H2O$	35.5	265	n.a.	1522
	36	280		
	35	281		
	35.2			
$Zn(NO_3)_2 - 6H_2O$	36	146.9	0.464 (liquid, 39.9˚C)	1828 (liquid, 36˚C)
	36.4	147	0.469 (liquid, 61.2˚C)	1937 (solid, 24˚C)
				2065 (solid, 14˚C)
$KF - 2H_2O$	41.4	n.a.	n.a.	n.a.
$K(CH_3COO) - 1\ ½\ H_2O$	42	n.a.	n.a.	n.a.
$K_3PO_4 - 7H_2O$	45	n.a.	n.a.	n.a.
$ZN(NO_3)_2 - 4H_2O$	45.5	n.a.	n.a.	n.a.
$Ca(NO_3)_2 - 4H_2O$	42.7	n.a.	n.a.	n.a.
	47			
$Na_2HPO_2 - 7H_2O$	48	n.a.	n.a.	n.a.
$Na_2S_2O_3 - 5H_2O$	48	201	n.a.	1600 (solid)
	48-49	209.3		
		187		
Zn(NO3)2 -2H2O	54	n.a.	n.a	n.a.
$NaOH - H_2O$	58.0	n.a.	n.a.	n.a.
$Na(CH_3COO) - 3H_2O$	58	264	n.a.	1450
	58.4	226		
$Cd(NO_3)_2 - 4H_2O$	59.5	n.a.	n.a.	n.a.
$Fe(NO_3)_2 - 6H_2O$	60	n.a.	n.a.	n.a.
NaOH	643	227.6	n.a.	1690
$Na_2B_2O_7 - 10H_2O$	68.1	n.a.	n.a.	n.a.
$Na_3PO_4 - 12H_2O$	69	n.a.	n.a.	n.a.
$Na_2P_2O_7 - 10H_2O$	70	184		
$Ba(OH)_2 - 8H_2O$	78	265.7	0.653 (liquid, 85.7 ˚C)	1937 (liquid, 84˚C)
		267	0.678 (liquid, 98.2˚C)	2070 (solid, 24˚C)
		280	1.255 (solid, 23˚C)	2180 (solid)
$AlK(SO_4)_2 - 12H_2O$	80	n.a.	n.a.	n.a.
$Kal(SO_4)_2 - 12H_2O$	85.8	n.a.	n.a.	n.a.
$Al2(SO_4)_3 - 18H_20$	88	n.a.	n.a.	n.a.
$Al(NO_3)_3 - 8H_2O$	89	n.a.	n.a.	n.a.
$Mg(NO_3)_2 - 6H_2O$	89	162.8	0.490 (liquid, 95˚C)	1550 (liquid, 94˚C)
	90	149.5	0.502 (liquid, 110˚C)	1636 (solid, 25˚C)
			0.611 (solid, 37˚C)	1640
			0.669 (solid, 55.6˚C)	
$(NH_4)Al(SO_4) - 6H_2O$	95	269	n.a.	n.a.

(Continued on next page)

Table 3.5 (Continued)

Compound	Melting temperature (°C)	Heat of fusion (kJ/kg)	Thermal conductivity (W/m K)	Density (kg/m3)
$CaBr_2 - 4H_2O$	110	n.a.	n.a.	n.a.
$MgCl_2 - 6H_2O$	117	168.6	0.570 (liquid, 120°C)	1450 (liquid, 120°C)
	115	165	0.598 (liquid, 140°C)	1442 (liquid, 78°C)
	116		0.694 (solid, 90°C)	1569 (solid, 20°C)
			0.704 (solid, 110°C)	1570 (solid, 20°C)
$Mg(NO_3) - 2H_2O$	130	n.a.	n.a.	n.a.
$NaNO_3$	307	172	0.5	2260
	308	174		2257
		199		
KNO_3	333	266	0.5	2.110
	336	116		
KOH	380	149.7	0.5	2.044
$MgCl_2$	714	452	n.a.	2140
NaCl	800	492	5	2160
	802	466.7		
Na_2CO_3	854	275.7	2	2.533
KF	857	452	n.a.	2370
K_2CO_3	897	235.8	2	2.290

n.a.: not available

3.3.4 Eutectics of organic and inorganic compounds

Eutectics are a combination of two mixtures of two or more salts that possess a fixed melting/freezing point. Some candidate materials having acceptable values of heat of fusion are pentaerythritol, pentaglycerine, neopentyl glycol and their mixtures. These eutectics can be used for cool and passive solar storage with low or medium temperature flat plate collectors, according to their melting point. Some of the eutectics are listed in Table 3.6. A highly crystalline polymer such as high density polyethylene (HDPE) offers definite advantages as a potential thermal energy storage material if it is rendered form stable by crosslinking. Crosslingked HDPE is an excellent thermal energy storage material and can be used in direct thermal contact with ethylene glycol and silicone oil (Hasnain, 1998).

Compound	Melting temperature (°C)	Heat of fusion (kJ/kg)	Thermal conductivity (W/m K)	Density (kg/m^3)
37.5% Urea + 63.5% acetamide	53	131.2	n.a.	n.a.
32.9% benzoic acid	48	144.5	0.130 (liquid, 100°C)	n.a.
			0.282 (solid, 38°C)	n.a.
			0.257 (solid, 52°C)	n.a.
Na_2SO_4(32.5%)H_2O(41.4%) NaCl(6.66%)NH_4Cl(6.16%)	13	146	n.a.	n.a.
49.3% $MgCl6H_2O$- 50.7%$Mg(NO_3)_26H_2O$	58	58	n.a.	n.a.
67.1% Naphthalene +	67	123.4	0.136 (liquid, 78.5° C)	n.a.
61.5%$Mg(NO_3)6H_2O$ +38.5%NH_4NO_3	51	131.3	n.a.	n.a.
58.3%$Mg(NO_3)6H_2O$ +41.7%$MgCl_26H_2O$	58	106	n.a.	n.a.
$CaCl_26H_2O$ +$CaBr_2$ 6 H_2O	14	140	n.a.	n.a.
Lauric-capric acid	18	120	n.a.	n.a.
Lauric-Palmitic	33	145	n.a.	n.a.
Lauric-Stearic	54	150	n.a.	n.a.
Palmitic-stearic	51	160	n.a.	

n.a. : not available

Table 3.6: Physical properties of eutectics (Hasnain, 1998)

3.4 Supercooling and stratification problem

Salt hydrates have high heats of fusion. Yet they are denser than water and therefore make a more compact storage medium. Serious disadvantages are that they do not always solidify at the right temperature and into the desired compound. Supercooling occurs when heat is being extracted from the latent heat storage, the material may cool past its melting temperature without releasing the latent heat or it may be recovered at a temperature significantly below the melting point (see Figure 3.3) (Burns, 1981). The supercooling phenomenon can be an important obstacle to the industrial use if it becomes too large. Salt hydrates behave in a more complex way than organic compounds because hydration and dehydration occurs. At a temperature below the hydration point, the anhydrate becomes hydrated and crystallizes with the evolution of heat. Upon heating the crystal dissolves in its water of hydration, thereby absorbing heat (Hariri, 1988).

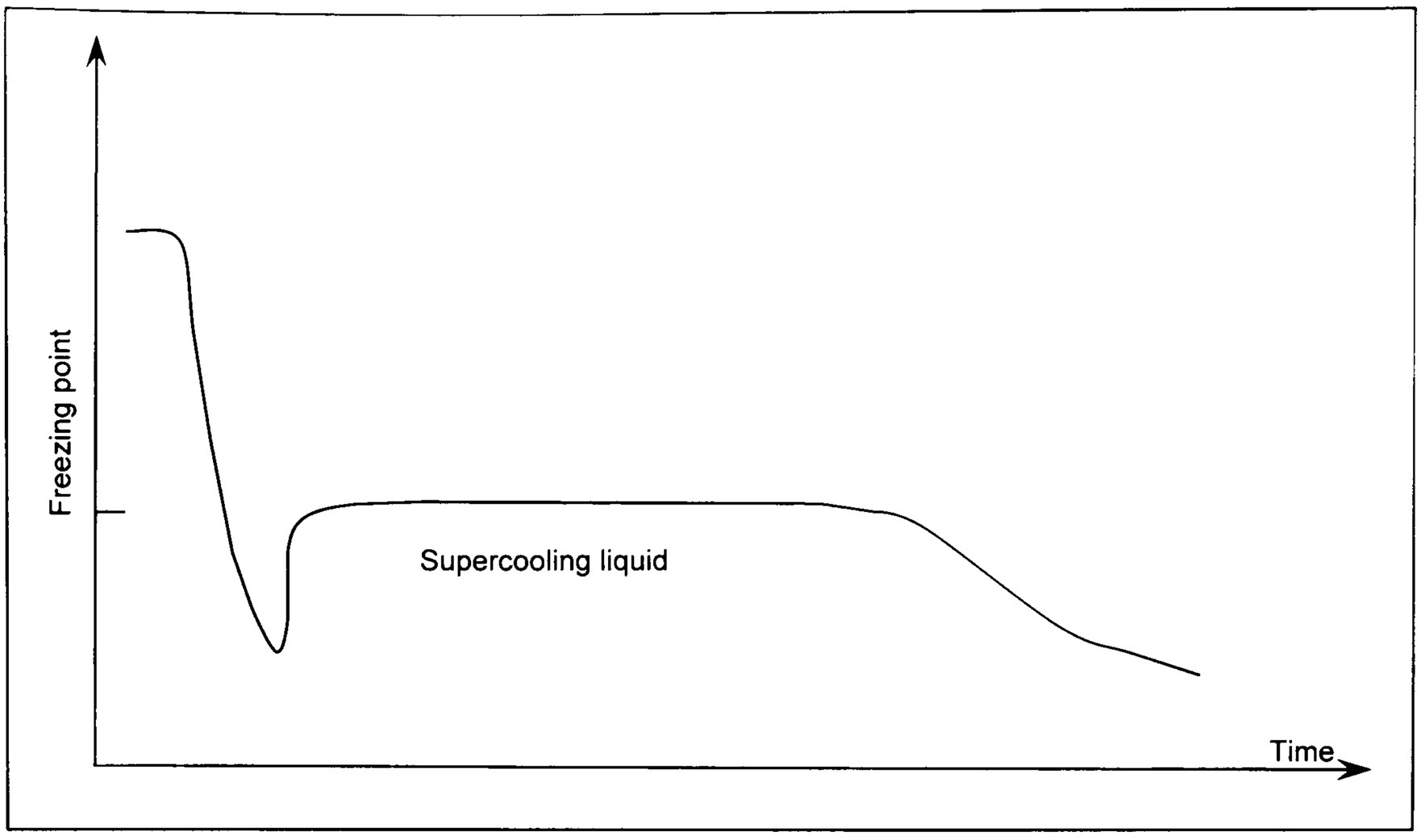

Figure 3.3: Supercooling of a phase change material (Burns, 1981)

Since solidification involves nucleation, numerous nucleating additives have been investigated in order to reduce the supercooling. A nucleating agent is a material having a crystal structure similar in lattice spacing to that of the heat storage substance. They serve as nuclei for the PCM crystals to grow on them during freezing of the PCM and are also termed as seed-crystals. The amount of supercooling could be reduced by using glass containers containing a shallow bed of the salt hydrate. The larger glass surface aided in somewhat improving the nucleation conditions in the melt and the shallow bed assisted in eliminating segregation effects in the molten material (Abhat, 1982). Ryu (1992) studies various inorganic salt hydrates as a latent heat storage medium. He found that, for thickened Glauber's salt, borax can reduce supercooling of the salt from 15 to 3-4°C. Three different powders of carbon (1.5-6.7 μm), copper (1.5-2.5 μm) and titanium oxide (2-200 μm) were found to reduce the supercooling of thickened $Na_2HPO_4 \cdot 12H_2O$. Also, by adding 2 wt% potassium sulphate the supercooling of thickened $CH_3COONa \cdot 3H_2O$ was reduced from 20 to 2–3°C (see Table 3.7).

PCM	Thickener	Melting temperature (°C)	Nucleating agent (size, µm)	Supercooling (°C) w/o nucleator	Supercooling (°C) w/ nucleator
$Na_2SO_4 \cdot 10H_2O$	SAP	32	Borax (20 x 50 – 200 x 250)	15 - 18	3 - 4
$Na_2HPO_4 \cdot 12H_2O$	SAP	36	Borax (20 x 50 – 200 x 250)	20	6-9
			Carbon (1.5-6.7)		0-1
			TiO_2 (2-200)		0-1
			Copper (1.5-6.7)		0-1
			Aluminum (8.5-20)		3-10
$CH_3COONa \cdot 3H_2O$	CMC	46	Na_2SO_4	20	4-6
			$SrSO_4$		0-2
			Carbon (1.5-6.7)		4-7
$Na_2S_2O_3 \cdot 5H_2O$	CMC	57	K_2SO_4	30	0-3
			$Na_2P_2O_7 \cdot 10H_2O$		0-2

Table 3.7: Supercooling range of thickened PCMs with different nucleating agents (Ryu, 1992)

Stratification (or irreversible phase change) is usually associated with phase separation after it cycles through the phase change process which limits the usefulness of salt hydrates. For example, Glauber's salt has an incongruent melting point, and as its temperature increases beyond the melting point it separates into a liquid phase and solid Na_2SO_4. Since a density of the salt is higher than a density of the solution, phase separation occurs. As a consequence, the salt settles to the bottom of the tank. With complete stratification, the storage ability of the salt decreases to about 40% (Hariri, 1988).

To overcome the problem, addition of suspension media or thickening agents to the salt hydrate to prevent separation of the solid and liquid phases has been recommended. The use of a thickener also assists in suspending the nucleating agents within the heat storage medium bulk, which otherwise tend to collect at the container bottom due to density differences. Thickening agents, however, displace a part of the salt hydrate in the heat store, thus, reducing the volumetric heat storage capacity of the heat store (ABhat, 1982). Ryu (1992) proposes to use a super-absorbent polymer (SAP) made from an acrylic acid copolymer as an effective thickener to prevent undesirable phase separation of the high hydrate inorganic salts such as $Na_2SO_4 \cdot 10H_2O$ and $Na_2CO_3 \cdot 10H_2O$ (see Table 3.7). Most

of these materials can be stabilized by the addition of 3 to 5 wt% SAP as a thickener. For the low hydrate inorganic salts such as $CH_3COONa\cdot 3H_2O$ and $Na_2S_2O_3\cdot 5H_2O$, carboxymethyl cellulose (CMC) is found to be an effective thickener.

Several techniques have been tried for preventing the phase separation, which results in loss of storage capacity, i.e., a rotating storage device and direct contact heat transfer. Another approach is to store salt solutions in a shallow pan or a long, thin tube (Hariri, 1988). In addition, a technique of using a macro-encapsulation of PCMs is found to avoid large phase separations. Results tested by Burns (1981) show that more than 2,000 cycle of PCM encapsulated change phase without any phase separation. The most cost-effective containers are plastic bottles and tin plated food cans/mild steel cans. However, corrosion could lead to disastrous consequences if internal and external lacquer finishes are not applied properly to the mild steel metal cans.

3.5 Thermal cycling

The most important criteria that have limited widespread use of phase change energy storage are a number of cycles they can withstand without any degradation in their properties and a useful life of PCMs–container systems. Insufficient long term stability of the storage materials is mainly due to poor stability of the materials' properties and corrosion between the PCM and container (Zalba, 2003). The heat storage materials must undergo thermal cycling tests, which involves in repeated melting and freezing of the phase change materials. Abhat (1982) observes that laboratory measurements comprising at least 1,000-2,000 cycles are recommended, particularly with the inorganic salt hydrates, to establish the long-term thermal stability of the PCM.

Mark (1980) used a standard calorimetric technique to investigate the heat storage in Glauber's salt as a function of thermal cycling. Two samples including $Na_2SO_410H_2O$ with 3% Borax and thickened material comprising 88% Glauber's salt + 2.64% Borax + 9.36% attapulgite clay were tested. Results show that the thermal capacity of the pure salt declines quickly from 238kJ/kg to 63kJ/kg after 40 cycles. The thermal capacity of the thickened salt also declines but slowly to 12kJ/kg after 140 cycles. A study by Cartsson (1979) also supports that as a result of phase separation with every melting/solidification cycle the heat capacity of Glauber salt may decrease by as much as 16% for each new cycle. Clearly, both samples are unfit for long-term use as latent heat storage materials.

In 1984, Kimura used NaCl to improve the stability of $CaCl_26H_2O$, containing slightly more water than the stoichiometric composition. Results are found to be very stable following more than 1000 heating–cooling cycles. In 1995 Gibbs and Hasnain studied the thermal stability of paraffins and found that the paraffins had excellent long-term stability as neither the cycles nor contact with metals degrades their thermal behaviour. An investigation on the phase change stability of some fatty acids subjected to 450 phase transition periods is conducted by Hasan (1994). Sar (2003) also studies the thermal stability of some fatty acids (e.g., stearic, palmitic myristic and lauric acid) by Differential Scanning Calorimeter (DSC) technique. The repeated thermal cycles of 40, 410, 700 and 910 has been tested. The measurements show that all fatty acids investigated as PCMs have a good thermal stability for an actual middle-term thermal energy storage.

3.6 Containment for the phase change substances

To ensure that a PCM storage unit remains cost effective it is important that not only the material itself but also a type of container used must be inexpensive. Suitability of the containment type for thermal energy storage applications depends primarily on a compatibility of a container material to transfer heat between the PCM and heat transfer fluid. Furthermore, container dimensions and construction are likely to have great bearing on the rate of heat transfer. The container should be capable of a change in volume, corrosion resistance and impermeable to the PCM and the heat transfer fluid.

3.6.1 PCMs and volumetric change in containers

Schroder (1979) studies on phase change showed that most hydrates involved a considerable change in volume. To avoid ruinous mechanical stress on a storage container, he found that, in the case of selected hydrates which expanded on melting, the problem could be solved by applying flat plate storage containers with flexible wall. In the case of water salt hydrate eutectics (the volume increases on solidification), this expansion destroyed even the flexible containers soon after a few storage cycles by local buckling. This serious problem can be over-come by adding a small amount of special substances, lower melting salt hydrate eutectics to the storage medium. Examples of which are, H_2O/NaF, H_2O/NaCl, H_2O/KF, etc.

A design for containers of the phase change substance requires specification of amounts of storage, pressure and material requirements for a tank, and an amount of insulation to be used. The containers must be leak proof, capable of withstanding long exposure to temperature cycles, and corrosion resistant. If a volume change accompanies phase change (30% is typical), the container must be capable of accommodating the change.

3.6.2 Corrosion of the materials

A compatibility of PCMs with conventional materials of construction is particularly important for an assurance of a life of a latent heat storage system. Gravimetric analysis, optical and scanning electron microscopy are conventional evaluation methods for corrosion tests. The gravimetric method provides a sample mass loss, from which a reduction in sample thickness with time and a corrosion rate can be computed. On the other hand, the microscopy technique provides information on a type of corrosion, for instance, pitting corrosion, cracks, etc.

Studies of PCMs including organics, inorganic salt hydrates and inorganic eutectic compounds for corrosion tests with storage containment have been carried out by Yoneda (1978), Heine (1978, 1981) and Schroder (1980). Results show that the most compatible materials with metal containers (i.e., stainless steel, mild steel, copper, tin plated mild steel and etc.) are organic materials. Porisini (1988) studies the corrosion resistance of metallic alloys (stainless steel, carbon steel, Al alloys, and Cu) to salt hydrates ($Na_2SO_4 \cdot 10H_2O$, $CaCl_2 \cdot 6H_2O$, $Na_2SO_4 \cdot 1/2NaCl \cdot 10H_2O$, $NaOH \cdot 3.5H_2O$). Results show that the most corrosion-resistant alloy to all the hydrated salts is stainless steel. Further investigations on corrosion tests with salt hydrates are performed by Groll (1990), Cabeza (2001) and Amaya (2003).

An investigation of fatty acids with corrosion resistance to some construction materials is undertaken by Sar (2001). The containment materials are stainless steel (SS 304L), carbon steel (steel C20), aluminium (Al) and copper (Cu). The gravimetric analysis on mass loss (mg/cm^2), corrosion rate (mg/day) and microscopic or metallographic investigation are performed for 910 thermal cycles. He concludes that stainless steel (SS 304L) with

chromium oxide (Cr_2O_3) surface layer and Al with aluminium oxide (Al_2O_3) surface layer is essentially compatible with the investigated fatty acids (stearic, palmitic, myristic and lauric acid).

From the above investigations, it can be concluded that stainless steel is the only metal that is compatible with all phase change materials. Mild steel is a fairly good material being corrosion resistant to most PCMs with an exception of $Zn(NO_3)_26H_2O$ and $Mg(NO_3)_2$ - $MgCl_2$ eutectic. Copper is compatible with all heat storage materials, except sodium thiosulphate 5-hydraate. Aluminum and aluminum alloy $AlMg_3$ are incompatible with the salt hydrates, with an exception of $Na_2S_2O_3$ $5H_2O$. Furthermore, common plastics are stated to be generally corrosion resistant to most inorganic salt hydrates and their eutectic compounds.

3.6.3 Capsule and tube in tube containers

Capsule container

Heat transfer performance can be affected by thermal conductivity of PCMs. Salt hydrates have thermal conductivities in a range of 0.5-1.5 W/mK whereas thermal conductivities of paraffins are between 0.15-0.21 W/mK. Manley (1983) suggests that in order to achieve high heat transfer rates the PCM should be subdivided by some form of encapsulation. Encapsulation effectively increases a heat transfer surface area per unit volume and thereby provides a correspondingly improved rate of heat transfer. They can be formed in button-shaped capsules ranging from 3/8 to several inches. The PCM powder is compacted into small pellets and then the pellets are encased in a tough, inert latex skin. The small size of the pellets minimizes stratification and separation problems. The capsules can be used in

packed-bed heat exchanger/storage unit with aqueous ethylene glycol heat exchanger fluid. The encapsulated containers are normally available in three geometries, rectangular, cylindrical and spherical type (see Figure 3.4).

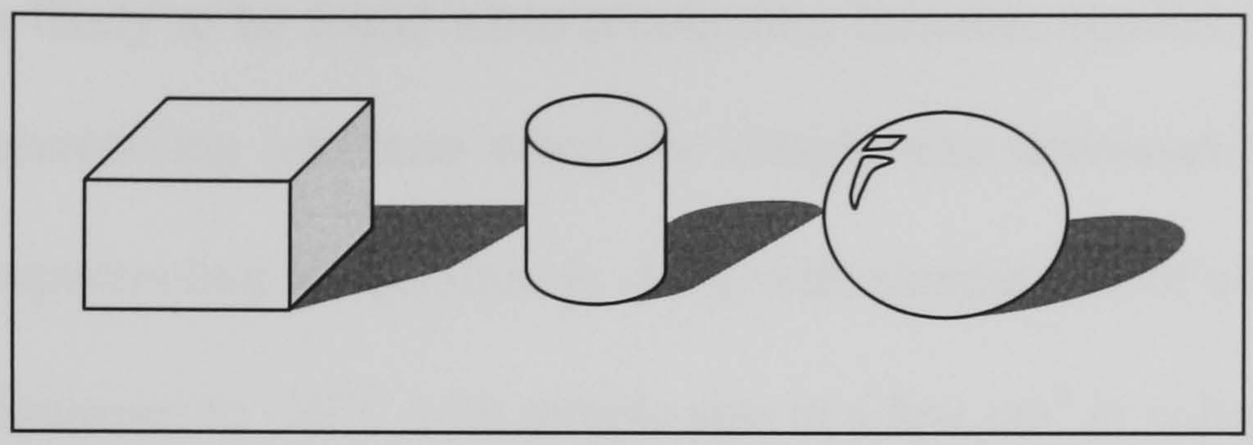

Figure 3.4: Type of encapsulation for PCM containment (rectangular, cylinder and spherical shape)

Barba (2003) studies behaviour of encapsulated salt hydrates as heat storage in a domestic hot water tank with three different geometrical configurations, e.g. slab, cylindrical and spherical polyethylene containers. He used a moving boundary model for the phase-change material during the discharging mode and the duration of the phenomenon. Results show that among different geometrical configurations of the PCM the shortest time for complete solidification is matched for small spherical capsules, with high Jacob numbers and thermal conductivity.

The rate of heat transfer to or from a packed bed of PCM containers is dominated by several factors. Manley (1983) shows that the performance of the bed is very dependent on the container size so that an available energy storage density of the store is directly related to the surface area density. Thus for a given energy density it is possible to define an upper limit for container size. He presents a design chart for selecting the maximum acceptable PCM container size for spherical and cylindrical containers according to a given power density, temperature difference and a target NTU of 2 (see Figure 3.5). For example, to

achieve power density of 20 kW/m^3 with a temperature difference of 20°C, an equivalent sphere diameter should not exceed 75mm; this is satisfied by a cylinder of diameter 50mm with aspect ratio 2.0 (height/diameter). However, it is worth mention that the supercooling phenomenon is likely to be found when a container becomes smaller. Bedecarrats (1995) reports that supercooling increases when the sample size decreases. He shows that for water/ice, the supercooling temperature is -14°C with sample size of a few cm^3 in volume, but the figure decreases to -36°C with sample size of a few μm^3 in volume.

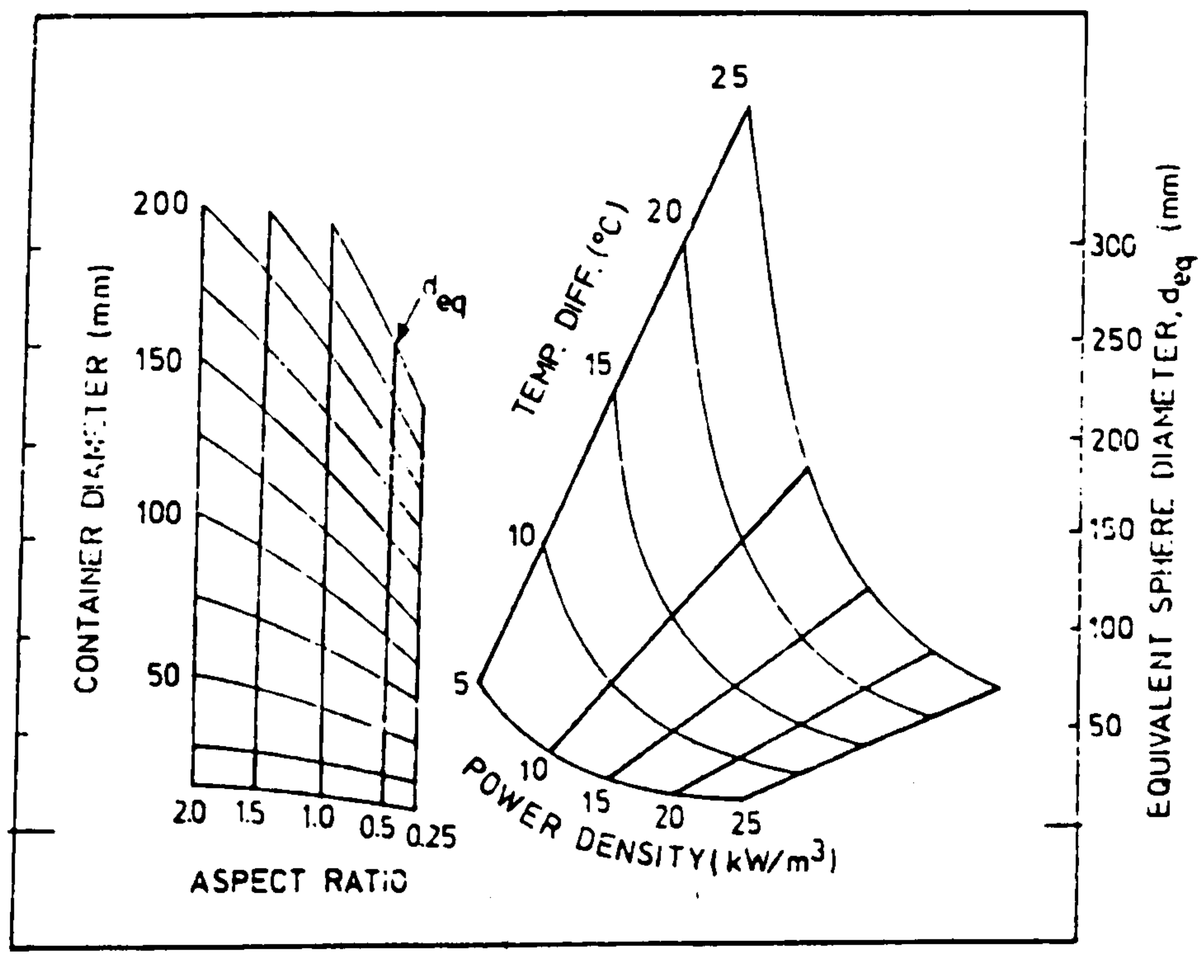

Figure 3.5 Container sizing chart (based on the following; U=40 W/m^{2}K, ε=0.38, NTU=2), (Manley, 1983)

Tube in tube type

A tube in tube concept has been developed whereby a PCM is sandwiched between an inner metal and outer insulated tube (Figure 3.6). The PCM is sealed inside a beam which enables a fluid to pass through the inner-pipe of the circular beam in order to provide heat exchange capability. Heat transfer between the hot/cold fluid which flows inside the pipe and the surrounding PCM takes place from the outer surface of the metal pipe. The beams

must also be able to eliminate a possibility of waterside contamination and avoid a possibility of PCM spills. The beams can be manufactured in any length. Standard lengths by EPS for PlusICE are 2, 4 and 6m lengths with diameter aspect ratios of 4-5 in order to achieve 7-8 hours charging operation. The thermal energy beams can be accommodated as part of a pipe network without a need for central thermal energy storage tank. Alternatively, the beams can be stacked on top of each other in order to provide a centralised thermal energy storage system.

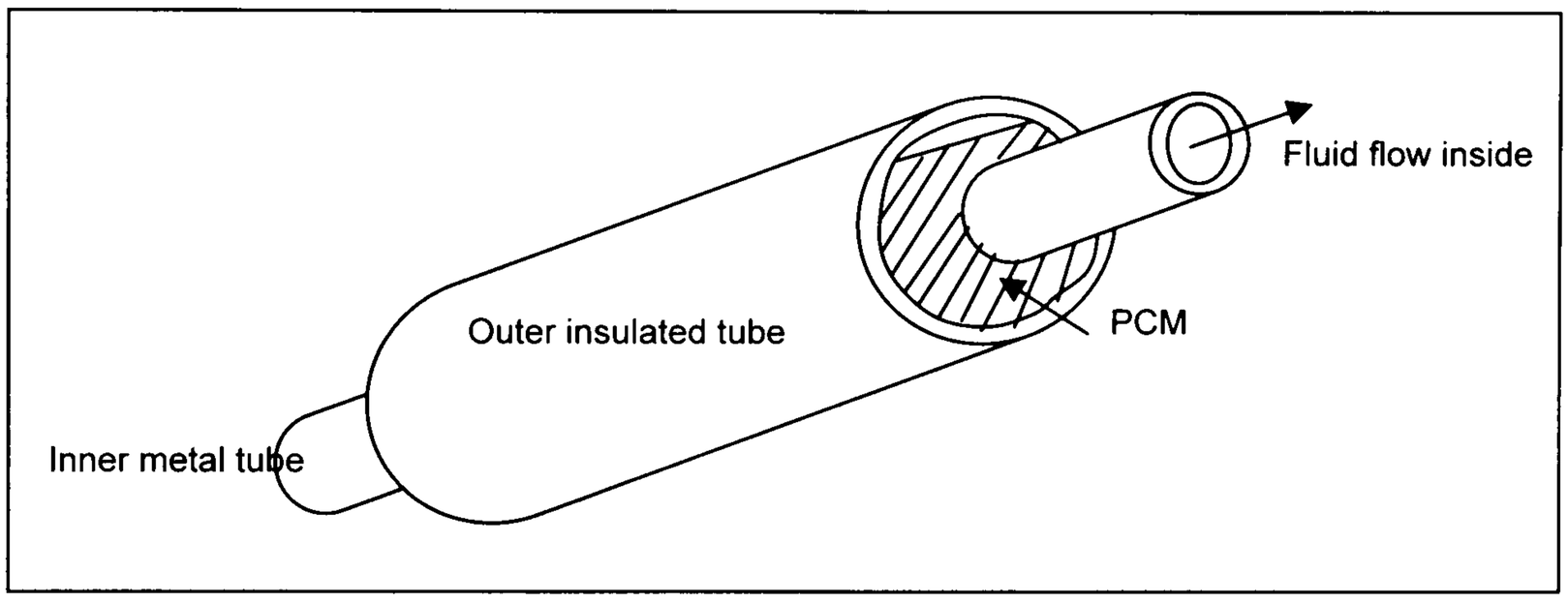

Figure 3.6: A tube in tube container for phase change materials

Latent heat storage systems using the beam PCMs have attracted more attention in recent years. An interesting technique of using multiple PCMs in a tube container is developed by Zhen-Xiang (1995). He proposes a novel thermal energy storage using a tube surrounded by an external coaxial cylinder of multiple phase change materials with different melting points (Figure 3.7). A hot or cold fluid flows through the inner tube to charge or discharge thermal energy. An experiment has been carried out to investigate heating performances of using multiple PCMs over a single PCM with high temperature (500-900°C). He concludes that charge-discharge rates of thermal energy can be greatly enhanced by using multiple PCMs with different melting points in comparison with a single PCM. Furthermore, a

fluctuation of an outlet temperature of the working fluid is found to be significantly reduced.

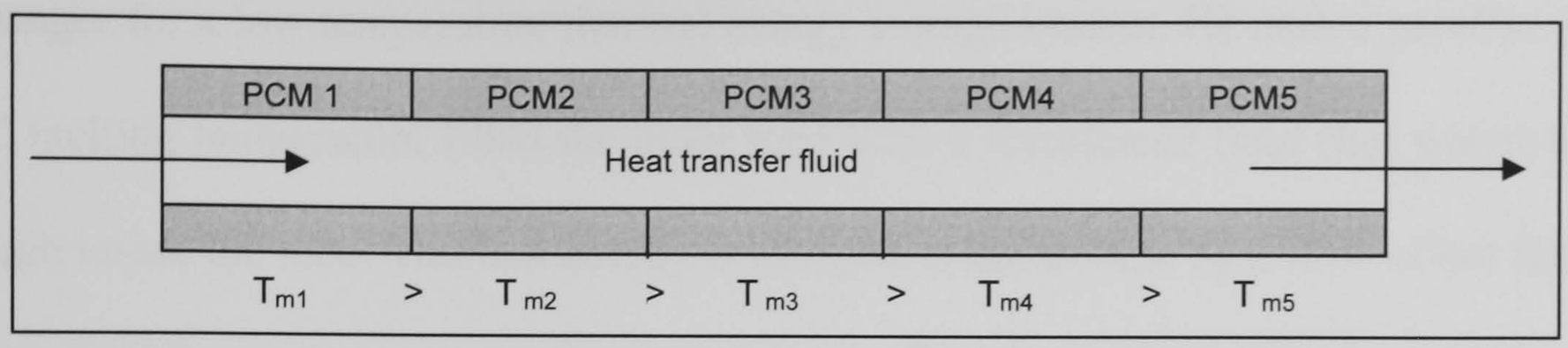

Figure 3.7: Physical model of a coaxial cylinder made up of several segments for different PCMs with different melting points (Zhen-Xiang, 1995)

3.7 PCM heat exchangers

One major problem for any latent heat thermal storage applications is that most PCMs with high energy storage density have an unacceptably low thermal conductivity (Velraj, 1997). Hence, heat transfer enhancement techniques are required. Heat exchangers play a major part in the latent heat storage system as they are used for transferring heat from a heat source to a heat storage substance and from the latter to a heat sink. Types of heat exchanging surface rule a design of a thermal storage system because it influences temperature gradients for charging and discharging of the storage. Heat exchangers can be classified by (i) flow arrangements, (ii) construction type, (iii) heat transfer mechanisms, (vi) surface density and (v) whether or not the fluids are in contact (white, 1991). The first two are the most common classifications. Several types of heat exchangers have been investigated to enhance heat transfer for the latent heat storage as reviewed below.

3.7.1 Double pipe heat exchangers

Hassan, F. (1991) investigates the performance of heat transfer in a double pipe heat exchanger for a low temperature thermal energy storage system. He uses a paraffin wax of 50°C melting temperature filled the outer tube with a transferred fluid (hot water) flowed through inside the tube. Thermal energy is charged to the storage by a flow of hot fluid and a cold fluid is used to extract the stored heat. Results indicate that increasing a heat exchanger length as well as a flow rate increases the heat transfer rate and accumulates stored energy. However, it is expected that there will be a limit of tube length after which it will have no effect. This limit occurs when an average fluid temperature approaches a PCM melting temperature. His further study in 1998 shows that most PCMs, especially in solid phase, exhibit insulating characteristics, thus creating a problem for the heat retrieval cycle. This problem can be eliminated by using metallic extended surfaces with bare heat carrying tubes or heat pipes.

To improve a charge/discharge capacity of a latent heat storage system several types of finned tubes with different configurations have been studied (Morcos, 1990), (Sadasuke, 1991), (Choi, 1994), (Zhang, 1996) and (Costa, 1998). Results reveal that heat flux for a finned tube is much improved comparing to that of a bare tube. A study by Choi (1994) shows that heat transfer coefficients in the unfinned-tube are in ranges of 40-170 W/m^2 whereas the finned tubes performs better with 80-320 W/m^2.

3.7.2 Shell-and-tube heat exchangers

Kamimoto (1986) develops a latent heat storage unit of 30 kWh using high density polyethylene (HDPE) rods for solar thermal applications. A direct contact heat transfer technique between HDPE rods and ethylene glycol is adopted. Their design shows that a hot fluid is introduced into a heat exchanger from a top end during an energy charge process. During a discharge process, a cold fluid is circulated from a bottom end. In 1993, Conti numerically simulates cyclic thermal processes in a shell and tube latent storage system. In his design, the hot and cold fluids are introduced from the same end of the heat exchanger for the successive charge and discharge processes. No explanation from both studies is given as to why such the operation mode is adopted and which one is better? To answer the question, Gong (1997) develops a finite element model to simulate the cyclic thermal process occurring in a shell and tube latent heat exchanger. The heat exchanger consisted of a tube which is surrounded by an external coaxial cylinder made up of a PCM. A working fluid flowed through the tube to store or extract thermal energy from the PCM. Numerical experiments indicate that introducing the hot and cold fluid from the same end of the storage exchanger is more desirable than introducing the hot and cold fluid from different ends of the storage exchanger.

Another parametric study is conducted by Conti (1996) to compare two different schemes of connection of a storage element to a heat engine, considering series and parallel set up. He addresses the thermodynamics and performance of heat storage using a PCM shell and tube heat exchanger, in which a solar power plant is provided to damp pulsed behavior of a heat source. Results show that a latent-heat thermal storage device, driven by a liquid metal heat transfer fluid, is more effective if used in parallel connection.

3.7.3 Direct contact heat transfer

Because most solid phase change materials usually have low thermal conductivity, therefore, during the discharging process, high thermal resistance occurs. To improve the performance of a rate of heat transfer, a technique of direct contact heat transfer (between a aqueous crystallizing solution and an immiscible heat transfer fluid) has been proposed by Sideman (1967). The essence of this technique is that a fluid (lower in density and immiscible with the aqueous salt solution) is entered at the bottom of the storage vessel as a dispersed phase (Figure 3.8). As bubbles of this fluid rise through a vessel, they transfer heat to or from the salt solution, and also agitate the vessel contents. The heat transfer fluid is pumped through the remainder of the primary heat transfer loop.

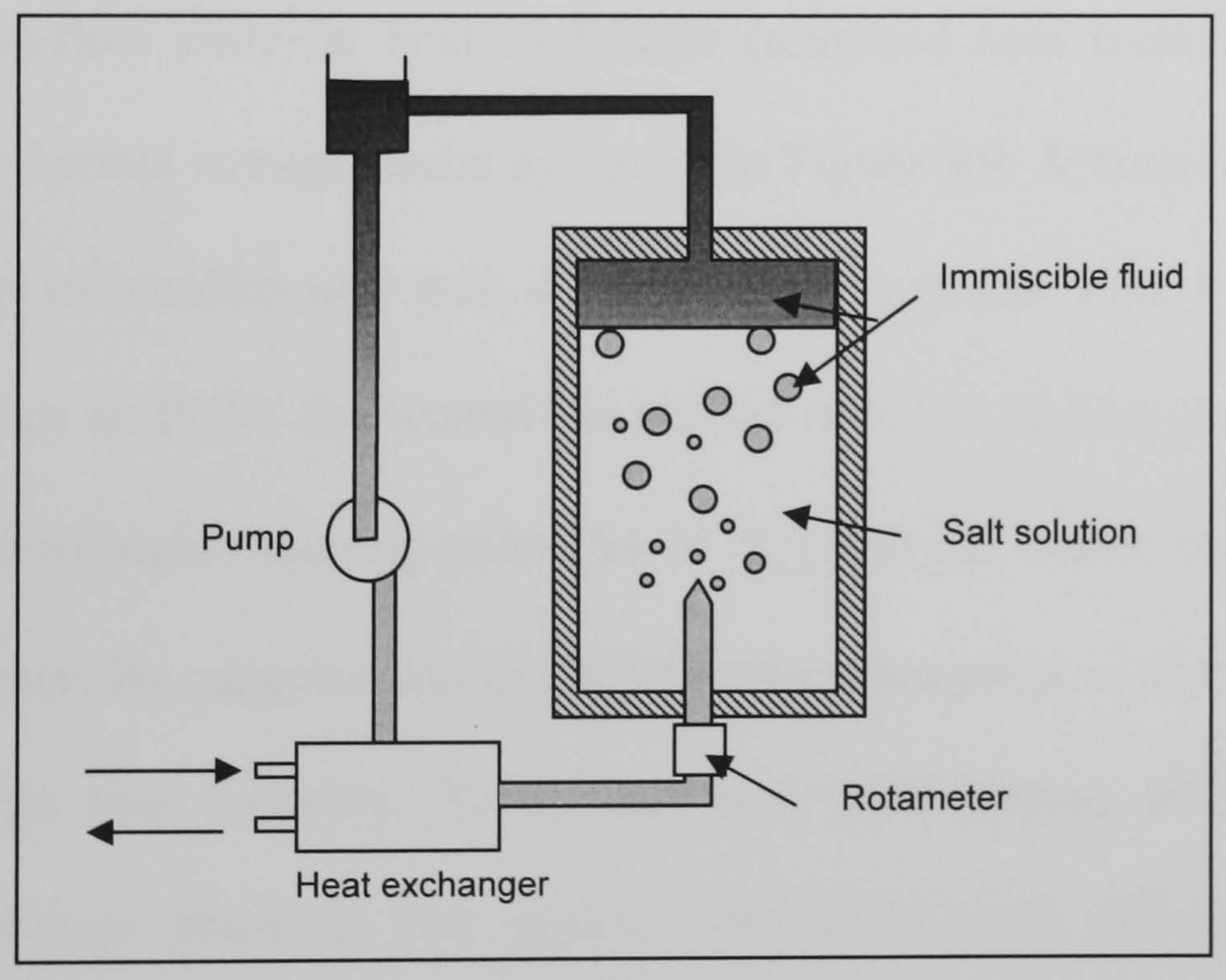

Figure 3.8: Immiscible fluid-Heat of fusion storage system (Burns, 1981)

Eddie (1981) compares the heat storage potential using various salt hydrate candidates (disodium phosphate, calcium chloride, sodium thiosulfate, sodium carbonate and calcium nitrate) for direct contact heat transfer. A light hydrocarbon, Varsol, is used as a heat transfer fluid. He concludes that sodium carbonate is unacceptable due to its nucleation

difficulty whereas calcium nitrate is ruled out because of excessive carryover. His further experiment, an investigation on the effect of system geometry to the rate of heat transfer, shows that doubling a column height increases storage efficiency by 6 to 17% depending on the salt used. Recently, many studies have shown that several salt hydrates perform satisfactorily (Shahidi,1995), (Fossa, 1995) and (Kiatsiriroat, 2000) .

3.7.4 Plate-fin heat exchangers

To smooth out intermittent supply of energy, Okada (1988) proposes a plate fin heat exchanger integrating n-octadecane PCM. This provided a desirable performance for the heat exchanger. In 1995, Okada carries on further work to investigate the performance of a single-pass cross-flow plate-fin heat exchanger (unmixed heat transfer fluid, air) using paraffin wax as thermal storage media as shown in Figure 3.9. A novel idea of his study is to use two kinds of paraffin wax with different melting points. Four heat exchangers are tested; the first has no PCM, the second has a PCM of lower melting point (38-47 °C), the third has a PCM of higher melting point (54-74 °C), and the fourth has both kind of wax distributed in space. He suggests that the PCM heat exchanger is useful for continuous and intermittent waste heat recovery. To achieve best performance, all PCMs in the heat storage must change phase in one period. The PCM with different melting points (distributed according to the temperature distribution of the heat exchanger) performs well under a wide range of operating conditions.

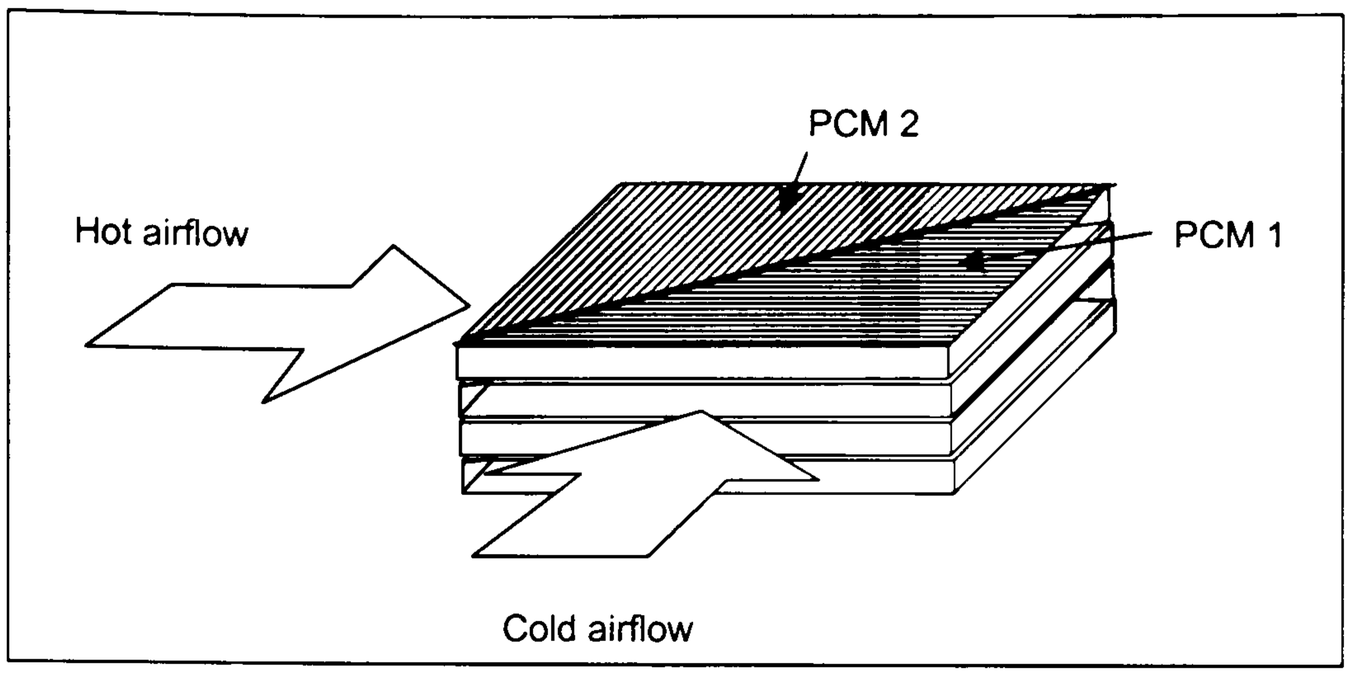

Figure 3.9: Distribution of the higher and lower melting point PCMs in the plate-fin heat exchanger (Okada, 1995)

3.8 Basic concept of thermodynamics for latent heat storage

A following review on basic thermodynamic for latent heat storage is based on studies of Hariri (1988) and Yunus (1989).A substance can exist at three different phases, liquid, solid and vapour. The three phases may exist together in equilibrium but the two phases are more common. Figure 3.10 shows the pressure-temperature diagram of a pure substance, called phase diagram (three phases are separated from each other by three lines). Along the sublimation line the solid and vapour phases exist in equilibrium, along the fusion (or melting) line the solid and liquid phases exists in equilibrium and along the vaporisation line the liquid and vapour phase are in equilibrium. These three lines meet at the triple point, where all three phases coexist in equilibrium. The vaporisation line ends at the critical point because no distinction can be made between liquid and vapour phases above the critical point.

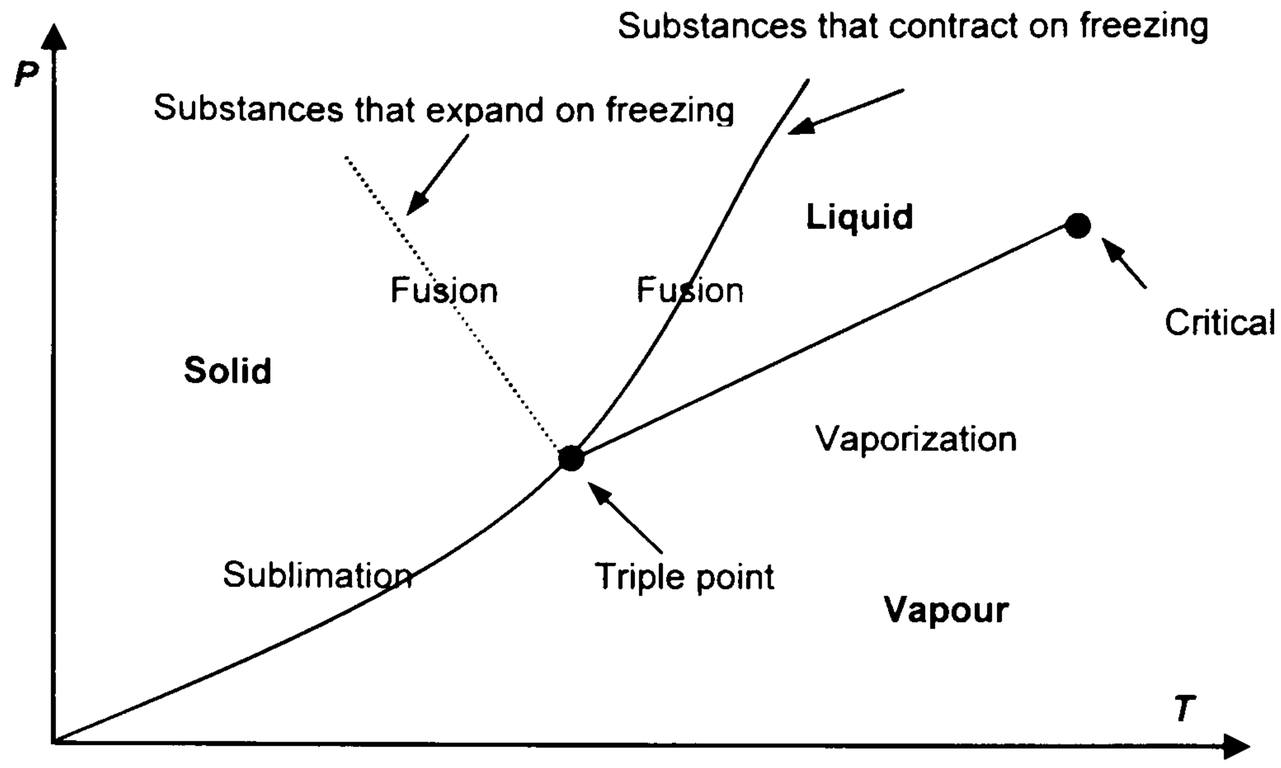

Figure 3.10: Pressure-temperature diagram of pure substances (Yunus, 1989)

Under equilibrium condition two phases of the same substances exist at the specified temperature and pressure. Enthalpy, entropy and Gibbs function (an indication of the amount of energy in a system) are three thermodynamic extensive (mass dependent) properties of a matter. The Gibbs function difference is the driving force for phase change, just as the temperature difference is the driving force for heat transfer. "...the two phases of a pure substance are in equilibrium when each phase has the same value of specific Gibbs function" (Yunus, 1989). This is due to having the two phases at the same pressure and temperature. This fact is relevant to different solid phases of a pure substance and is important in metallurgical applications of thermodynamics. It can be expressed as:

$$G = H\text{-}TS \qquad (3.1)$$

where H is enthalpy in energy, T is temperature and S is entropy in energy.

Clapeyron equation is another important thermodynamics relation for understanding a phase change process. It involves the saturation pressure and temperature, the change of enthalpy associated with a change of phase and the specific volume of the two phases. During a phase change process, the pressure is the saturation pressure, which depends on

the temperature only and is independent of the volume. Consider the third Maxwell relation:

$$\frac{dP}{dT} = \frac{\Delta S}{\Delta V} \qquad (3.2)$$

where dP/dT is the slope of the pressure-temperature diagram which is independent of the volume, ΔS the entropy change and ΔV the volume change for the phase transition. By substituting entropy with the latent heat of the phase transition ΔH divided by the temperature T at which the change is occurring, we obtain:

$$\frac{dP}{dT} = \frac{\Delta H}{T\Delta V} \qquad (3.3)$$

This is called the Clapeyron equation which applies to any change of state: fusion, vaporisation, sublimation and changes between crystallisation forms. This is an important thermodynamic relationship, since it enables us to determine the enthalpy of vaporisation at a given temperature by simply measuring the slope of the saturation curve on a P-T diagram and the specific volume of saturated liquid and saturated vapour at the given temperature.

The total amount of heat stored by a substance in a solid phase when the temperature is increased from T_s to the temperature of boiling T_b via the temperature of fusion T_f can be expressed as:

$$Q = n\int_{T_s}^{T_f} C_{ps}dT + n\Delta H_f + n\int_{T_f}^{T_b} C_{pl}dT + n\Delta H_v \qquad (3.4)$$

where n is the quantity of the material in moles, C_{ps} and C_{pl} the molar heat capacity at constant pressure of the solid and liquid phases (sensible heat), respectively, ΔH_f the enthalpy of fusion, and ΔH_v the enthalpy of vaporisation. The second and fourth terms

indicate the amount of heat involved in the phase change at the points of melting and boiling, respectively.

Figure 3.11 shows the change in enthalpy according to the transition temperature. The enthalpy H has an infinite slope at the fusion temperature, T_f, and this kind of phenomena called 'first order phase transition'. It has the implication that the heat capacity, C_p (defined as the gradient of enthalpy with respect to temperature), becomes also infinite. The physical reason for this is the addition of heat to a system at its first order transition temperature is used in pushing the transition rather than in changing the temperature of the system. It follows that a first order transition may be characterised by an infinite heat capacity at the transition point. This is the reason why phase change materials are attractive as heat storage media.

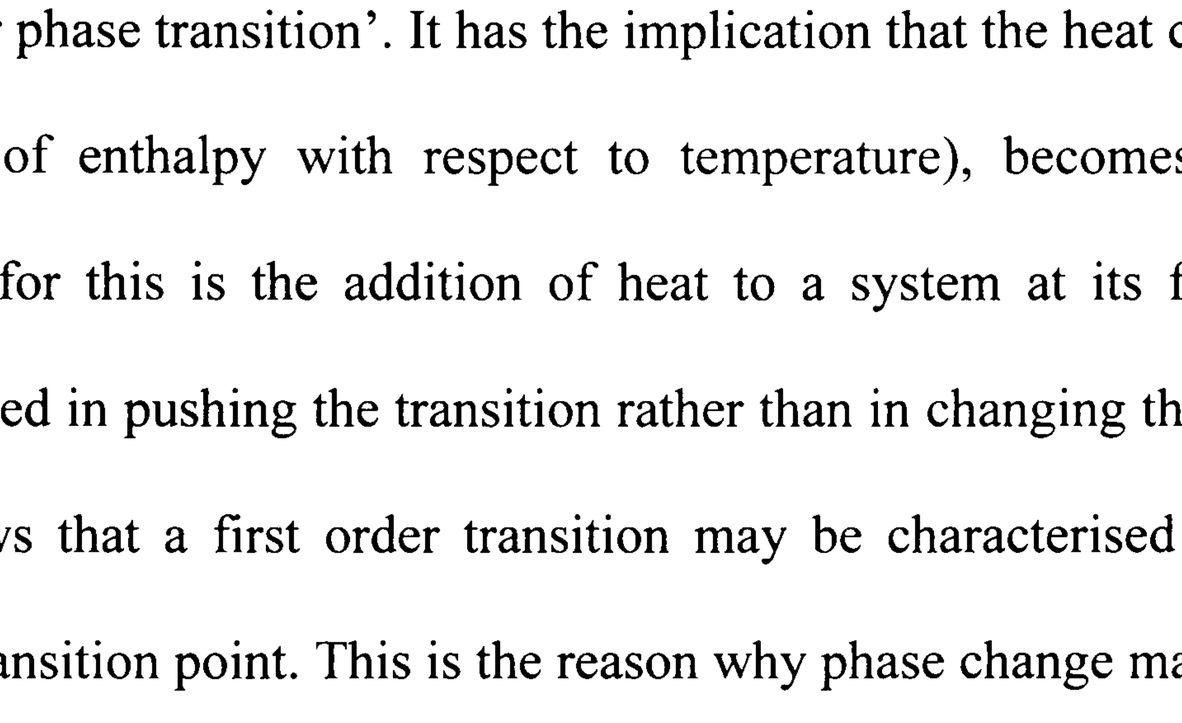

Figure 3.11: Change in enthalpy at transition temperature (Hariri, 1988)

3.9 PCM applications

Table 3.8 categorises PCM energy storage applications. These applications can be divided into two groups, thermal inertia and thermal storage. A difference between these two relates to thermal conductivity of a substance. Zelba (2003) points out that in the case of

thermal inertia it is appropriate to have low conductivity values, while in thermal storage such low values can produce a real problem since there can be sufficient energy stored but insufficient capacity to dispose of this energy quickly enough. Some interesting techniques using PCMs as heat storage applications for space heating or cooling and water heating for residential demand are presented below.

Application
▪ Thermal storage of solar energy
▪ Passive storage in bioclimatic building/ architecture (HDPE + paraffin)
▪ Cooling: use of off-peak rates and reduction of installed power, ice-bank
▪ Heating and sanitary hot water: using off-peak rate and adapting unloading curves
▪ Safety: temperature maintenance in rooms with computers or electrical appliances
▪ Thermal protection of food: transport, hotel trade, ice-cream, etc.
▪ Food agro industry, wine, milk products (absorbing, peaks in demand), greenhouses
▪ Thermal protection of electronic devices (integrated in the appliance)
▪ Medical applications: transport of blood, operating tables, hot-cold therapies
▪ Cooling of engines (electric and combustion)
▪ Thermal comfort in vehicles
▪ Softening of exothermic temperature peaks in chemical reactions
▪ Spacecraft thermal systems
▪ Solar power plants

Table 3.8: Applications using PCM for thermal energy storage (Zelba, 2003)

3.9.1 Heat pipes embedded in PCMs

Heat pipes have been used for a wide variety of applications, such as solar energy collectors and waste heat recovery. Hepp (1976) proposes a solar energy storage system with a heat pipe condenser embedded in a PCM jacket, and an evaporator connected to a solar collector. During the day, the PCM melts and stores latent heat as a source for water heating. Two years later, Abhat (1978) developes a design of a heat exchanger using a series of axial fins to enhance heat transfer from a heat pipe to the PCM.

Heat pipes discussed above are irreversible showing that the evaporator was always at the same end. Turnpenny (1999) outlines a novel night ventilation system using a PCM embedded in heat pipes which are reversible for space cooling. Heat is transferred to the PCM and melts it during the day enabling the lower room temperature. At night, heat is extracted from the melted PCM by drawing cool air from outside over the heat pipes. Therefore, the evaporator end becomes the condenser. This new developing technique avoids the need for complex heat exchange geometry on the PCM surface exposed to the air.

3.9.2 PCMs in greenhouses

An investigation of PCM containers buried underground for greenhouses is carried out by Jaffrin *et al* (1987) (see Figure 3.12). The containers are placed in concrete shelves with five layers in semi-circular tunnels contained calcium chloride hexa hydrate. Heat is transferred by passing air through the units. He points out that a possible energy saving of 80% can be achieved in comparison with conventional greenhouses and of 60% compared to double-covered greenhouses.

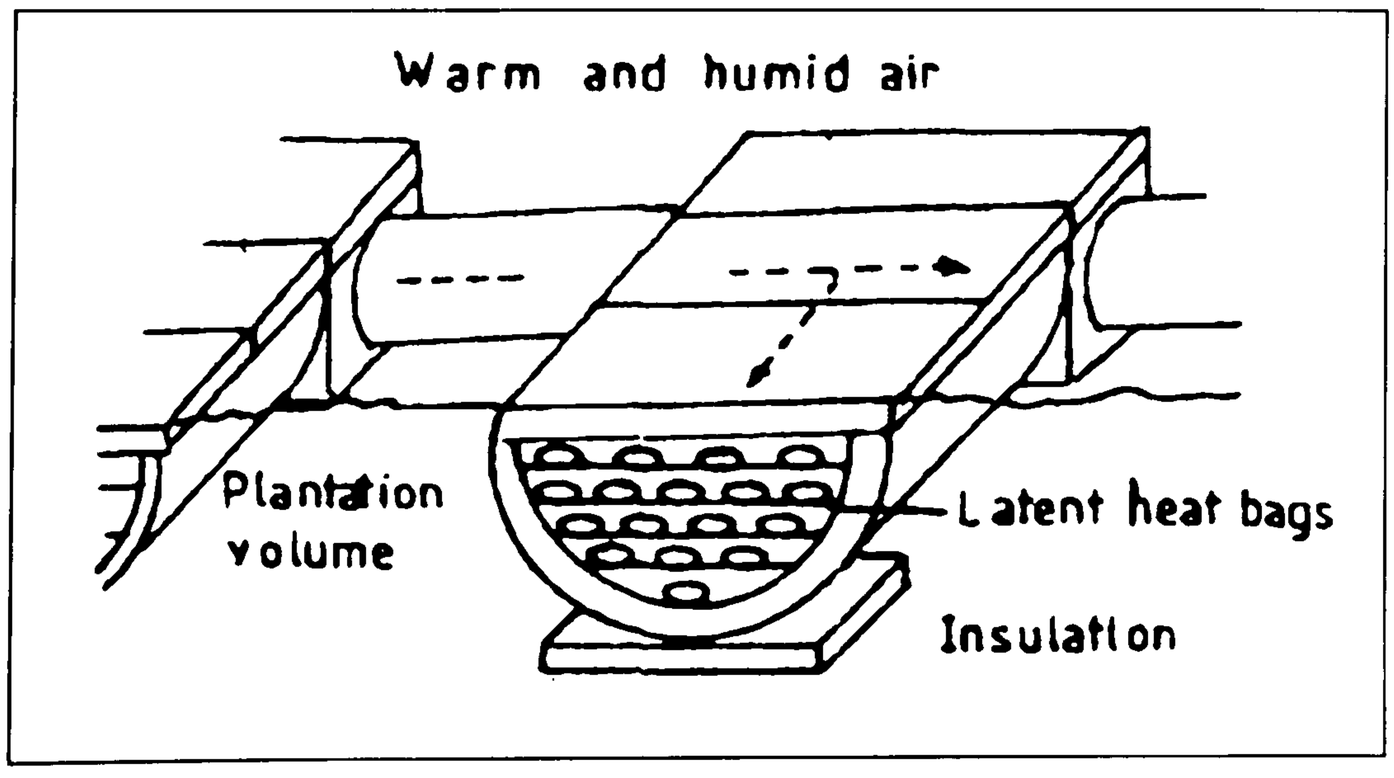

Figure 3.12: Arrangement of the PCM containers underground (Jaffrin, 1987)

Kurklu (1998) reviews the use of PCMs for energy saving and management in greenhouses. An investigation is carried out by classified PCMs in three most used groups based on salt hydrates, paraffins and polyethylene glycol. Figure 3.13 shows an example of energy storage units of the greenhouses. Applications can be integrated into inside and outside of the greenhouses. While the energy storage unit inside the greenhouse collected warm air from the ridge of the greenhouse during the day time, the direction of air flow is reversed for the energy releasing process at night. For the outside unit, this one also reverses the air flow during energy withdrawal from the store. Results from the study indicates that while the external unit releases about 80-90% of the energy absorbed, this is 60-80% for the internal energy storage unit.

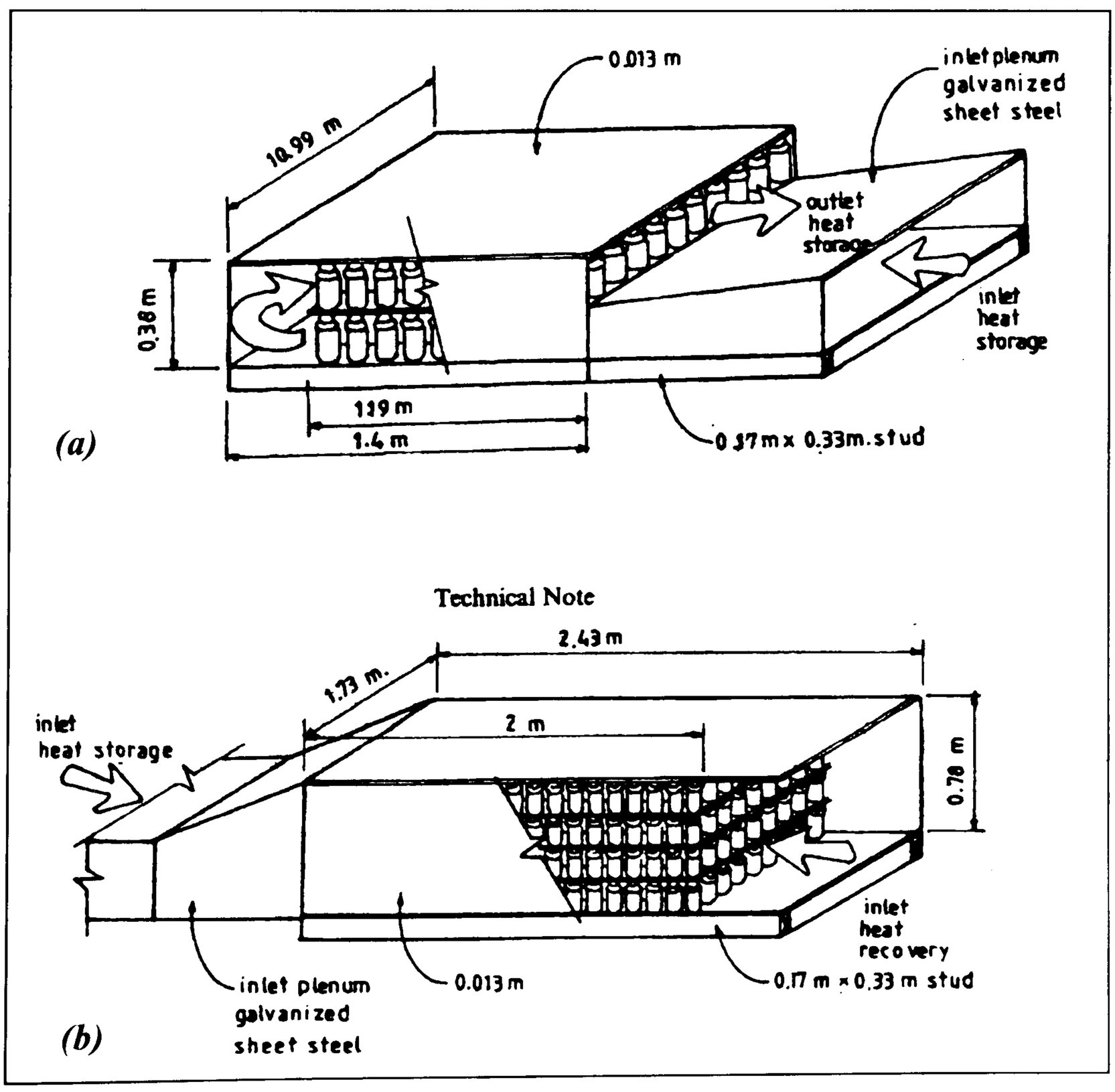

Figure 3.13: Energy storage unit (a) inside and (b) outside the greenhouse (Kurklu, 1998)

3.9.3 PCMs floor heating

Parts of a building structure can be used as a heat store and emitter. Austen (1990) suggests if a building surface is to be used for the emission of heat, then the thermal comfort of occupants in correlation to the surface temperature must be considered. This is especially for floor heating where actual physical contact between occupant and surface will take place. It is noted that for floor warming the temperature should not exceed 26-27°C.

In sensible heat storage applications, an ability to release the energy stored diminishes as the temperature of the store reduces. On the other hand, raising the temperature stored to overcome the problem extends a consequence of overheating. There are mainly two benefits of using latent heat storage systems. Firstly, storage capacity is greatly enhanced and, secondly, the rate of heat transferred occurred at near constant temperature.

Figure 3.14 shows a basic configuration of floor PCM. PCM must be hermetically sealed against contamination. This also gives advantages on good heat exchanger and suitable requirements of floor warming application. A conically shaped capsule is recommended by Austen (1990) with its high surface area for the quantity of PCM contained. Normally, a number of conically PCM is installed together with heating elements. It may be laid above a layer of insulation or directly on to a floor slab where the insulation is below over site concrete. A latent heat capacity of 400-550 Wh/m^2 can be achieved.

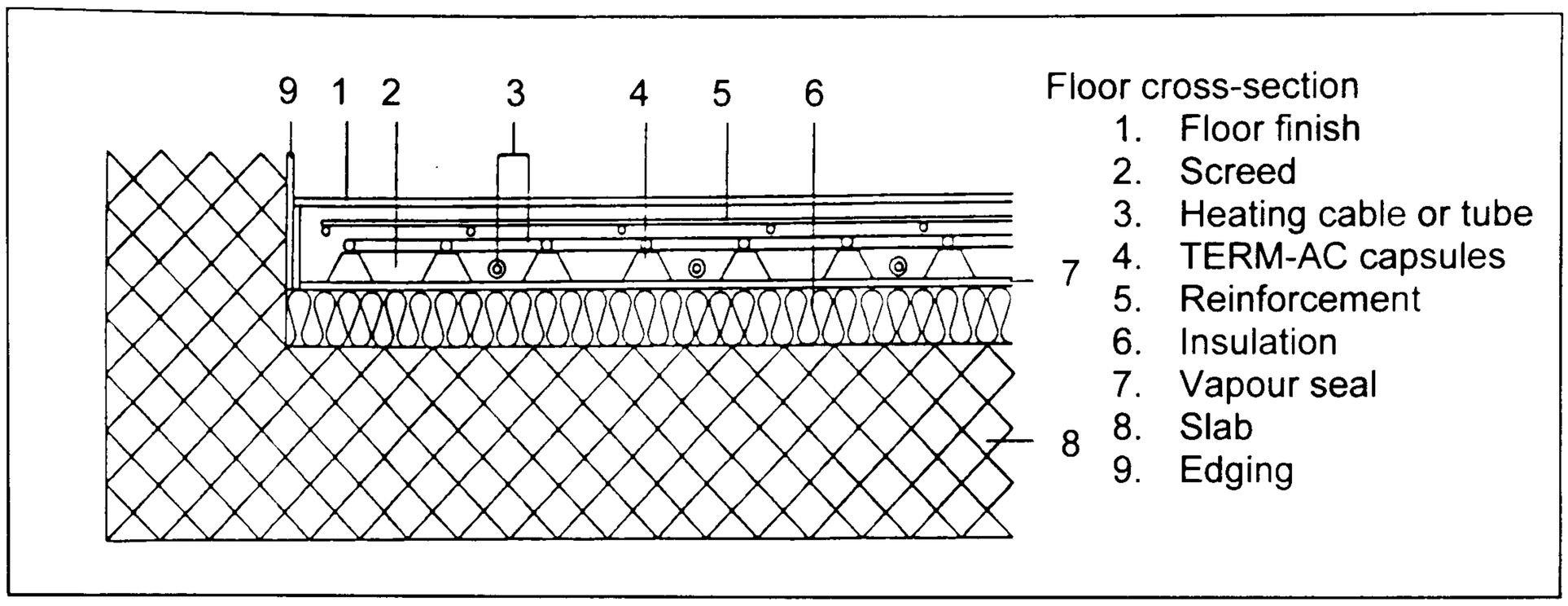

Figure 3.14: Cross-section through PCM floor heating system (Austen, 1990)

In achieving a sense comfort, ideal temperatures are considered to be 24°C at floor level and 19°C at head level. Figure 3.15 shows how floor warming approach to these conditions. This is because of its latent heat released at constant temperature. During the charge period, the slab temperature needs to be about 29°C in order to sustain the ideal surface temperature of 24°C. Energy will be absorbed by the PCM as fusion into the liquid state takes place. During the discharge period energy will be released from the capsules for warming purposes as crystallisation of the PCM into the solid state takes place. This process will continue at constant temperature until the capsules are fully discharged or charging recommences. Austen (1990) compares the thermal performance and payback period of floor warming systems of with and without PCM storage. It is found that the floor system using PCM storage increases the heating capacity over the conventional floor system by six times.

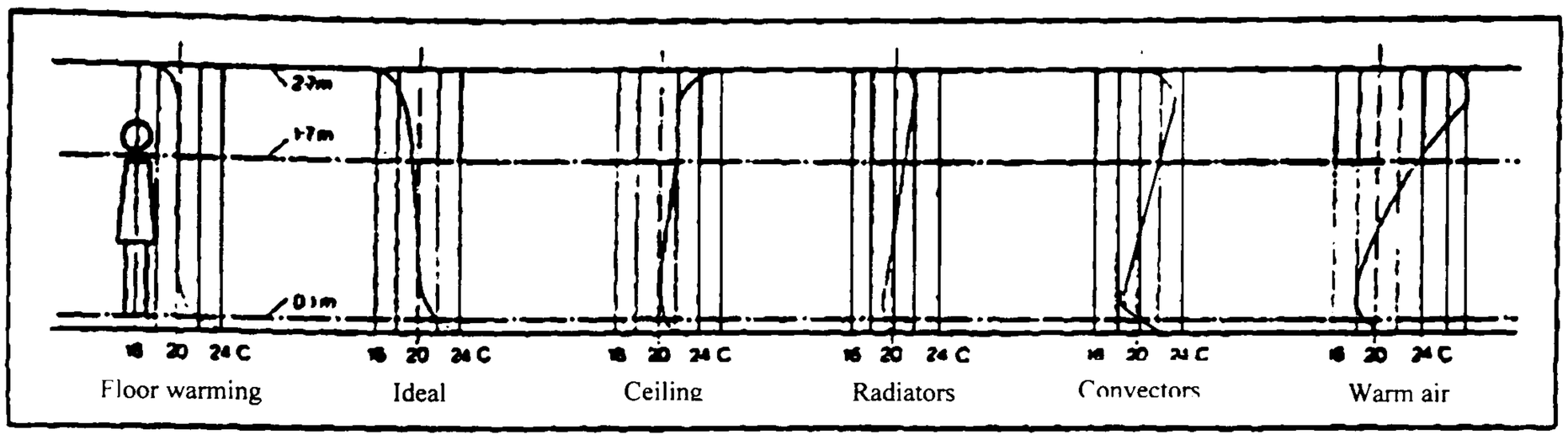

Figure 3.15: Temperature gradients for various heating methods (Austen, 1990)

An investigation of heat storage-type floor heating using a heat pump driven with nighttime electricity, as the heat source, is carried out by Yamaguchi (1997). The PCM is a package of mirabilite ($Na_2SO_4 10H_2O$) with the melting and freezing point of 32°C and 30°C, respectively. A wet film-type vertical heat extracting tube with a built-in Freon flashing pump is introduced in order to extract heat necessity for 24hrs in 8-hrs operation. Results show that the amount of heat does not reach the goal of 4.5 kW and is approximately 2.5 kW. This is because an underground temperature during the tests is stable in the low temperature, -1°C and also the resistance to heat transfer underground is larger than expected, resulting in less heat extracted.

3.9.4 Space heating by PCMs

In passive solar design, PCMs are potentially very attractive because they offer a possibility of lightweight thermal storage with minimal over heating. For these purposes, PCMs are being offered with phase change temperature varying from 21°C to 27°C. It might be expected that high phase change temperatures (27°C) can lead to overheating and a consequent discomfort. Low phase change temperatures (21°C) may require

impractically large or expensive surface areas of storage in order to produce sufficient heat transfer between storage and building interior.

Carter (1981) investigates an effect of phase change temperature of 21°C and 27°C on an efficiency of phase change storage in passive solar homes. He concludes that the 27°C material requires a high fraction of the solar input to go directly into the storage in order to avoid overheating. The 21°C material generally performs better, but in cold climates it might be difficult to obtain sufficient natural heat transfer between the store and the building interior to maintain acceptable temperatures from solar heat alone. He suggests that a phase change temperature slightly higher than 21°C could be used to solve this problem.

Dubois (1983) studies a water space heating system using paraffin wax as latent heat storage supplied by a heat pump. An energy use for space heating could be reduced by shifting electricity consumption from higher to lower tariff hours.

3.9.5 Wall PCMs

Studies have shown the use of an absorption of phase change materials into commonly used building materials. The use of carboxylic acids makes it possible to achieve considerable increases in capacity. However, the drawback of carboxylic acids is their liquidity which in practice means that the building materials must be coated in one way or another after their absorption. The simplest way to incorporate the PCM into the building materials is by immersion the building materials into the hot PCM which absorbed into the pores by capillary suction. Another technique is to use a water solution of the PCM to be

absorbed into the building materials at room temperature and when the water evaporates, the PCM remains in the materials.

Feldman (1991) examines the feasibility of incorporating a typical PCM in the early stage of gypsum wallboard production and to characterize the obtained energy storing wallboard obtained thereby. The butyl stearate, BS, is chosen as a heat storage material because it meets the thermodynamic and kinetic criteria for low temperature heat storage. BS consisted of 49% butyl stearate and 48% butyl palmitate is incorporated into wallboard by immersion technique. The freeze-thaw cycling tests are carried out in a chamber for a period of 100 cycles. It is shown that there are no apparent physical changes such as deterioration of the matrix, cracking, blistering or spotting of the paint and peeling of the paperboard after 100 cycles. For a rise of 4°C through the melting range of PCM, $1m^2$ of energy storing wallboard with BS had a total thermal storage capacity of 370kJ. This capacity is computed by adding the sensible heat capacity of gypsum alone (33kJ) with the sensible heat capacity of BS (16kJ) and the latent heat capacity of BS (321kJ).

Kaasinen (1991) carries out an experiment using PCMs absorbed into ordinary building materials, namely, gypsum board, wood-particle board, porous wallboard, timber (pine), cellular concrete, brick, concrete and sand-lime brick. Carboxylic acids and polyalcohols are used as latent heat storage materials. It is indicated that in comparison with storage capacities of untreated building materials the largest increase occurs in the porous wallboard by a factor of 4.5. The increases in capacity of concrete, gypsum board and brick are almost non-existent.

Stritih (1996) proposes a solar wall that absorbs solar energy into a PCM. Black paraffin wax is used as storage medium and stores heat for heating air for ventilation of a house. The wall construction operates on following principles. Short-wave solar radiation passes through glass with transparent insulation material (TIM), which prevents convective and short wave radiation heat transfer. Heat is absorbed and stored into the paraffin wax as latent heat. Air is heated as it passes thorough a channel (between the paraffin wax and the TIM) and lead into a room. Results show that thickness of a panel dictated an amount of stored heat. An analysis for a heating season gives an optimum thickness of 50mm and a melting point a few degrees above the room temperature. An efficiency of the proposed wall is 45% on average.

Ismail (1997) experimentally studies the performance of thermal insulation using PCM (glycol wax) incorporated into walls and roofs under real operational conditions for achieving passive thermal comfort. An experimental setup consists of a small room with PCM enclosed between two walls. Comparative tests are made between with and with out PCM enclosed. Results indicate that the thickness of the PCM layer is an important factor in shielding the external heat flux. For example, an indoor temperature does not change and remains constant around 23°C when the PCM gap is increased from 20mm to 40mm. In the case of the PCM wall/ceiling, the internal temperature seems to be unaffected by variations in the external temperature until the PCM layer is totally in the liquid phase. After this condition occurs, the increase in the external temperature leads to a corresponding increase in the PCM and the indoor wall temperatures. Furthermore, he reports that the use of PCM embedded in walls and roofs as a thermal barrier shows its potential and effectiveness in maintaining comfort temperature resulting in a reduction in the necessary installed capacity of air-conditioning units.

3.10 Conclusions

Latent heat storage system is a technique of storing heat by a transition of phase from solid to liquid or from liquid to vapour of a substance with no change in temperature. Nowadays this technique has received a great deal of interest due to the high energy storage capacity of phase change materials. However, a number of problems still remains to be tackled, including phase separation and supercooling, before economically and technically favorable latent heat energy storage systems can be made available for widespread use.

The two most common groups of phase change materials (PCMs) are organic and inorganic compounds. Most of the organic group are chemically stable (exhibit little or no supercooling) and non-corrosive. They have a high latent heat per unit weight and low vapour pressure and are compatible with most building materials. Their main disadvantages are flammability, high changes in volume on phase transition and low thermal conductivity. In comparison to organic compounds, inorganic PCMs exhibit a higher latent heat per unit volume and high thermal conductivity. They are lower in cost and are non-flammable. However, the major drawbacks are corrosion to most metals and suffering from supercooling and decomposition that can affect their phase change properties. Thus, in the applications of inorganic PCMs the use of nucleating and thickening agents to minimize supercooling and phase segregation are recommended.

Over a few decades a wide range of applications using PCMs in heat storage systems have been studied. Significant efforts in which the PCMs can be applied, for heating and cooling buildings, are such as PCM embedded into buildings materials including wall, floor or ceiling, an integration of PCMs in heat pipes, PCMs in greenhouses, etc. These

applications can be very effective in shifting the heating and cooling load to off peak electricity periods. Yet, many more applications are to be discovered.

Chapter 4 Thermal properties of microencapsulated phase change material slurry (MCPCM slurry)

4.1 Introduction

Previously, we see that latent energy storage is one of the key technologies for energy conservation and is of great practical importance. In this chapter another technique of utilising PCMs in energy storage and thermal control systems has been studied. In this approach, the PCM is microencapsulated and suspended in a heat transfer fluid to form a phase change slurry. In conventional thermal energy storage systems, many applications often operate by using the sensible heat of a single-phase working fluid (e.g. water, oil) which mostly requires high volumetric flow rate. Increasing convective heat transfer coefficient of a working fluid would permit the use of a smaller volumetric flow rate which reduces pumping power. A two-component slurry incorporated the latent heat of phase change particles is a useful medium to enhance both thermal energy storage and heat transportation. In the context, experimental investigations for viscosity and pressure loss of the slurries are presented. Measurements of thermal capacity of the novel slurries are performed using two techniques, standard differential scanning calorimeter (DSC) and thermal analysis (TA). Experimental results can be found in Appendix.

4.2 Background

Use of PCMs is becoming popular for many energy storage and thermal control systems for both high and low temperature applications. This is because the use of PCMs provides thermal energy storage from the latent heat associated with small temperature variation. Microencapsulation is a method used to obtain products with controlled release properties.

It is a process that allows isolating an active product from an external environment by forming microcapsules. Microencapsulated phase change material (MCPCM) is very attractive since the rate of heat transfer per unit volume to or from the material in particles is high and the ratio of surface area to volume of small particles is relatively large (Charunyakorn, 1991). In addition, encapsulating the PCM in small capsules can eliminate any segregation during phase change.

The use of MCPCM particles suspended in a single-phase working fluid would provide additional thermal capacity from the latent heat associated with the solid-liquid phase change. Although the latent heat of fusion is generally less than that of vaporisation and sublimation, the change in volume of phase change materials during fusion or solidification is usually very small. The slurry also serves as both the energy storage and heat transfer media, and the requirement of separate heat transfer media is therefore eliminated.

Over a few decades, many researchers have shown advantages and possible utilisation of MCPCM slurry. A study concerning the thermal use of MCPCM slurries is reported in 1979 by Mehalick and Tweedie. Since 1983 SBIR investigations for NASA have demonstrated the effective of this novel coolant in significantly enhancing the effective thermal capacitance allowing to minimising the weight and volume of a thermal storage in spacecraft. Kasza (1985) also reports that convective heat transfer coefficient of a working fluid is increased as the utilisation of MCPCM suspension. This is a result of increasing in the effective thermal conductivity and the effective thermal capacity. Chen (1987) carries out an analytical and experimental study on the augmentation of laminar flow heat transfer using a phase-change slurry. He shows that the convective heat transfer rate for a phase-

change slurry flow is proportional to the square root of the Reynolds, and inversely proportional to the cubic root of the Jakob number of the slurry. Charunyakorn (1991) develops a theoretical model describing the forced convection heat transfer with a phase change slurry in a circular duct flow and notices that the Nusselt number of the phase change slurry flow is 2-4 times higher than that of the single-phase flow. Recently more scientific papers have been published concerned with the feasibility of using MCPCM to enhance the convective heat transfer in a working fluid [Roy (1991, 1997), Colvin (1992), Goel (1994), Choi (1994) and Yamagishi (1996, 1999)].

4.3 Microencapsulated phase change material (MCPCM)

4.3.1 MCPCM particles

A new technique of utilising encapsulated PCM in energy storage has been developed. There are two principal means of encapsulation. The first one is macroencapsulation, which comprises the inclusion of PCM in some form of package such as tubes, pouches, spheres, panels or other receptacle. These containers can serve directly as heat exchangers or they can be incorporated in building products. The second containment method is microencapsulation, whereby small spherical particles are enclosed in a thin, high molecular weight polymeric film. The coated particles can then be incorporated in any matrix that is compatible with the encapsulating film. The film must be compatible with both the PCM and the matrix (Amar, 2003). Microencapsulation also allows the PCM to be incorporated into conventional construction materials. However, there are drawbacks, for instance, impregnating the MCPCM into concrete is found very effective, but it may affect the mechanical strength of the concrete (Fraunhofer, 2002).

Microencapsulation can be range in size from less than 1 μm to more than 300μm. The PCM in microcapsules can be selected to melt and freeze at desired temperatures. The surrounding shell encapsulates the melted core material and prevents it from mixing with the carrier fluid, contaminating sensitive materials, or depositing inside system components. Heat is absorbed as the PCM is melted and released upon freezing. The wall material of the capsule can be formulated by using a wide variety of materials including natural and synthetic polymers. Microencapsulation of phase change substance can be prepared by using two processes, complex coacervation and spray-drying method.

Benita (1996) and Hawlader (2003) showed that the complex coacervation method can be processed as following; typically, microencapsulation involved the use of more than one colloid. Ten percent of gelatine and acacia solutions are prepared with distilled water as coating materials. Then, paraffin wax is melted into the gelatine solution at 10,000 rpm with a homogenizer. Here, an acacia solution is added drop by drop with the temperature maintained at 65 °C throughout emulsification. The individual coacervated droplets attract and coalesce around core particles, which are immiscible in the system. Then, the temperature of solution is dropped to the room temperature and the coacervated particles separated out into new phases, rich and poor phases in colloid concentration. The final step is hardening and isolation of microcapsules. Cross-link agent is used for hardening process which takes about 16 hours. Then, the suspension is filtered, and the precipitate is soaked in absolute ethanol to get free flowing microcapsules before dried in a vacuum oven.

With spray drying method, emulsion of paraffin wax and the solutions of coating materials are prepared through a similar process to the coacervation method. Then, they are spray-dried in the cocurrent mode using a dryer with an inner chamber diameter of 1.6m.

Emulsions are atomised with a feed rate of 20ml/min by a centrifugal atomiser operated at 25,000rpm with the inlet and outlet temperature of 130 and 80°C, respectively. Finally, the microcapsules are collected at the bottom (Hawlader, 2003). Results obtained from a differential scanning calorimeter show that microcapsules of paraffin wax could be well prepared by both spray drying and complex coacervation methods and are suitable for a solar energy storage material. Microencapsulation efficiency also depends on the process parameters, for example, core-to-coating ratio, amount of crosslink agent and emulsifying time.

Properties desired in PCM micro spheres are similar to those necessary for a thermal energy storage system. Phase change particles used in the present study is paraffin wax. The advantages of microencapsulated paraffin wax are high latent heat of fusion, low vapor pressure in the melt, negligible supercooling, no phase segregation and commercial availability at reasonable cost. The *n*-eicosane paraffin waxes with melting points of around 28°C, 35 °C and 50°C are chosen in the research supplied by Frisby Technologies Inc. They are encapsulated in millions of durable capsules of 15 to 40 microns in diameter (see Figure 4.1). The microcapsule comprises of 80-85% of the material weight and has an impermeable shell wall of less than one micron. The paraffin wax is encapsulated in flexible and strong-thermoset plastic wall and has claimed by the manufacturer to pass through 150,000 cycle tests with minimal degradation under thermal and pressure operations. Table 4.1 shows the specifications of the MCPCM.

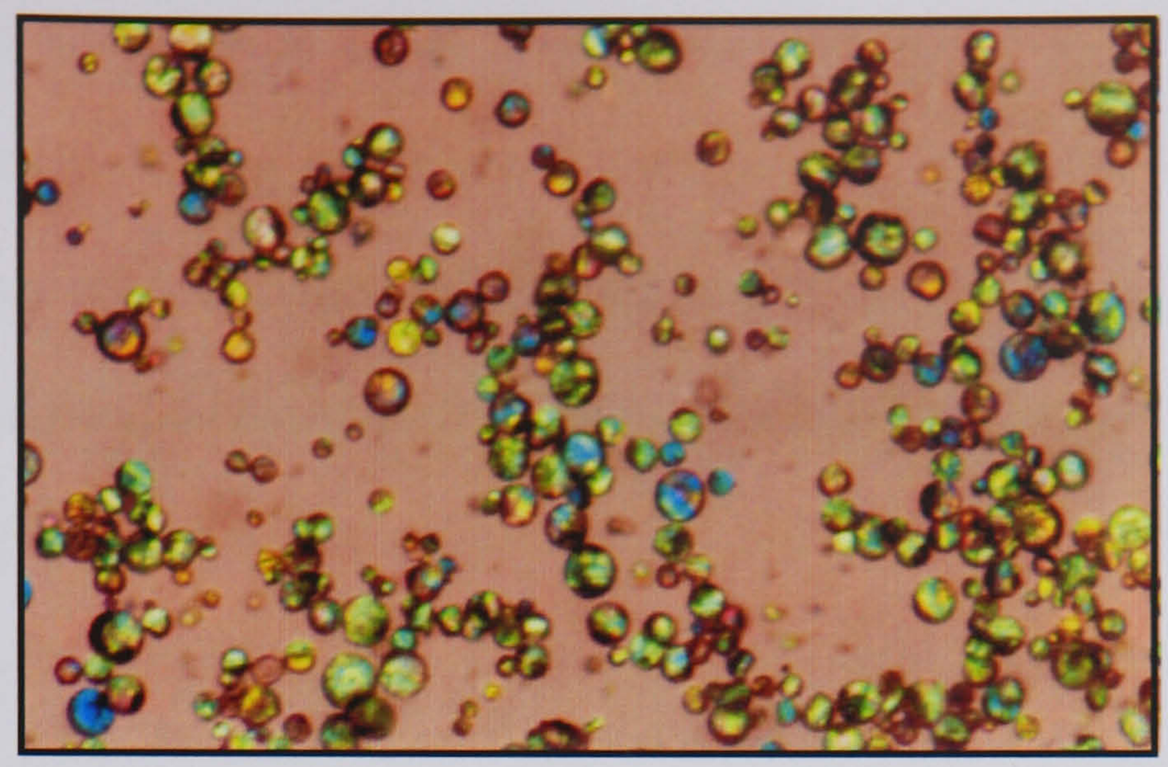

Figure 4.1: Photomicrograph of microencapsulated phase change material

	Paraffin Wax	Melting Temperature (°C)	Density (kg/m^3)	Specific Heat (kJ/kg°C)	Thermal conductivity (W/m°C)	Latent heat (kJ/kg)	Particle Size (microns)
1	*n*-eicosane	28	894	2.14	0.178	186	15-40
2	*n*-eicosane	35	899	2.13	0.179	180	15-40
3	*n*-eicosane	50	897	2.14	0.178	160	15-40

Table 4.1: Physical properties of the MCPCM particles with melting temperature of around 28°C, 35°C and 50°C (Frisby Technologies Inc., 2004)

4.3.2 MCPCM Slurry

In order to select a fluid as an energy transport medium, Goel (1994) notes that two main criteria have to be considered which are high thermal conductivity and high specific heat. However, as *n*-eicosane is selected as a heat storage medium in the phase change slurry, a selection of the working fluid is governed by another important factor that is its compatibility with *n*-eicosane and the wall of capsules. As a carrier fluid for the MCPCM, water can be used without any inconvenience. It is easy to handle, has low viscosity and no effect on the phase change material or the microcapsule wall. However, at temperature below 0°C, Yamagishi (1996) suggests using glycol solution or brines ($CaCl_2$ or NaCl).

Mixing the microencapsulated phase change particles and water is one of the most common operations for preparing the phase change slurry. The term 'mixing' is applied to a process used to reduce a degree of non-uniformity or gradient of a property such as concentration, viscosity, temperature and so on. Mixing the slurry can be done by moving material from one region to another. To promote a high rate of heat transfer, well mixing is required to achieve a desired degree of homogeneity. Thus, an electric stirrer was used to prepare the MCPCM slurry. However, after the homogeneity of MCPCM slurry has been achieved and the stirrer was turned off, phase separation caused by gravity or centrifugal force between the suspended particles and water could be observed within seven minutes. The capsules of PCM are lighter than water and generally float to the surface (see Figure 4.2).

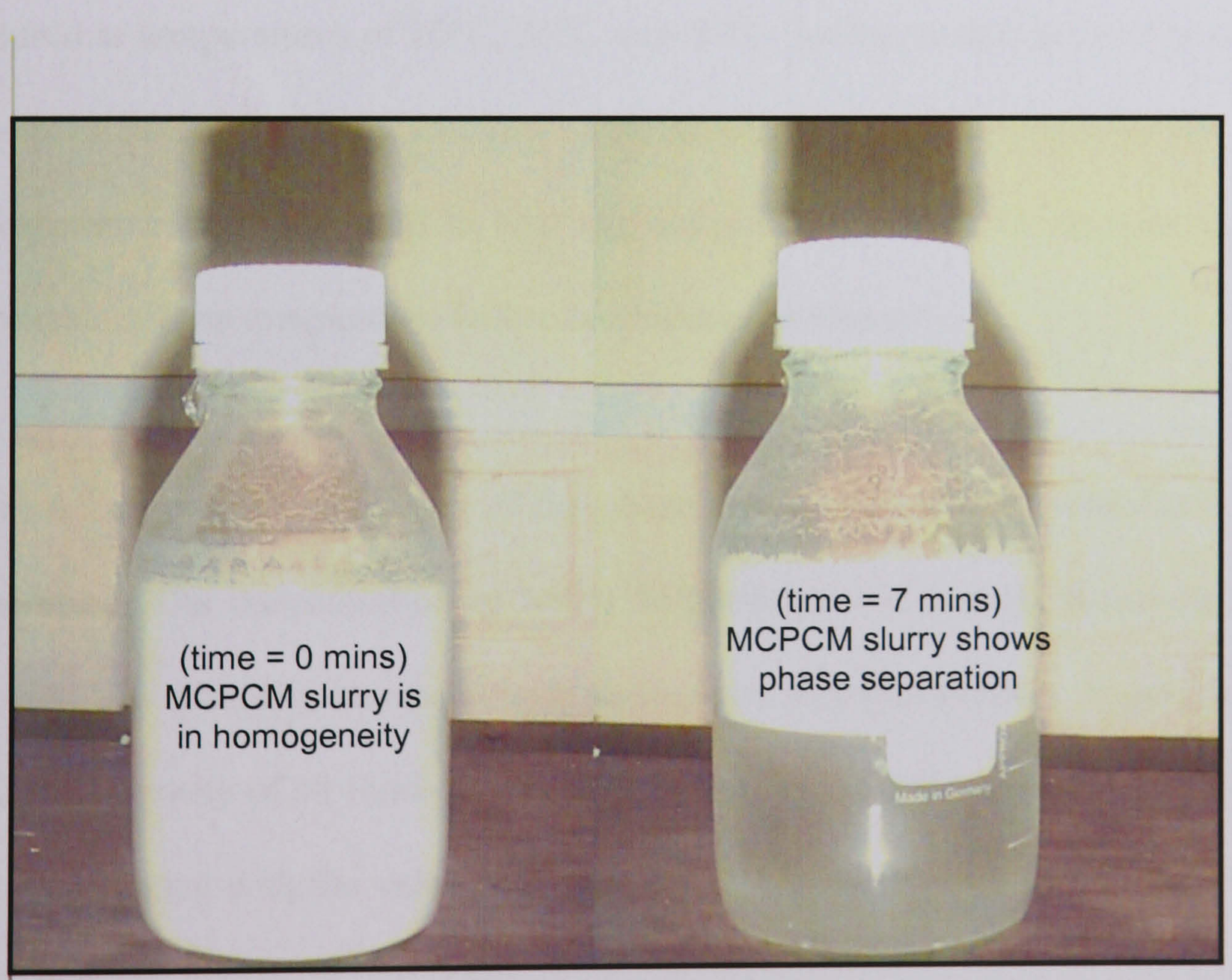

Figure 4.2: Stratification of MCPCM slurry

4.4 Phelogical properties of MCPCM slurry

4.4.1 Viscosity measurement

Viscosity of a fluid is a measure of its resistance to flow represented by a ratio of shear stress to shear rate. It is a strong function of temperature. The viscosity of liquid generally decreases with temperature, whilst the viscosity of gas increases with temperature (Perry, 1997). In the present experiment viscosities of MCPCM slurries were measured by a Brookfield viscometer from the School of Chemical Engineering, which is a rotational viscometer. Initially, six samples were prepared using the MCPCM particles with a melting point of 35°C. Concentrations were made at 0% (pure water), 2.5%, 3.5%, 10%, 20%, 30% and 40% (volumetric percentage of MCPCM in water). The viscosities of the samples were measured at temperatures of 20°C, 35°C and 40°C (below, at and above the melting point of the paraffin wax) to study an effect of the suspended particles with solid and liquid core. A temperature bath was used to heat the samples for at least 15 minutes to maintain a desire and uniform temperature before measuring the viscosity.

Figure 4.3 shows the viscosities of the phase change slurries and water as a function of temperature. The concentration of MCPCM particles was a main factor dominating the viscosity. The viscosity increased with an increase in concentration. In ranges of 20°C to 40°C, the viscosity of all fluid decreased slightly. The viscosity of water was found to have a big discrepancy with the value cited elsewhere. The viscometer should read the viscosity of water at 1cP instead of 3cP. Thus, all results measured in the present experiment need to be checked because the viscometer may not be accurate. This might relate to the use of a number-one needle of the rotational viscometer which was designed for high viscosity measurement of up to 20,000cP.

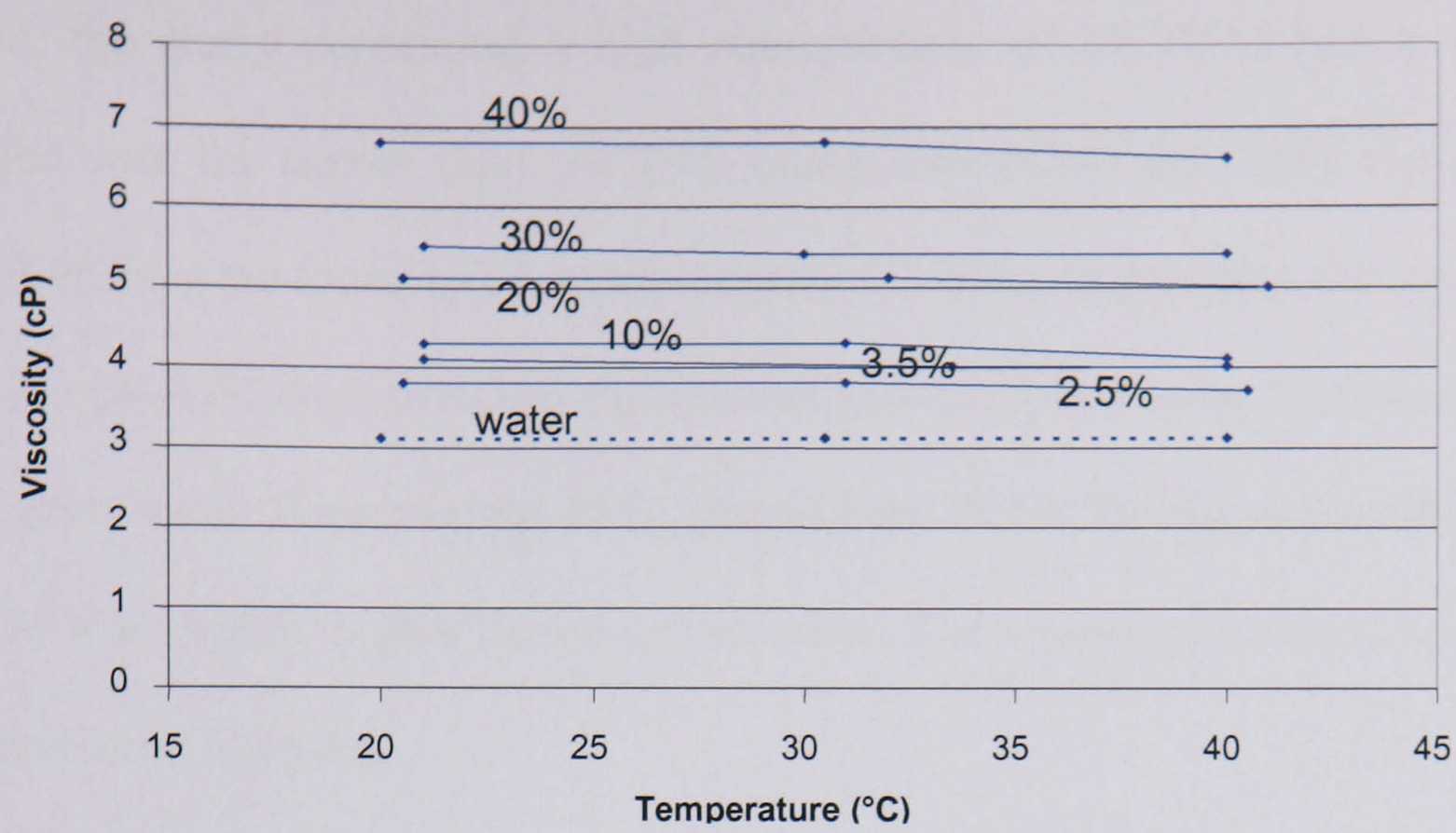

Figure 4.3: Viscosity of MCPCM Slurries (vol. % of MCPCM in water)

The viscosities of the slurries were measured again using a Bohlin CS rheometer from the School of Food and Science. Fifteen samples were prepared among the paraffin wax with melting points of 28°C, 35°C and 50°C, which was 0% (pure water), 10%, 20%, 30% and 40% of MCPCM in water (volumetric percentage). Tests were conducted with slurry temperatures of 20°C and 60°C (below and above the melting point of paraffin waxes). A temperature bath with a magnetic stirrer was used to heat and mix the samples for at least 15 minutes prior to the measurement of viscosity. This is to ensure that a uniform temperature and homogeneity have been achieved.

Figure 4.4 plots the relationship of apparent viscosity and shear rate of (a) 28°C, (b) 35°C and (c) 50°C MCPCM slurry. These figures were then compared with the viscosity of water. Noting that the MCPCM particles with different melting used in the present experiment had the same range of diameter between 15 and 40 microns. In the case of pure water, the viscosity was in good agreement with values sited elsewhere. As seen in the figures, the viscosity of the fluid depended on two main parameters; the temperature of the slurry and the concentration. The viscosity decreased with an increase in temperature. In

addition, the slurry containing a high concentration of MCPCM had a high viscosity compared with the carrier fluid. At $T<T_f$ (solid core PCM) the slurry viscosities for 10-20% MCPCM were found to be approximately 1-3 times higher than the viscosity of pure water. For 30-40% concentration, the viscosities were found to be 5-10 times higher than that of pure water. However, At $T>T_f$, (liquid core PCM) the slurry viscosity for 10-30% MCPCM was slightly higher than the pure water. The viscosity increased nonlinearly with particle volume fractions.

Figure 4.4: Apparent viscosity of 10-40% MCPCM slurry against shear rate for the paraffin wax with the melting point of (a) 28°C (b) 35°C and (c) 50°C

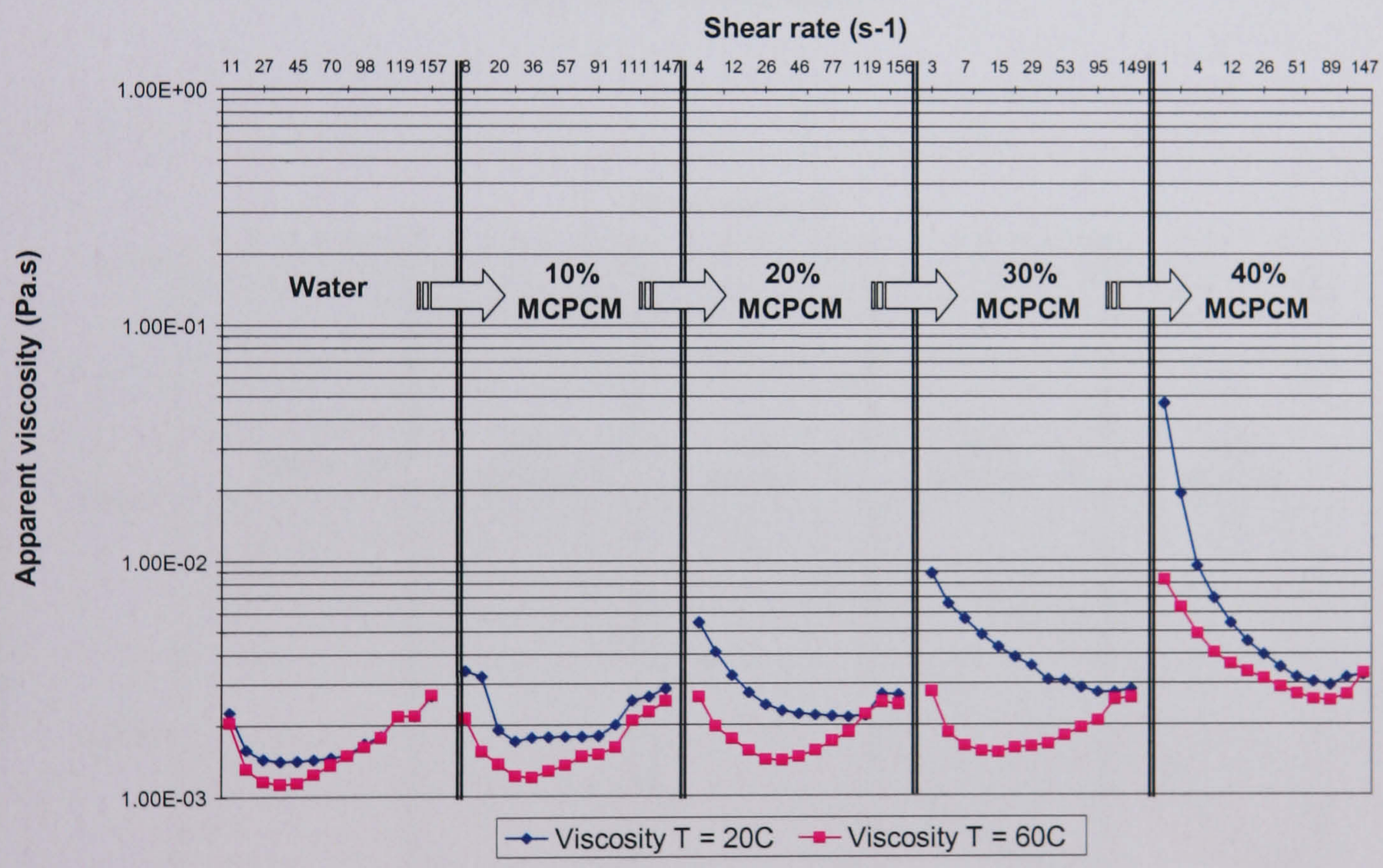

(a) 28°C n-eicosane

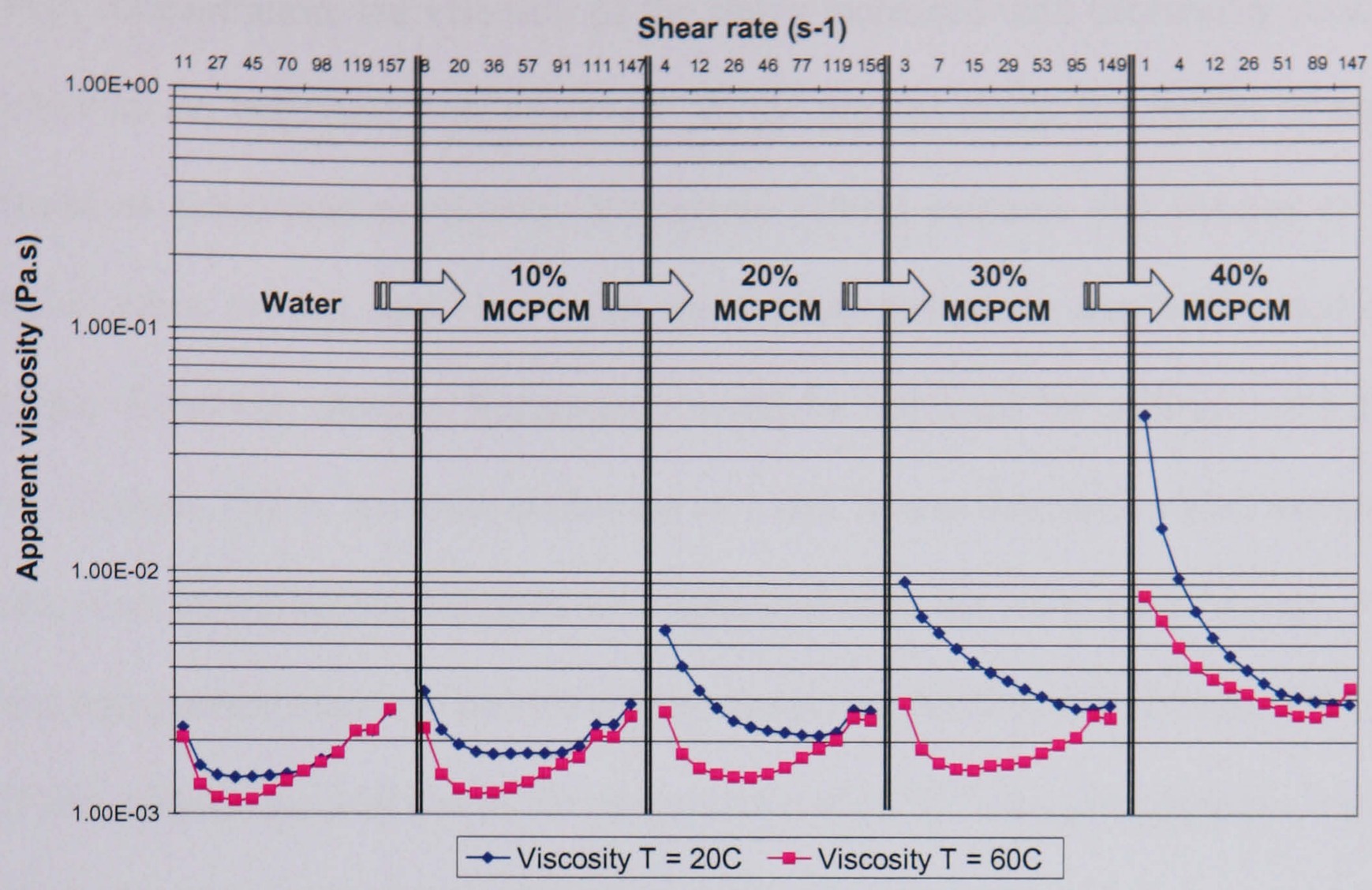

(b) 35°C n-eicosane

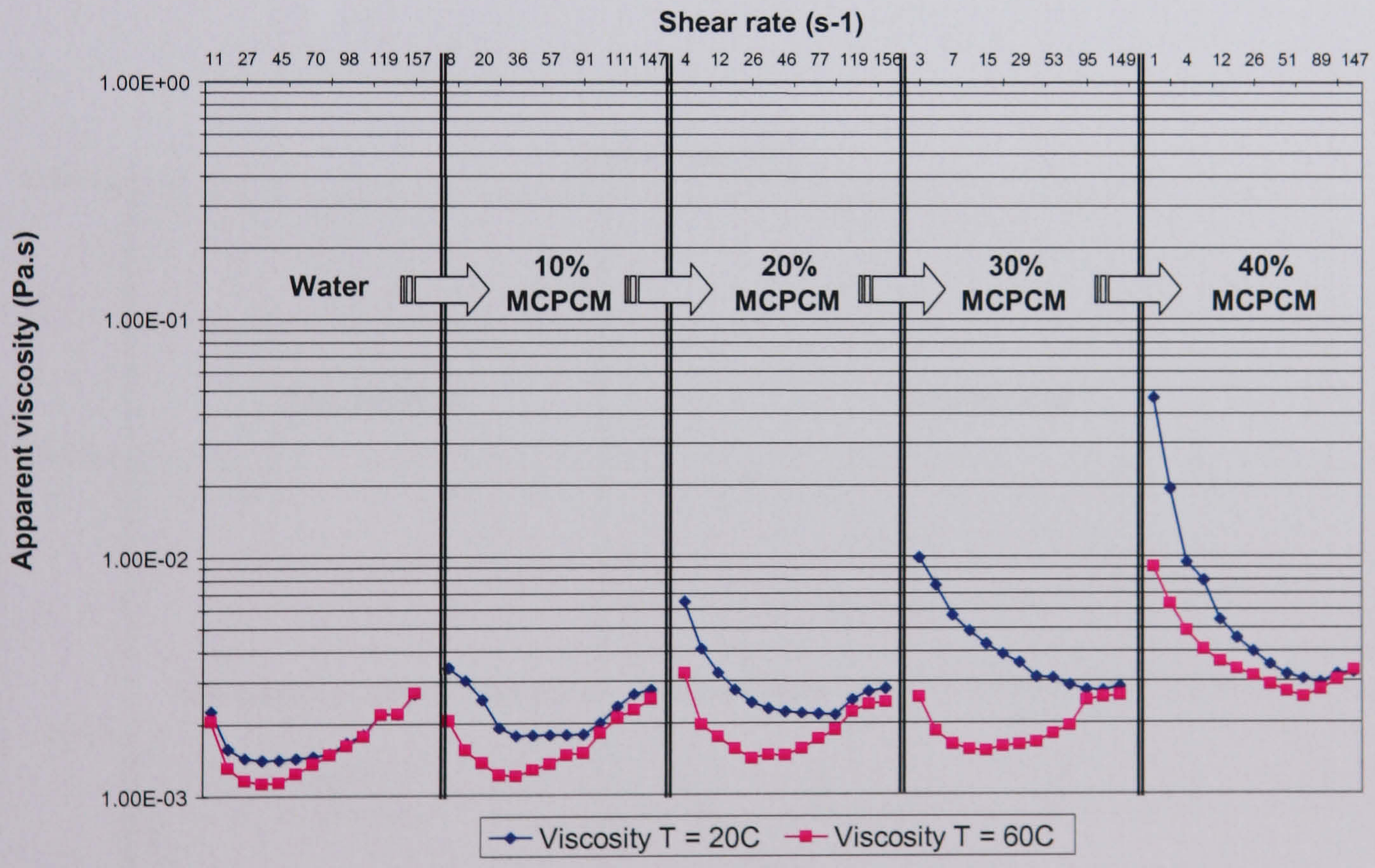

(c) 50°C n-eicosane

At high concentration, the viscosity of the slurry increased with decreasing shear rate, i.e. non-Newtonian behaviour was observed. In the present study, the feature of aggregation occurred as mentioned previously. Yamagishi (1999) explains that slurries of very fine particles often exhibit non-Newtonian rheological behaviour due to fluctuation of the particles. However, particle flocculation could be inhibited by addition of a dispersing agent (Eveson, 1957). An ionic surfactant of 1 vol. % was therefore added into the slurries for the next investigation. Samples were prepared with the 35°C paraffin wax. Figure 4.5 shows the apparent viscosity plotted against shear rate for 20% and 40% MCPCM slurry of with and without the additive at the temperature of 25°C. Using the additive was found to improve the degree of particle dispersion and effectively reduced the apparent viscosity. With the additive present, the slurry behaved practically as a Newtonian fluid. Adding more than 2% additive did not provide a further reduction in slurry viscosity.

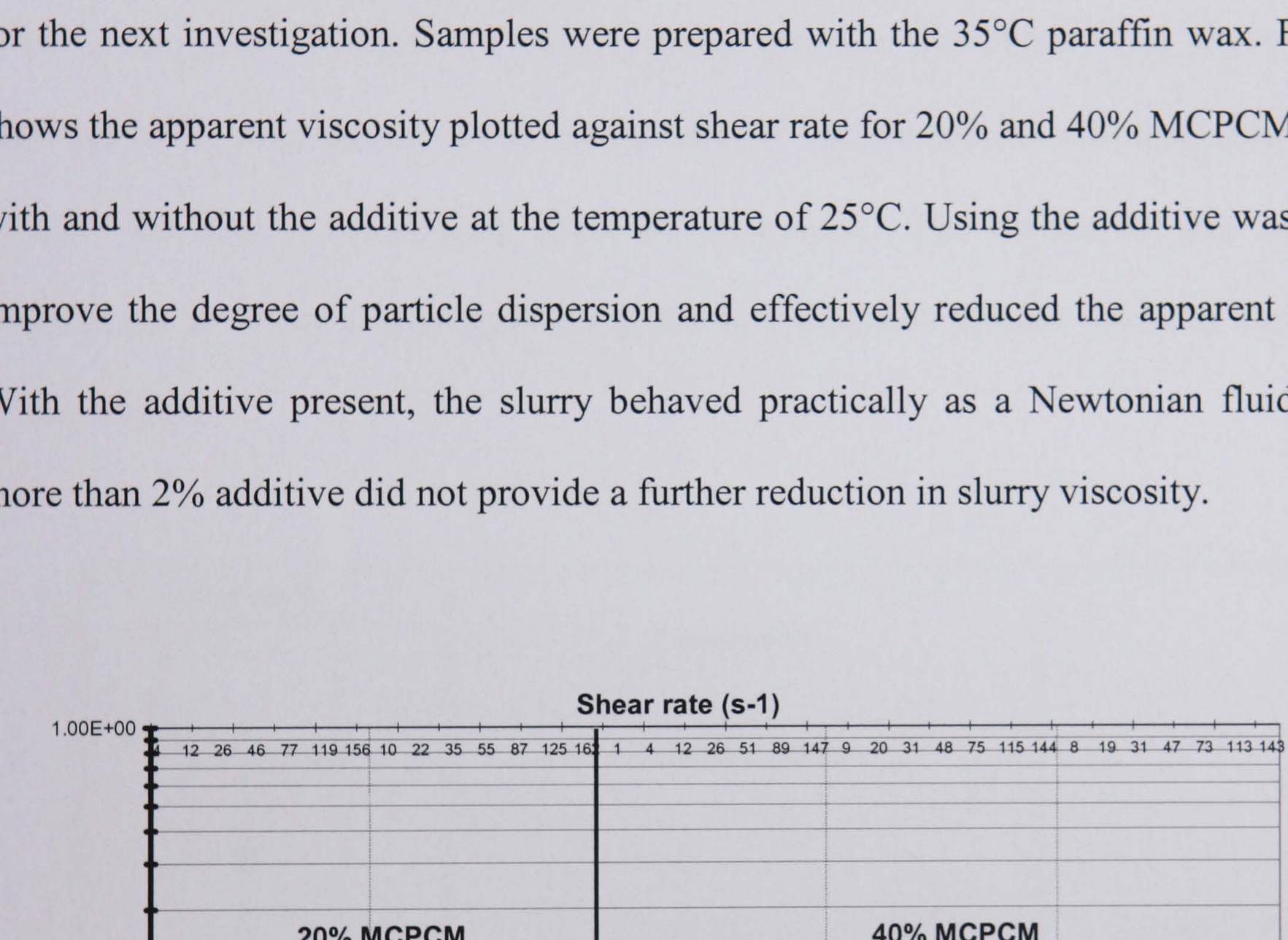

Figure 4.5: Apparent viscosity for 20% and 40% MCPCM slurry with 35°C n-eicosane of with and without additive at the slurry temperature of 25°C

4.4.2 Pressure drop measurement

Figure 4.6 shows a schematic diagram of experimental apparatus for pressure drop measurement. Tests were conducted with 35°C paraffin wax for the mixture of 5-40% MCPCM slurries. The slurry of 28°C and 50°C MCPCM particles were excluded from the experiment because they had the same particle diameter of 15-40 microns. Test section of the apparatus was made of a circular pipe with 15mm diameter and 1.5m long. Flow rates were in ranges of 2-6l/min. To investigate the pressure loss of MCPCM slurry with solid core particles, temperature of the fluid at inlet of the test section was maintained at 25°C, which was below the melting point of *n*-eicosane. The reason for not running the experiment with liquid core particles is because they had smaller viscosity comparing to the solid core.

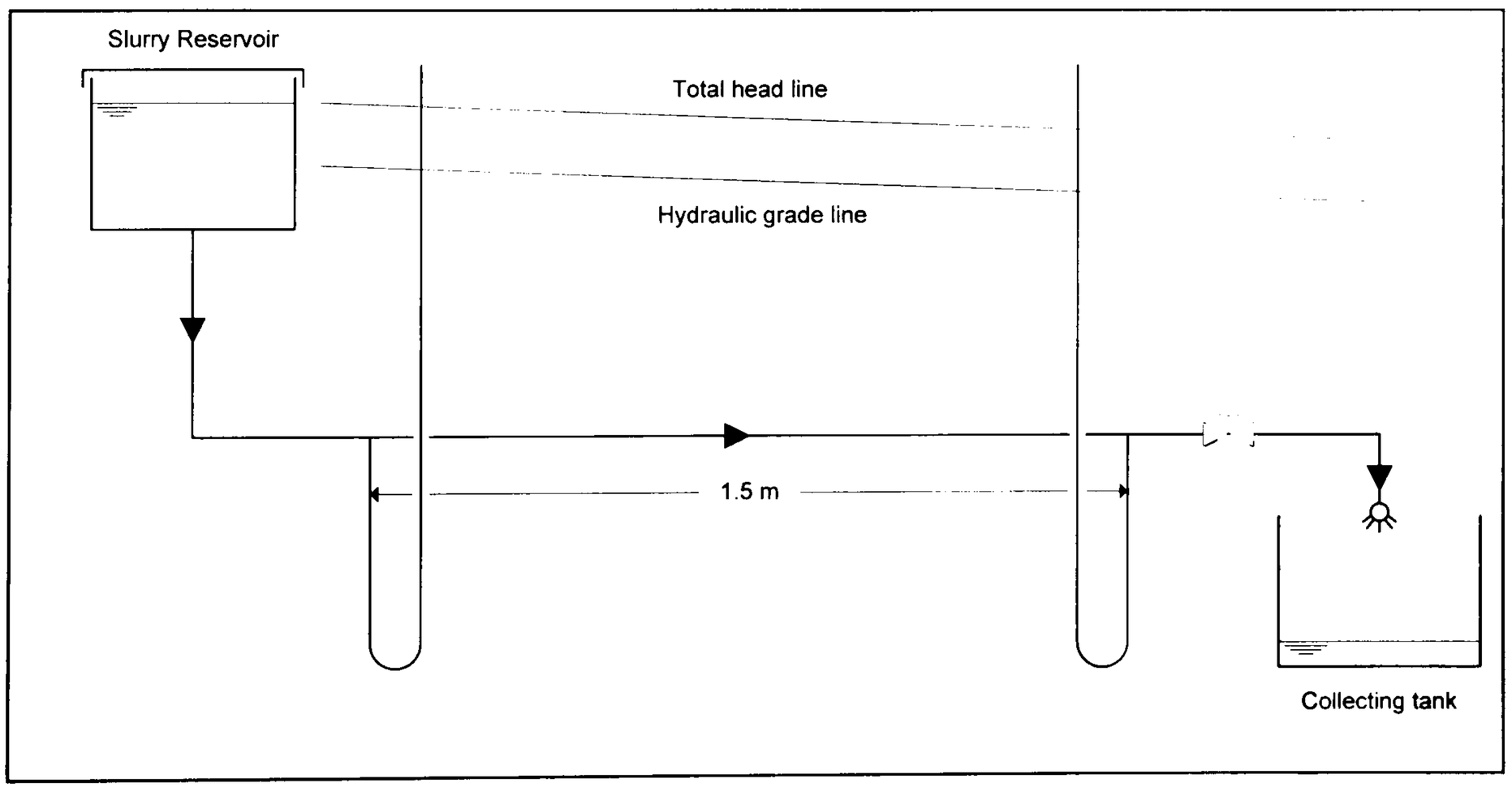

Figure 4.6: Experimental apparatus for the pressure drop measurement

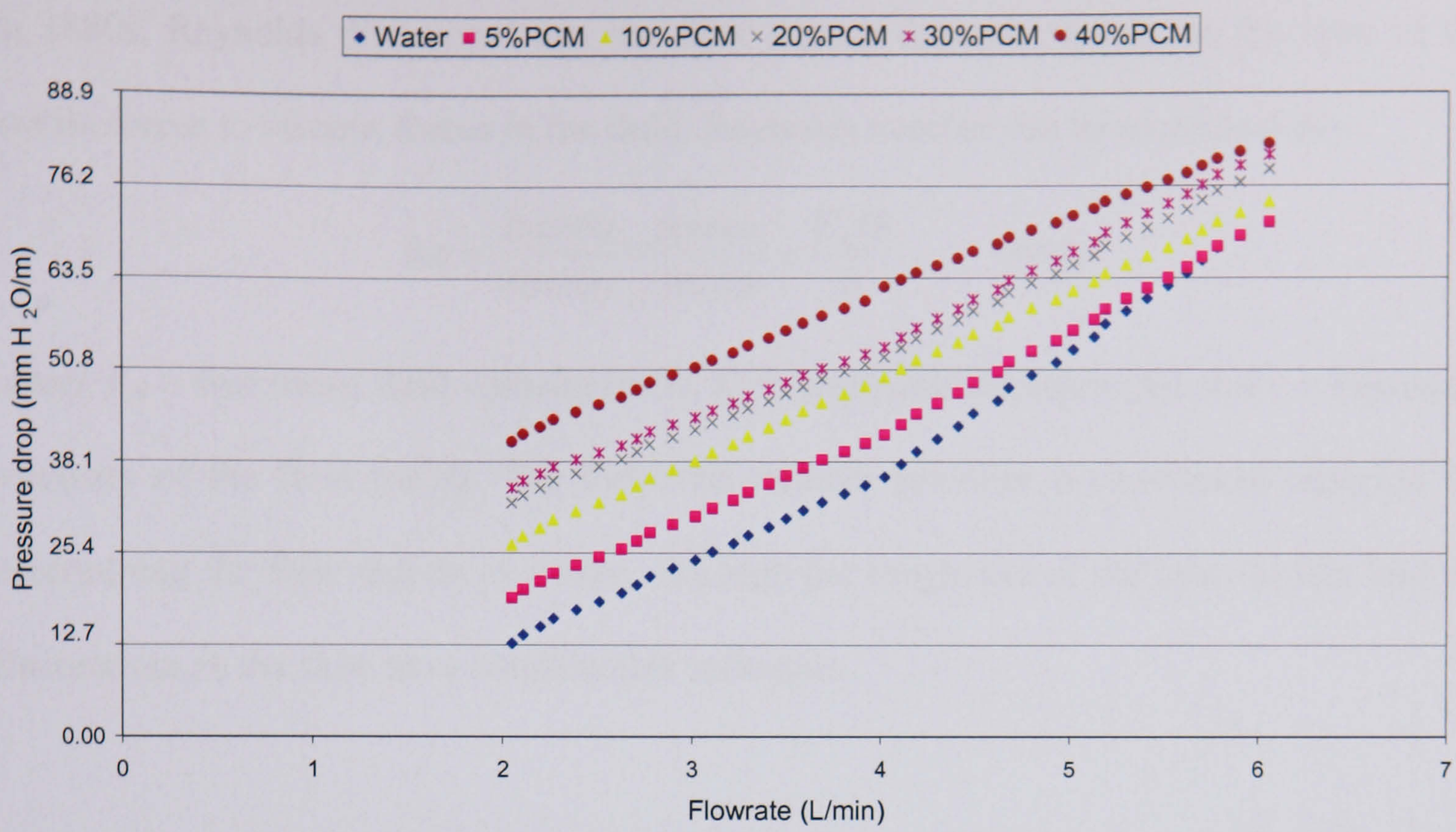

Figure 4.7: Pressure drop plotted against volumetric flow rate for water and 5-40% MCPCM slurry at 25℃

Figure 4.7 illustrated the pressure drop measurement per unit length (mm H_2O/m) of water and 5-40% MCPCM slurries over the flow rate of 2 to 6l/min. It was observed that the pressure drop increased over the entire range of flow rates. The pressure drop of the slurry with more particle fractions showed higher value of pressure drop comparing with the slurry with small concentration. For example, the pressure drop of 40% MCPCM slurry was found to be 40mm H_2O/m comparing with 26mm H_2O/m of 10% MCPCM slurry. The figure increased by 54%. This can be attributed to the increased slurry viscosity according to the increasing particle fraction. At 2l/min, the pressure drop of 10% MCPCM slurry was found to be around twice that of water. However, at 6l/min, the pressure drop of 10% MCPCM slurry and water were seen in equivalence. This is because the pressure drop of water rose rapidly at around 3.5l/min and approached the figure of 10% MCPCM slurry. To explain this phenomenon it should be noted that flow style in a tube can be laminar or turbulent, depending on the flow conditions.

In 1880s, Reynolds discovered that the flow regime depends mainly on the ratio of the inertia forces to viscous forces in the fluid. Reynolds number can be expressed as

$$\mathrm{Re} = \frac{Inertia\_forces}{Viscous\_forces} = \frac{V_m D}{\nu} \qquad (4.1)$$

where V_m = free mean fluid velocity (m/s), D = a circular diameter (m) and ν = kinematic viscosity of the fluid (m^2/s). The Reynolds number provides a convenient criterion for determining the flow regime in a tube, although the roughness of the tube surface and the fluctuations in the flow have considerable influence.

Figure 4.8 shows the dependence relationship of friction factors on the Reynolds number for pure water and slurry of 10% to 40% MCPCM. The friction factor was calculated from

$$f = \Delta P \frac{2D}{L\rho V_m^{\ 2}} \qquad (4.2)$$

where ΔP = pressure drop (N/m^2), D = pipe diameter (m), L = pipe length, ρ = density of fluid (kg/m^3) and V_m = mean fluid velocity (m/s). These values were calculated from the pressure drop and the apparent viscosity which were measured by the Bohlin CS rheometer. In the range of Re<2,000~4,000, the friction factor of all samples are close to the line which corresponds to the known dependence of laminar flow. In the range of Re>4,000, the friction factor approaches the line for turbulent flow as described by Blasius equation. The transition from a laminar to turbulent flow occurred in the Reynolds number range of 2,000 to 4,000, which is in good agreement with the values cited elsewhere.

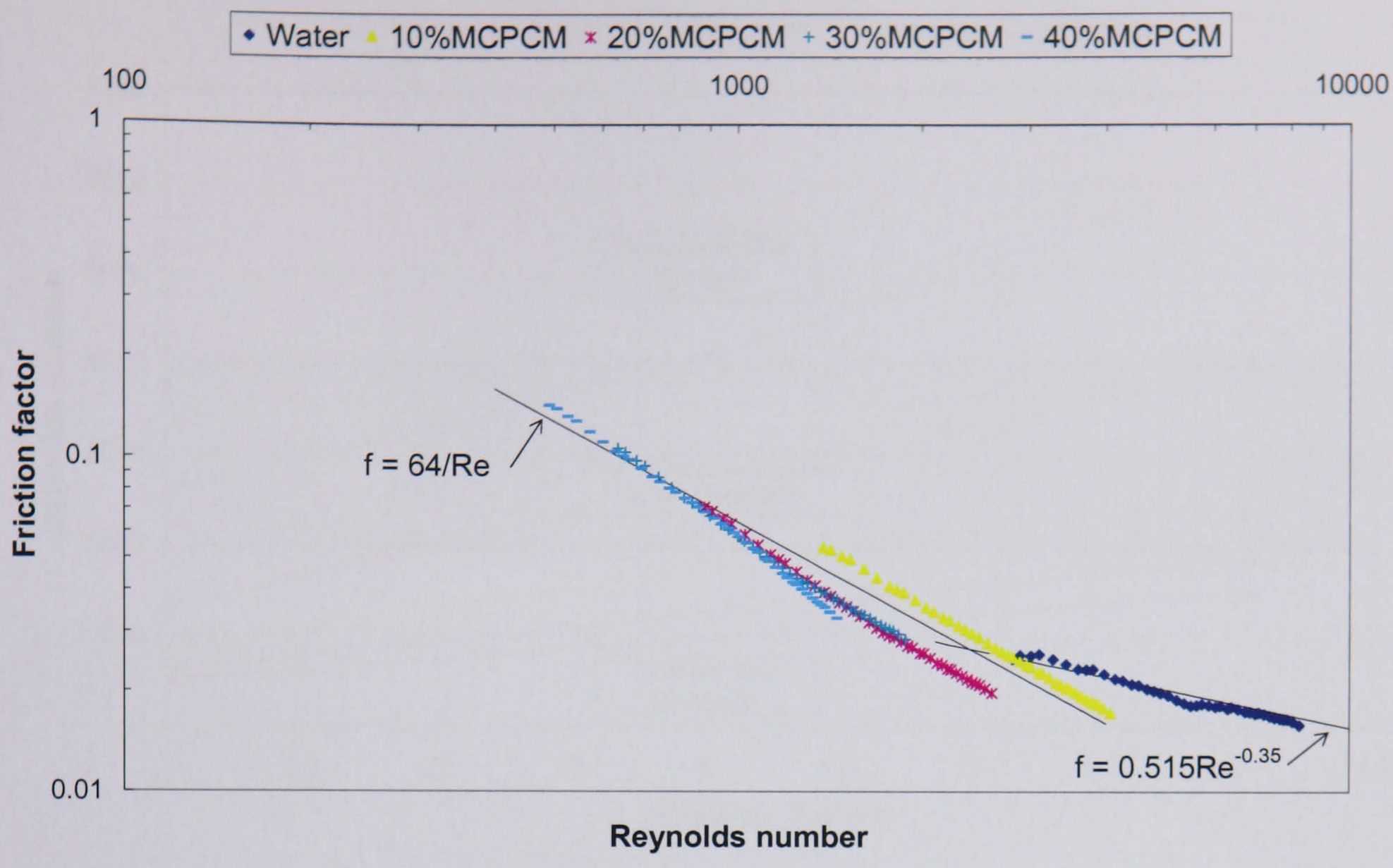

Figure 4.8 Friction factor plotted against Reynolds number for pure water and 10%-40% MCPCM slurry at 25°C

Figure 4.9 plots the relationship of Reynolds number for water and 10%-40% MCPCM slurry against the flow rates. The flow structure of MCPCM slurry changed from turbulent to laminar as the particle volume fractions in the slurry increased under a constant flow rate condition. The pressure drop of water increased rapidly around 3.5l/min, which was due to the change of flow style from laminar to turbulent flow. Yamagishi (1996) also reports the similar phenomenon that the pressure drop of the slurry flow depends on not only the concentration but also the flow-style of the slurry (at a certain flow rate).

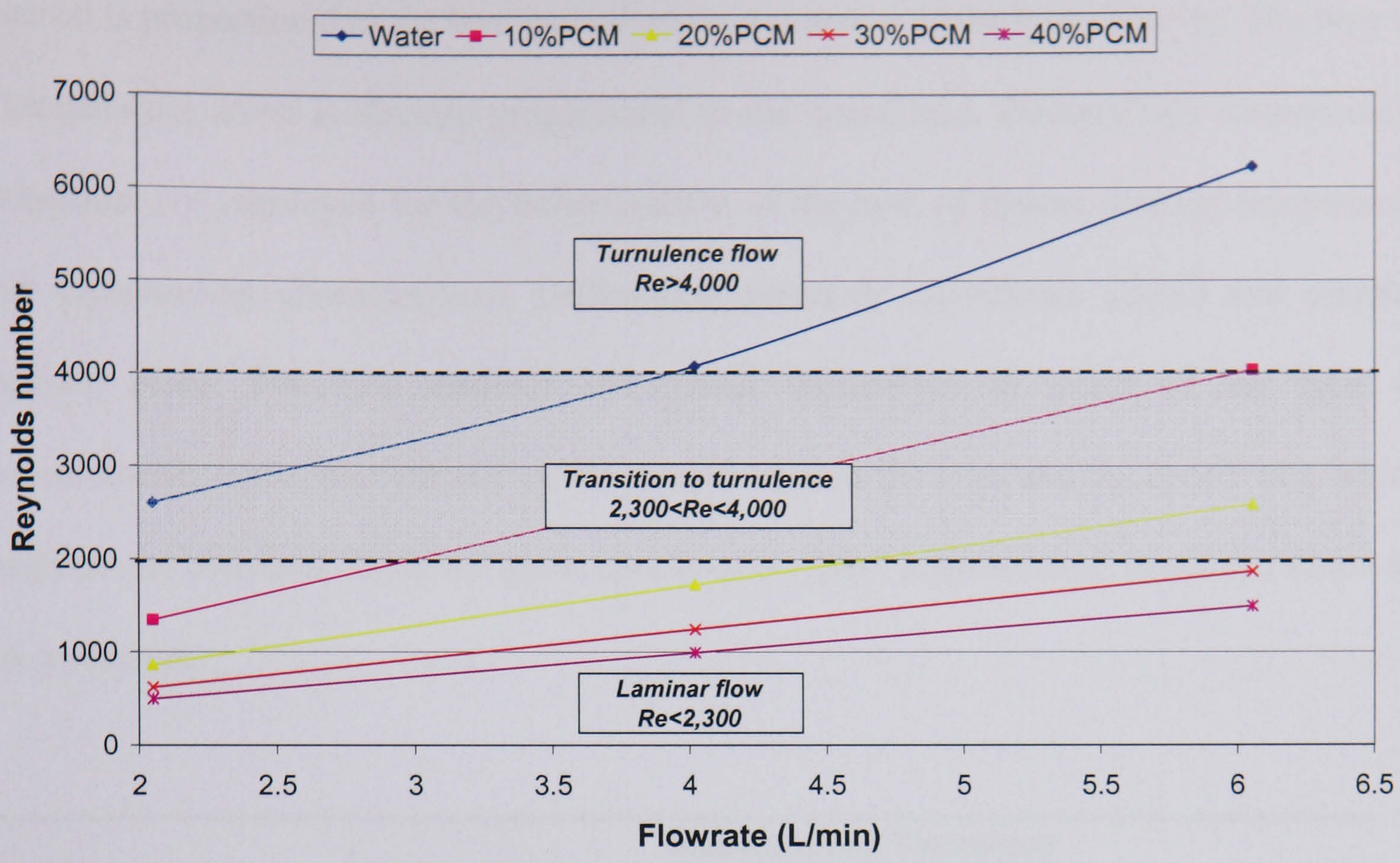

Figure 4.9: Reynolds number plotted against volumetric flow rate for water and 10%-40% MCPCM slurry at 25 °C

4.5 Latent Heat of Fusion

The determination of latent heat is not simple. It requires a temperature control system to bring the test sample to its melting temperature. A method for measuring the amount of heat absorbed at this temperature is required and is usually complicated. Latent heat is derived from calculations of other variables or from specialised equipment. One simple method given by Hale in 1971 consists of placing the test material in an insulated refractory container with differential thermocouple junctions inside and outside the container. The container with a sample is placed in a furnace whose heating rate is controlled so that a constant temperature gradient is maintained across the container walls. The heat flow to the sample is thus almost constant and the heat received by the sample in a given time is determined. The time the sample takes to go through a given temperature

interval is proportional to the heat gained and is a measure of the heat capacity. The time of a temperature arrest is directly proportional to the latent heat. Primary two measurement techniques are employed for the determination of the heat of fusion, melting temperature and supercooling characteristics; Differential scanning calorimeter (DSC) and thermal analysis (TA). The two methods distinguish themselves in terms of the type of measurements made, the quantity of the sample used in the tests and the speed with which result can be obtained. Table 4.2 gives details of the DSC measurement in comparison with TA technique.

	Measurement Technique	
	DSC	**TA**
Quantity of substance	1-10 mg	10 g – 10 kg
Measurements made	Temporal variation of the thermal energy exchanged with the sample to enable it to undergo heating or cooling at a constant predetermined rate, The output of the measurements is the energy-time diagram, also called thermogram	Temporal variation of temperature at selected locations within the heat storage substance resulting from energy input/output to the sample. The output of the measurements is the temperature time diagram
Data evaluated	▪ Form of the endothermic of exothermic peaks on the thermogram ▪ Melting point/range ▪ Freezing point/range ▪ Degree of supercooling ▪ Heats of fusion and solidification ▪ Specific heat as a function of temperature	▪ Shape of the temperature-time diagram, melting and freezing plateaus, homogeneity of the original substance following melting, etc ▪ Melting point/range ▪ Freezing point/range ▪ Degree of supercooling ▪ Congruent/incongruent melting ▪ Decomposition of the original substance, formation of new phases, segregation effects

Table 4.2: Details of differential scanning calorimeter and thermal analysis measurement techniques (Abhat, 1982)

4.5.1 Differential scanning calorimeter (DSC) measurement

A Differential Scanning Calorimeter (DSC) is a useful instrument for measuring heat of fusion and specific heat which provides quick and reliable results in the form of energy-time diagrams (thermograms). Evaluation of the thermograms yields rather precise values of the phase transition temperatures during melting and freezing of the sample, the heats of fusion and solidification and the specific heat variation as a function of temperature (Abhat, 1982). Usually, the quantity of the sample used in the tests are very small, e.g. 1-10 mg. Experiments can be made in hermetically sealed pans with a choice of atmosphere with a number of heating rates. The DSC is, however, a severe test for substances that supercool, since the supercooling tendencies are maximised due to the small quantities of the samples and the poor nucleation conditions in the DSC testing pans. Some DSC has the additional feature of low temperature auxiliary equipment using liquid nitrogen.

Experiments were conducted to study the latent heat of fusion and changes in melting point of the paraffin waxes. A DSC manufactured by Perkin Elmer (Model: Pyris 1) from the School of Mechanical Engineering was used for the investigations. Initially, three samples of pure MCPCM particles with the melting point of 28°C, 35°C and 50°C were examined. Then, the thermal behaviours of MCPCM slurries with 10%, 20%, 30% and 40% vol. concentration were investigated using 35°C paraffin wax. The slurries were prepared and mixed for 15 minutes at a temperature below the melting point of PCM. The samples were put in aluminium pans covered by aluminium lids. The inner diameter and height of the container were measured at 5 and 2mm, respectively. In the DSC measurement, the sample and reference material were heated at a constant rate of 5.0°C/min. The temperature difference between them was proportional to the difference in heat flow between the two materials. The latent heat of fusion was calculated using the area under the peak of the

DSC thermograms and the melting temperature was identified by the temperature established the thermograms at the peak point. The experiments were performed under heating and cooling modes to investigate the supercooling phenomenon.

Figure 4.10 (a, b and c) shows the typical DSC curves, which plotted the rate of energy absorption against temperature, of pure paraffin waxes of 28, 35 and 50°C melting point. The quantities of the materials for the 28°C, 35°C and 50°C MCPCM were 14.34, 15.21 and 16.45mg, respectively. One thermal cycle was conducted shown as a heating and cooling curve. The latent heat of fusion was observed as the curves rapidly rose when the MCPCM started melting and crystallisation. The measured latent heat of fusion and the melting/crystallisation temperature of MCPCM are given in Table 4.3. The latent heat of fusion of the paraffin waxes was in good agreement with the data provided by the manufacturer being 183, 174 and 162kJ/kg for 28°C, 35°C and 50°C MCPCM, respectively. However, the crystallisation temperatures of all tested materials were smaller than the melting temperatures around 2°C to 4.5°C. Thus, the supercooling phenomenon was observed.

Figure 4.10: DSC thermogram (heating and cooling curves) of pure MCPCM with the melting point of a) 28°C b) 35°C and c) 50°C

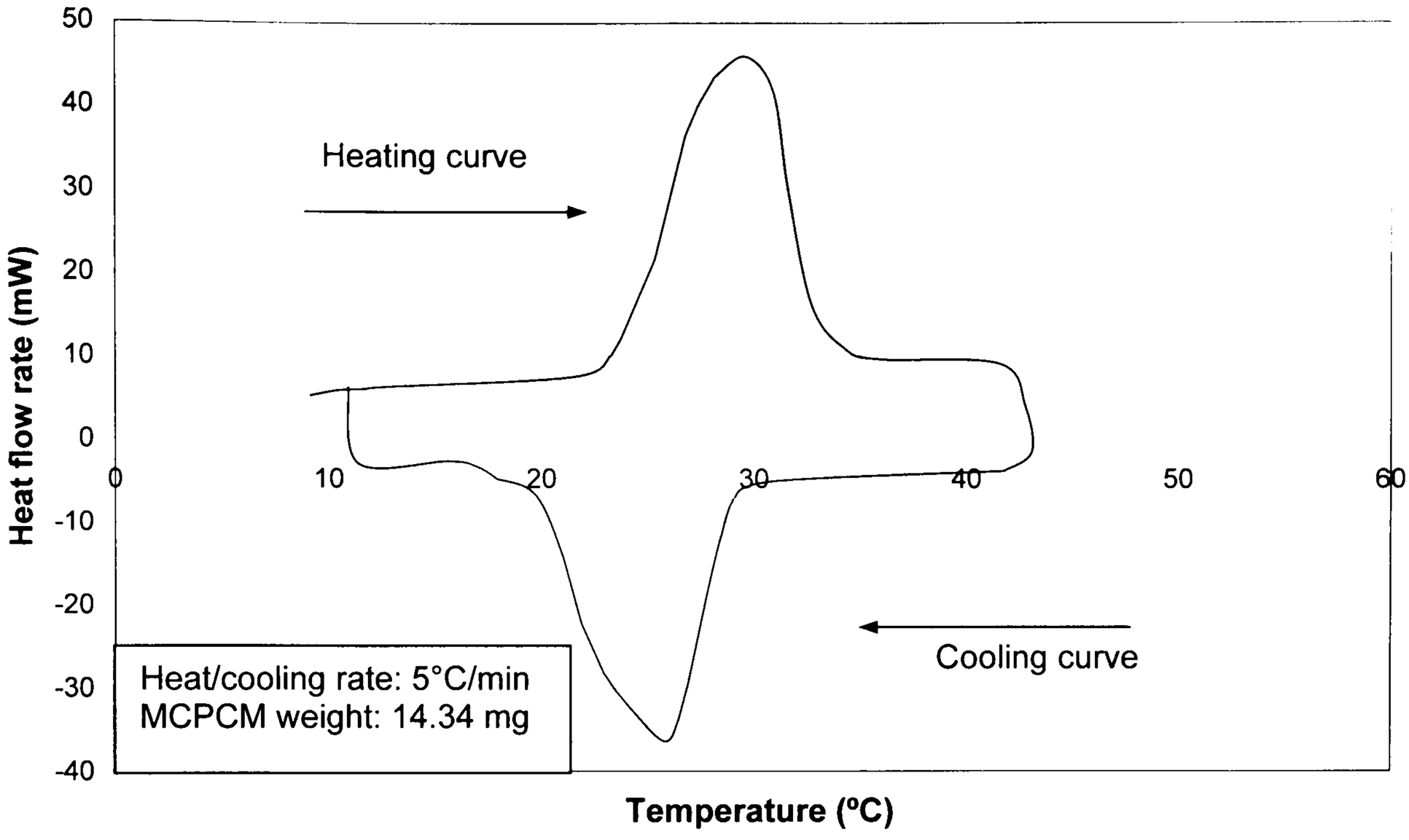

(a) 28°C n-eicosane

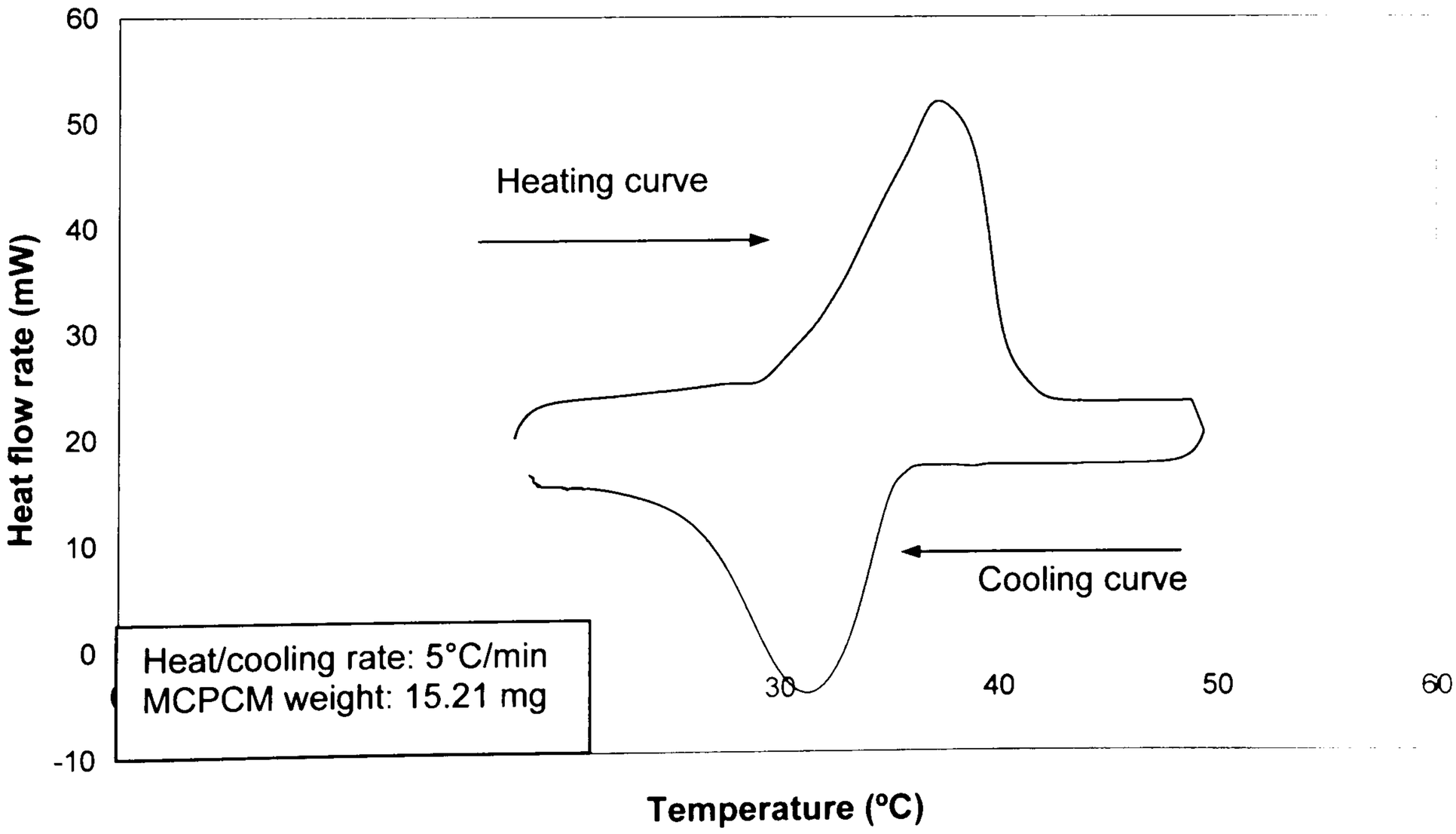

(b) 35°C n-eicosane

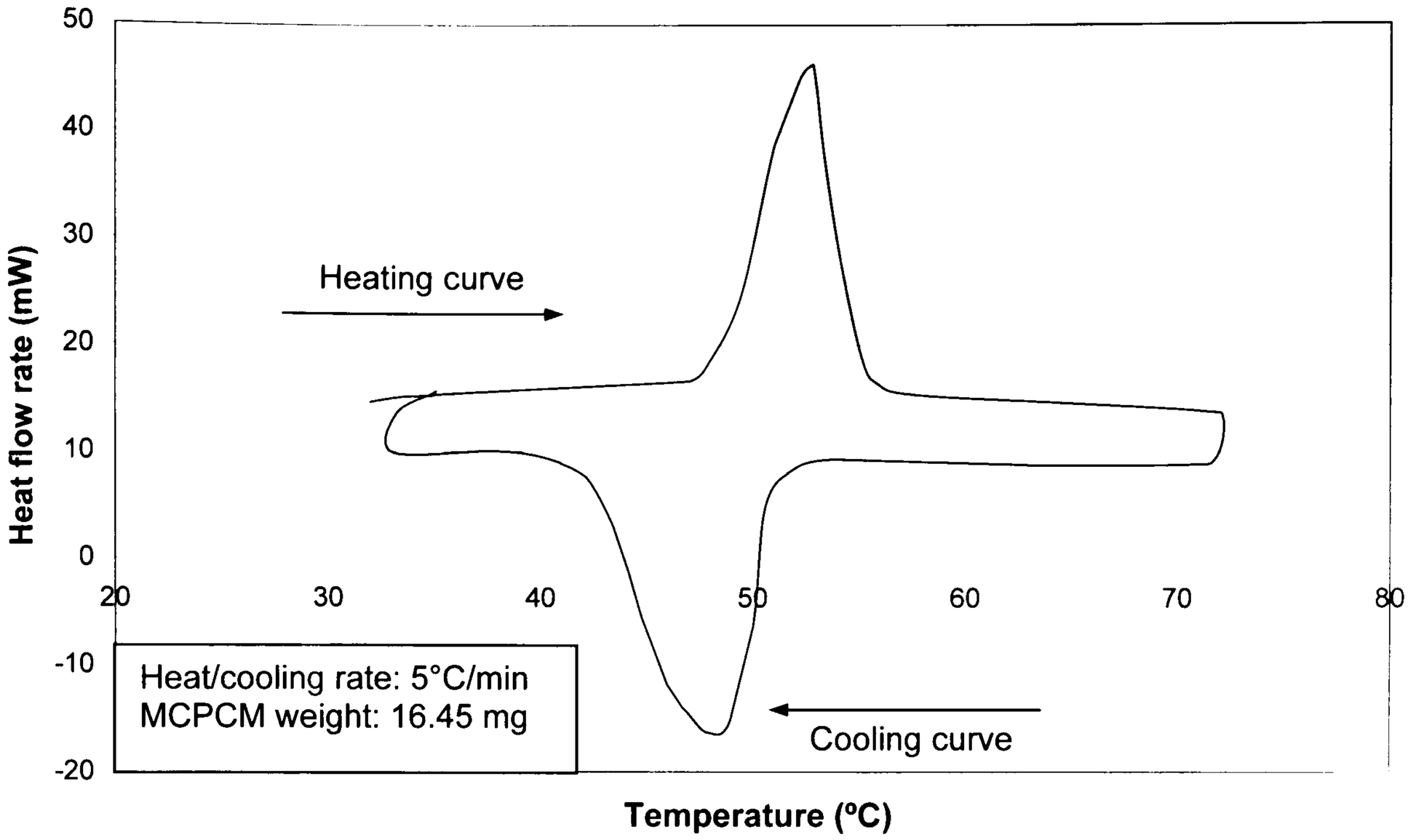

(c) 50°C n-eicosane

An investigation of the supercooling phenomenon by Yamgishi (1996) shows that of the size of microspheres ranged from 5 to 100μm the crystallisation temperatures are lower as the micro sphere sizes decrease. He points out that the supercooling increases with reducing the size of microcapsule because the number of nuclei in each droplet decreases as the droplet size reduces. The crystallisation inside a droplet starts from the generation of a small crystalline nucleus. There are two processes to form the nuclei; the nuclei forms inside the liquid (homogeneous nucleation) or on the interface solid substances (heterogeneous nucleation). He observes that the crystallisation behaviours of the microcapsules could occur after either of the mentioned nucleation. When the nucleus forms in a MCPCM, it grows until the core material has entirely crystallised. The heterogeneous nucleation occurs at a higher temperature as compared with the case of homogeneous nucleation.

	Paraffin Wax	Melting Temperature (°C)	Crystallisation Temperature (°C)	Latent heat (kJ/kg)
1	*n*-eicosane	28.5	26.5	183.42
2	*n*-eicosane	36.6	32.2	173.75
3	*n*-eicosane	52.2	47.6	162.65

Table 4.3: Measured latent heat of fusion and melting and crystallisation temperature of paraffin waxes

Figure 4.11 shows the DSC thermograms of the MCPCM slurries using 35°C paraffin wax with 10%-40% vol. concentration. The samples weighed around 17.59 to 20.23mg and were heated at a rate of 5°C/min from 20°C to 50°C. Evaluation of the peak around 36°C showed that the paraffin wax released the latent heat of fusion and underwent solid-liquid phase transition. The benefit of adding more concentration of phase change particles seemed to increase the enthalpy of the working fluid. This can be observed at the curves around the PCM melting temperature where the MCPCM slurry with more concentration showed the higher peak comparing to the MCPCM slurry with small concentration.

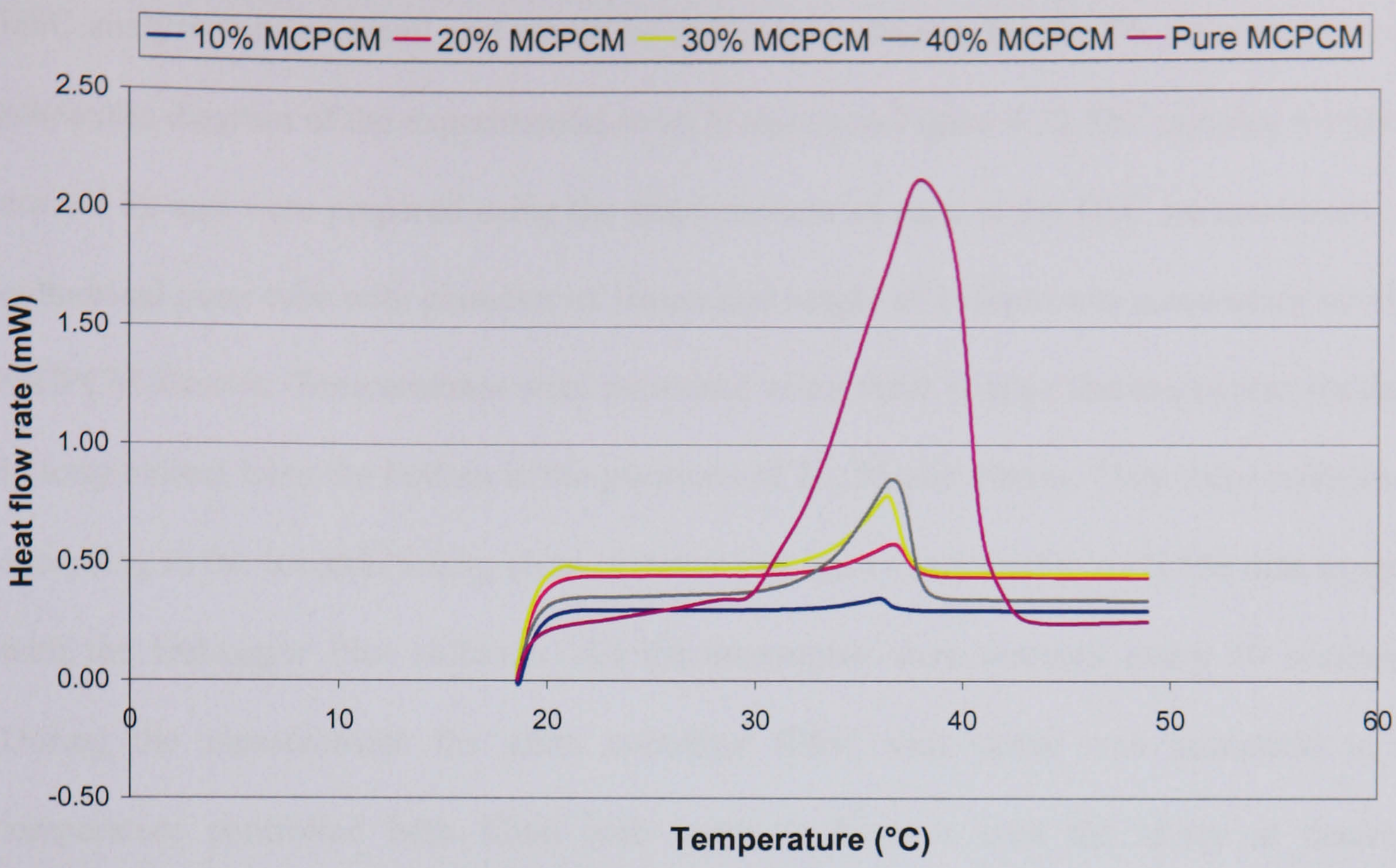

Figure 4.11: DSC thermogram (heating curves) for MCPCM slurries (10%-40%)

4.5.2 Thermal analysis (TA) measurement

Another measurement technique for the determination of melting and freezing characteristics is thermal analysis (TA). The TA technique involves the determination of temperature-time diagrams, or the heating and cooling curves, recorded during the melting and freezing of the sample. It uses about 10g – 10kg of the sample, depending on the type of an apparatus and usually is slower than the DSC. With proper care, the rate of heating and cooling can be well controlled and relatively accurate results can be gained (Abhat, 1982).

Pure water and MCPCM slurries of 20%, 30% and 40% concentration using the paraffin waxes of 28°C, 35°C and 50°C melting point were evaluated using the TA technique. 10% concentration was not investigated because the effect of latent heat of fusion found in the

DSC analysis was so small and would be difficult to observe by the TA measurement. A schematic diagram of the experimental setup is shown in Figure 4.12.The samples weighed around 8g and were prepared using the same process as seen in the DSC measurement. A cylindrical glass tube with diameter of 10mm and height of 150mm was a container for the MCPCM slurries. Temperatures were measured using three K-type thermocouples located in longitudinal from the bottom at the positions of 20, 35 and 50mm. They were calibrated according to the ice and boiling point of water and were connected to a DT500 data logger with the DeLogger Plus software. All thermocouples were scanned every 10 seconds. During the measurement the glass container filled with slurry was immersed in a temperature controlled bath filled with water to heat or cool the slurry at desired temperatures.

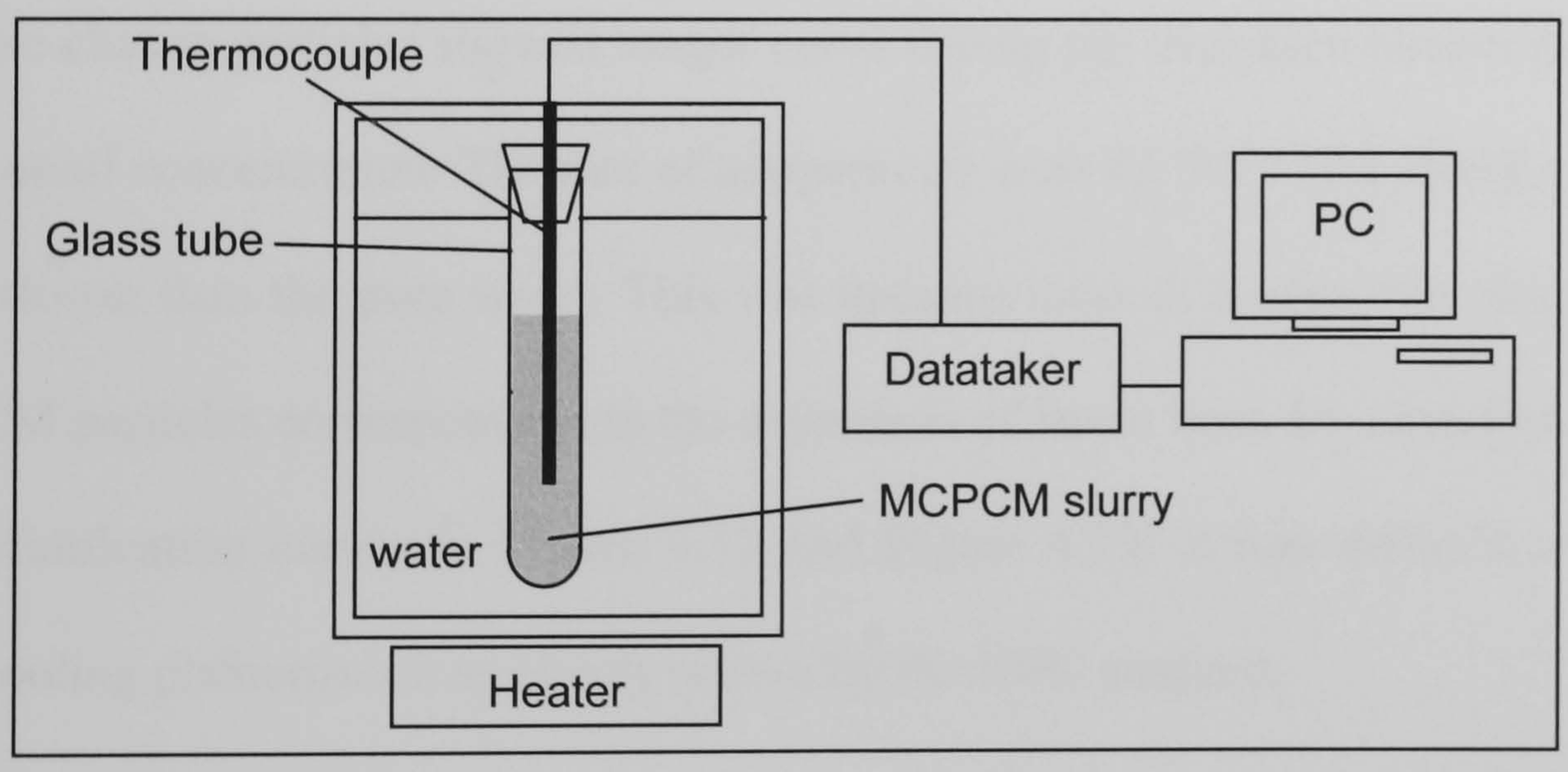

Figure 4.12: Glass test tube apparatus for TA measurement

Figure 4.13 (a, b and c) and Figure 4.14 (a, b, and c) shows typical heating and cooling curves of the TA measurement using the slurry of 28°C, 35°C and 50°C MCPCM, respectively. Results were presented with an average temperature of the fluid obtained from three thermocouples. The figures of phase change slurries were then compared with

that of the pure water. Notably, all experiments were finished within 7 minutes before the phase separation occurred.

As seen in Figure 4.13, at the initial stage of the melting process, the temperature increase of MCPCM slurries was linear, and then it was non-linear in shape with nearly zero-slope where the non-linear temperature interval corresponded to the paraffin melting temperature range. At high concentration the graph of MCPCM slurries showed longer curve during the melting temperature compared to the small concentration. Melting temperatures obtained from the TA measurement were in the same range as investigated by the DSC technique.

In cooling mode, the rate of temperature drop for MCPCM slurries seemed to be slower around the solidification temperature (see Figure 4.14). The slurry with high concentration of phase change particles showed longer curve during the transition temperature compared to the small concentration. The rate of temperature drop for MCPCM slurries seemed to be much slower than the pure water. This was because most of energy was absorbed into the MCPCM particles corresponding to the utilisation of latent heat. By examining the melting and solidification curves in Figure 4.12 and Figure 4.13, it was difficult to observe the supercooling phenomenon as clearly shown by the DSC analysis.

Figure 4.13: Temperature variations of MCPCM slurries (10% to 40%) in heating mode with a) 28°C b)35°C and c)50°C melting point

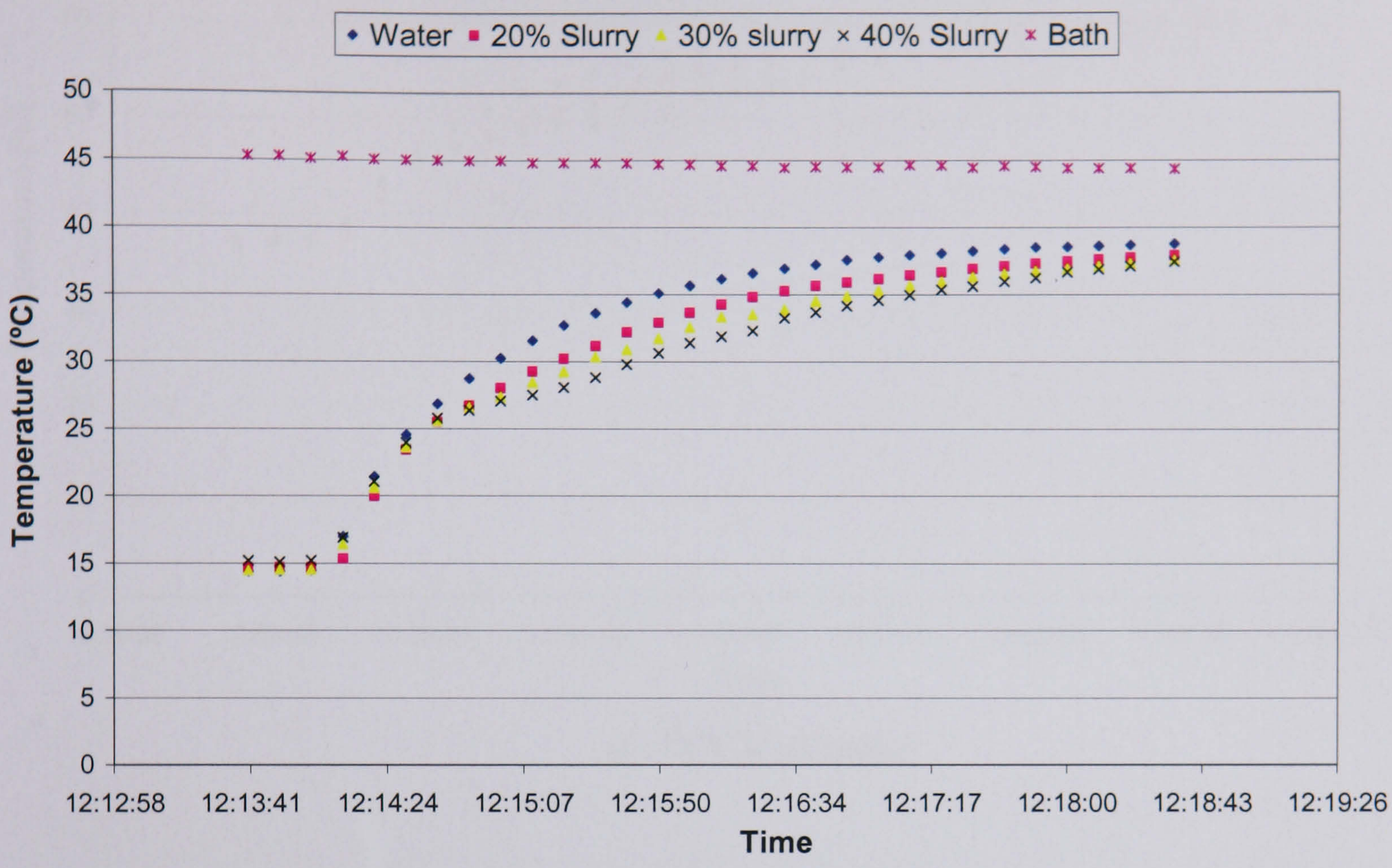

a) 28°C n-eicosane

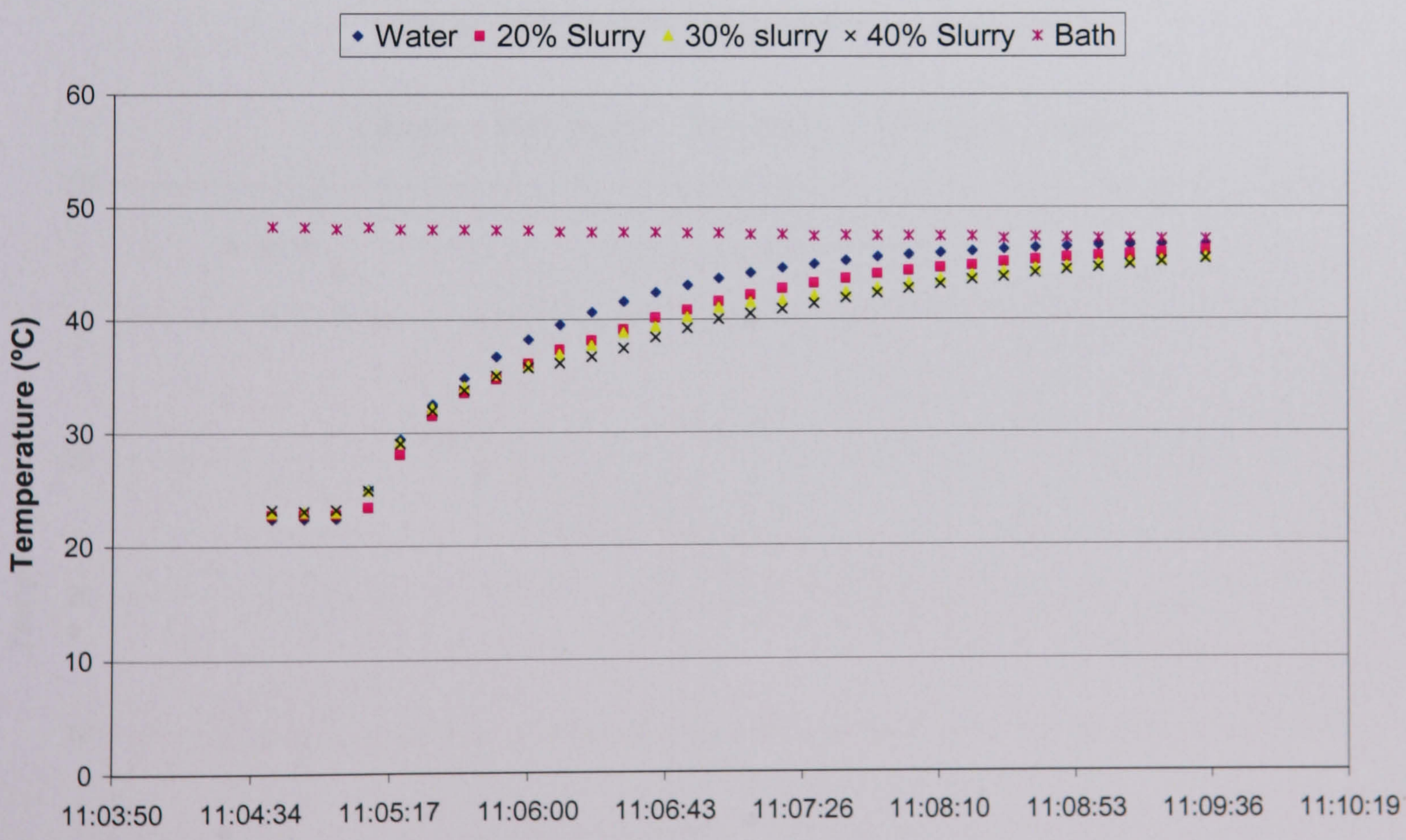

b) 35°C n-eicosane

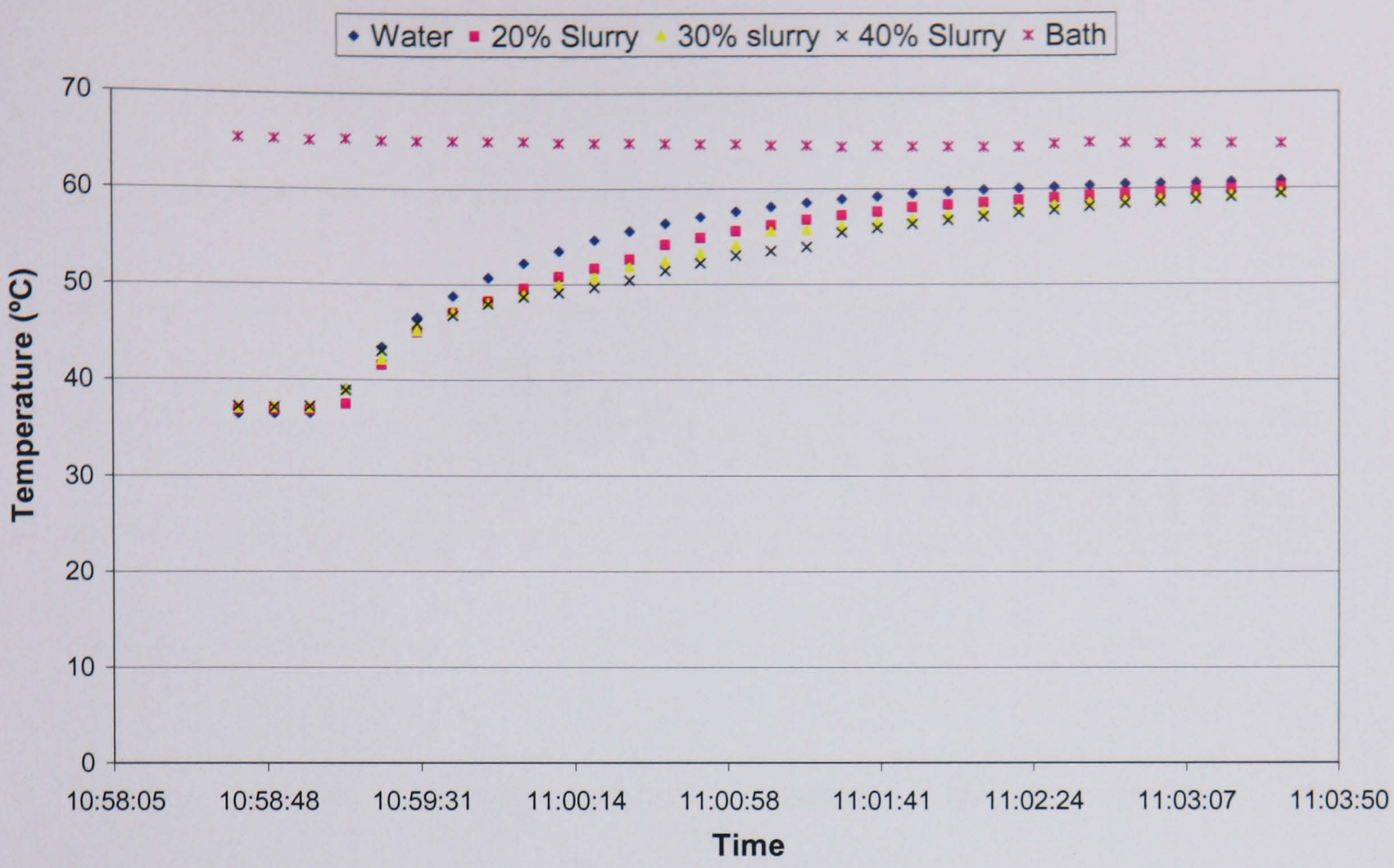

c) 50°C n-eicosane

Figure 4.14: Temperature variations of MCPCM slurries (10% to 40%) in cooling mode with a) 28°C b)35°C and c)50°C melting point

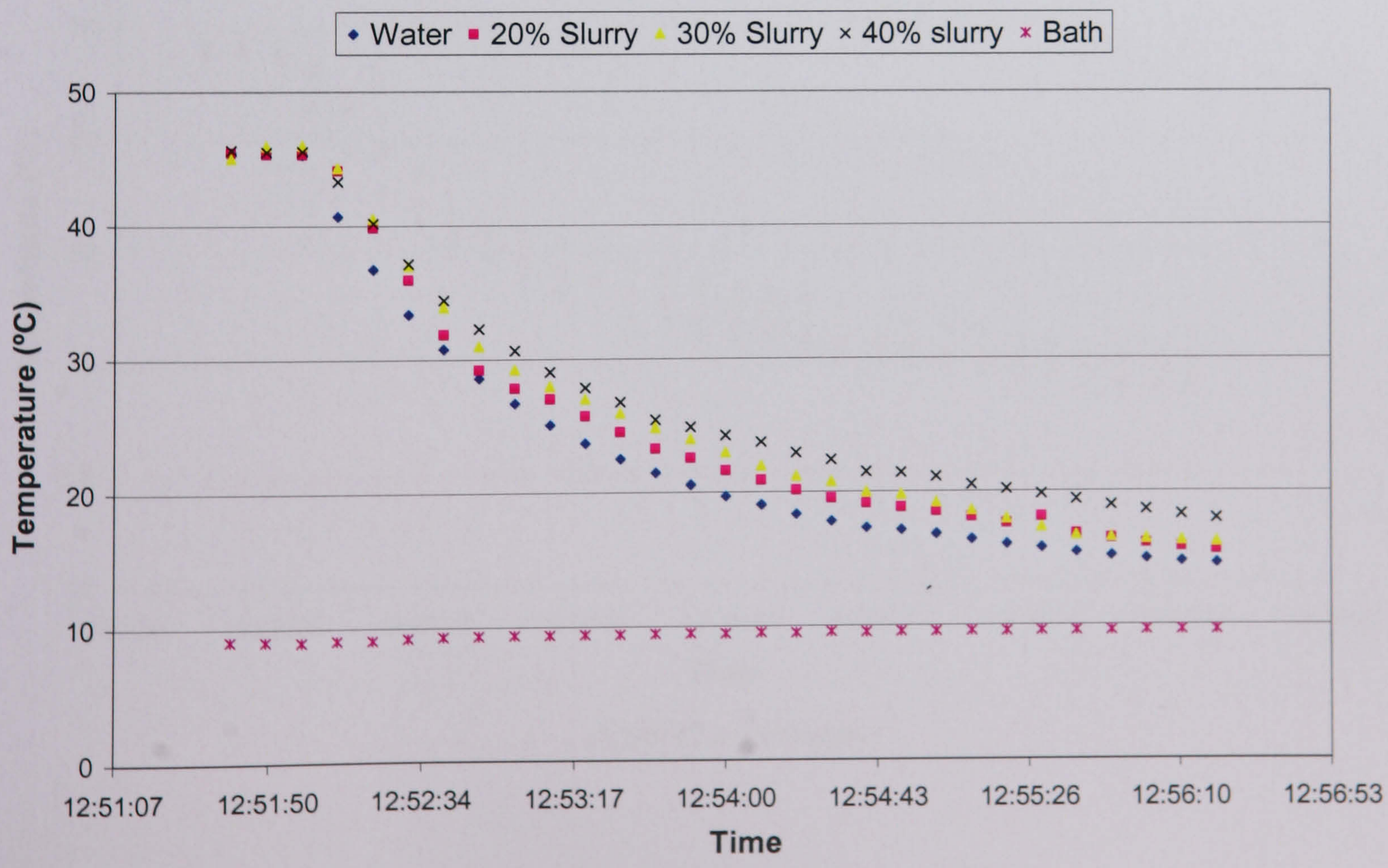

a) 28°C n-eicosane

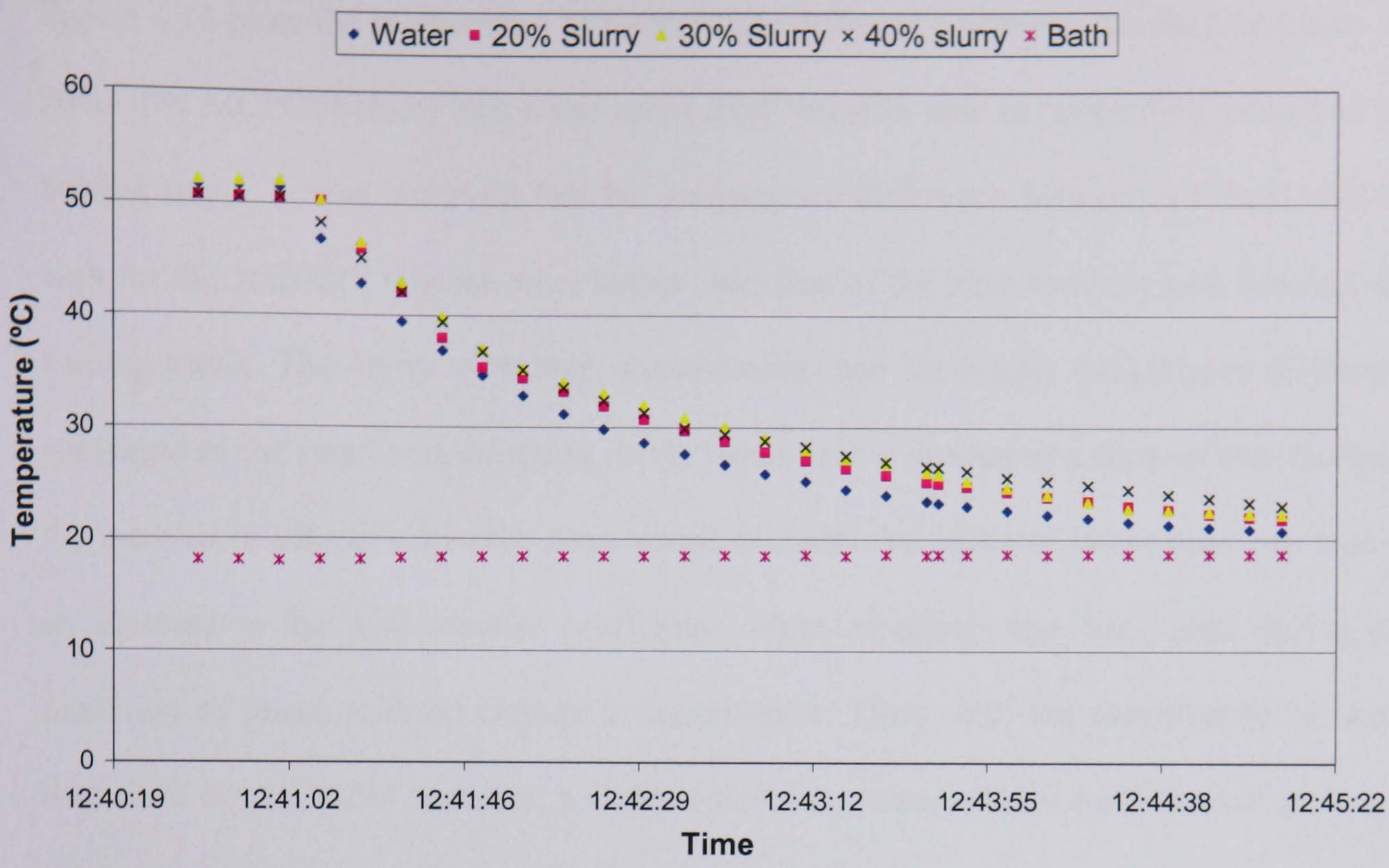

b) 35°C n-eicosane

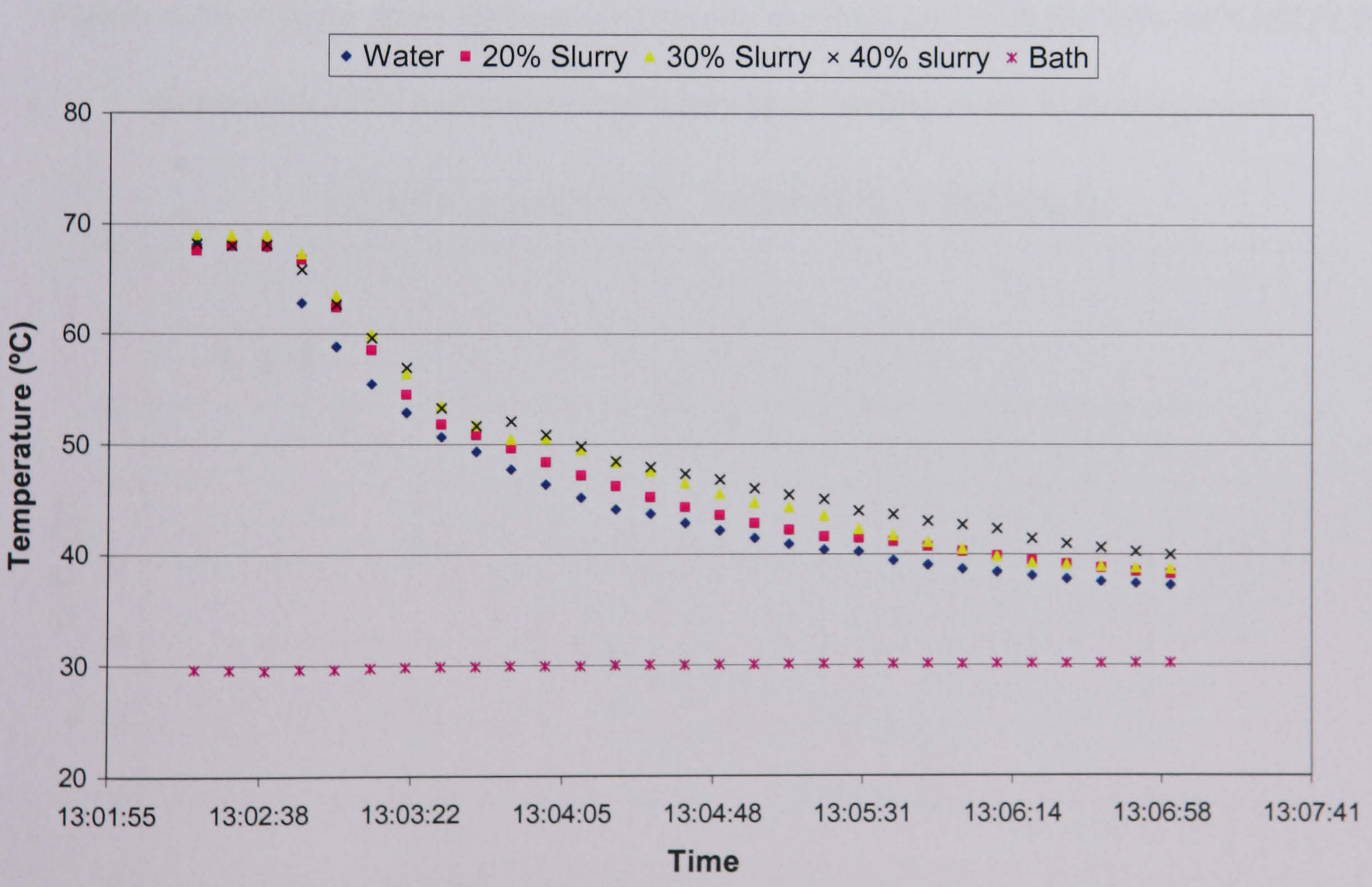

c) 50°C n-eicosane

Figure 4.15 plots the relationship of temperature difference between the fluid and bath for 20%-40% MCPCM slurry and water using 35°C paraffin wax in (a) cooling mode and (b) heating mode. It was observed that the temperature difference between the fluid and the bath for the MCPCM slurries were higher than that of the pure water in both heating and cooling mode. The slurry with high concentration had the bigger temperature difference compared to the small concentration. If the latent heat is viewed as a form of specific heat, the increase in effective specific heat, which includes the effect of latent heat, can lead to an increase in the heat transfer coefficient. Most of energy has been used during the transition of phase with no change in temperature. Thus, with the contribution of latent heat from the MCPCM particles, a slurry containing phase change particles can store and release more heat than a single phase fluid such as water.

Figure 4.15: Temperature differences between the fluid and bath for 20%-40%MCPCM slurry with 35°C n-eicosane and water in a) cooling mode b) heating mode

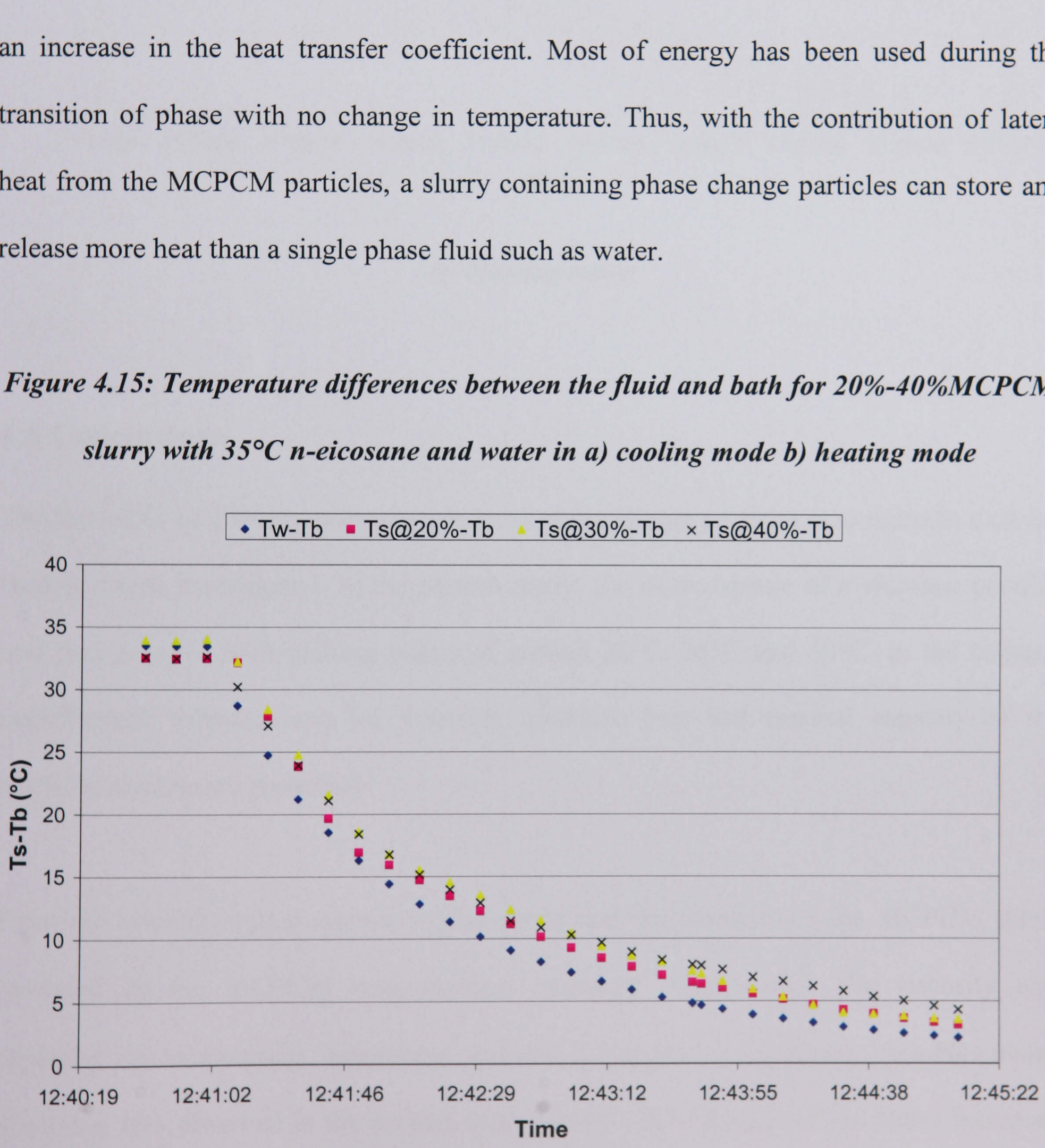

a) Cooling mode

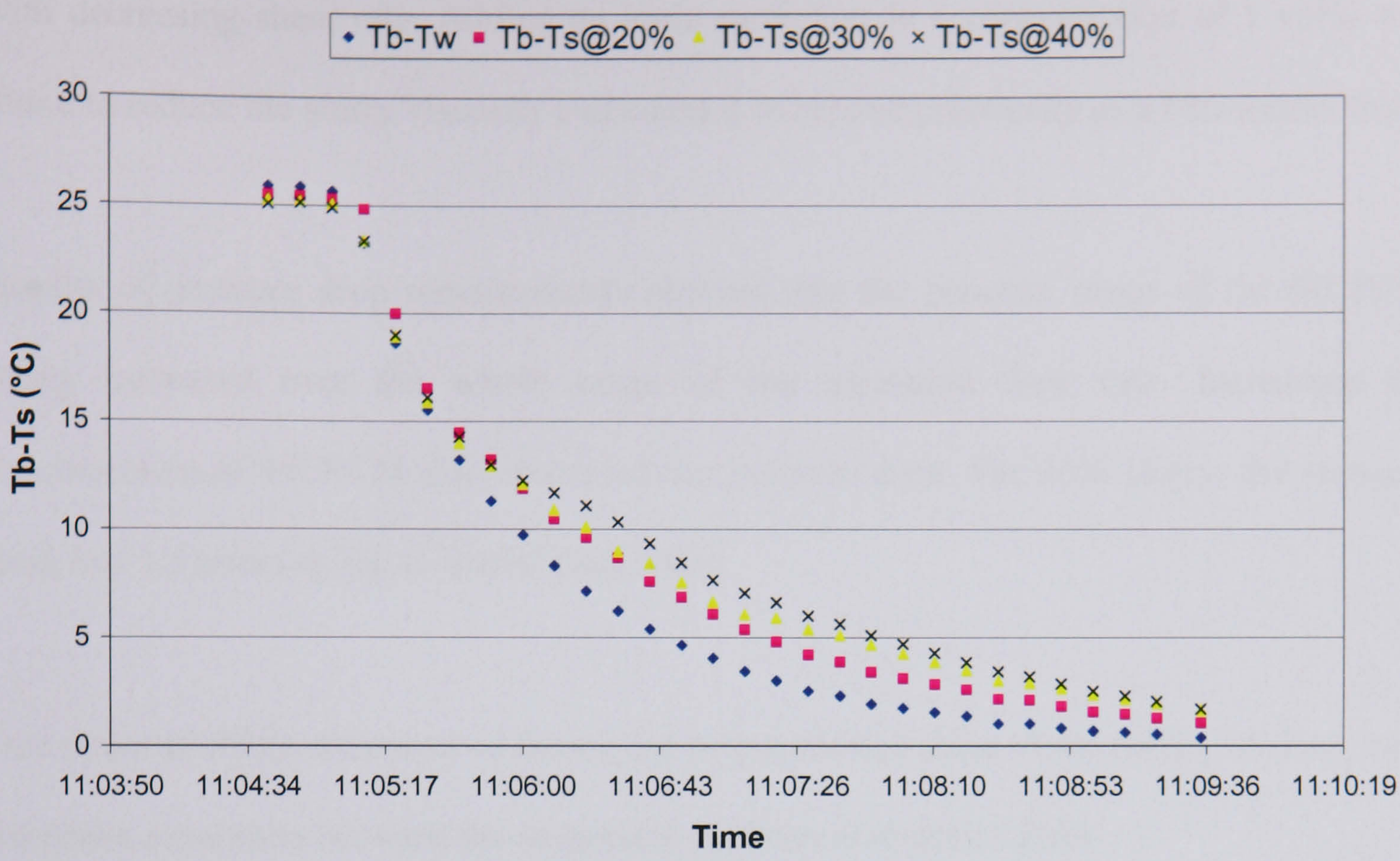

b) Heating mode

4.6 Conclusions

The feasibility of utilising microencapsulated phase change particles suspended in a carrier fluid has been investigated. In the present study, the microcapsule of *n*-eicosane paraffin wax was selected with melting points of around 28°C, 35°C and 50°C. In the context, experimental investigations for viscosity, pressure loss and thermal capacity of the MCPCM slurries are presented.

From the viscosity measurement, it was found that the viscosity of the MCPCM slurry increased as the MCPCM concentration increased. Furthermore, the viscosity also depended on temperature, decreasing with the increase in temperature. Non-Newtonian behaviour was observed in the present study whereas the viscosity of the slurry increased

with decreasing shear rate. Adding an ionic surfactant in a concentration of 1 vol% was found to reduce the slurry viscosity and cause it to behave practically as a Newtonian fluid.

Results of pressure drop measurements showed that the pressure drops of the MCPCM slurry increased over the whole range of the measured flow rate. Increasing the concentration of MCPCM also increased the pressure drop. For 20% slurry, the pressure drop was 1.5 times as big as that of pure water.

One major problem encountered during the preparation process of the MCPCM slurry was the phase separation between the suspended particles and carrier fluid.

Results from the DSC analysis showed that the latent heat of fusion for 28°C, 35°C, and 50°C paraffin waxes were 183.42, 173.75 and 162.65kJ/kg, respectively. The crystallisation temperatures of the paraffin waxes were lower than their melting point of around 2°C to 4.6°C as a result of supercooling phenomenon.

The suspension of MCPCM particles in a carrier fluid was found to increase the heat transportation of the working fluid. Results from the TA technique showed that the temperature gap between the MCPCM slurries and bath during the melting and solidification process increased with increasing concentration. This was because most of energy has been used during the transition of phase with no change in temperature. Thus, the slurries containing phase change particles could store more energy than the single phase fluid. Under isothermal condition the MCPCM slurry is suitable for use as the working fluid.

Chapter 5 An investigation of microencapsulated phase change material slurry in a closed loop system

5.1 Introduction

We can now see that the heat transportation of a working fluid can be significantly enhanced by an introduction of latent heat of fusion from suspensions of phase change particles. This chapter studies the feasibility of using a slurry containing micro encapsulated phase change material (MCPCM) of *n*-eicosane as a heat transfer fluid. The effects of repeated use of liquid-solid phase change particles upon melting and solidifying in a slurry were studied using a small-scale rig of closed loop circuit. The primary parameters for the investigation were volumetric concentrations and flow rates. The heat transportation and pumping power of the slurries were measured in order to determine the most suitable concentration of MCPCM used in the slurry. Experimental results can be found in Appendix.

5.2 Background

Parameters affecting the heat storage performance of MCPCM slurry are such as bulk Stefan number, volumetric concentration etc. The bulk Stefan number is defined as the ratio of the sensible heat capacity of the suspension to its latent heat capacity. Charunyakorn (1991) notes that the bulk Stefan number significantly dominates the heat transfer performance of the MCPCM slurry. The Nusselt number can be considerably improved 1.5-2.5 times by reducing the bulk Stefan number, which corresponds to increasing the latent heat of the slurry. The effect of increasing the concentration is twofold; it decreases the Stefan number and raises the conductivity enhancement factor.

Goel (1994) shows that the bulk Stefan number is the most dominant parameter. His results show that up to 50% reduction in the wall temperature rise can be obtained by using the MCPCM suspension in place of a single-phase fluid. He concludes that for best results, the bulk Stefan number should be maintained low ($Ste \leq 1.0$). This can be achieved either by selecting a PCM such that its ratio of sensible heat capacity is high, by increasing the concentration of the MCPCM or by reducing the duct radius. The concentration does play an indirect role in heat transfer through the bulk Stefan number.

Choi (1994) studies the effects of PCM–water slurry on the convective heat transfer coefficient in a turbulent flow and suggests that the effect of latent heat on the local heat transfer coefficients may also depend upon the slurry flow structure. In 1999, Yamagishi investigates the effect of turbulent and laminar slurry flows on local heat transfer coefficients. His results interestingly show that when flows of the MCPCM slurries are at approximately the same mean flow velocity, the flow of higher particle fraction of 15% has a lower heat transfer augmentation than the 7% MCPCM slurry. This is because the flow of 7% slurry has higher Reynolds numbers than that of the 15% slurry. However, if the particle volume fractions are the same for both laminar and turbulent flows, the heat transfer in the turbulent flow is more effective than that in the laminar flow. The heat transfer augmentation associated with phase change depends upon not only the fraction of solid particles in the slurry but upon the degree of turbulence.

The effects of duct-to-particle diameter ratio and degree of homogeneity of the suspension do not have a significant effect on the heat transfer characteristics of the phase change slurry (Goel, 1994). Two other parameters that their effects could be negligible are the

particle-to-fluid thermal conductivity ratio and modified particle Peclet number (Charunyakorn, 1991)

Recently, more papers have been published on theoretical or experimental approaches to clarify the merits of this medium. These studies focus mainly on heat capacitance and heat transfer coefficient. Although they indicate promising applications, they are limited in scope. The data necessary for engineering design of a thermal-energy system using MCPCM slurry are not available in the literature. The major challenge in applying liquid-solid PCM to a convection heat transfer system is to show how to circulate the particles continuously and successfully through the heat transfer flow loop. This study employs a small-scale rig with a closed loop circuit (see Figure 5.1b), instead of a one-way-flow rig as used by many studies (see Figure 5.1a), in order to circulate the suspension from the slurry reservoir through the test section and back to the reservoir (as used in real applications). The effects of repeated use of the slurry with liquid-solid phase change particles upon melting and solidifying can be investigated.

a)

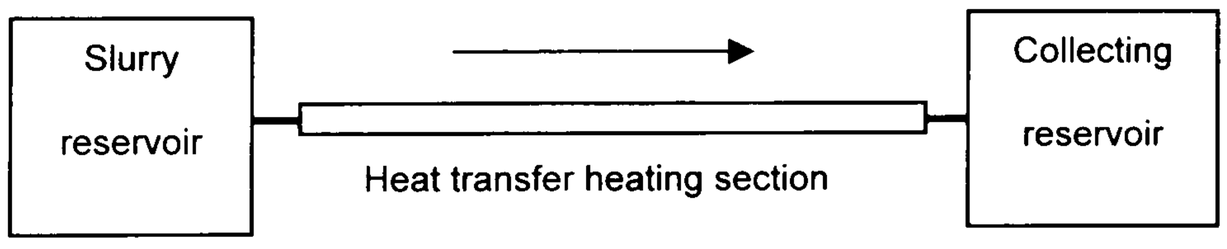

b)

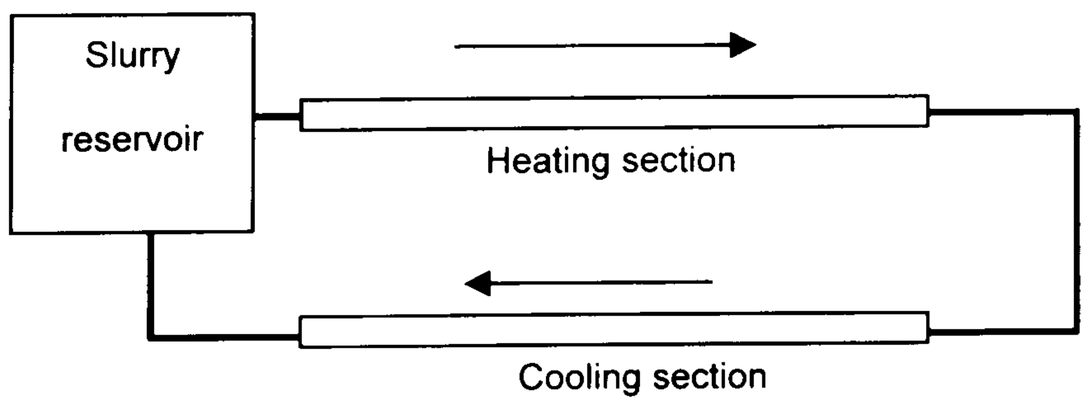

Figure 5.1: a) One-way-flow rig b) Closed loop rig

5.3 An investigation of a small scale closed loop rig

5.3.1 MCPCM slurry

The MCPCM used in this study was a paraffin wax of *n*-eicosane with a melting point of 28°C, 35 °C and 50°C. The paraffin wax was encapsulated in capsules of 15 to 40 microns in diameter. Water was used as a carrier fluid to prepare the working fluid of 5%-40% vol. concentration as shown in Table 5.1.

	Paraffin Wax	Melting Temperature (°C)	Density (kg/m^3)	Latent heat (kJ/kg)	MCPCM Slurry Concentration (%Vol.)				
1	*n*-eicosane	28	894	186	5%	10%	20%	30%	40%
2	*n*-eicosane	35	899	180	5%	10%	20%	30%	40%
3	*n*-eicosane	50	897	160	5%	10%	20%	30%	40%

Table 5.1: Physical properties of the MCPCM particles

(Frisby Technologies Inc., 2004)

5.3.2 Experimental apparatus and method

Figure 5.2 and 5.3 shows the schematic diagram and the experimental apparatus of the system, which consists of a slurry reservoir, a heating reservoir, a hydrodynamic entry and heat transfer test section, a cooling heat exchanger, an electric mixer, a static mixer, a double-diaphragm pump, a turbine flow sensor, a breath valve, two heaters, a voltmeter, an ammeter, an AC power supply, and a power meter. The heating reservoir was filled with water and insulated with 19-mm neoprene insulation to prevent heat loss. Two 3kW-heaters were mounted at the bottom of the heating reservoir to continuously supply heat for the system and were monitored by the volt and amp meter. To ensure the uniform temperature of hot water in the heating reservoir, a submersible pump was installed to

circulate the hot water from the bottom of the tank into the surface (the heaters were fitted at the bottom of the tank).

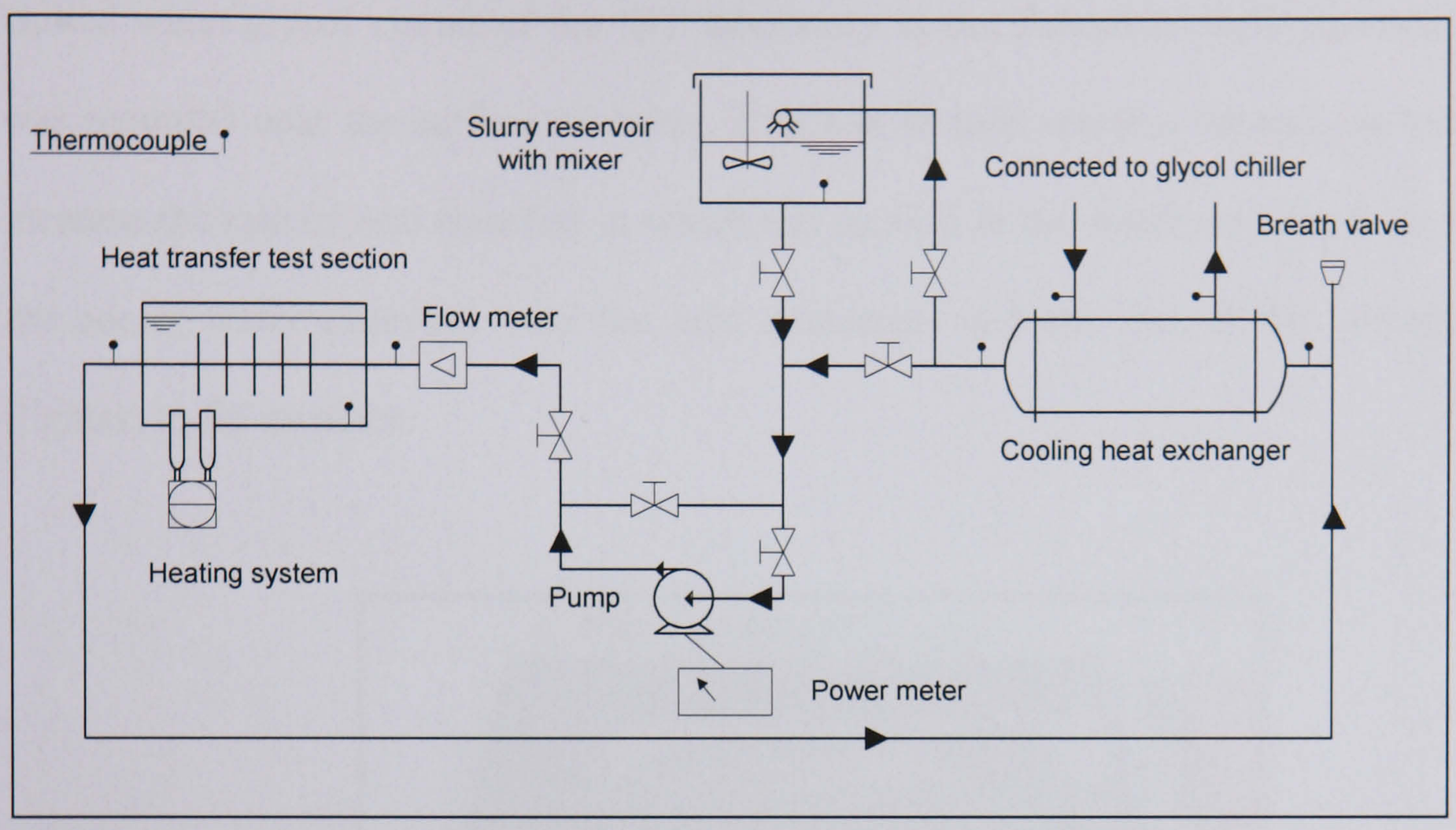

Figure 5.2: Schematic diagram of the small scale rig

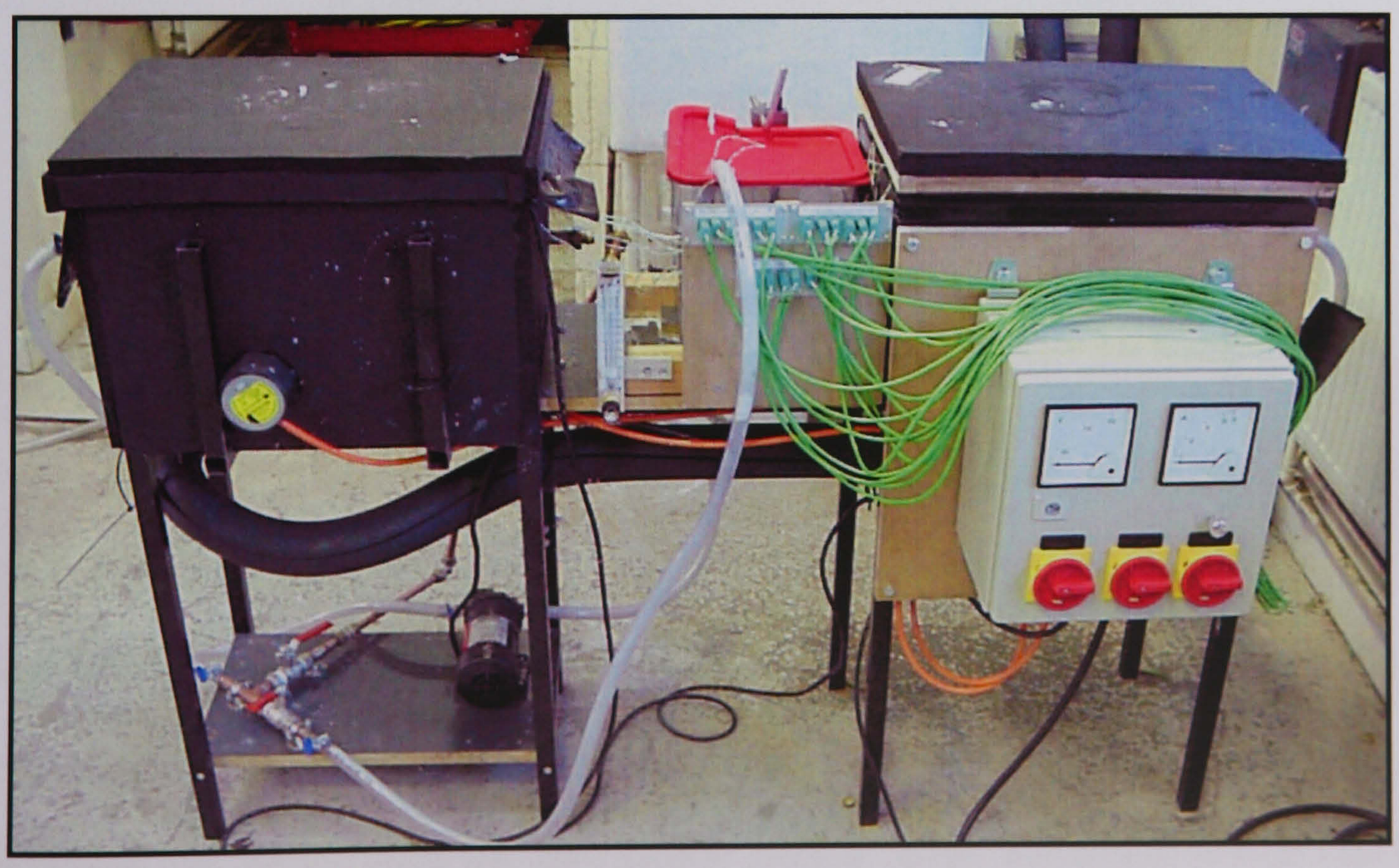

Figure 5.3: Experimental apparatus

The cooling heat exchanger is illustrated in Figure 5.4 which connected to the closed-loop chilled water/glycol circuit of the IBT laboratory in the School of Built Environment. It was mounted near the surface of water. This was to help create a natural convection (to increase the rate of heat transfer) in which any motion in the water was due to the sink of the cooler water (heavier) near the heat exchanger and the rise of the warmer water (lighter) to fill its place.

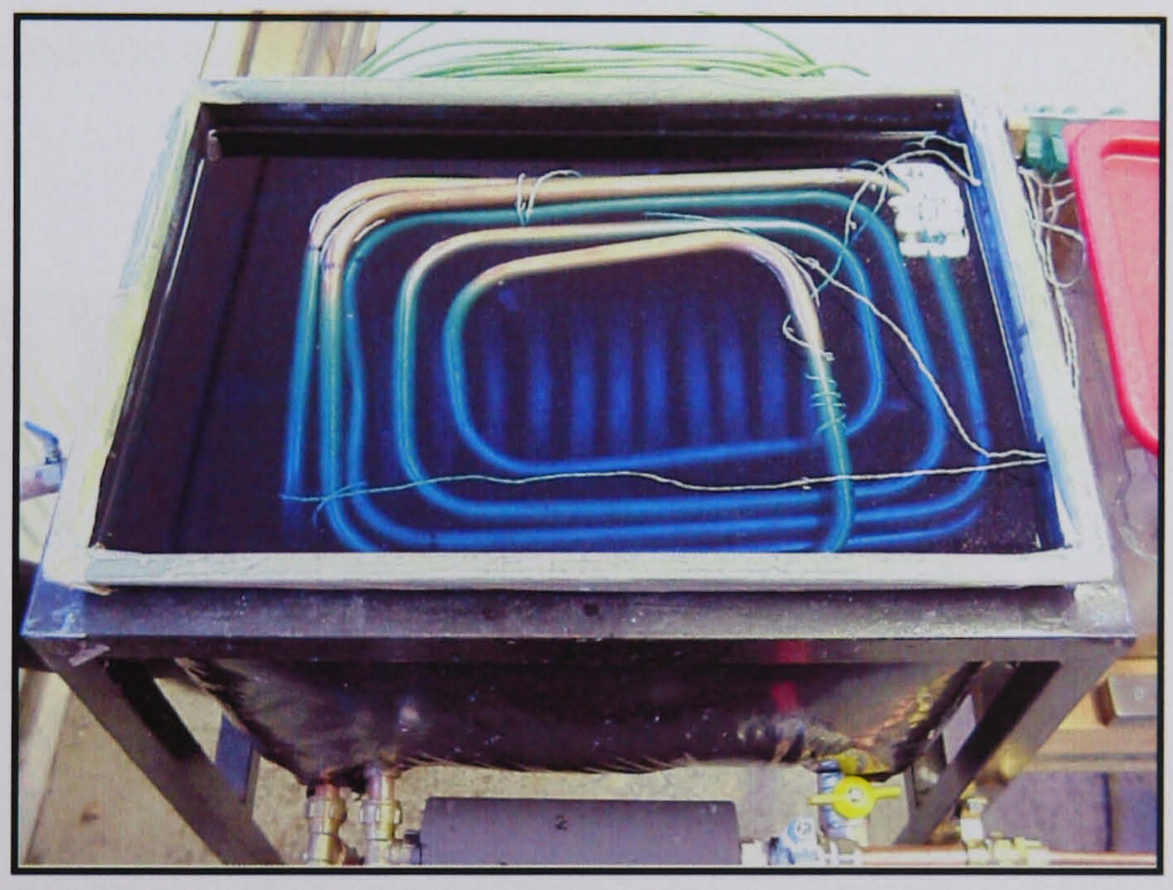

Figure 5.4: Cooling heat exchanger

The power meter was used to monitor the power consumption of the pump. The electric mixer was used at the beginning of the test in the slurry reservoir to mix the water and MCPCM into a homogeneous mixture. The static mixer was installed between the cooling heat exchanger and the test section in order to ensure a well mixed suspension. The temperature of the slurry at the inlet and outlet of the test section and cooling reservoirs, including the temperature of the glycol chillier were monitored using the K-type thermocouples attached to the outer tube wall. They were taped securely to the pipes and

insulated. The thermocouples were connected to a DT500 datalogger, which downloaded information onto a PC by means of an RS-232 interface and the DeLogger Plus software. All thermocouples were scanned every 5 seconds.

The heating heat exchanger was made up of a helically coiled copper tube (with a diameter of 12 mm and a wall thickness of 0.8 mm) as illustrated in Figure 5.5. The length of the tube was found to be approximately 330-350 diameters. The hydrodynamic entry section was 15-20 diameters to ensure that the flow entering the test section was developed. A submerge pump was used in the reservoir to help circulating warm water through out the tank to achieve the uniform temperature.

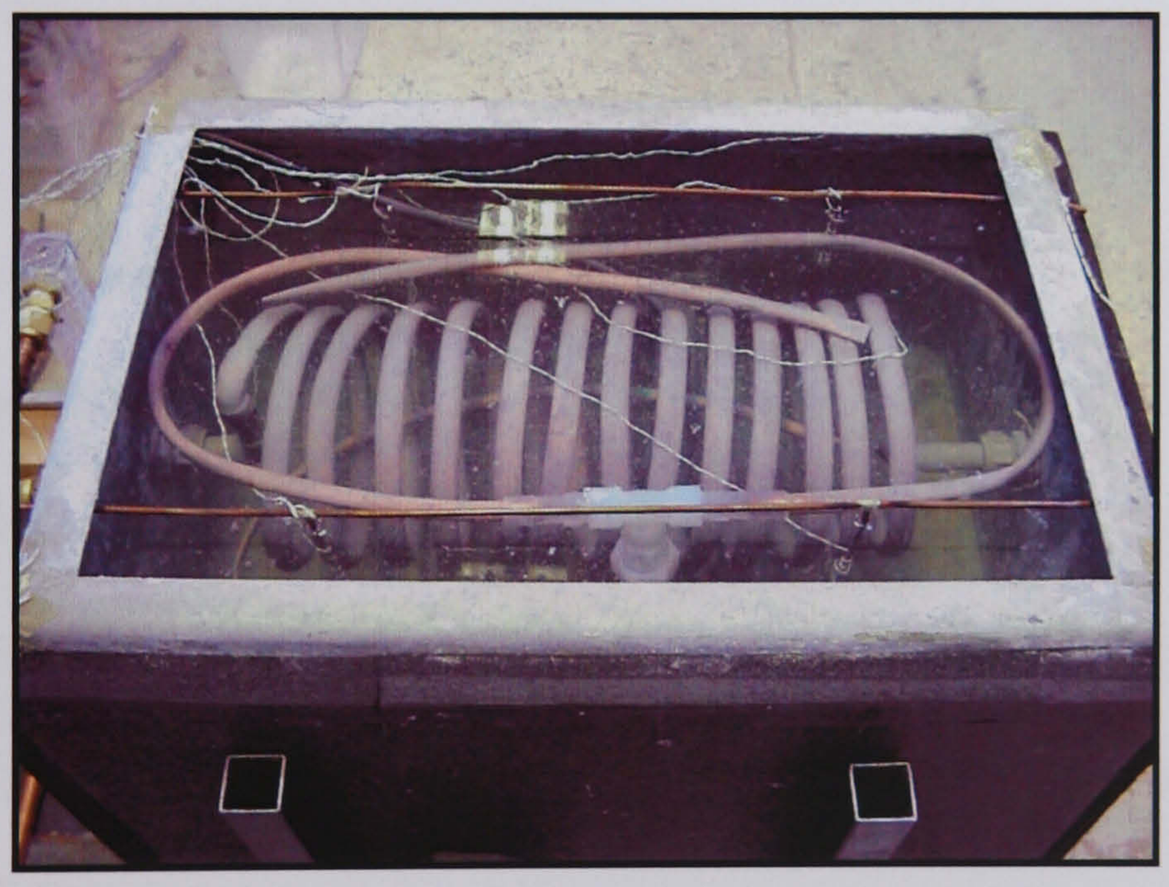

Figure 5.5: Helically coiled tube heating test section

Ali (1998) carries out a study on heat transfer coefficient inside the coils since the criterion for transition from laminar to turbulent in curved pipes is established. He studies a steady state natural convection from uniformly heated helical coiled tubes and notices that laminar regime starts first followed by transition to turbulent regime almost at the middle of the coil. This laminar regime is characterised by a decrease in the heat transfer coefficient

while transition to turbulent regime is characterised by a wave variation of average heat transfer coefficient with increasing the number of coil turned. The heat transfer coefficient in the fully developed flow region of the helically coiled tube does not remain constant as found in the straight tube.

Chen (1999) also reports that the flow patterns in horizontal helically coiled tubes may change along the axial length compared to the flow characteristics in a horizontal straight pipelines because of the combined effects of gravitational and centrifugal forces. He notes that the flow characteristics in helically coiled tubes are very complex and unique due to the combination effects of gravitational and centrifugal forces, especially in a horizontal coiled tube, where the angle between the gravity and centrifugal forces changes along the axial direction within one turn.

Notably, the present study did not investigate the effect of turbulent or laminar flows on heat transfer characteristic of the MCPCM slurry due to the complexity of the flow inside the helically coiled tubes. The primary parameters for the investigation were MCPCM volumetric concentration and various flow rates. A curve for heat transfer with a single-phase fluid was presented so that the standard single-phase results can be compared with those of the MCPCM slurry.

The rate of convective heat transfer into the flowing slurry can be calculated by *Newton's law of cooling*, $Q=hA(T_s-T_f)$, or the conservation of energy equation, $Q=\dot{m}\,C_p(T_o-T_i)$, where Q is the rate of heat transfer, h is heat transfer coefficient, m is mass flowrate, C_p is specific heat, A is surface area and T is temperature. In the case of pure water, the local bulk mean temperature can be easily estimated from a linear temperature rise along the test

section under the condition of uniform heat flux. When no phase change is involved in the slurry, the temperature at any location in the test section can be readily calculated. However, when a phase change occurs, the temperature rise across the melting temperature of *n*-eicosane is not linear because of latent heat (neither the local heat transfer coefficient, nor the thermal capacity is constant along the flow direction).

The experiment was conducted to monitor the rate of heat transfer into the system provided by the heaters, instead of measuring the rate of heat removed from the system by the flowing slurry (see Figure 5.6). This was to minimise uncertainty in the measurements of local bulk mean temperature of the slurry during phase change. Under a steady state condition, the change in total energy of the control volume during a process is zero. The amount of energy leaving the control volume from the flowing slurry plus heat losses must be equal to the amount of energy entering it (from the heaters). Hence, the heat transportation of phase change slurry can be determined from the rate of heat transfer into the system provided by the heaters minus heat losses.

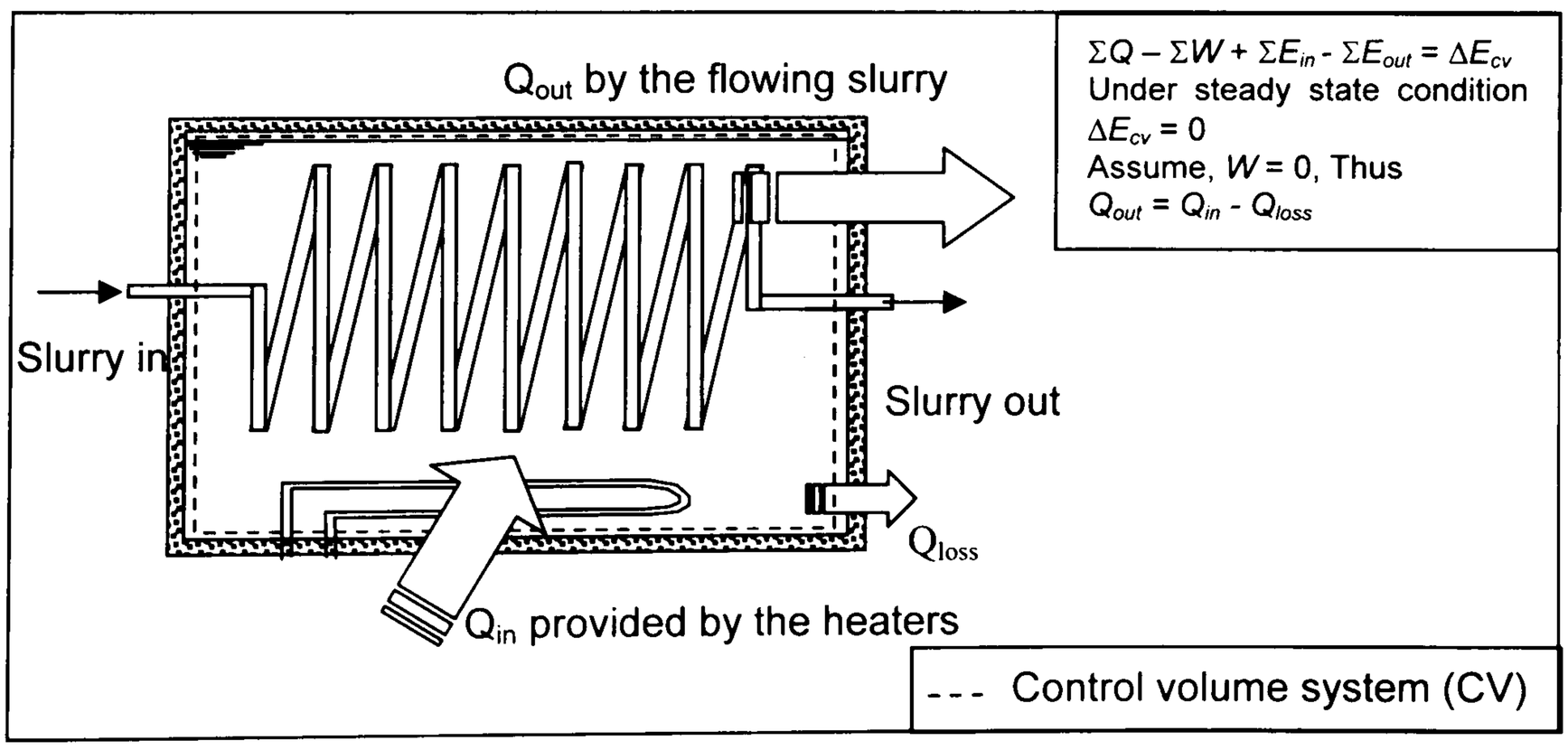

Figure 5.6: Control volume system of the test section

When the slurry was circulated through the test section at a certain flow rate, the experiment was carried out by adjusting the current of AC power supply of the heaters (connected to the ammeter rated at 25A max) until the steady state condition of the heating reservoir was achieved. The thermal steady state was judged when the temperature of water inside the heating reservoir remained constant for at least 10 minutes. Six K-type thermocouples were used at different locations to indicate the temperatures of water.

Flow rates of the slurry were measured in a volumetric unit by a turbine flow sensor, and were in the range of 2 to 6 l/min. The slurry was circulated through the heating test section where the solid PCM in the shells melted into a liquid phase releasing latent heat (see Figure 5.7). To ensure that the entire phase change phenomenon occurred in the test section, the temperature of the slurry leaving this section was maintained above the PCM melting point. The slurry was then pumped through the cooling coil heat exchanger where the liquid particles re-solidified. The temperature of the slurry leaving the cooling section was maintained below the solidification temperature of *n*-eicosane by 4°C due to the supercooling phenomena.

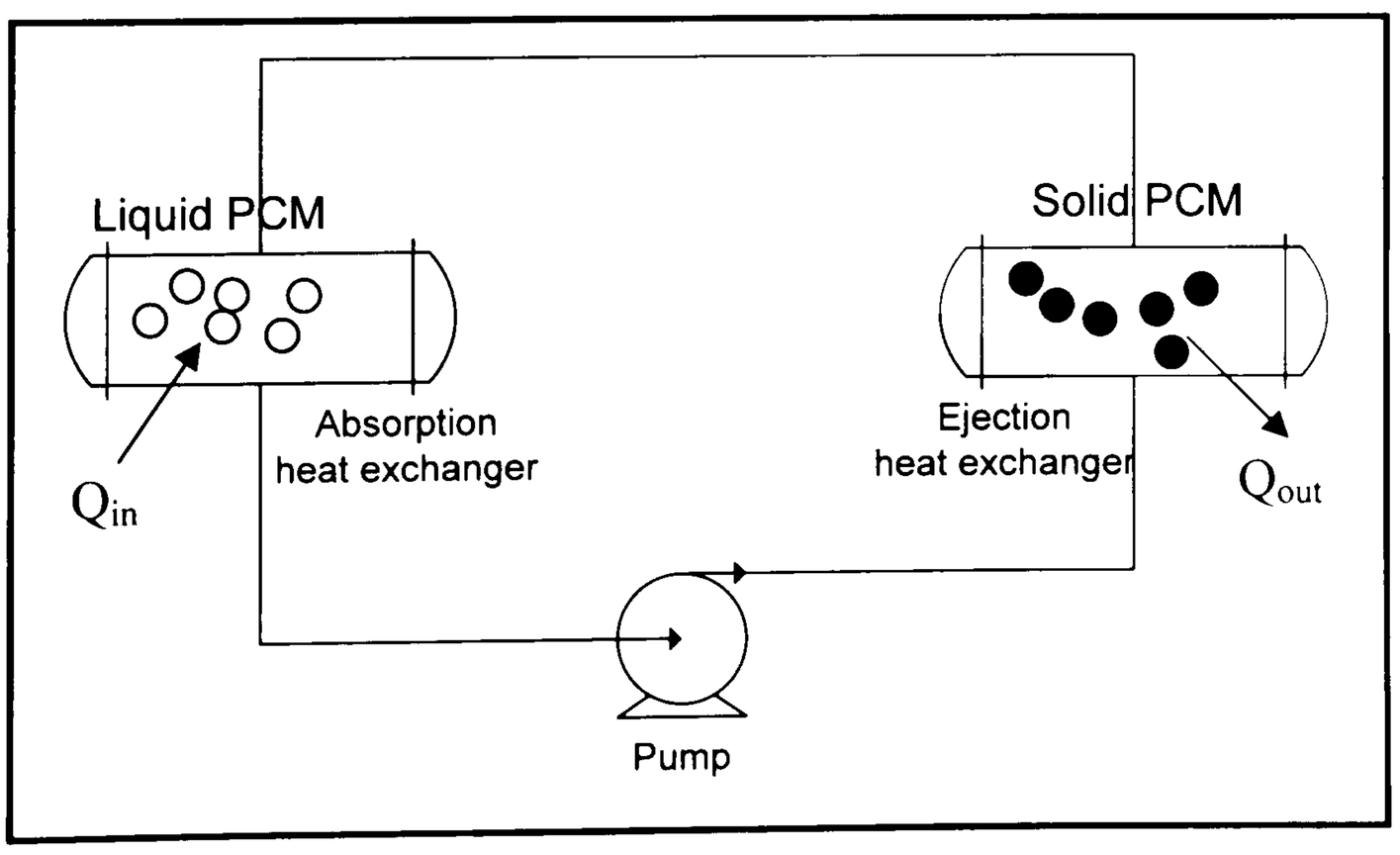

Figure 5.7: Melting and solidificantion of phasse change particles

5.3.3 Summary of data acquired

Operational problems encountered during experimental measurements are summarised as following. In an initial test, there was a problem concerned with the use of a variable area flowmeter. A float in a transparent tapered tube made a very simple flowmeter, but with the MCPCM slurry, the float could not be seen because of an opaque colour of the slurry. This resulted in a difficulty for indicating the correct flowrates. As the flow varied, the float rose or dropped along a guide rod. In case of water, it easily moved through the float with virtually no fluid sticking to the float. However, when the slurry containing the suspended particles (higher viscosity than water) made its way through the float, some particles could stick to the float and guide rod building layer upon layer. This effect would not permit the float to move freely along the guide rod and could result in reading errors.

Studies show that the floated flowmeter accuracy can quickly degrade due to changing in density and viscosity of liquid. Even the viscosity is only 15 centipoises the variable area flowmeter that calibrates for water read two times too high. At higher viscosities, this effect is even more pronounced. This is because at constant flow, the float is in equilibrium between the upward force of the fluid and the downward force of gravity. As the fluid viscosity increases and creates layers of fluid drag zones, each with a different relative velocity. This effect will cause a slow moving viscous liquid to yield the same buoyant force as a fast moving low viscosity liquid and reduce in accuracy of measurement (Swearingen, 1998).

A flow technology that relies on some static property of the fluid, like conductivity, incompressibility or heat capacity can be used. One technology such as an oval gear flowmeter that uses the property of incompressibility results a high accuracy and is almost

negligible effects of varying fluid viscosity, density and temperature. During operation, each gear rotation in the oval-gear meter traps a pocket of fluid between the gear and the outer chamber walls. However, with the MCPCM slurry there is a risk of the particles passed through the gear teeth and being crushed. Alternatively, turbine flowmeters are high accurate. The advanced technology will allow the meter to automatically compensate for viscosity and density effects and can be used with small particles. However, with infrared turbine flow sensors, the fluid must be clear or translucent liquid capable of transmitting IR light. With MCPCM slurry, the colour of slurry could have an effect on the accuracy of the device.

The flowmeter used in the present experiment was the turbine type (the Blancett Model 220210), using magnetic pick-up and pre-amplifier. It works as fluid moving through the turbine flow meter causes the rotor to rotate at a speed proportional to the fluid velocity. As rotor blades pass though the magnetic field produced by the magnetic pick-up, the pick-up will generate a frequency signal proportional the rate of flow. This allowed the meter to automatically compensate for viscosity and density effects and was suitable for use with small particles of up to 250-micron.

Another problem found in the experiment was the stratification of solid particles in the carrier fluid caused by gravity or centrifugal forces (see Figure 5.8). During the preparation process, phase separation between water and the particles was observed in the slurry reservoir. Because the density of suspended particles was smaller than the density of water, the particles naturally rose to the surface. This phenomenon could reduce a number of phase change particles flowing back into the system which decreases the use of latent

energy. To overcome the problem a method combining both open and closed systems was introduced.

Figure 5.8: MCPCM particles float at the surface (non homogeneous suspension)

The criterion used in the experiment was to divide the operation into three stages. The first stage used the open system to prepare the MCPCM slurry before feeding them into the system (Figure 5.9a). The mechanical mixer was used in the slurry reservoir to mix the slurry into homogeneity. A 1% additive was also added to reduce the slurry viscosity. During operation, the system was switched to stage II, the close system, where the slurry path was diverted from the slurry reservoir. In this case the slurry was only circulated inside the piping system of a closed loop circuit (Figure 5.9b). Thus, without the slurry flowing back into the container, there was no place for the particles and carrier fluid to be separated. Forced circulation from a pump could also help to stir and mix the solution. Stage III of the operation involved switching the system to the open system again. In this stage the mixer was turned off in order to deposit most particles back into the container and so prevent particle blockage, especially at the junctions. Because such particles of MCPCM are slightly sticky and can stick together to form large lumps, clogging often

occurs in a piping system, resulting in failure to circulate the slurry through the system (see Figure 5.10).

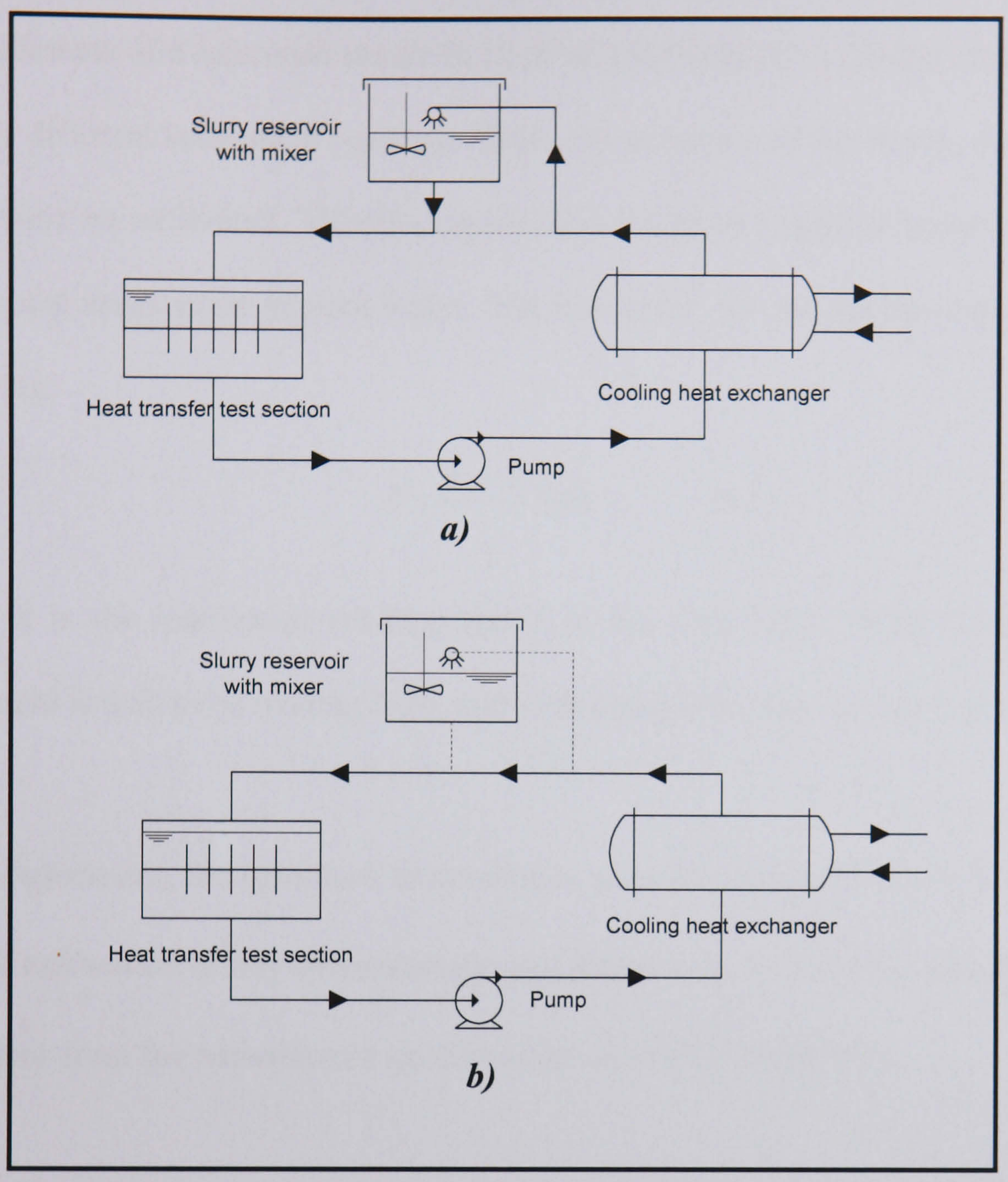

Figure 5.9: a) Open system b) Closed system

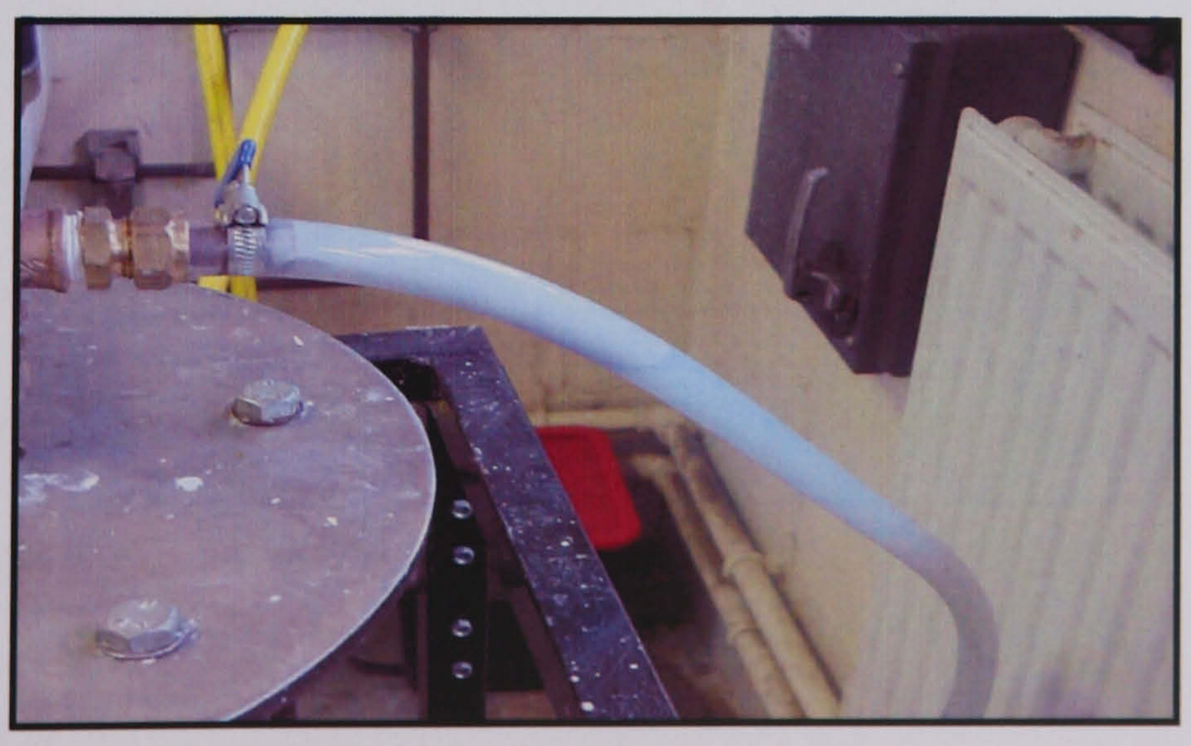

Figure 5.10: Phase change particles separated from water forming sticky large lumps clogging the pipe

5.3.4 Calibration and verification

Errors are inherent in all measurement. Even under ideal conditions, repeated measurements of a reference standard, such as a standard mass placed on a scale, will give slightly different instrument readings. Thus, the accuracy of the device used in the present study must be calibrated. Thermocouples were calibrated against known temperatures of the ice and steam point of pure water. The bias error[2] for the devices can be calculated as following;

$$B = \frac{I_i - I_t}{I_t} 100 \qquad (5.1)$$

where I_i is the instrument reading and I_t is the true value. With a positive bias, the instrument is said to be reading high, and with a negative bias reading low.

In the experiment, the operation temperatures were in a range of 10-60°C and the average error of calibration of any thermocouple was found to be ± 0.251°C. The figure falls in the limit error from the manufacture specification of ± 0.375 (0.0075T).

The flowmeter was calibrated using static weighing method to establish the relationship between the meter indicated flow rate and the measured true rate. The working fluid was diverted into the collecting tank for a fix period and the tank can then be measured with the fluid static in the tank. The net mass of fluid was divided by the measured diversion time to obtain the true mass flow rate. The average error was found to be –6.4% that agreed well with the manufacturer's claim at ±7%.

---

[2] The different between the most likely value (the average) and the true value, as established by a reference standard, is the bias error (Miller, 1989).

To reduce heat losses from the controlled system, the tank was enclosed with 19-mm neoprene insulation. The rate of heat losses of 28.22W was found. Comparing to the operation heat input of 1200W the above figure can be neglected.

At first, the apparatus was verified using water as the heat transfer fluid to check the accuracy of measurements. The test was conducted with the flowrate of 2l/min, the bath temperature of 50°C and the water inlet temperature of 30°C. Results showed that the energy balance, which defined as the ratio of the rate of heat removed by the working fluid to the electrical energy supply, was in the big deviation of 30% ($Q_{in}=i*v=10\times242=2{,}420$W and $Q_{out}=\rho \dot{m} C_p \Delta T=997\text{x}2/60/1000\times4180\times(43.5\text{-}31.4)= 1{,}680$W). This discrepancy led to a more careful evaluation of the experimental apparatus. Thus, the heating system which provided the heat input, Q_{in}, was calibrated.

Notably, the experiment was carried out under the steady state condition, in which the temperature in the controlled system did not change with time. However, to calibrate the heating system, the controlled system was considered as in a transient state condition, in which the temperature of the system varied with time (assuming that the temperature remained uniform throughout the system at any time). Thus, the rate of heat transfer into the system during Δt must be equal to the increasing energy of the system during Δt (neglecting heat losses).

The calibration was carried out with the heat inputs (Q_{in}) of 1,200, 2,400, 3,600 and 4,800W, which were monitored by the voltmeter (reading at 240V) and the ammeter (reading at 5, 10, 15 and 20A). The increasing energy of the system (ΔE) was determined when the temperature of the system rose by 10°C. The rate of heat transfer was calculated

by dividing ΔE with the measured diversion time (Δt). Results were compared with the rate of heat input indicated from the voltmeter and the ammeter. For example, at Q_{in} = 1200W, the voltmeter and the ammeter were indicated at 240V and 5A, respectively. The result showed that it took 38 min to raise the temperature of the system from 20°C to 30°C. Thus $\Delta E/\Delta t$, defined as $mC_p\Delta T/\Delta t$, was 686W. Comparing to the indicated heat input of 1200W the error was found to be 43%. Table 5.2 shows the average data of calibration and the bias error. Figure 5.12 shows the correction factor of the heating system, which plots against the indicated Q_{in}. The device was considered accurate with the correction. Keeping this in mind, the correction factor has been applied to all results presented in this paper.

	Q_{in} (W)	$\Delta E/\Delta t$ (W)	%Error
I = 5, V = 242	1210	627	48.18
I = 10, V = 245	2450	2187	10.73
I = 15, V = 245	3675	3509	4.52
I = 20, V = 243	4860	4412	9.22

Table 5.2: Results of the heater calibration

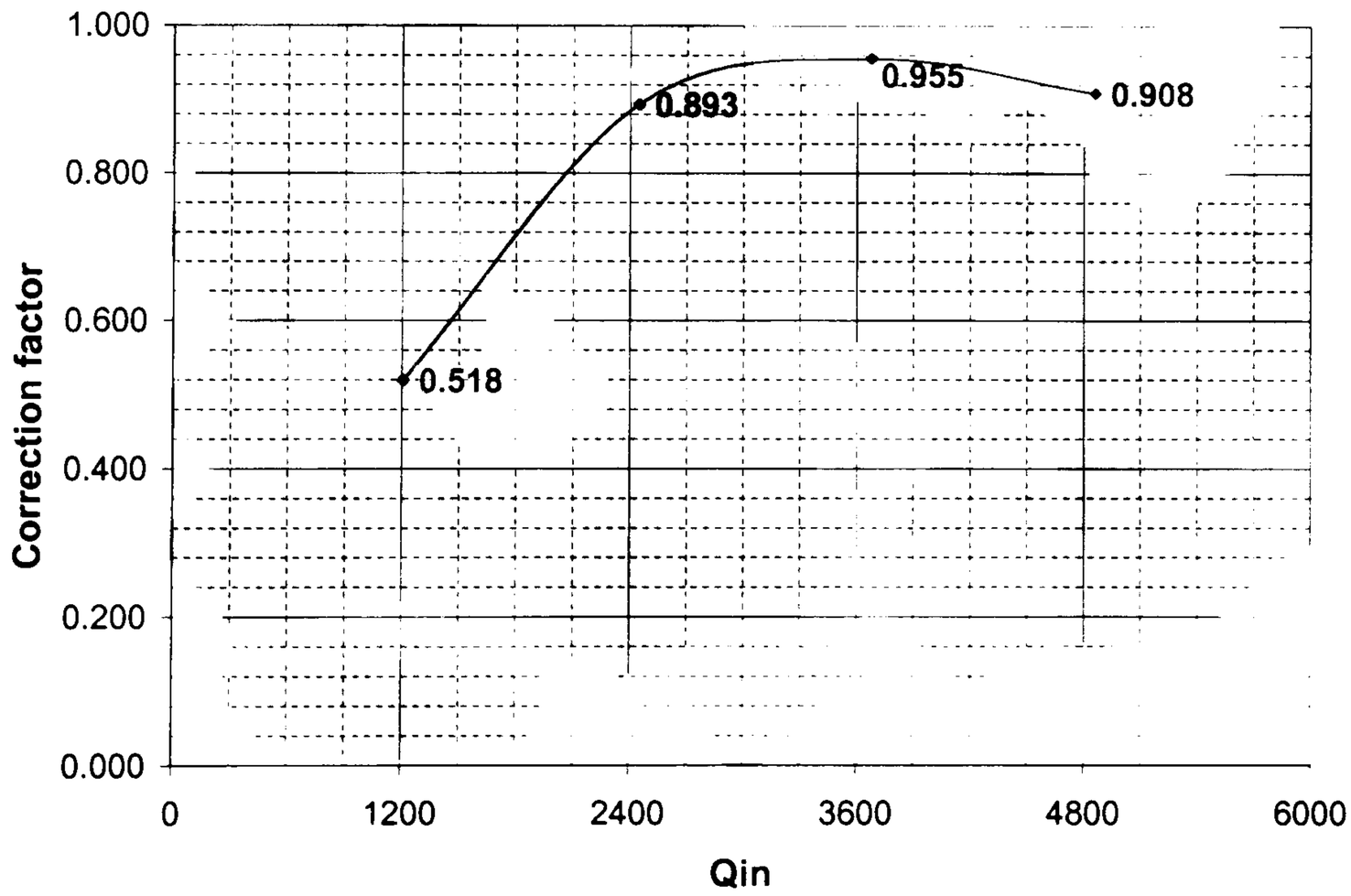

Figure 5.11: Correction factor for the heating system

5.4 Heat transportation of MCPCM slurries

5.4.1 Heat transfer characteristic

Figure 5.13a, b and c show local bath temperatures measured at six locations using water as the working fluid with the flowrate of 2 L/min and the inlet temperature of 30°C. The heating rates applied for the test were 2.662 kW (high Q_{in}), 2.178 kW (low Q_{in}), and 2.420 kW (medium Q_{in}), respectively. It can be seen that the curve of the local bath temperature increased linearly in Figure 5.13a, decreased gradually in Figure 5.13b and remained constant at 50°C in Figure 5.13c. Figure 5.13a and b imply that the systems were not in the steady state condition because the change in total energy of the control volume during the process was not zero. The curve with the increasing temperature showed that the electrical power input was higher than the thermal energy removed by the water and vice versa with the decreasing graph. To achieve the steady state condition either the flowrate or the heating rate should be adjusted. In the present study the flowrate was fixed so that only the heat input was adjusted to determine the thermal equilibrium of the system. Figure 5.13c shows that the rate of heat transfer provided by the heaters was in equilibrium to the rate of heat removed by the water (achieving the steady state condition).

Figure 5.12: The local bath temperature using water as the working fluid with the flowrate of 2 L/min and the inlet temperature of 30 ℃ with a) the heating rates of 2.662 kW (high Q_{in}), b) 2.178 kW (low Q_{in}), and c) 2.420 kW (medium Q_{in})

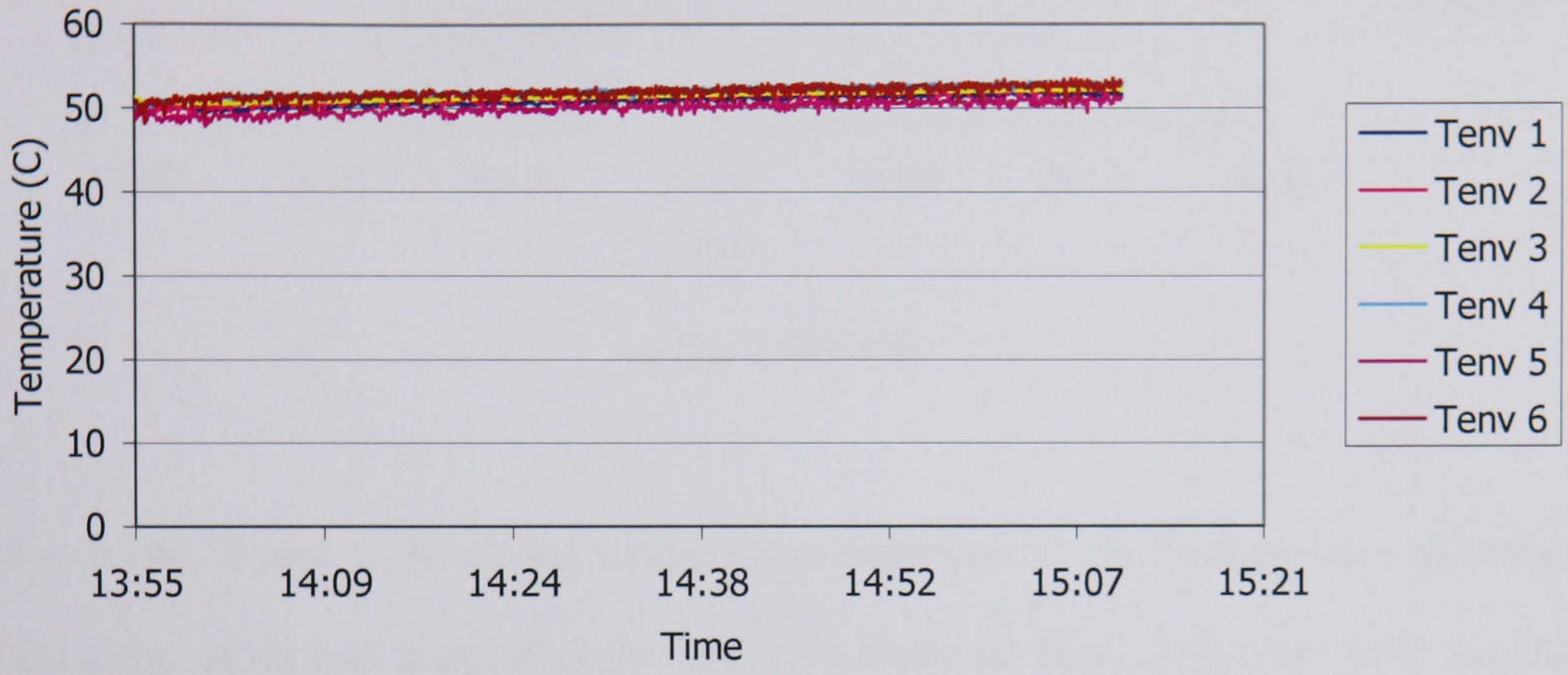

a) Q_{in} 2.662 kW

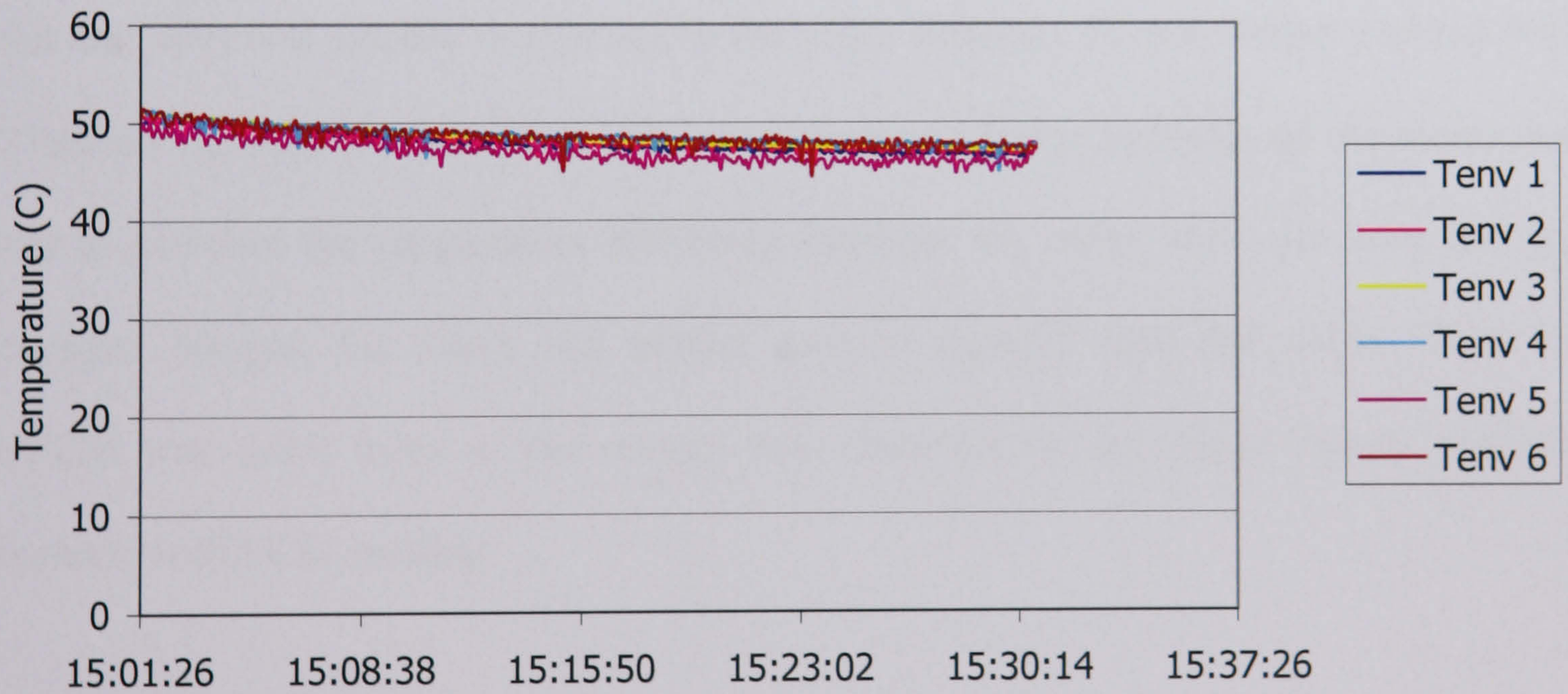

b) Q_{in} 2.178 kW

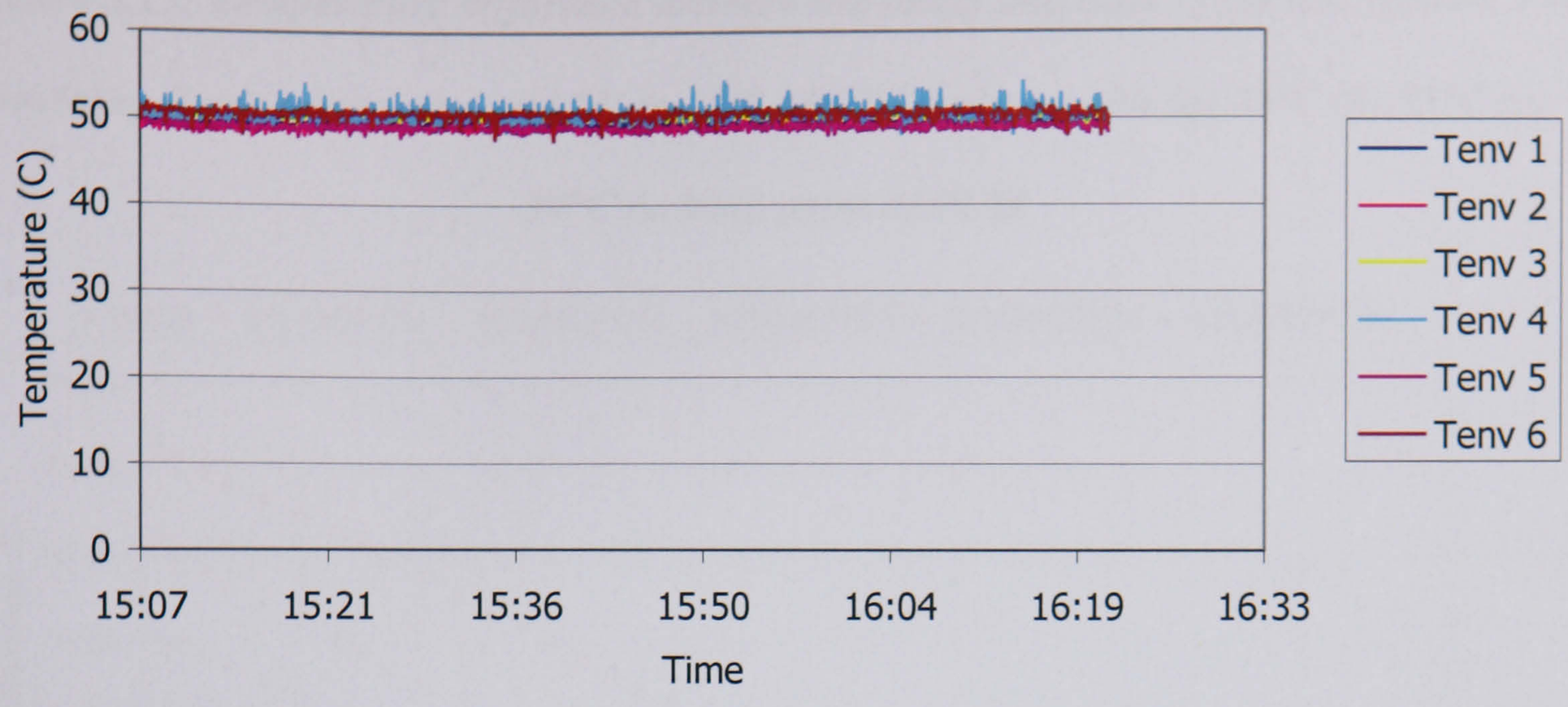

c) Q_{in} 2.420 kW

Figure 5.14a, b and c shows the temperature difference at the heating heat exchanger between the outlet and inlet using the MCPCM slurry of 28°C, 35°C and 50°C paraffin wax, respectively. A graph of pure water was presented in order to compare the result with the phase change slurries. At high flowrate, 6l/min, the temperature difference between the outlet and inlet was smaller comparing to the small flowrate, 2l/min, which resulted from the increase amount of mass flow. The use of phase change particles of the slurry was found to decrease the temperature difference between the outlet and inlet from the heat exchanger, because the slurry had greater thermal capacity than the water. When the MCPCM was used, most of the energy was absorbed by the phase change particles associated with PCM melting.

Figure 5.13: Temperature difference between the outlet and inlet of the test section. The working fluids were water and 5% to 40% MCPCM slurry with (a) 28°C (b) 35°C (c) 50°C melting point of PCM

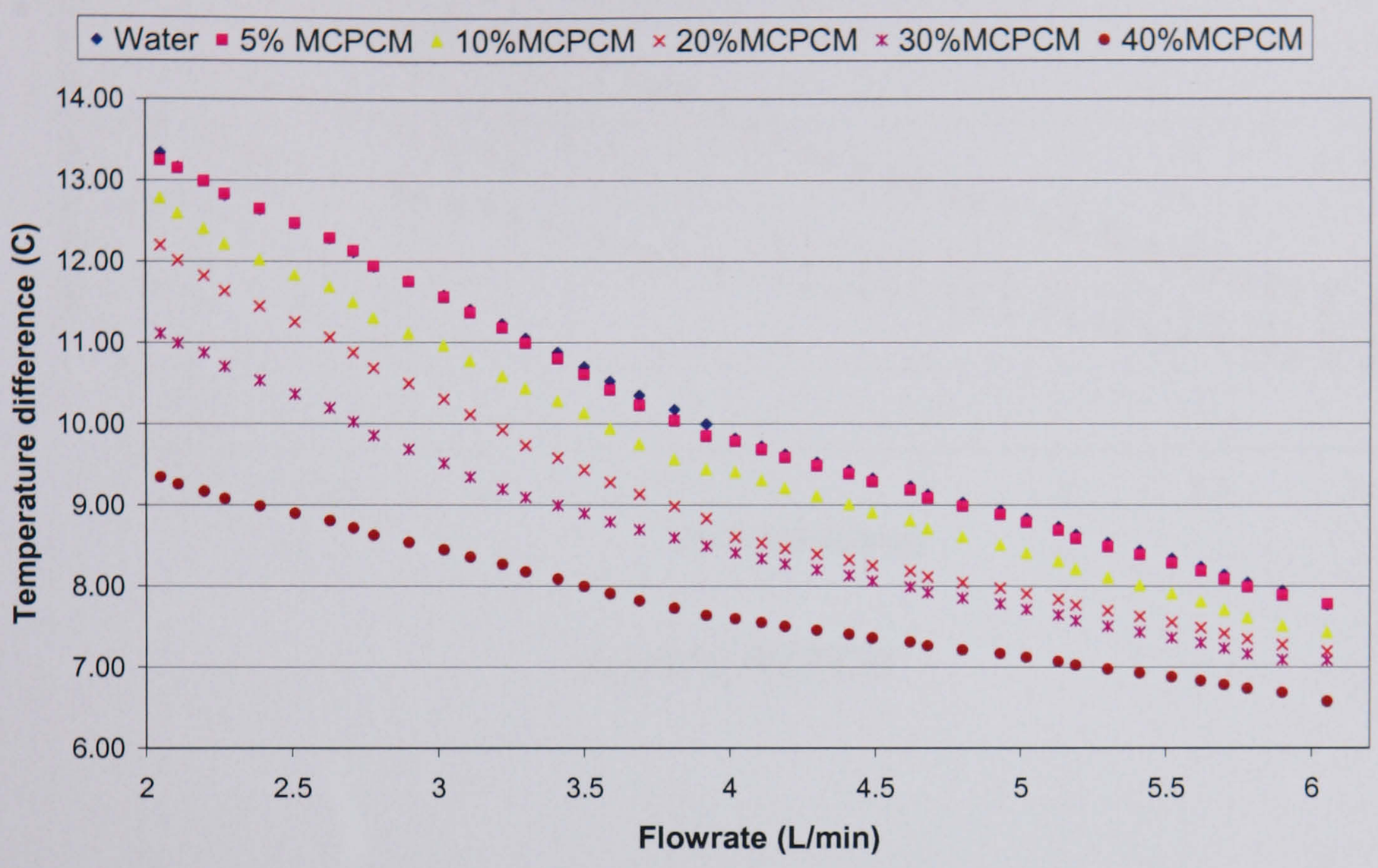

(a) 28°C MCPCM

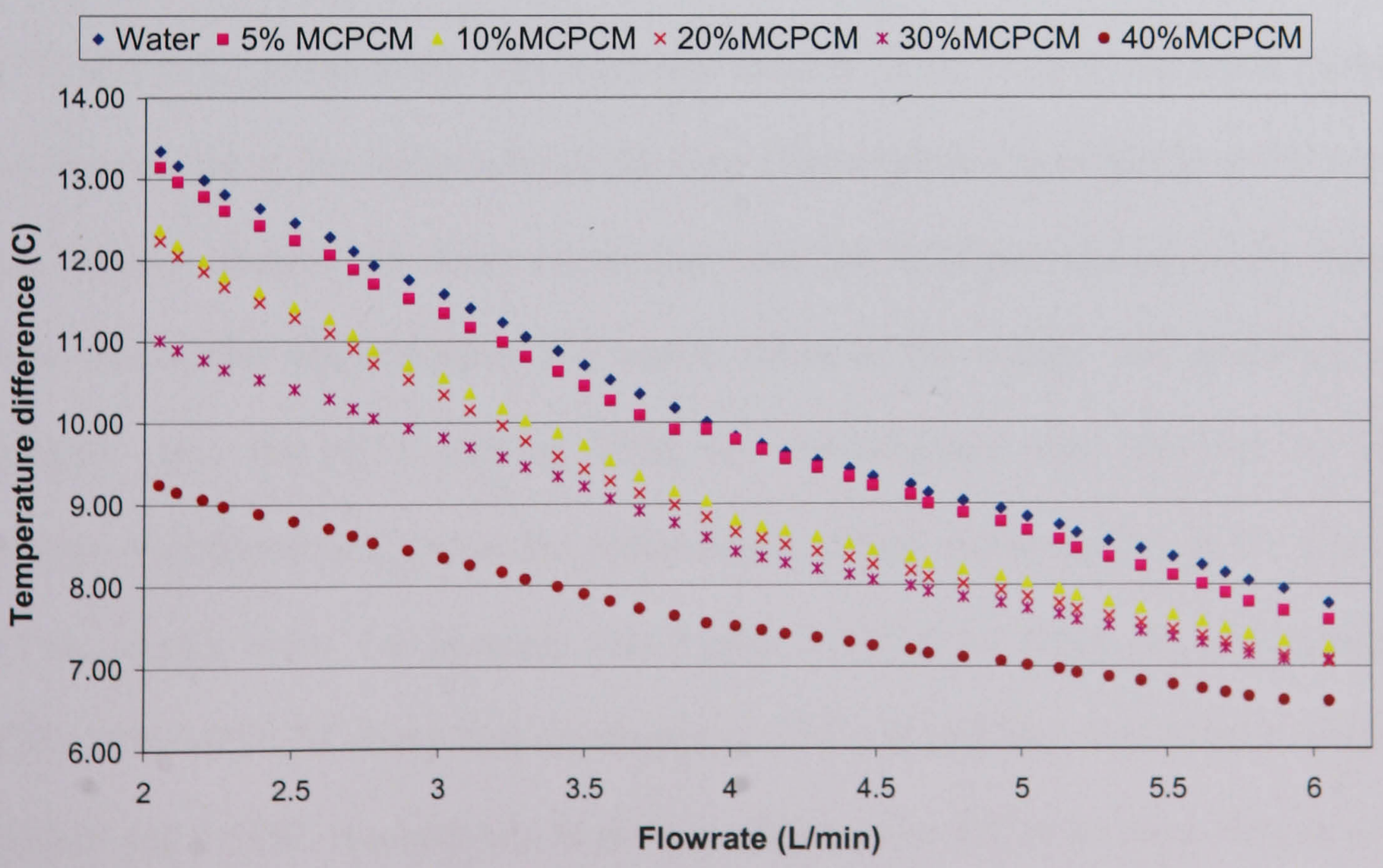

(b) 35°C MCPCM

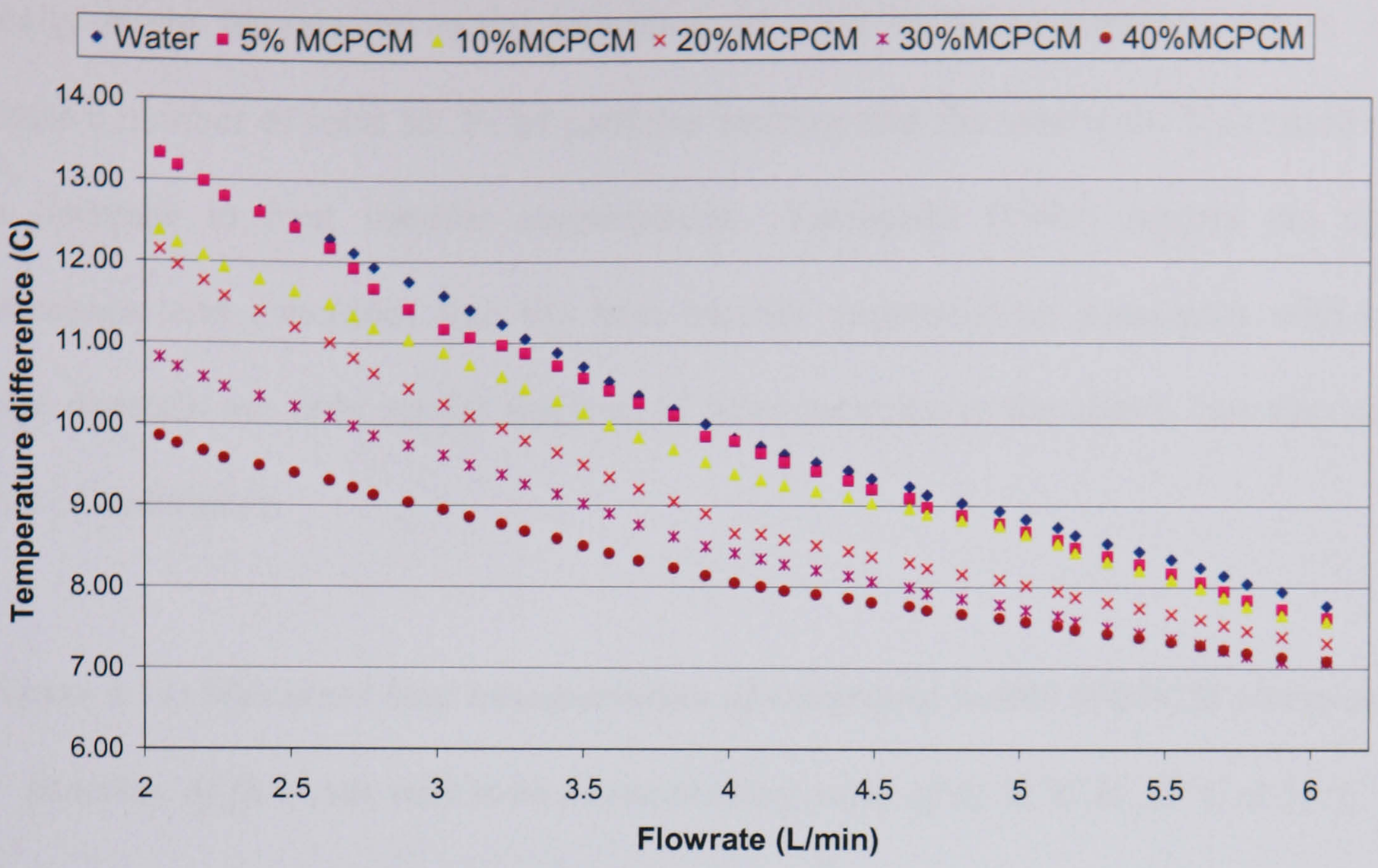

(c) 50°C MCPCM

5.4.2 Performance of MCPCM slurry

Figure 5.15 a, b and c compares the measured heat transportation of 5-40% MCPCM slurries and water with flowrates of 2-6 l/min using n-eicosane with melting point of 28°C, 35°C and 50°C, respectively. The Reynolds number of the slurries and water could not be determined due to the complexity of the flow characteristics in helically coiled tubes. The heat transportation of the slurry containing more MCPCM particles is usually higher than those of smaller concentration and water. Most of the energy was absorbed into the particles upon the PCM melting. Thus, the use of latent heat provided by MCPCM particles was found to improve the performance of heat transportation of the slurries over the use of pure water. For example, (see Figure 5.15b) at 2.7 l/min, the heat transportation of the 30% MCPCM slurry was approximately 52% higher than that of pure water, being 3.85kW and 2.5kW, respectively. However, adding more MCPCM from 30% to 40% only resulted in 3-6% improvement in performance. This could be because the increase slurry

viscosity might impede the radial migration of solid MCPCM particles, which would decrease a number of solid MCPCM particles melting near the tube wall. This could result in a decrease in heat transfer augmentation. Yamagishi (1999) reports the similar phenomenon and concludes that the heat transfer augmentation associated with phase change depends not only on the fraction of solid particles in the slurry, but also on the degree of turbulence.

Figure 5.14: Measured heat transportation of water and 5-40% MCPCM slurry as a function of flow rate with n-eicosane melting point of a) 28°C b) 35°C c) 50°C

(a) 28°C

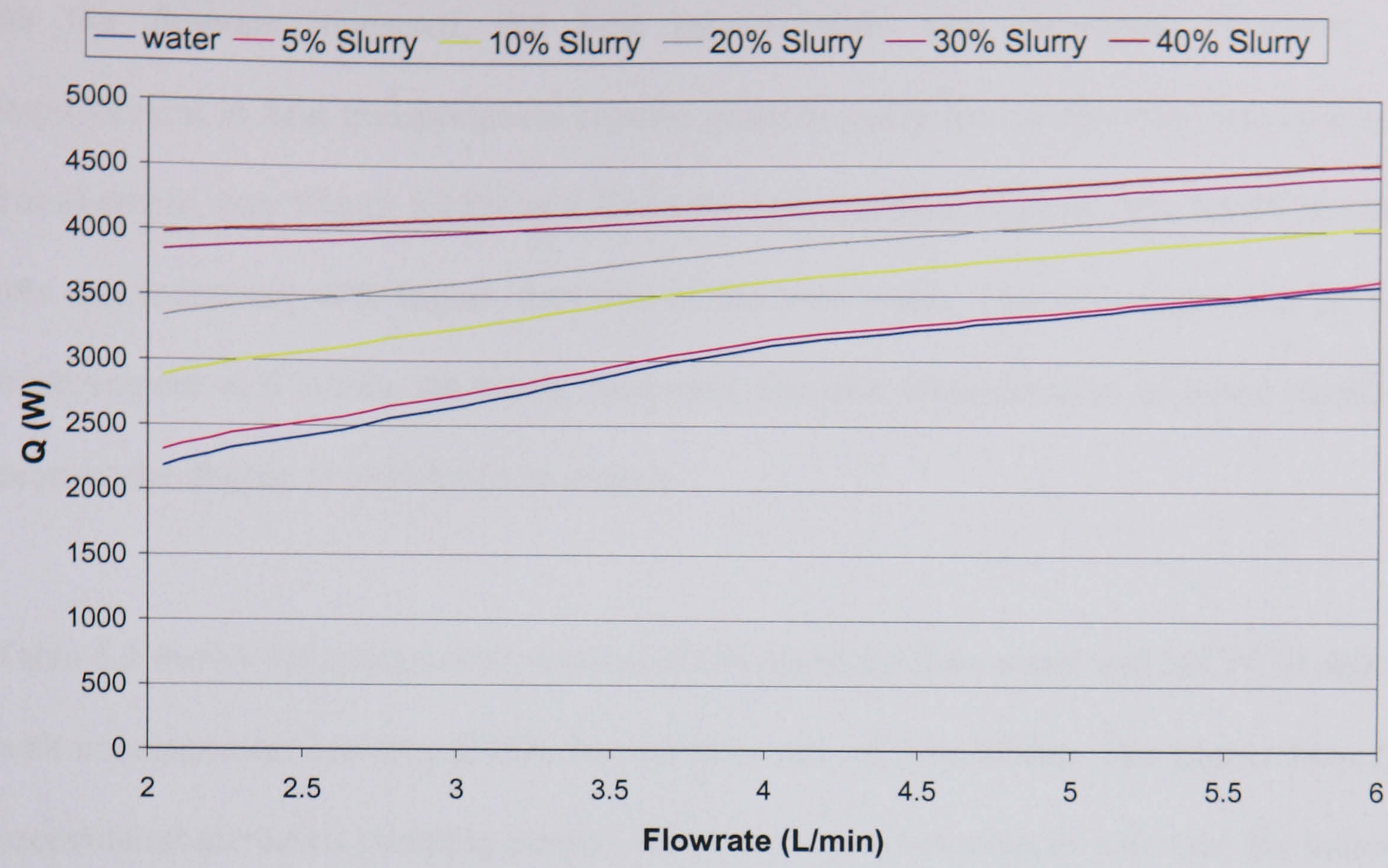
water
5% Slurry
10% Slurry
20% Slurry
30% Slurry
40% Slurry
5000
4500
4000
3500
3000
2500
2000
1500
1000
500
0
Q (W)
2
2.5
3
3.5
4
4.5
5
5.5
6
Flowrate (L/min)

(b) 35°C


water
5% Slurry
10% Slurry
20% Slurry
30% Slurry
40% Slurry
5000
4500
4000
3500
3000
2500
2000
1500
1000
500
0
Q (W)
2
2.5
3
3.5
4
4.5
5
5.5
6
Flowrate (L/min)

(c) 50°C

As the flowrate increased, the heat transportation also increased. However, the improvement in heat transportation became proportionally less as the flow rate increased. For example, (see Figure 5.15b) at 2 l/min the heat transportation of 20% MCPCM slurry was approximately 40% higher than that of the pure water. This is compared to an 18% improvement at 6 L/min. At higher flow rate, the heat transportation of water increased because the degree of turbulence increased.

Table 5.3 shows the energy consumption of the pump for pure water and MCPCM slurries with concentration between 5-40% for the flow rate of 2 to 6l/min. The higher flow rate necessitated increased pumping power. However, it is interesting to note that the increase in pressure drop due to the high concentration of MCPCM (see Figure 4.7) did not give a significant requirement for pumping power. The power consumption to pump 30% MCPCM slurry at 2l/min was found to be just 4.7% more than that to pump the pure water. This could be due to the use of an ionic surfactant of 1 vol. % in the slurry, which was found to improve the degree of particle dispersion and effectively reduced the apparent viscosity.

Slurry concentration	Pumping power (W)		
	at 2 l/min	at 4 l/min	at 6 l/min
Pure Water	70.02	77.51	85.01
5% MCPCM Slurry	71.27	77.70	84.02
10% MCPCM Slurry	71.22	78.94	87.69
20% MCPCM Slurry	72.61	77.87	85.66
30% MCPCM Slurry	73.30	80.11	86.28
40% MCPCM slurry	73.29	79.69	86.83

Table 5.3: Pumping power requirement for flow rate of 2, 4 and 6 l/min

5.5 CONCLUSION

This chapter studies the performance of the MCPCM slurry as a working fluid using a small-scale closed loop circuit. The parameters of interest were volumetric concentrations and flow rates. The following conclusions were made from this experimental study.

One major problem encountered during an experimental measurement was stratification between the solid particles and water caused by gravity in the slurry reservoir. This phenomenon was found to reduce a number of MCPCM particles flowing back into the system and decreased the efficiency of using the latent energy. The problem can be overcome by combining both an open and close system with a technique to divide the operation into three stages, open-close-open system.

The heat transportation of a working fluid containing MCPCM particles could be significantly improved compared to the use of pure water. For example, at 2.7l/min the heat transportation of a 30% MCPCM slurry was about 52% higher than the pure water. An increase in thermal capacity of a working fluid due to the use of phase change material could permit to use a smaller flowrate, which could save the pumping power. For example, to deliver 3.5kW of heat, the 30% MCPCM slurry of 35°C paraffin wax could allow using a flowrate of 2.7l/min instead of 5.7l/min with the use of pure water. A reduction in flow rate of 52% was found. This resulted in a saving of 12% in pumping power (from 84.5W to 74.5W).

As the flowrate increased the heat transportation also increased. However, it would require more pumping power. In addition, a high concentration of microcapsules signified large energy storage capability of the suspension. On the other hand, the drawback was that it

led to increase viscosity of the suspension, which required more pumping power, and at high concentrations, non-Newtonian behaviour. However, the use of an ionic surfactant in the slurry could improve the degree of particle dispersion and reduce the viscosity and pumping power. In the present study, the concentration of 5% to 10% did not show a good improvement in heat transportation. The concentration between 20-30% would be the best working fluid because of its relatively high heat capacity with a reasonable pressure drop. The use of 40% MCPCM slurry was not attractive because its performance was only up to 6% better than the 30% concentration.

Chapter 6 Fluidised-MCPCM glazed energy storage system

6.1 Introduction

In this chapter, the fluidised-MCPCM glazed energy storage system has been investigated to optimise its performance through a parametric study for which an indoor experimental rig was constructed. The solar radiation was simulated using lamps which had a light spectrum closely resembling that of sunlight. Initially, the flat plate solar thermal collector was used for the investigation. Then, the fluidised double glazed panel was constructed and tested. The working fluid used in the present study was a 20% MCPCM slurry employed 35°C *n*-eicosane. The heat transfer characteristics and efficiency of the system were examined. Experimental results can be found in Appendix.

6.2 Description of the proposed system

The proposed research is based on incorporating MCPCM slurry within a fluidised and sealed double-glazed system. The system could be integrated into building fabrics as shown in Figure 6.1. The components and operation of the system are described as following (see Figure 6.2).

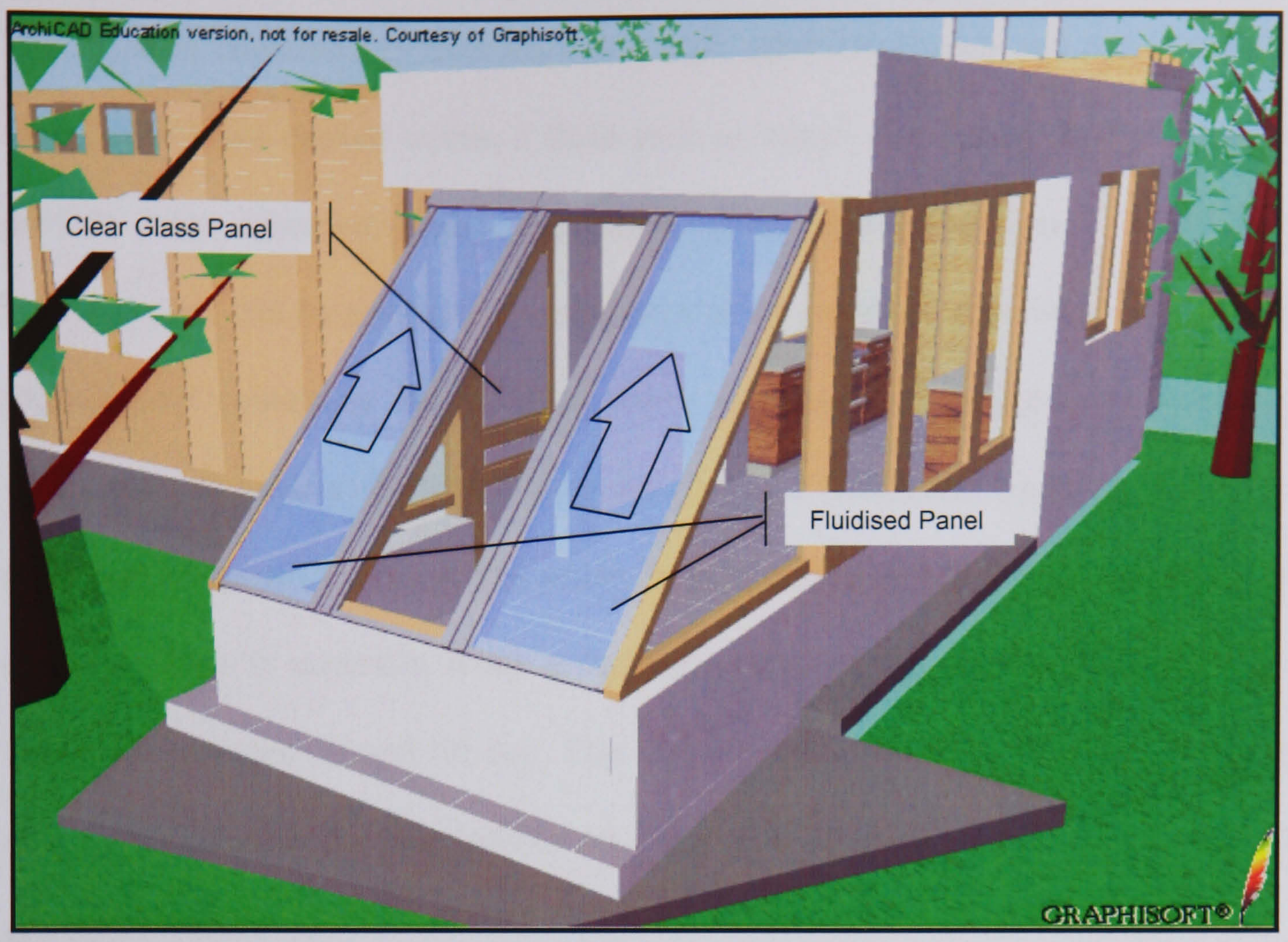

Figure 6.1: A typical building incorporating the proposed system

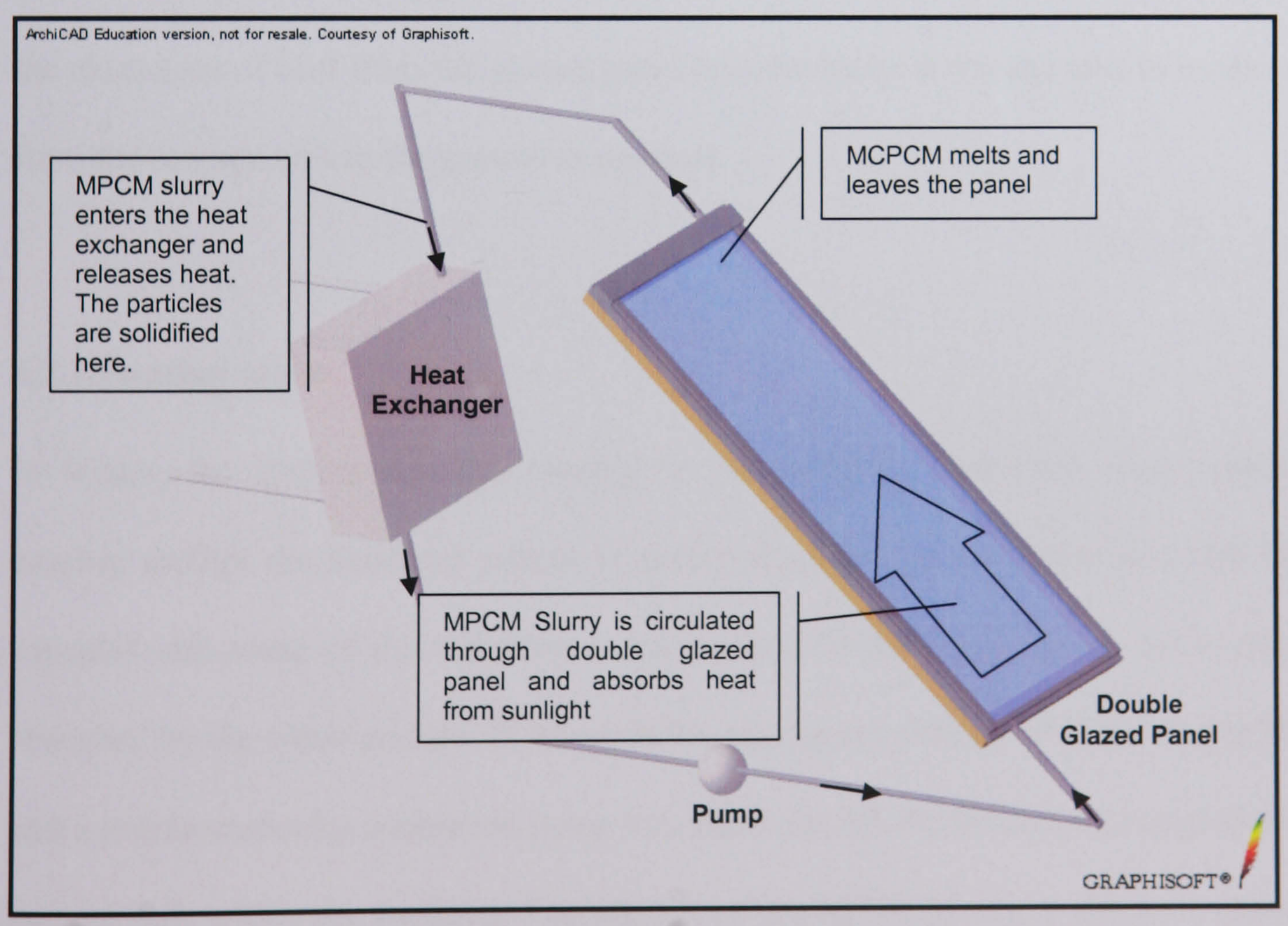

Figure 6.2: System components and operations

The PCM is contained in microcapsules with spherical shapes and thin conductive shells, which are carried within a fluid such as water. The phase change slurry can provide heat transport under practically isothermal conditions. The PCM in microcapsules can be selected to melt/freeze at the desired temperature. The doubled glazed panel containing the MCPCM slurry is linked to a piping system extended, which runs through a thermal storage unit located within the building. The glazed panel can be adjusted to a desired angle. In terms of energy collection efficiency, the collector slope is normally fixed at an angle equal to the site latitude. The UK is bound by latitudes 50 and 60 deg. The water medium can be coloured using a dye mixture to increase the absorptivity of water to solar radiation passing through the system in winter.

It is anticipated that a pump will be needed to circulate the fluid mixture to increase the extraction of heat from the glazed panel into the thermal storage unit in winter and from the storage unit to the ground in summer.

6.2.1 Heating mode

In winter, the system provides heating to the building. The short wave radiation passing though the fluidised panels is partly absorbed by the water dye and PCM capsules and some of the radiation is transmitted to the living space. Solar energy absorbed by the water and the PCM capsules, produces a change of phase in the PCM and a thermostatically controlled pump circulates the MCPCM slurry through thermal storage unit within the building. Circulation of the MCPCM slurry allows a quantity of heat to be transferred to the storage unit inside the building. Passing through this cooler medium, the PCM capsules and the carrier fluid lose heat and the MCPCM

solidifies once more. The cycle would continue as long as there is solar radiation impacting on the fluidised panels and the carrier fluid temperature reaches the phase change temperature of the PCM. The heat storage unit within the building needs to be designed so that it can store maximum possible energy without causing overheating of the living space. Any surplus energy gained could be used as heat source for other applications, for instance, hot water supply, heat pump or ejector refrigeration system.

6.2.2 Cooling mode

In summer, the system operates in a cooling mode to provide cooling for the building. The glazed units accommodating the MCPCM slurry will be shaded from direct sunlight, using movable insulation. As the indoor temperature rises above the PCM's phase change temperature, the PCM capsules melt. A pump then starts to circulate the MCPCM slurry through the section of the system buried in the ground, where the temperature is usually lower than that of the room air. Alternatively, this heat could be used as a heat source for the other applications, as mentioned previously. The cycle continues until the room temperature falls below the design temperature.

6.3 Solar collector test rig

6.3.1 Experimental apparatus and method

Figure 6.3 and 6.4 illustrates the schematic diagram of the experimental apparatus and the view of experimental rig. The rig consisted of two closed circuits, the primary and secondary circuit. The primary circuit consisted of a flat plate solar collector, lighting system (4,500W), heat exchanger, MCPCM slurry tank, electric mixer, double-diaphragm pump and flowrate transmitter (turbine type). The secondary circuit

comprised of a water storage tank, pump and variable area flowmeter. The temperatures of the working fluid at the inlet and outlet of the solar collector, heat exchanger and water reservoir were monitored using the K-type thermocouples attached to the outer wall of the pipes. The temperatures of the water inside the tank were monitored by 6 thermocouples which were located at different places and depths. The water reservoir, heat exchanger and pipes were insulated in order to minimise heat loss through the system. A DT500 data logger is connected to the thermocouples and the turbine flowmeter to upload information into a PC. All thermocouples were scanned every 5 seconds.

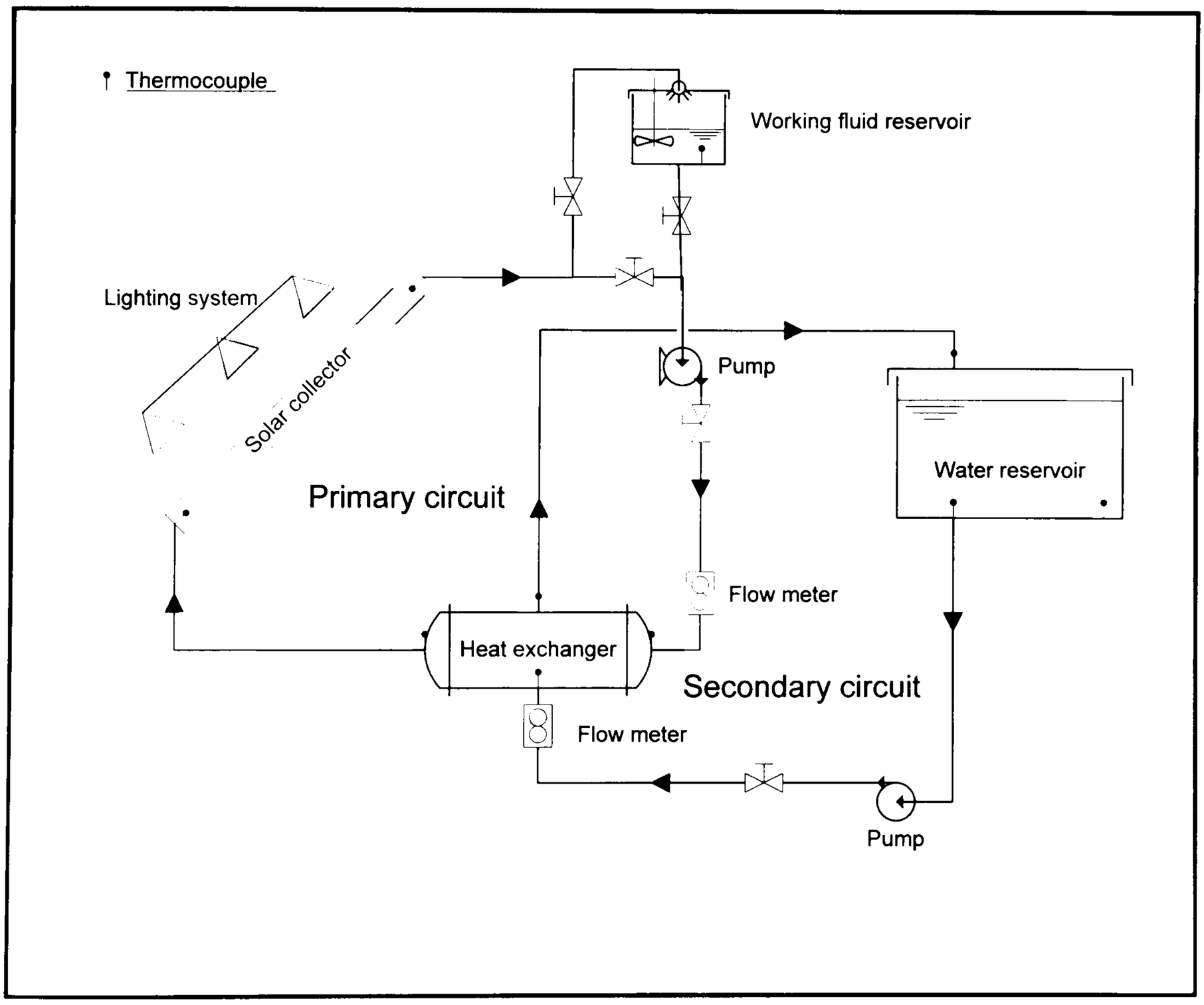

Figure 6.3: Flat plate solar collector schematic diagram

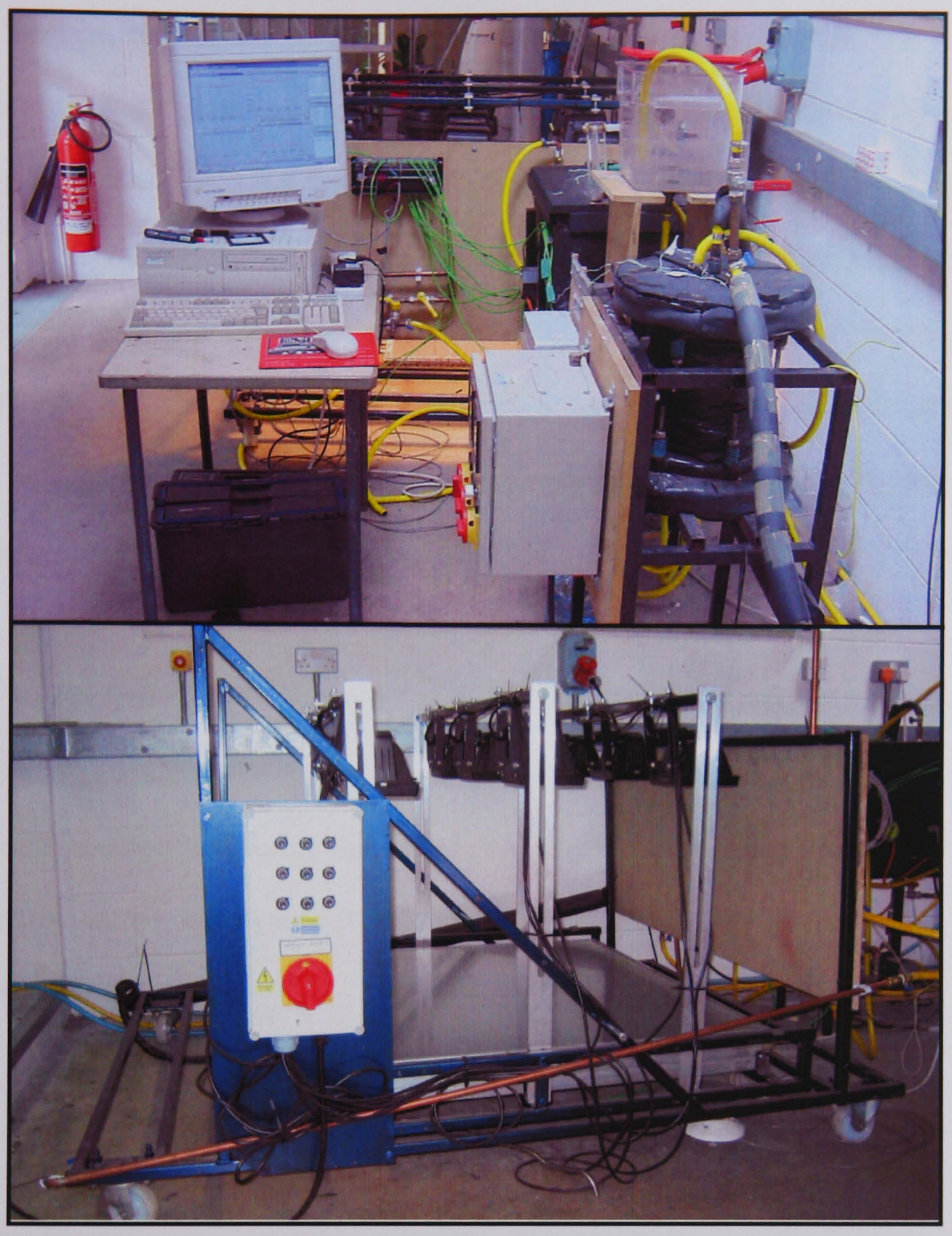

Figure 6.4: View of experimental rig

The heat exchanger used in the present study was a shell and coil construction. The coil was 200mm diameter and 300mm height made from 12mm soft copper tubing. The water reservoir was constructed from steel and its volume capacity was 37.58 litres.

The lighting system consisted of nine 500W halogen lights which were mounted on the bars on top of the frame to provide illumination for the collector. Each bar consisted of 3 lights and could be moved vertically up or down for adjusting the intensity of the light. Each lamp could be moved closer or apart from each other along the bar. The radiant flux of each light could be individually adjusted by varying current of electricity supplied to a lamp from a control knob. The irradiance at the surface of the solar collector was measured using a pyranometer which connected to the data logger. It worked by generating a voltage that was directly related by a scaling factor to the power of the lights on the collector.

The solar collector had a measured surface area of 1.212 m^2. Figure 6.5 shows details of the solar collector which consisted of a flat black plate through which the liquid flowed. The box containing the flat plate was constructed from aluminium and was insulated on the bottom side. Table 6.1 shows technical specification of the flat plate solar collector.

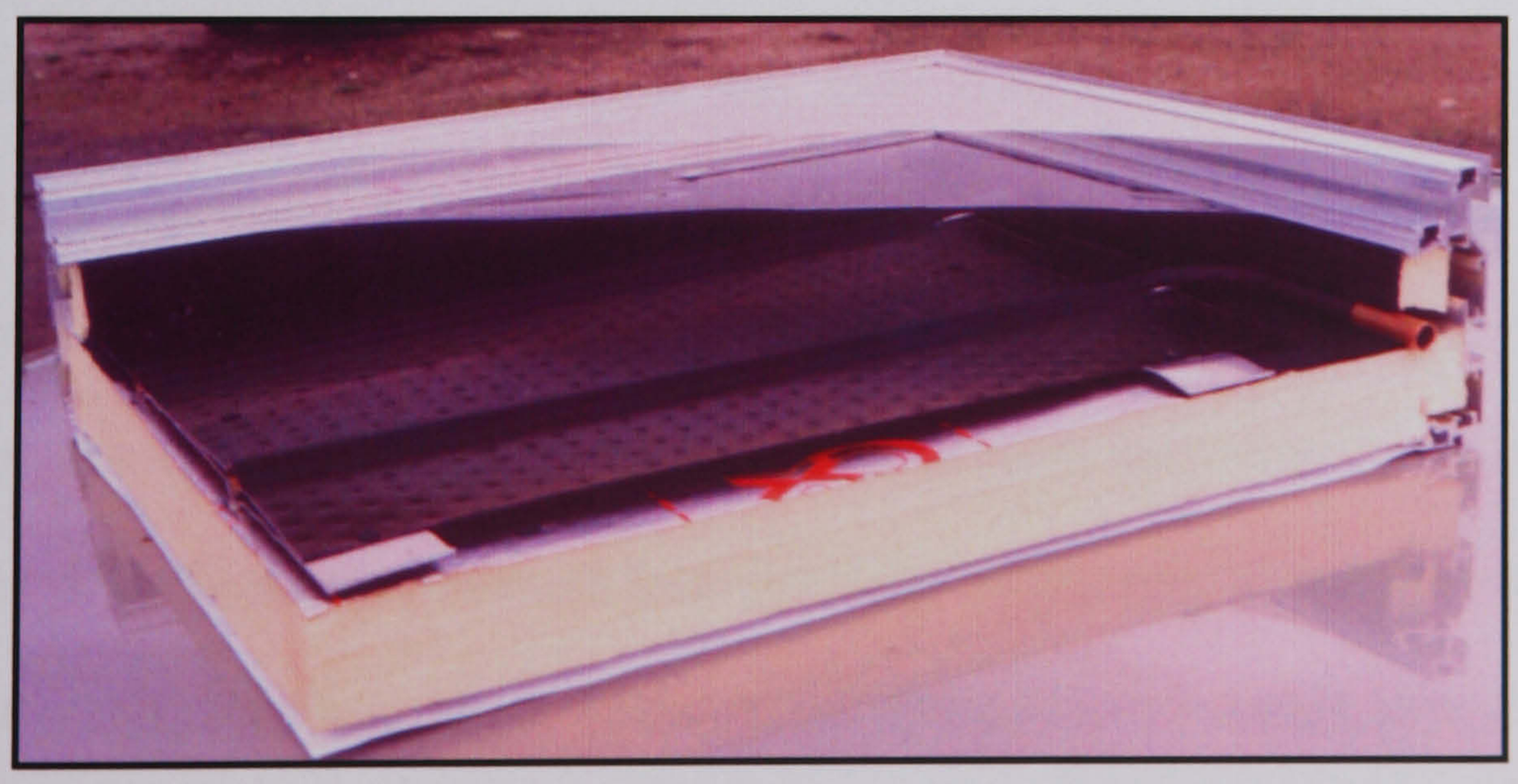

Figure 6.5: Details of flat plate solar collector

HEIGHT: WIDTH: WEIGHT	1175mm 1032mm 11kg
ABSORBER PLATE:	Aluminium fins metallurgically bonded to rhombic shaped copper water ways providing large water to wall contact for maximum heat transfer
	Selectively coated surface layer:, combines metallic nickel in aluminium oxide. Absorption coefficient = 0.97; emission coefficient = 0.13
GLAZING:	One outer layer of Tedlar film and one inner layer of Teflon, both manufactured by DuPont, minimises heat loss and ensures minimal weight Overall light transmittance = 95%
BACKING:	Melinex film ensuring the collectors are completely waterproof
COLLECTOR BOX:	Heavy aluminium box section with all round fixing channels for easy fitting. A sensor pocket is fitted at the appropriate location
INSULATION:	All insulation materials are 100% CFC-free
FLOW AND RETURN:	15mm copper for serpentine operation, 22mm for Headers & Risers
FLUID CONTENT:	0.6 litre per 1 square metre of collector area
RECOMMENDED	
FLOW RATE:	1 litre per square metre of collector area per minute
TRANSFER FLUID:	70% water, 30% Propylene Glycol
TEST PRESSURE:	15 Bar
MAXIMUM PRESSURE:	10 Bar
PRESSURE DROP:	10 kPa at flow rate of 0.03 litres per second, per 1 square metre of collector area

Table 6.1: Technical specification of the flat plate solar collector (AES Ltd., 2003)

The paraffin wax of 35°C *n*-eicosane was used as suspended particles for the MCPCM slurry. The mixture was made with a concentration of 20% due to its relatively high heat capacity and it was more reliable than a 30% concentration. Figure 6.6 illustrates an operation cycle of the experiment using the flat plate solar collector. Initially, the MCPCM slurry was prepared and mixed in the reservoir before fed into the system using the technique of open-close-open system as described in Chapter 6. Radiant flux generated from the lights would pass through the glazing and reach the absorber plate, which heated up, charging irradiant energy into heat energy. Heat was transferred into the working fluid passing through the pipe attached to the absorber plate. As the temperature of the slurry rose above the phase change temperature the MCPCM particles would melt, which stored the latent heat of fusion.

The working fluid was then circulated through the heat exchanger to reject heat into the secondary working fluid, which was water. Here, the MCPCM particles solidified. Then, the slurry was circulated back into the solar collector and the process started again. Meanwhile, the secondary working fluid entered the water reservoir to deposit heat and cooled down.

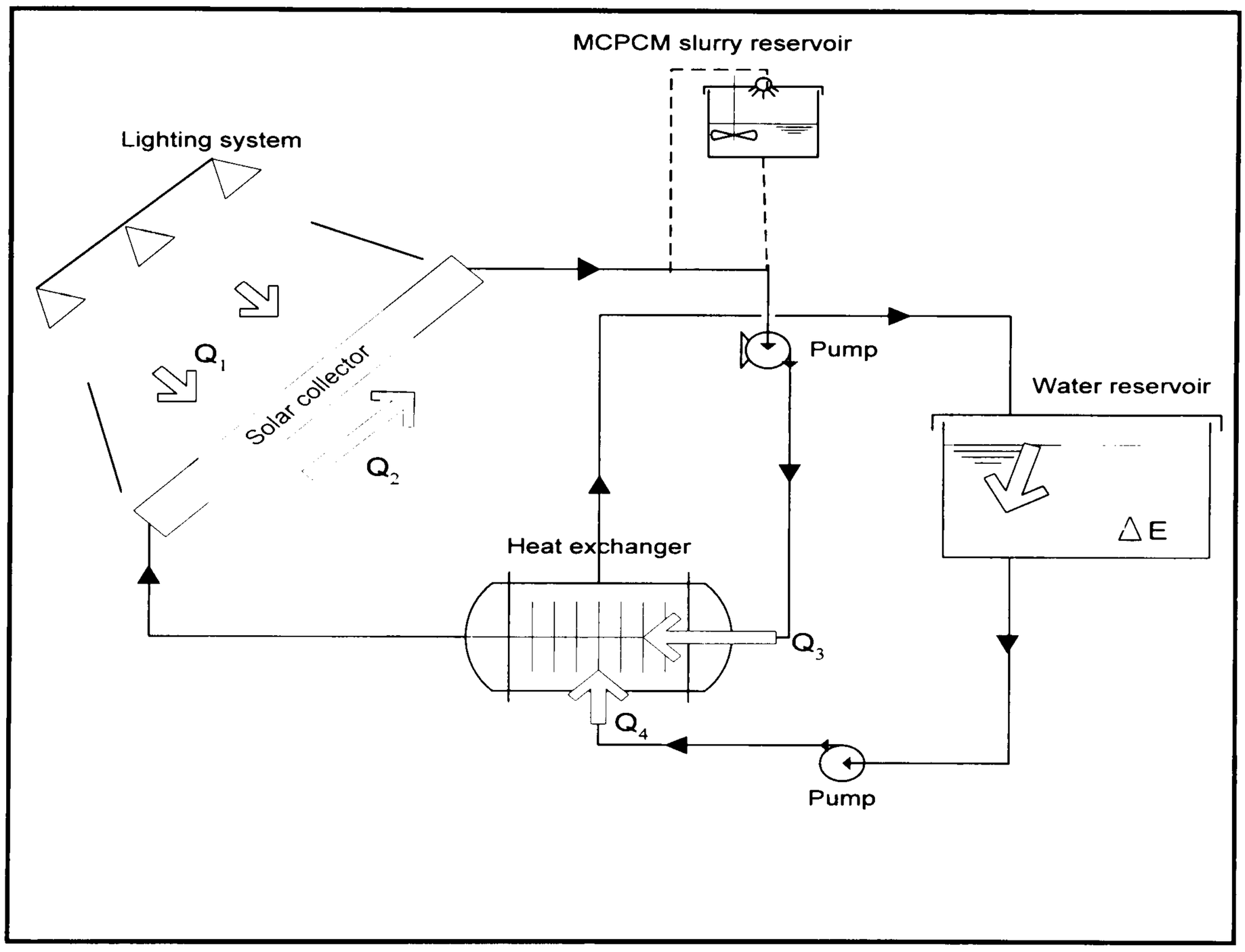

Figure 6.6: Operation cycle of the experiment

The irradiance from lights was measured on surface of the solar collector which was divided into thirty areas representing by 6 columns and 5 rows with equal space. The average irradiant value measured on the collector can be calculated as illustrated in Figure 6.7 and was the energy input ($Q_1=I_{av}*A_A$) for the solar collector. As mentioned earlier, it is not suitable to use the log-mean-temperature-difference (LMTD) method for the MCPCM slurry because neither the thermal capacity nor the local heat transf

coefficient is constant along the flow direction. Thus, measurement of the amount of heat (Q_2) absorbed by the MCPCM slurry could be determined from the amount of heat received by the secondary fluid ($Q_4 = \dot{m} C_p \Delta T$) or the amount of heat stored in the water reservoir, $\Delta E/\Delta t$. It was assumed that the heat loss of the system was small and could be neglected, thus, $Q_2 = Q_3 \approx Q_4 = \Delta E/\Delta t$.

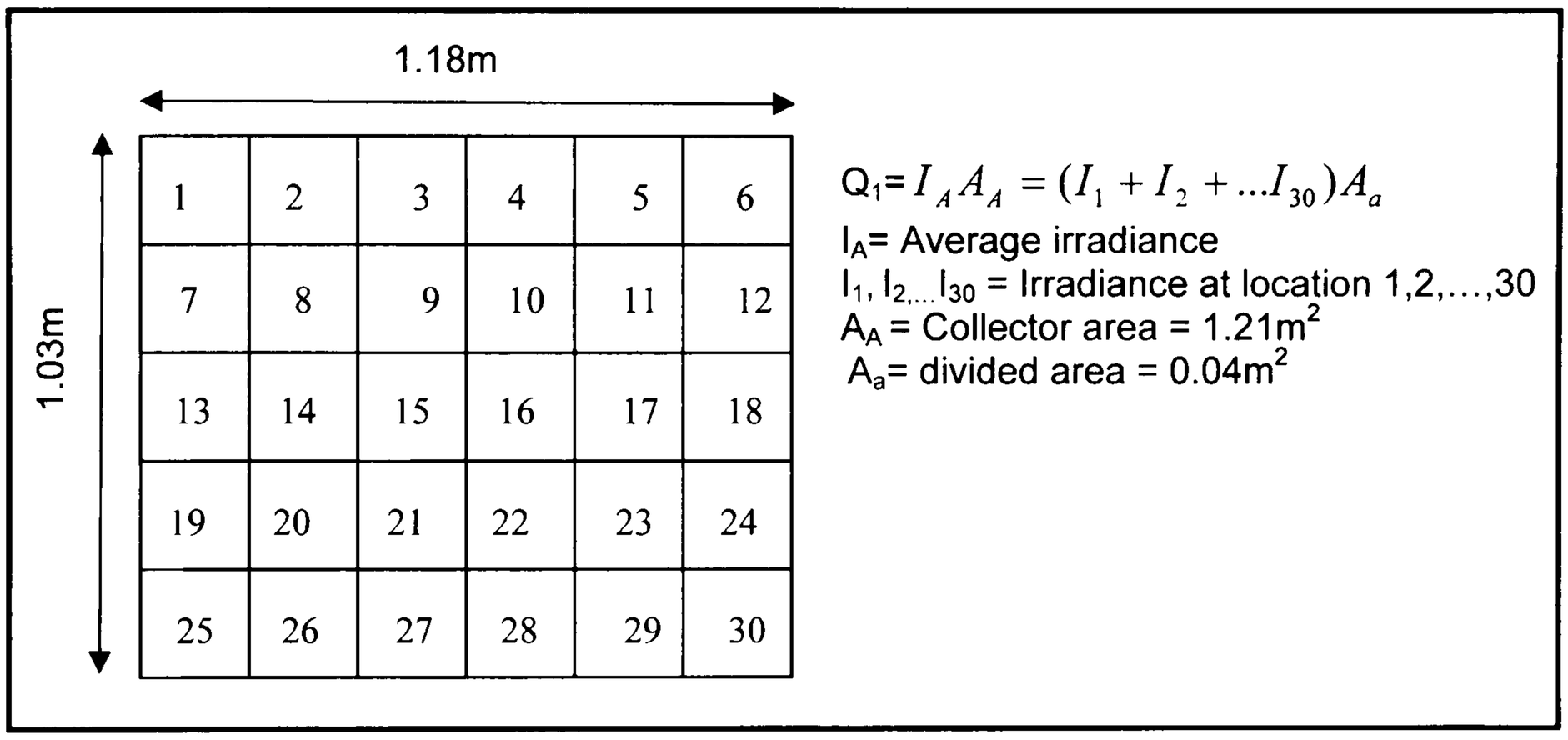

Figure 6.7: Solar collector area

The test procedure for the solar collector rig was carried out in a number of steps which were:

1. The experiments were operated with the insolation of approximately 200W/m^2, 400W/m^2, 600W/m^2 and 800W/m^2 by adjusting the lighting system to obtain the average irradiation.
2. Preheat the primary working fluid, MCPCM slurry, to the temperature of 28°C, which was below the phase change temperature.
3. Circulate the primary working fluid to collect heat from the solar collector
4. Adjust the flowrate of the primary working fluid to 1 l/min

5. Preheat the secondary working fluid, pure water, to the temperature of 20°C
6. Circulate the secondary working fluid to pick up heat from the primary working fluid in the heat exchanger
7. Adjust the flow rate of the secondary working fluid to 1l/min
8. Running the system until an outlet temperature of the primary working fluid from the solar collector reach 38°C (above the PCM melting point)
9. Temperature profiles and flow rates for each of the major components were taken from thermocouples located on the inlet and outlets to the heat exchanger and water reservoir.

6.3.2 Calibration and verification

Initially, water was used as a primary working fluid to check heat losses of the system. The devices used in the present study have already been calibrated during last experiment and was considered accurate with the correction. Table 6.2 illustrates measurement of irradiance (I) and calculation of the rate of heat transfer for Q_2, Q_3, Q_4 and $\Delta E/\Delta t$ from the solar collector rig using water as the primary working fluid. Heat loss through the system for the primary circuit between Q_2 and Q_3 was shown at around 5W and for the secondary circuit between Q_4 and $\Delta E/\Delta t$ was found at around 3 to 30W. Results show good agreement between the rate of heat input provided by the primary working fluid (Q_3) and the rate of heat transfer absorbed by the secondary working fluid (Q_4) with relatively low heat loss of 10 to 25W. Hence, it is acceptable to determine the rate of heat transfer for the primary working fluid by the calculation of the rate of heat transfer from the secondary fluid ($Q_2 \approx Q_3 = Q_4 + Q_{loss}$).

I (W/m^2)	Q_2(W)	Q_3(W)	Q_4(W)	$\Delta E/\Delta t$ (W)
779	447	442	425	395
602	366	362	344	321
393	245	242	216	206
203	127	123	112	99

Table 6.2: Heat input and output of the solar collector system (I, Q_2, Q_3, Q_4 and $\Delta E/\Delta t$) using water as the primary working fluid

6.4 Performance of the solar collector with the use of MCPCM slurry

6.4.1 Insolation pattern

Figure 6.8 illustrates the insolation pattern of lights on the solar collector with an average irradiance of (a) 779 W/m^2, (b) 599 W/m^2, (c) 396 W/m^2 and (d) 217 W/m^2. The distribution of light on the collectors can be seen to be variable. This may have some effect on the performance of the collectors under laboratory conditions as more light is falling on some parts than others. However, as the average insolation levels were used for the calculations it is unlikely that this will have affected the experiments significantly.

Figure 6.8: Insulation map for the solar collector a) I_{av} = 779W/m² b) I_{av} = 599W/m² c) I_{av} = 396W/m² d) I_{av} = 217W/m²

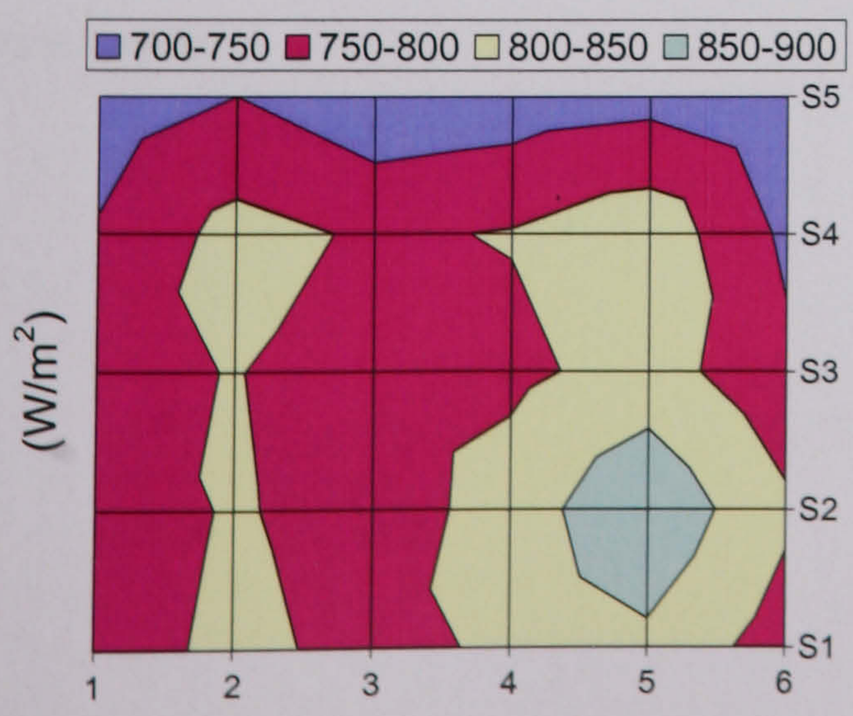

(a)

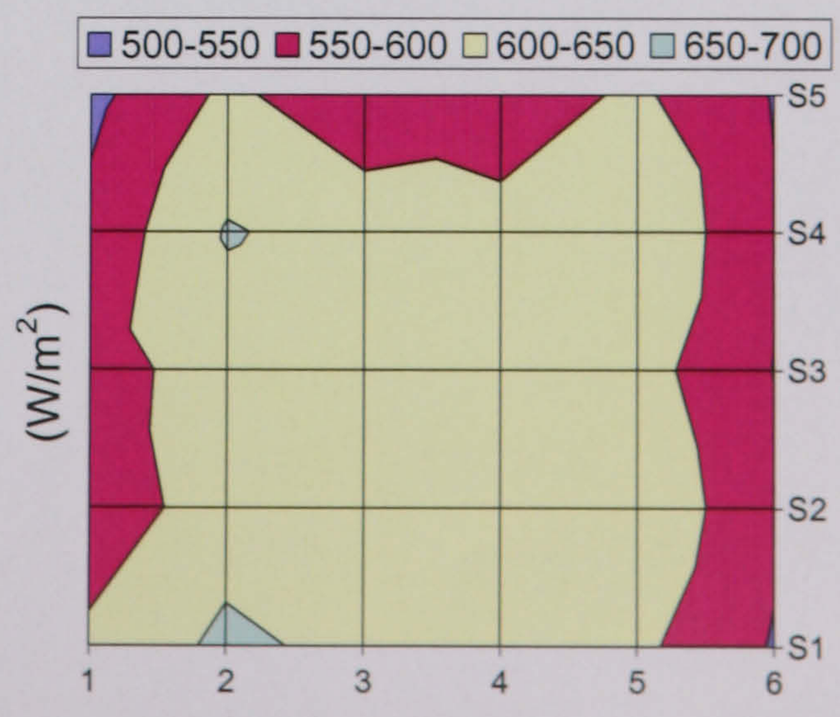

(b)

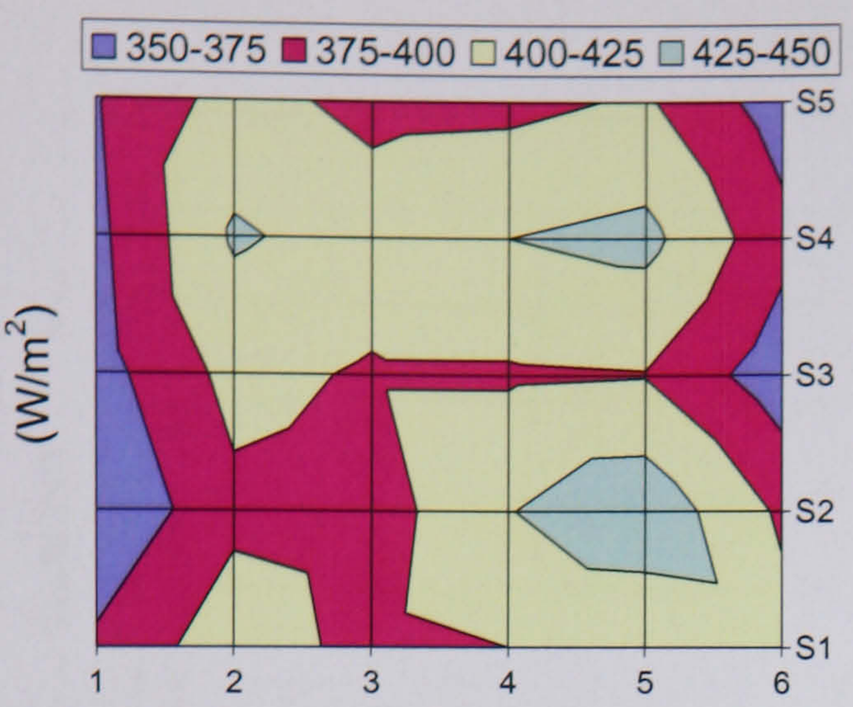

(c)

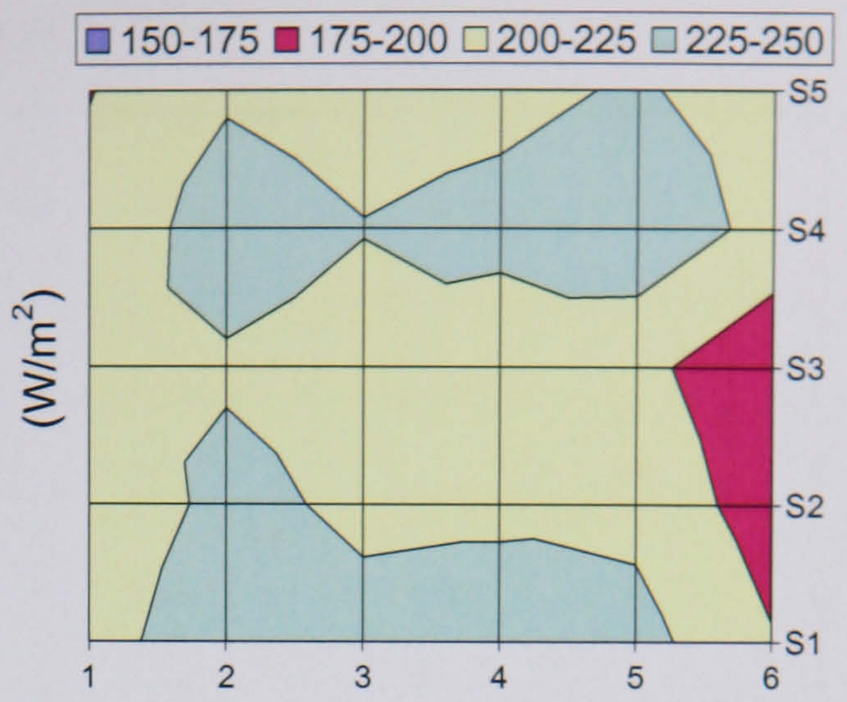

(d)

6.4.2 Heat transfer characteristic

Figure 6.9 illustrates the temperature difference between the inlet and outlet of the solar collector for the primary working fluid using water and 20% MCPCM slurry plotted against irradiance between 200W/m^2 and 800W/m^2. At high irradiance, 800W/m^2, the temperature differences of the working fluid between the inlet and outlet of the solar collector were higher than those of the small irradiance, 200W/m^2, which resulted from the increased amount of heat flux. The use of phase change slurry was found to decrease the temperature difference between the inlet and outlet of the solar collector, because the slurry had greater thermal capacity than water. For example, at 800W/m^2, the temperature difference between the inlet and outlet of the solar collector for 20%MCPCM slurry was around 2.5°C comparing to 4°C of the pure water.

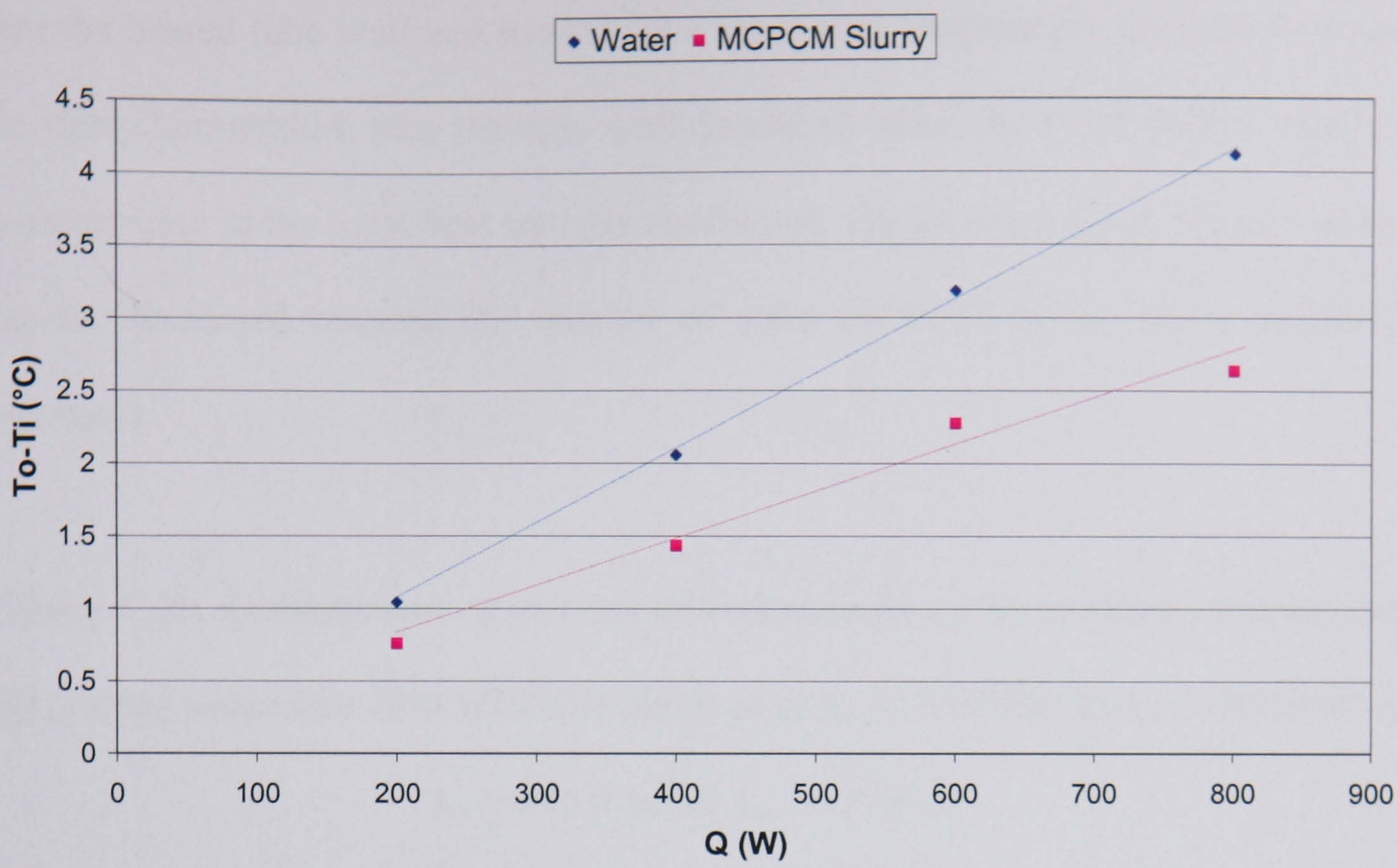

Figure 6.9 Temperature difference between the inlet and outlet of the solar collector using water and 20%MCPCM slurry against irradiance between 200W and 800W/m^2

Figure 6.10 illustrates the rate of heat transfer of the primary working fluids (Q_2) for 20% MCPCM slurry using the calculation of the rate of heat transfer from the secondary working fluid under insolation of (a) 779W/m^2, (b) 599W/m^2, (c) 396W/m^2 and (d) 217W/m^2. Results from the initial experiment using water as the primary working fluid has been plotted for comparison with the use of MCPCM slurry. Overall, the rate of heat transfer of the MCPCM slurry was higher than that of the pure water. As seen in Figure 6.10, the rate of heat transfer for the MCPCM slurry was in a significant variation comparing to curve of water. The rate of heat transfer increased gradually until it reached the peak. The curve then began to drop and maintain slightly above the figure of the pure water. Choi (1994) also speculated that the variation in the local heat transfer coefficient would depend upon the number of solid PCM particles that migrated from the turbulent core region to the flow fields

near the heated tube wall and melted. The inner-wall temperature decreased because the slurry temperature near the tube wall decreased when the PCM melted, resulting in an increase in the local heat transfer coefficient. On the other hand, the rate of heat transfer decreased because the number of solid MCPCM in the slurry eventually decreased.

Figure 6.10: A comparison of the rate of heat transfer of the primary working fluid (Q_2) using water and 20% MCPCM slurry at a) $I_{av} = 779W/m^2$ b) $I_{av} = 599W/m^2$ c) $I_{av} = 396W/m^2$ d) $I_{av} = 217W/m^2$

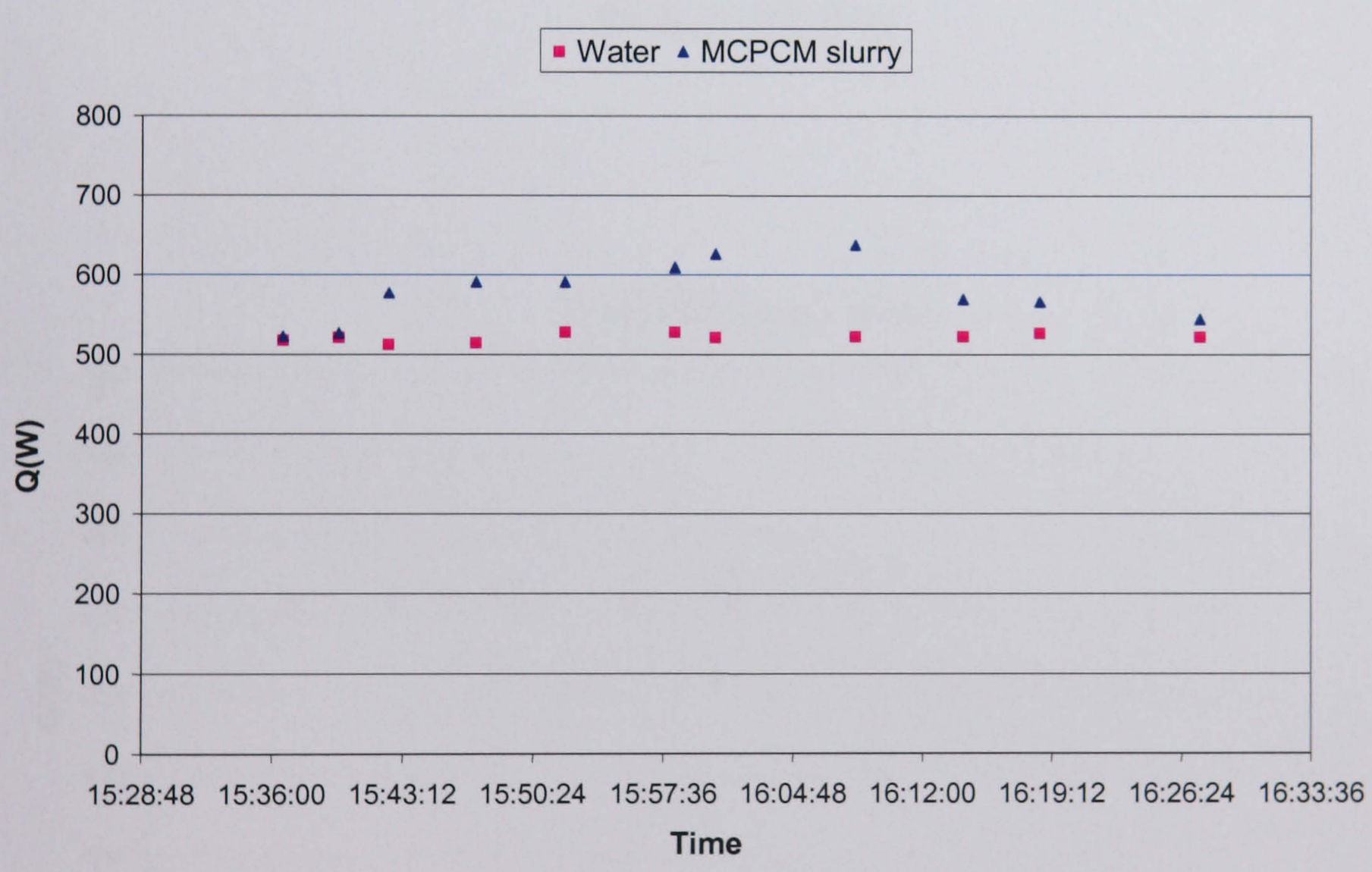

(a) $I_{av} = 779\ W/m^2$

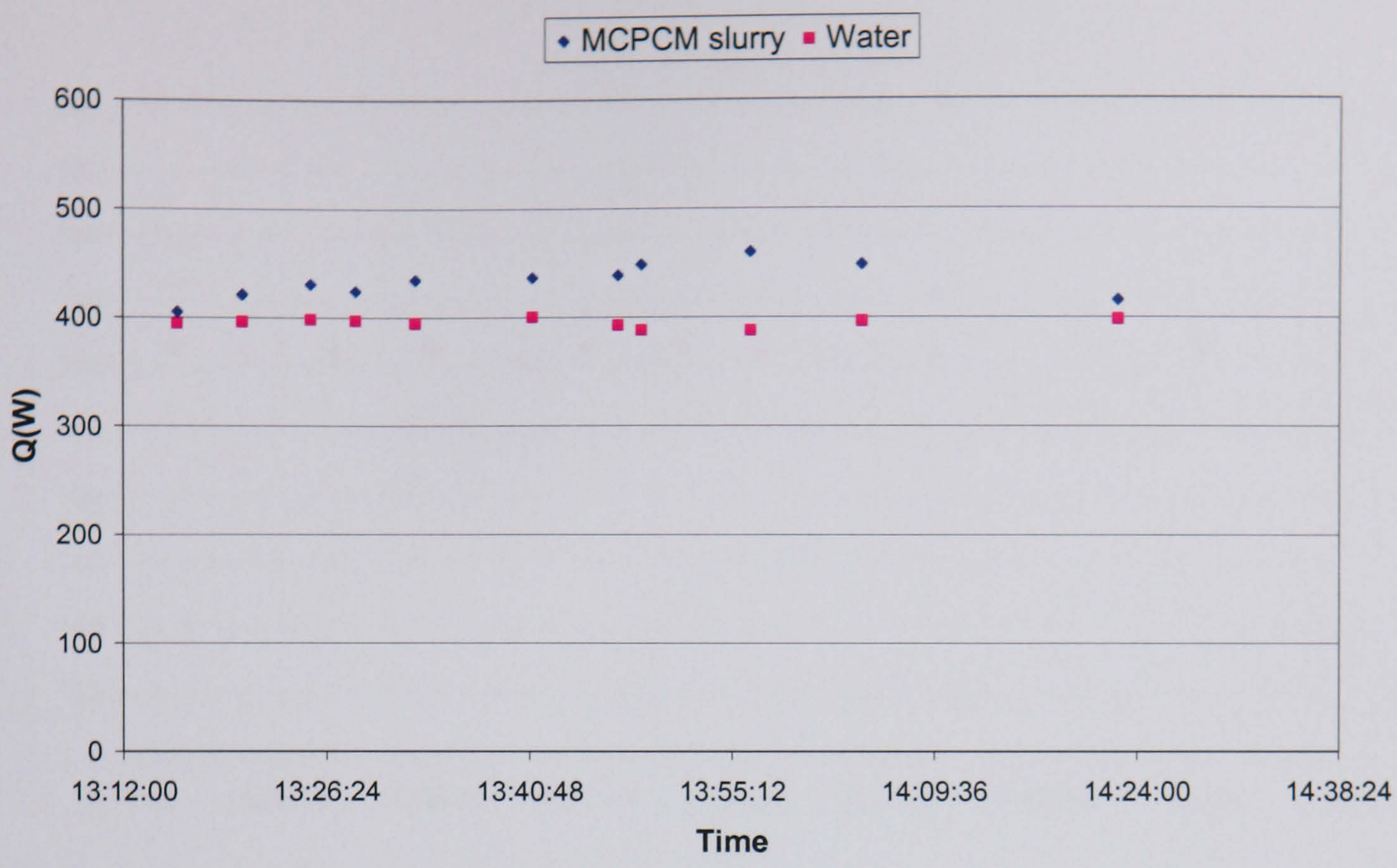

(b) $I_{av} = 599\ W/m^2$

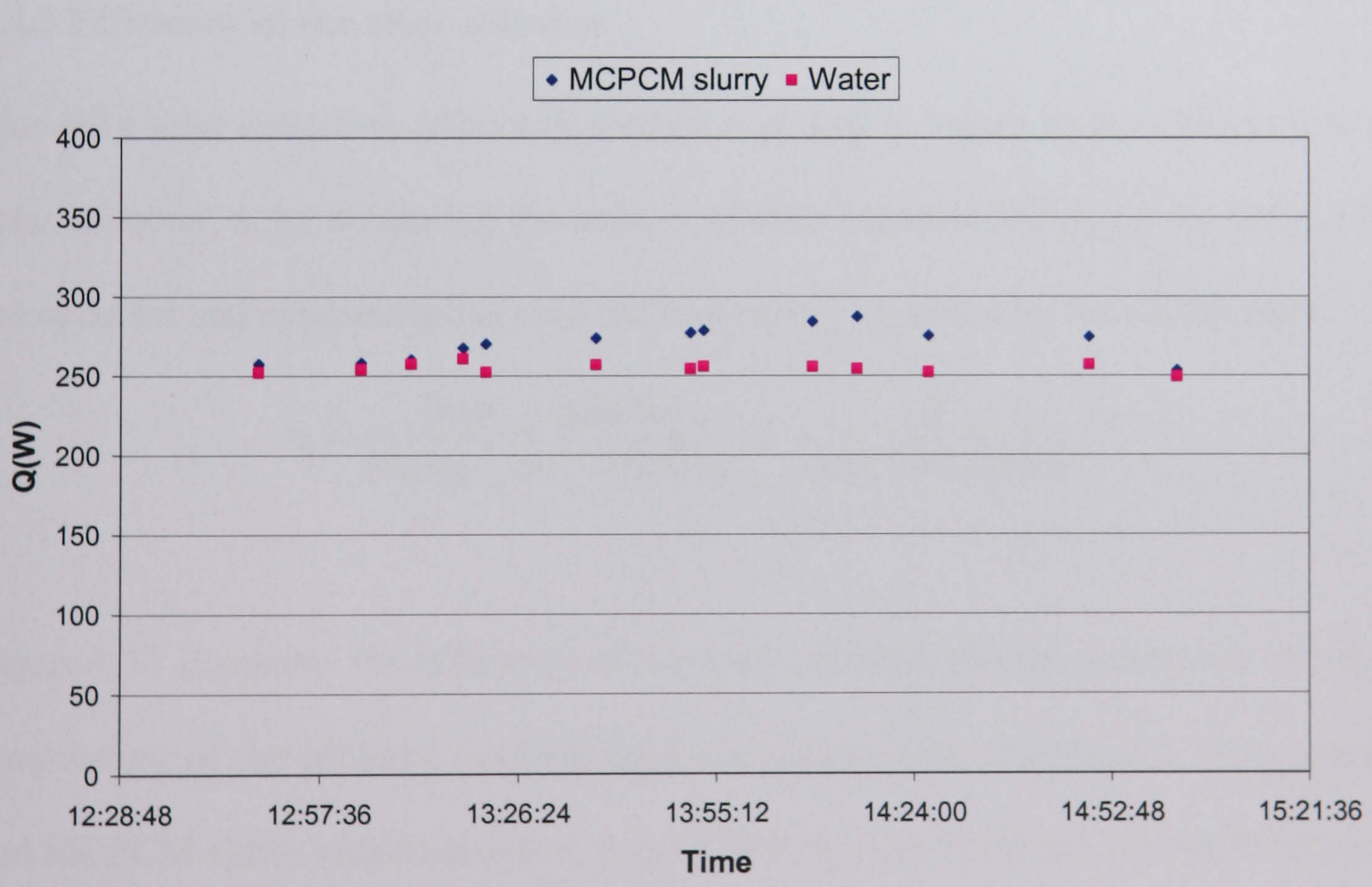

(c) $I_{av} = 396\ W/m^2$

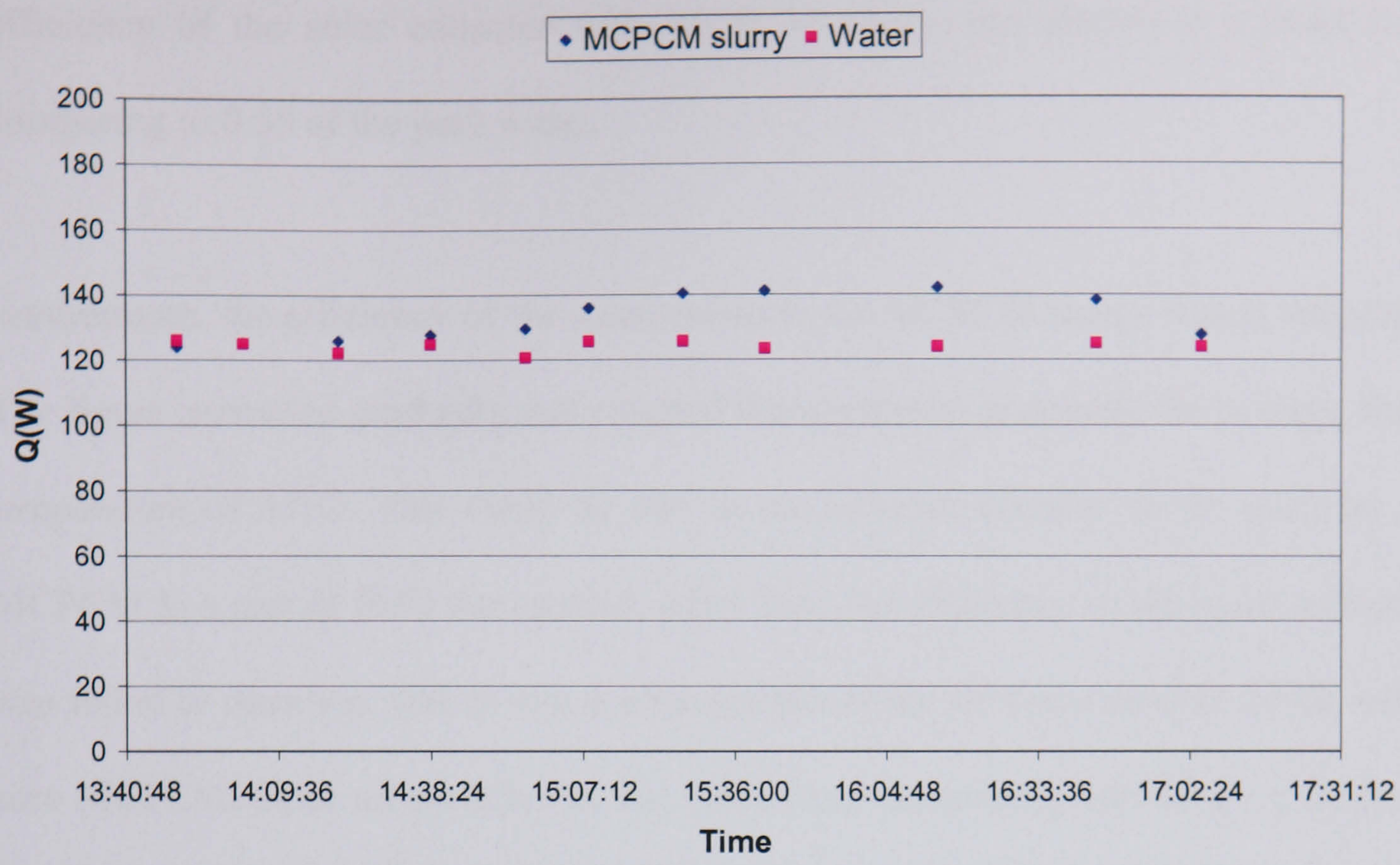

(d) I_{av} = 217 W/m^2

6.4.3 Efficiency of the solar collector

The daily solar collection efficiency method was used to calculate the efficiency of a solar collector, η, by measuring the amount of solar radiation falling on the surface of the collector and comparing this with the heat energy absorbed by the carrier fluid.

$$\eta = \frac{Heat\_collected}{Energy\_on\_absorber} = \frac{Q}{Area * Insolation}$$

Figure 6.11 illustrates the efficiency of the solar collector plotted against the average temperature of the primary working fluid, calculated from $(T_{in}+T_{out})/2$, using water and MCPCM slurry under insolation of (a) 779W/m^2, (b) 599W/m^2, (c) 396W/m^2 and (d) 217W/m^2. The use of MCPCM slurry was found to improve the efficiency of the solar collector over the single phase working fluid. For example, at 779W/m^2, the

efficiency of the solar collector with MCPCM slurry was shown at around 0.65 comparing to 0.55 of the pure water.

Furthermore, the efficiency of the solar collector for MCPCM slurry was in variation. The figure increased gradually and reached the maximum at around the average fluid temperature of 33°C. This could be due to the increase number of the particles of MCPCM in a carrier fluid that melted. After that, the efficiency of the solar collector was found to decrease, which was a consequence of the decrease number of the solid core MCPCM. Once all particles in the slurry have completely melted the efficiency approached the minimum value. To maximise the benefit from the latent heat of fusion of this phase change slurry, it was recommended to maintain an average slurry temperature of around the range of 33°C to 34°C. In this condition, the performance of the solar collector could be improved by as much as 20% comparing to the use of a single phase working fluid.

Figure 6.11 Solar collector efficiency plotted against average fluid temperature, $(T_{in}+T_{out})/2$, using MCPCM slurry and water for a) $I_{av} = 779W/m^2$ b) $I_{av} = 599W/m^2$ c) $I_{av} = 396W/m^2$ d) $I_{av} = 217W/m^2$

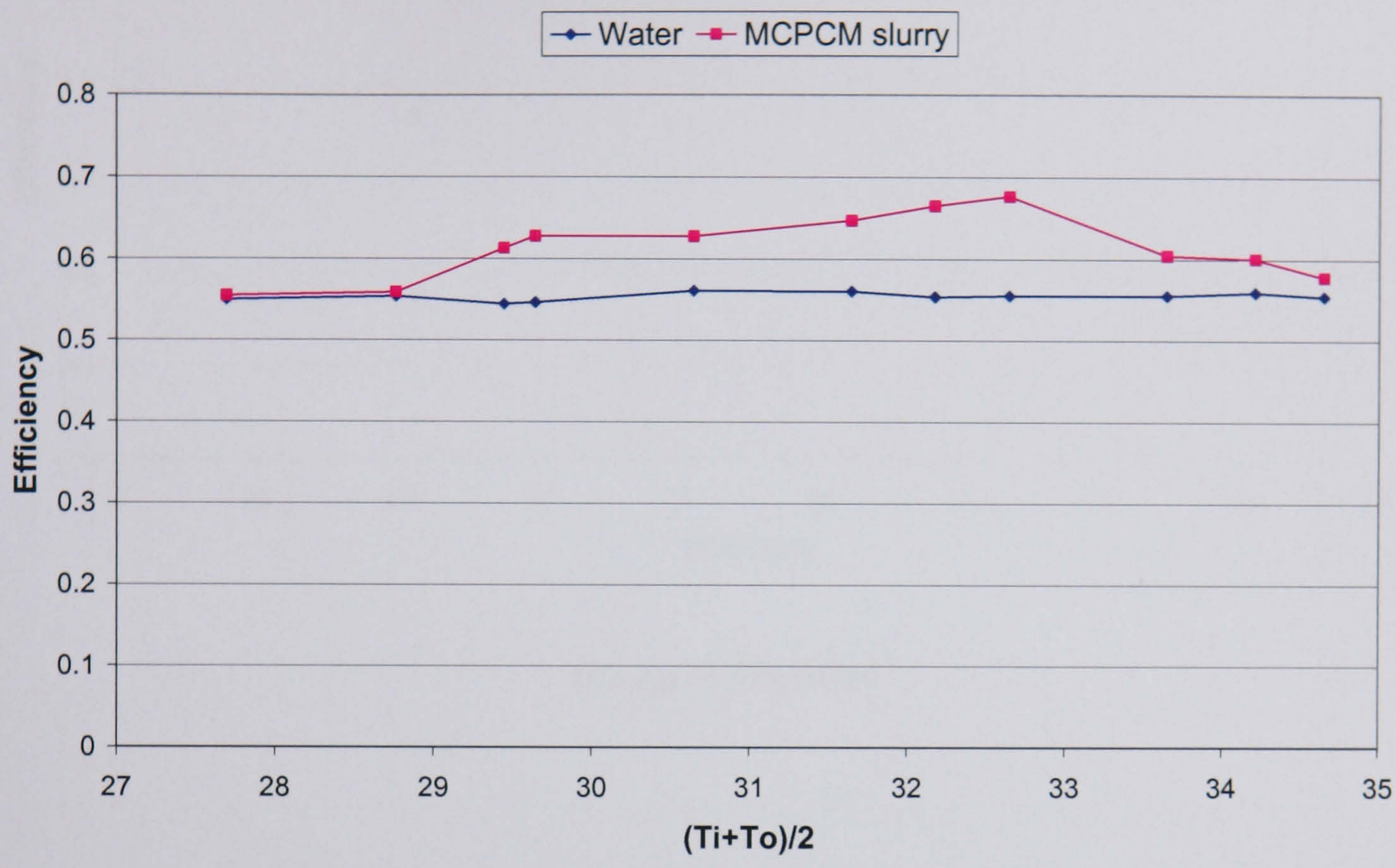

(a) I_{av} = 779 W/m2

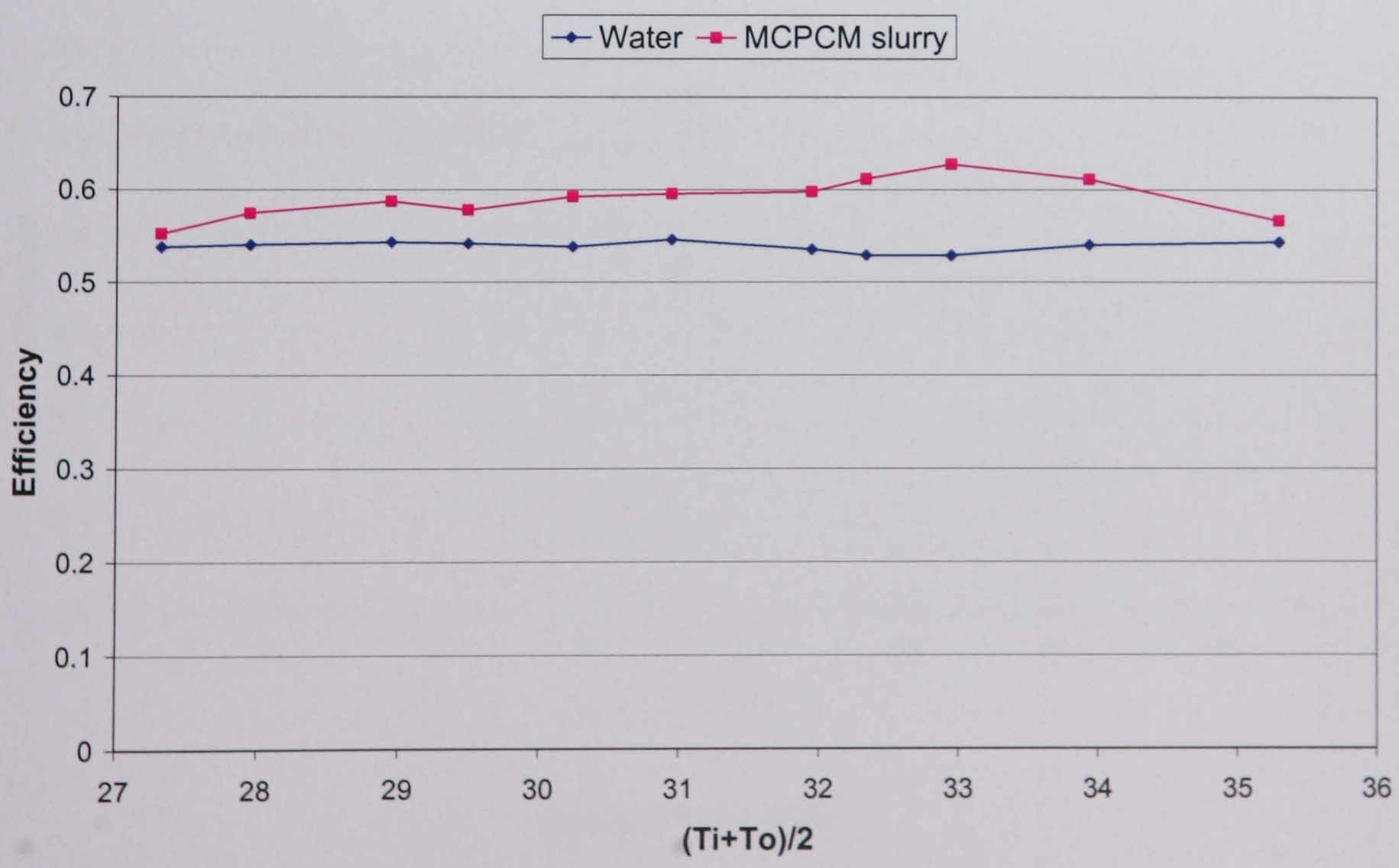

(b) $I_{av} = 599\ W/m^2$

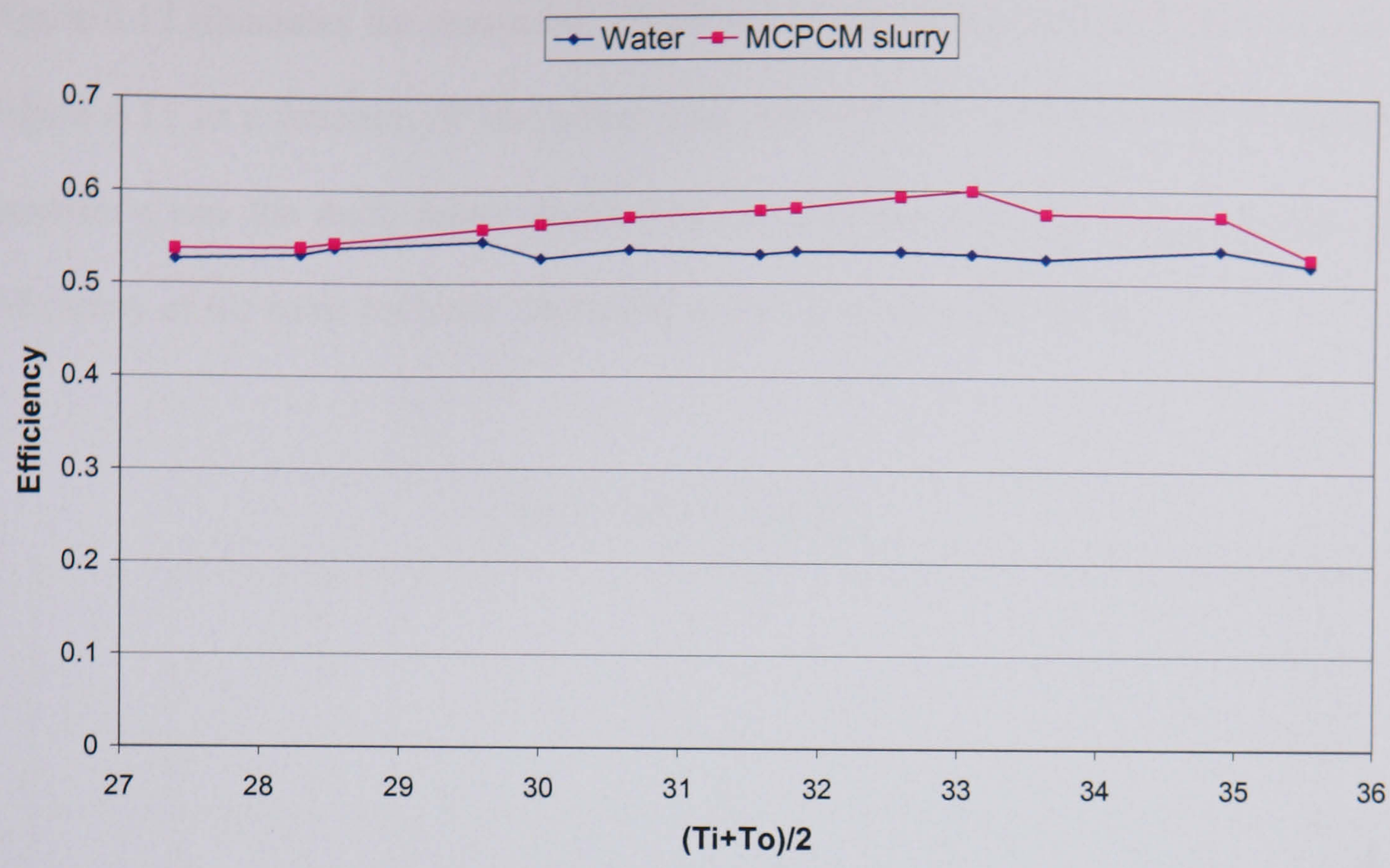

(c) $I_{av} = 396\ W/m^2$

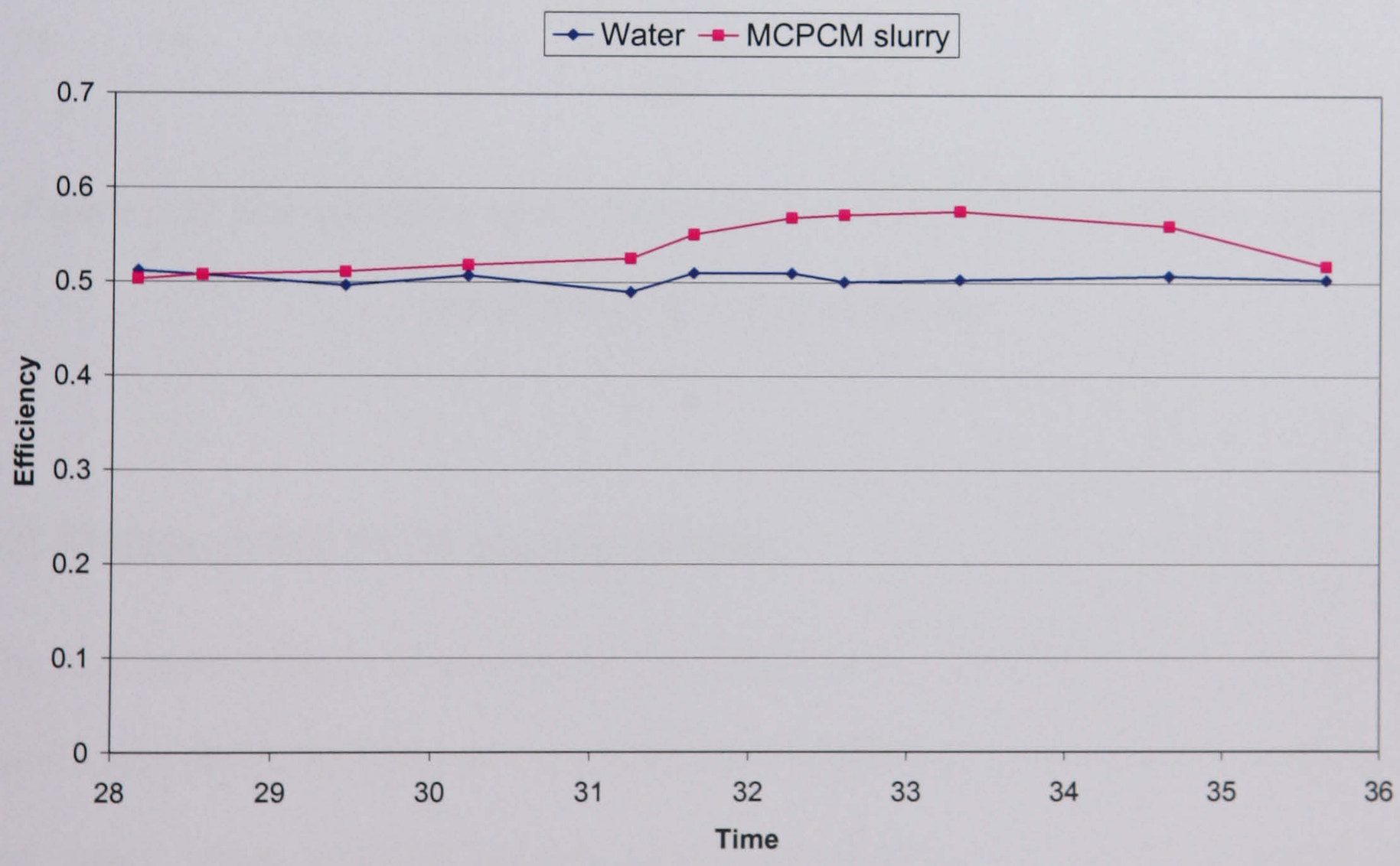

(d) $I_{av} = 217\ W/m^2$

Figure 6.12 illustrates the maximum efficiency of the solar collector determined from Figure 6.11 as a function of insolation from 200W/m^2 to 800W/m^2. The intensity of irradiance was the main factor dominated the efficiency of the solar collector. The efficiency of the solar collector decreased as the insolation decreased.

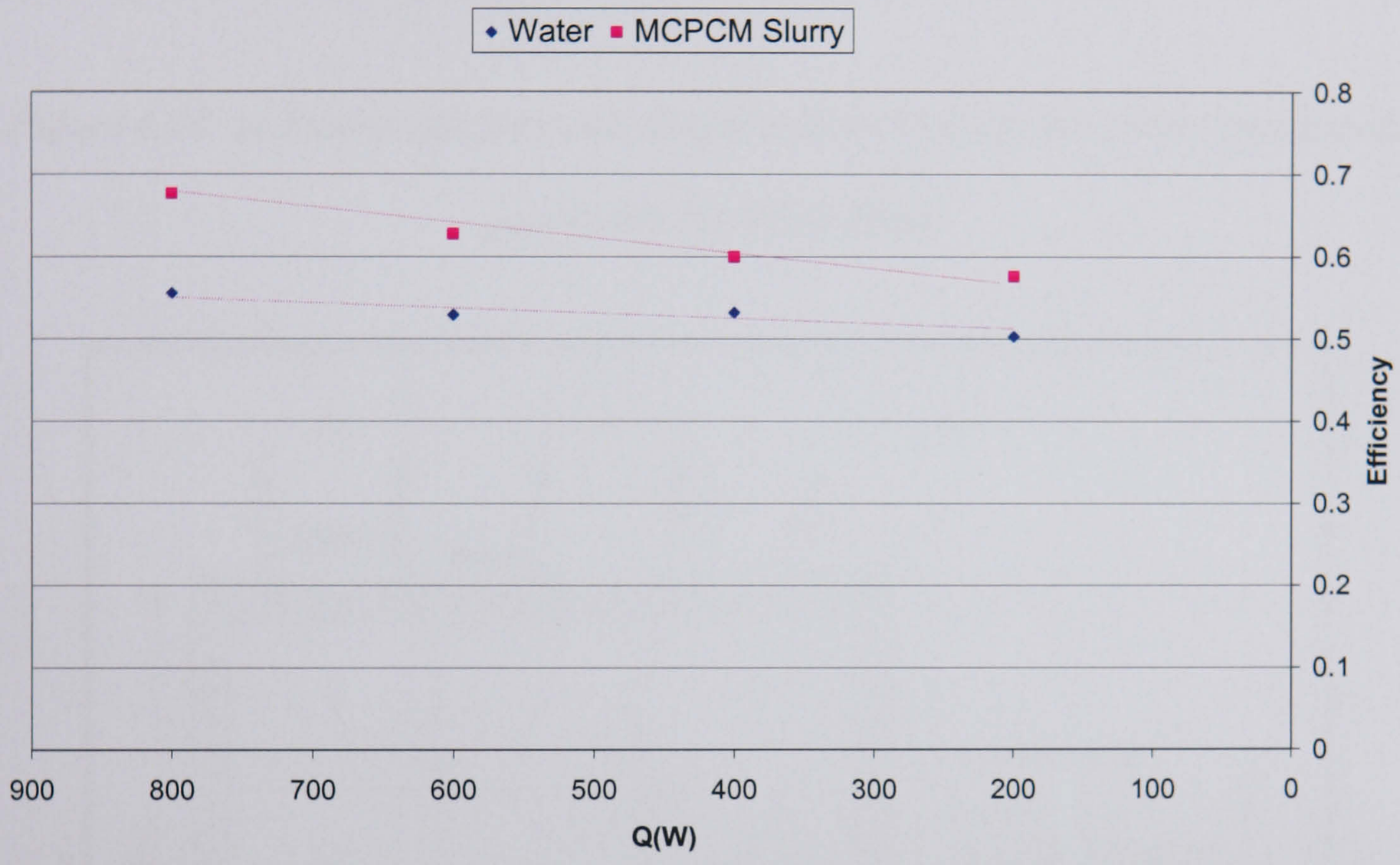

Figure 6.12 The efficiency of the solar collector at difference insolation with the use of MCPCM slurry and water

6.5 Fluidised-MCPCM glazing system

The next experiment is to investigate the performance of the fluidised double glazed panel using MCPCM slurry as a working fluid, which was constructed in a laboratory and tested under artificial lighting conditions. Figure 6.13 (a, b, c) shows the construction of double glazed panel. The panel was made of a plastic sheet instead of a glass sheet because the glass panel was too brittle to drill holes when bolting the sheet into a metal frame. Initially, the prototype was design with the dimension of

1m*1m. But because the big size of double glazed panel incur more pressure (due to the weight of fluid), this could lead to buckling and leakage problem. Thus the smaller scale with a surface area of 0.25m^2 (0.5m*0.5m) was constructed and a thickness of the sheet was 5mm. Silicon sealant was used for preventing leakage of fluid around the edge.

Figure 6.13: a) Double glazed panel diagram b) view of double glazed panel c) the panel with MCPCM slurry

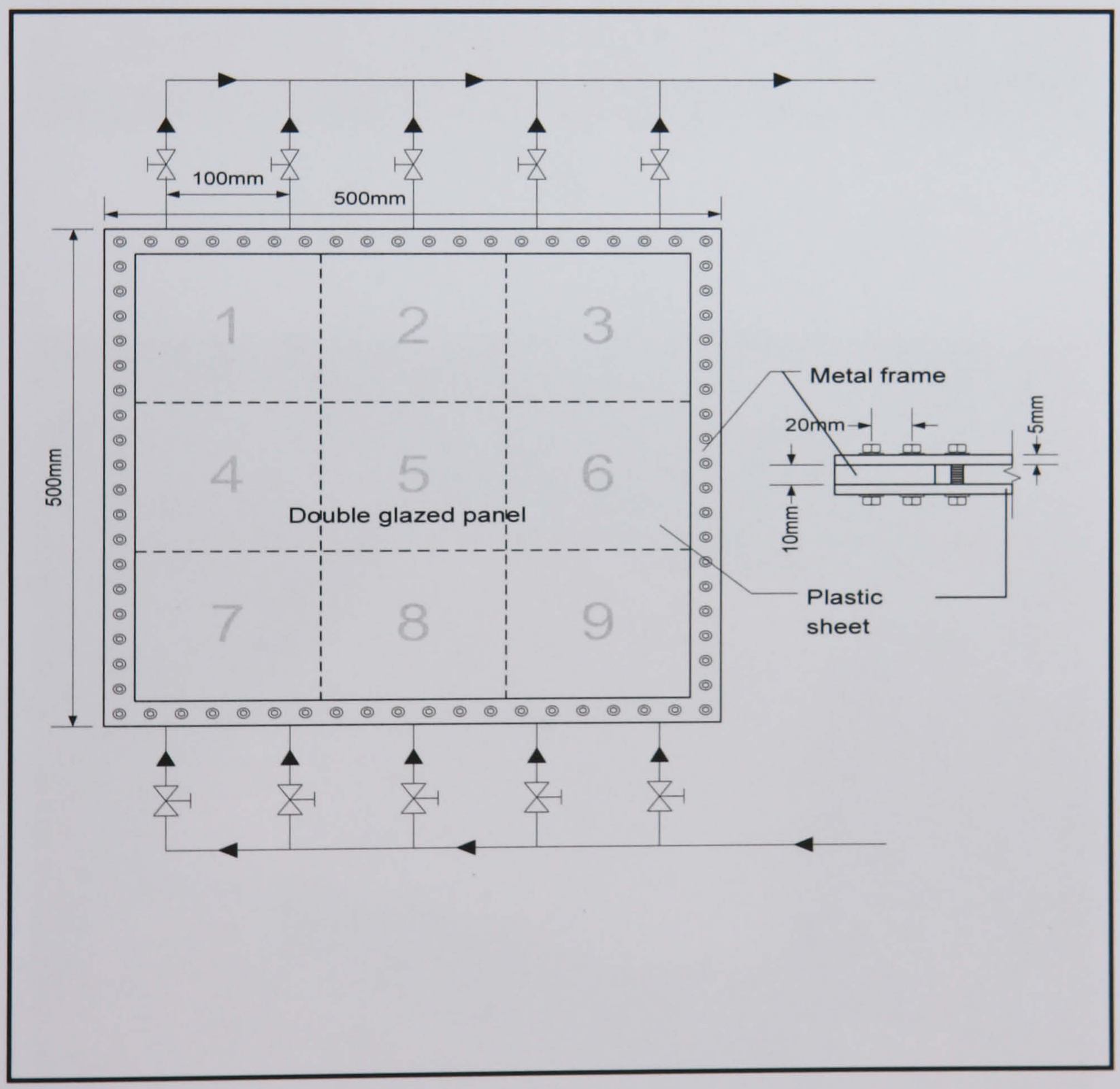

(a)

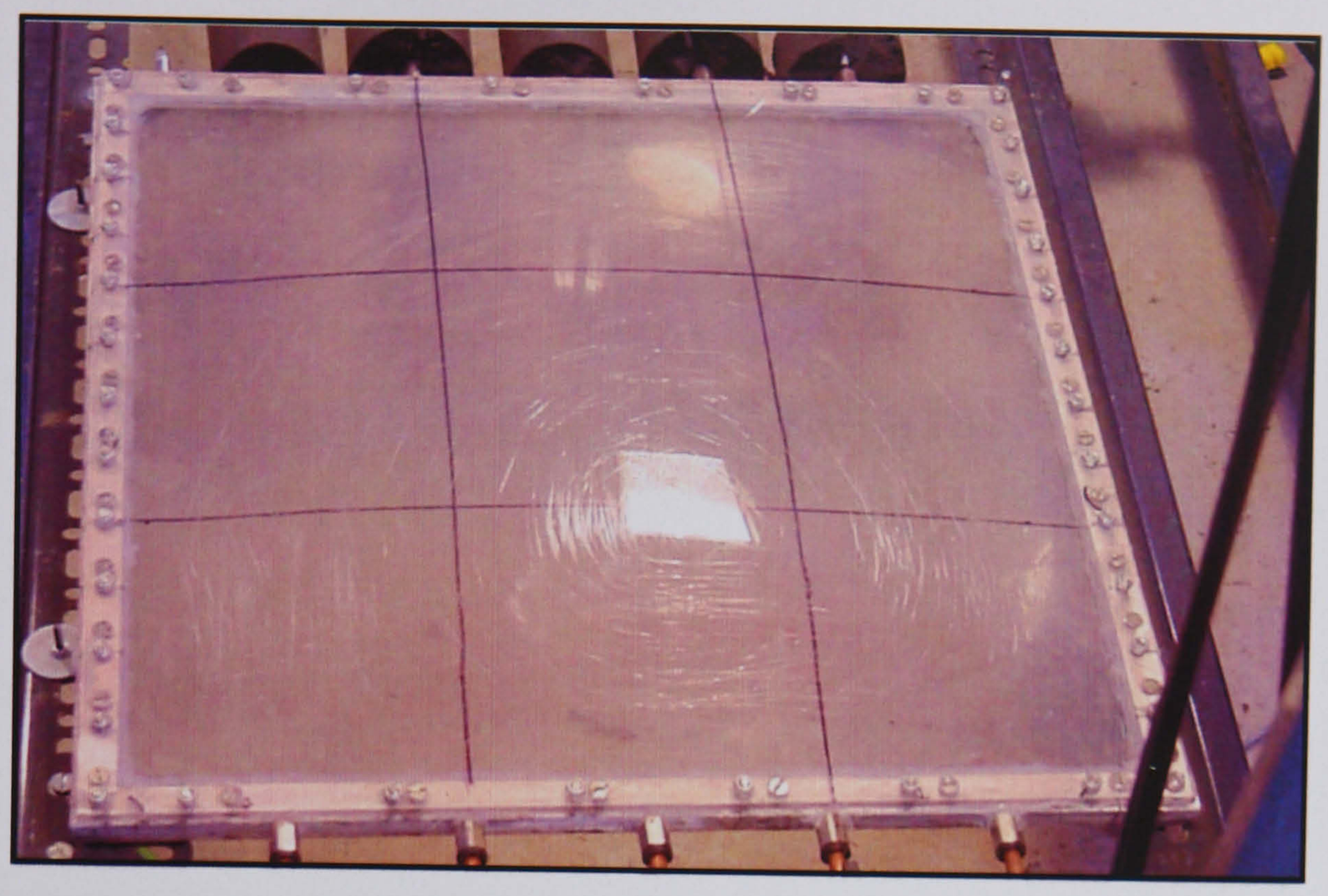

(b)

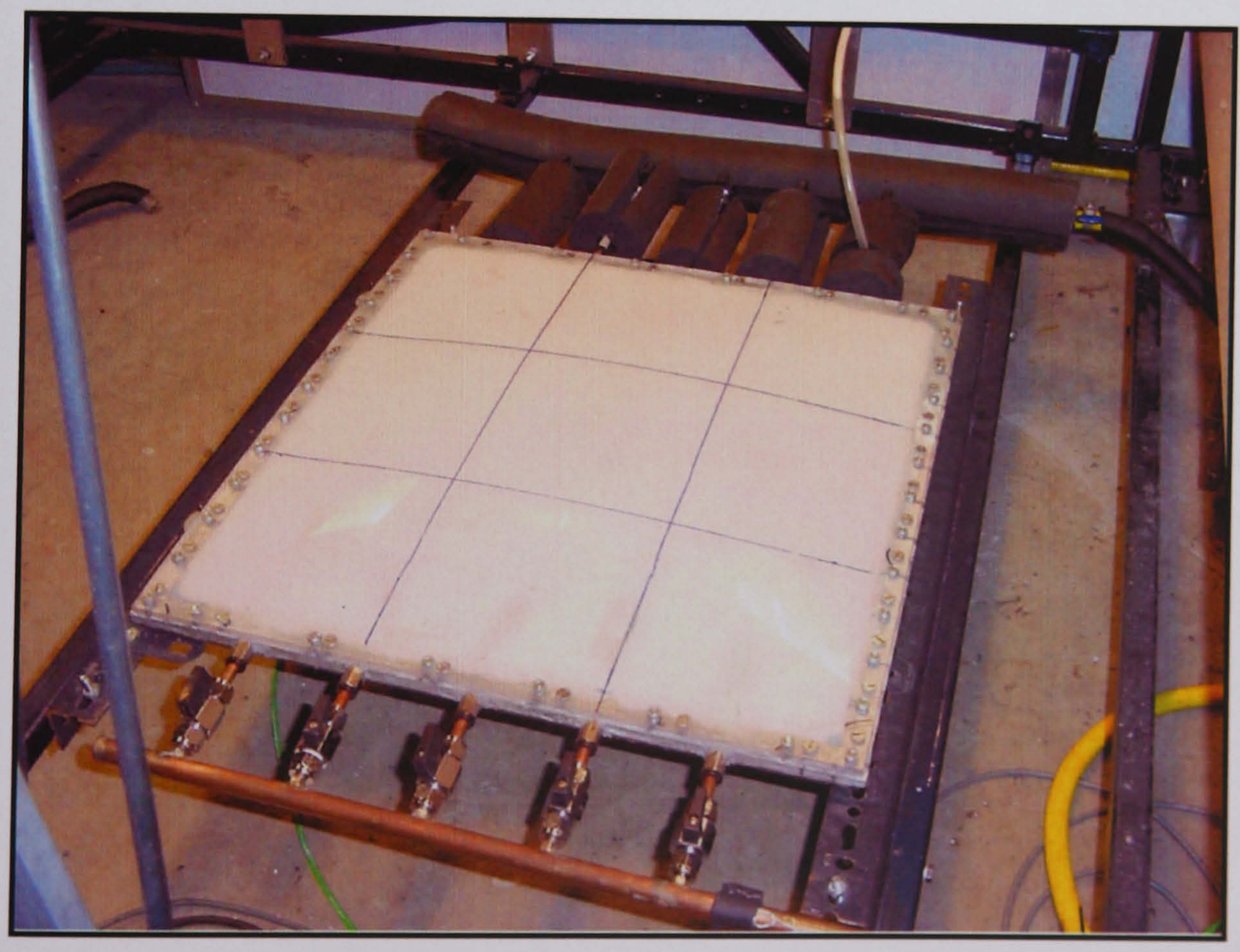

(c)

Figure 6.14 illustrates the schematic diagram of fluidised-MCPCM glazed energy storage system. The rig consists of a primary and secondary circuit and lighting system, which were similar to the previous experiment. There were five channels of inlets and outlets into the double glazed panel which linked by the main pipeline. The test procedure and operational cycle of this experiment was similar to the study of the solar collector. The phase change particle employed *n*-eicosane with the melting point of 35°C was used in the present study with 20% mixture (vol.%). The average insolation was calculated from the irradiance measured from nine equal spaces of the glazing area (see Figure 6.13a). The amount of heat carried by the primary working fluid (Q_2) can be estimated from the amount of heat received by the secondary working fluid (Q_4) as illustrated in Figure 6.6.

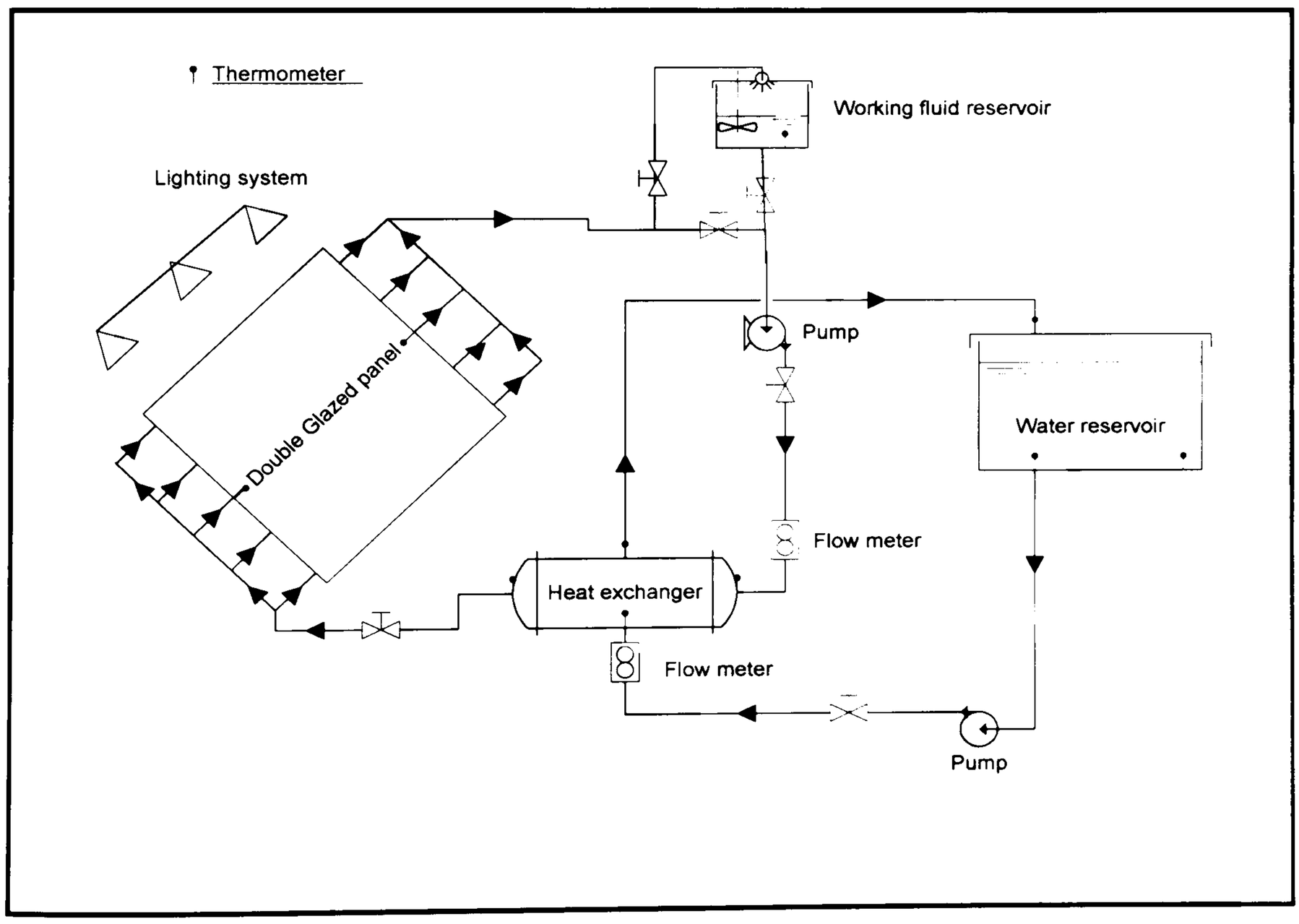

Figure 6.14: Fluidised double glazed energy storage schematic diagram

6.6 Performance of the fluidised MCPCM glazed energy storage system

6.6.1 Insolation pattern

Figure 6.15 (a to d) shows the irradiance map of lights on the glazing panel with the average measurement of 806W/m^2, 601W/m^2, 399W/m^2 and 200W/m^2, respectively. The distribution of light on the surface was seen to be variable of around ±10% with more intensity towards the middle area of the panel. However, it was unlikely that this would affect the experiments significantly because the average insolation levels were used in the calculations.

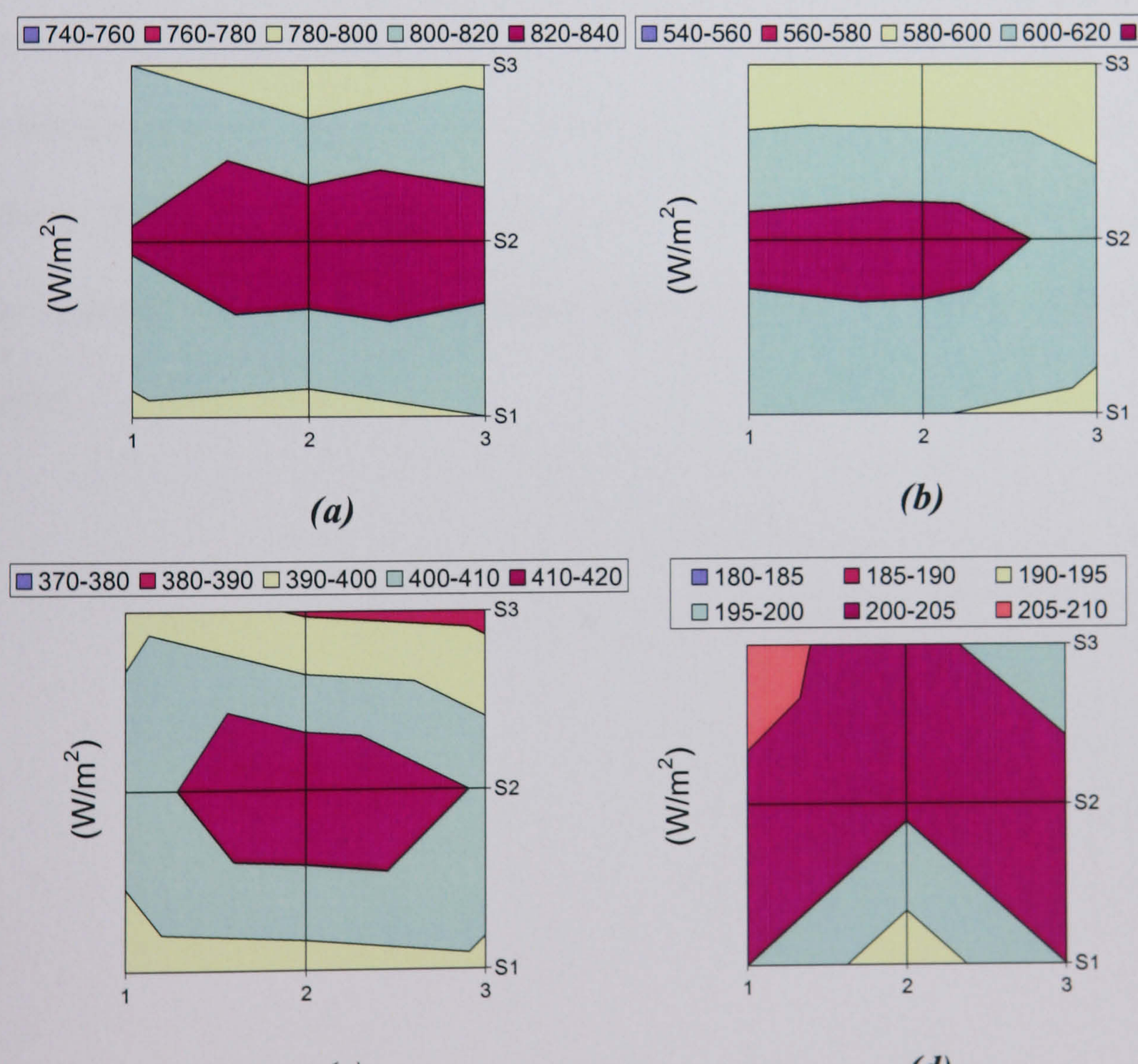

Figure 6.15: Insulation map for the double glazed panel with (a) I_{av} = 806W/m^2 (b) I_{av} = 601W/m^2 (c) I_{av} = 399W/m^2 (d) I_{av} = 200 W/m^2

6.6.2 Heat transfer characteristic

Figure 6.16 (a) to (d) illustrates the rate of heat transfer of the primary working fluid using 20% MCPCM slurry, which was estimated from the calculation of the secondary working fluid, water, under different irradiance from 800W/m^2 to 200W/m^2, respectively. Results were compared with the figure of pure water. At an average irradiance of 200W/m^2, 400 W/m^2, 600 W/m^2 and 800W/m^2, the maximum rates of heat transfer of the fluidised MCPCM glazed energy storage system were approximately 28W, 59W, 94W and 128W, respectively. Overall, with the use of MCPCM slurry as the primary working fluid the rate of heat transfer was enhanced by approximately up to 18% over the pure water. The rate of heat transfer of double glazed energy storage system was much smaller than that of the solar collector. This was because the surface area of the glazing panel was only one-fourth of the solar collector. However, this study does not aim to compare the performance between the solar collector and the double glazed panel according to different functions of the systems.

Figure 6.16: A comparison of the rate of heat transfer of the primary working fluid (Q_2) using water and 20% MCPCM slurry at (a) I_{av} = 806 W/m^2 (b) I_{av} = 601 W/m^2 (c) I_{av} = 399 W/m^2 (d) I_{av} = 200 W/m^2

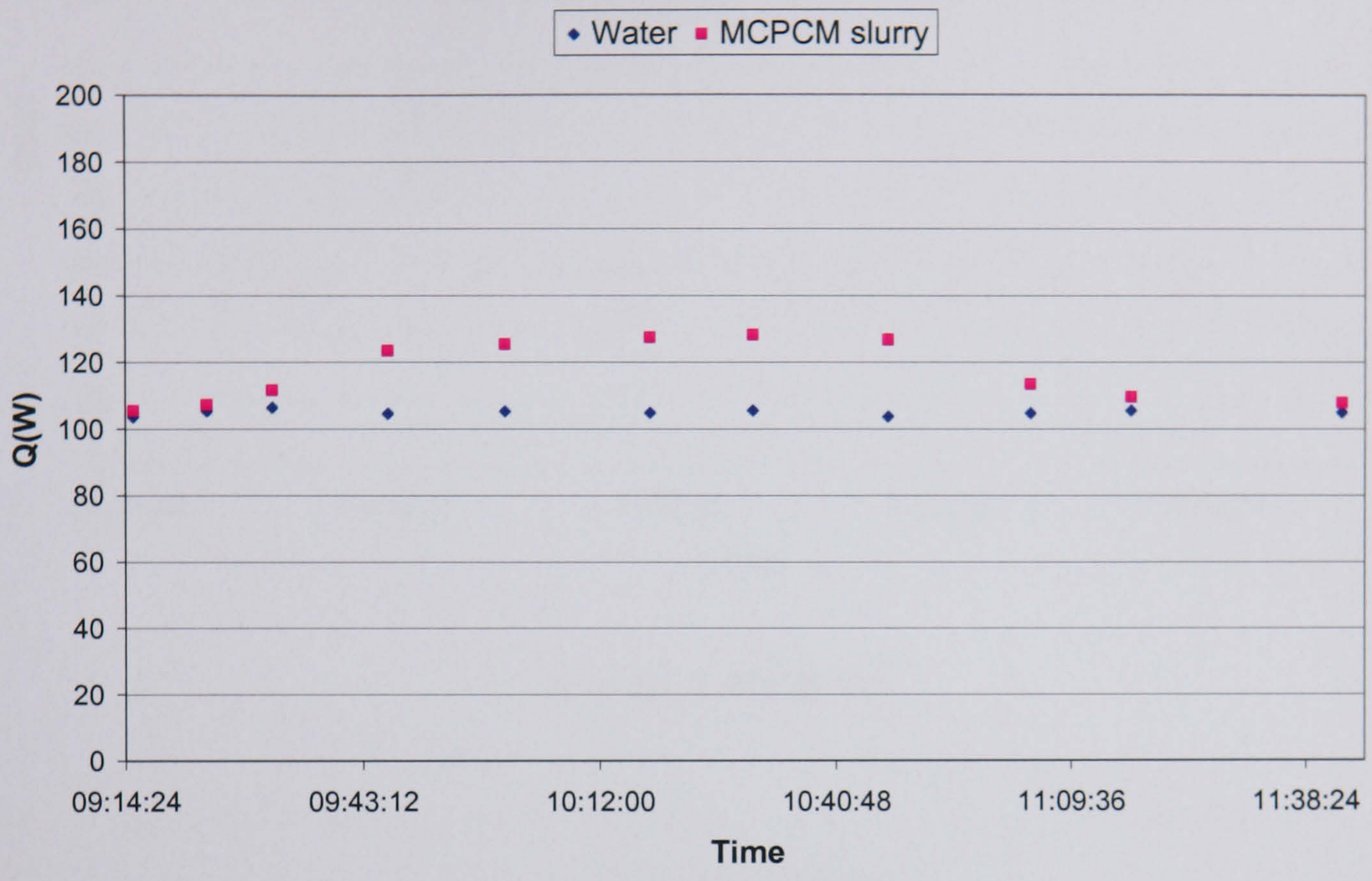

(a) I_{av} = 806 W/m^2

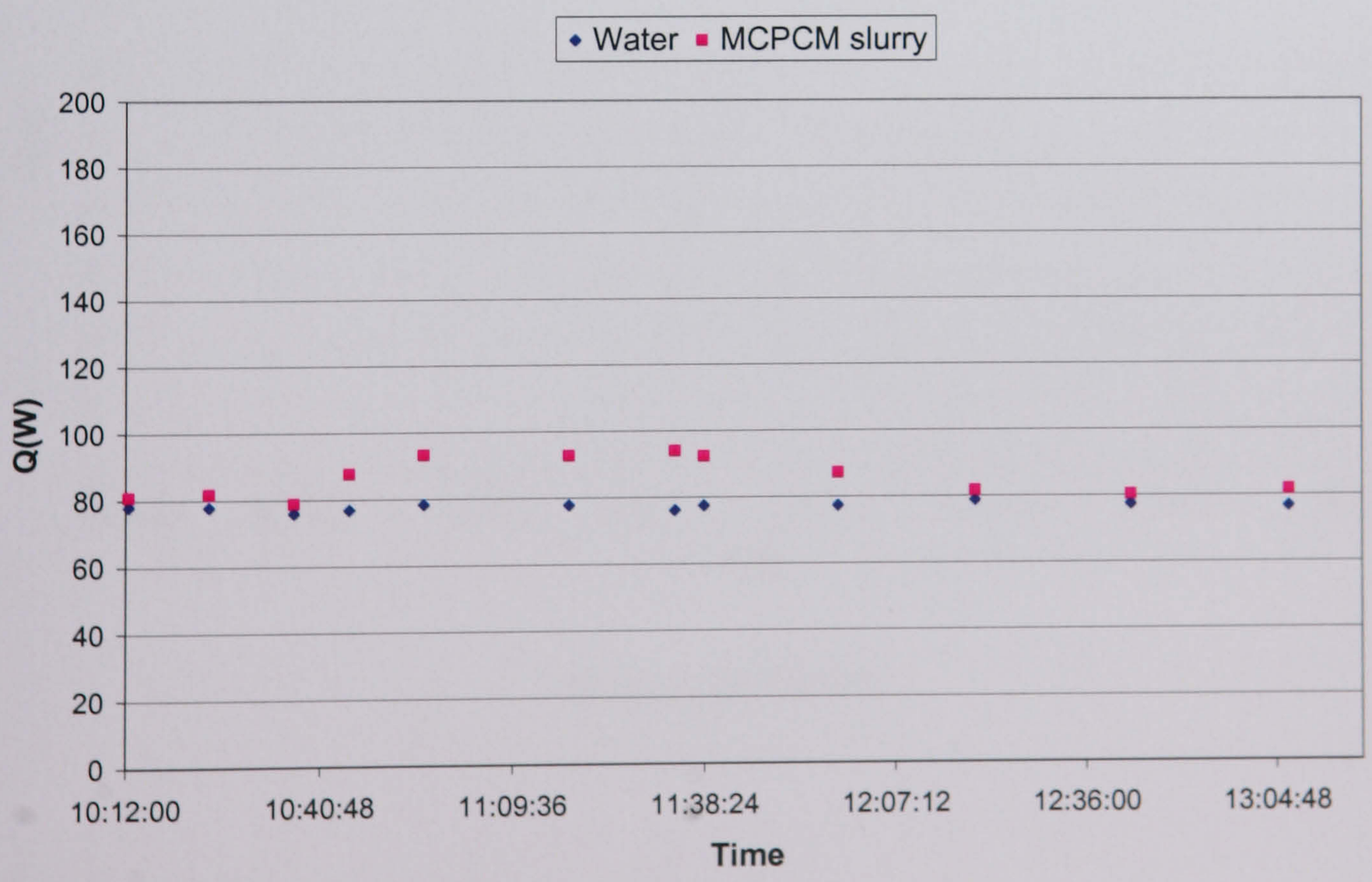

(b) I_{av} = 601 W/m^2

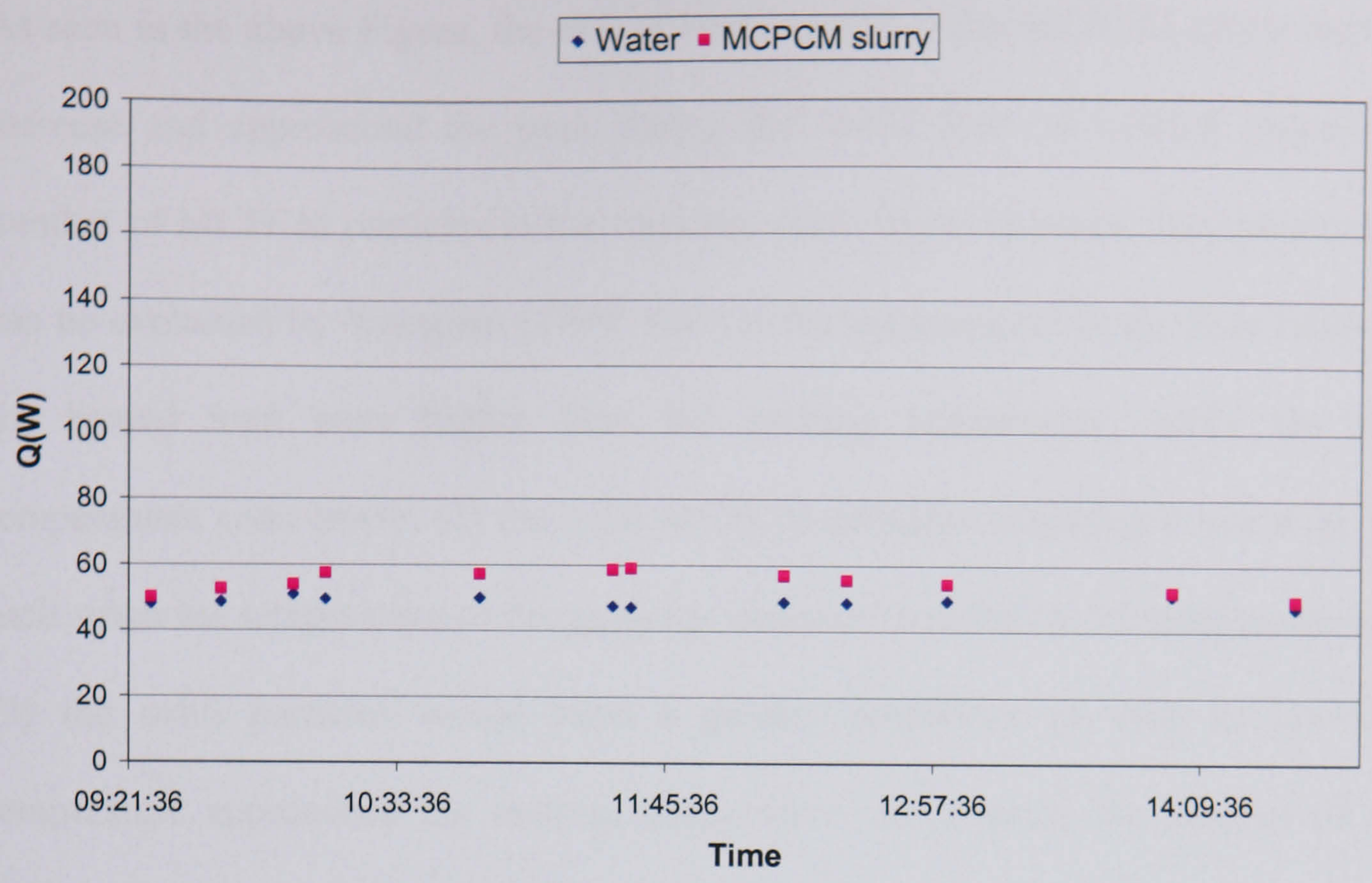

(c) I_{av} = 399 W/m^2

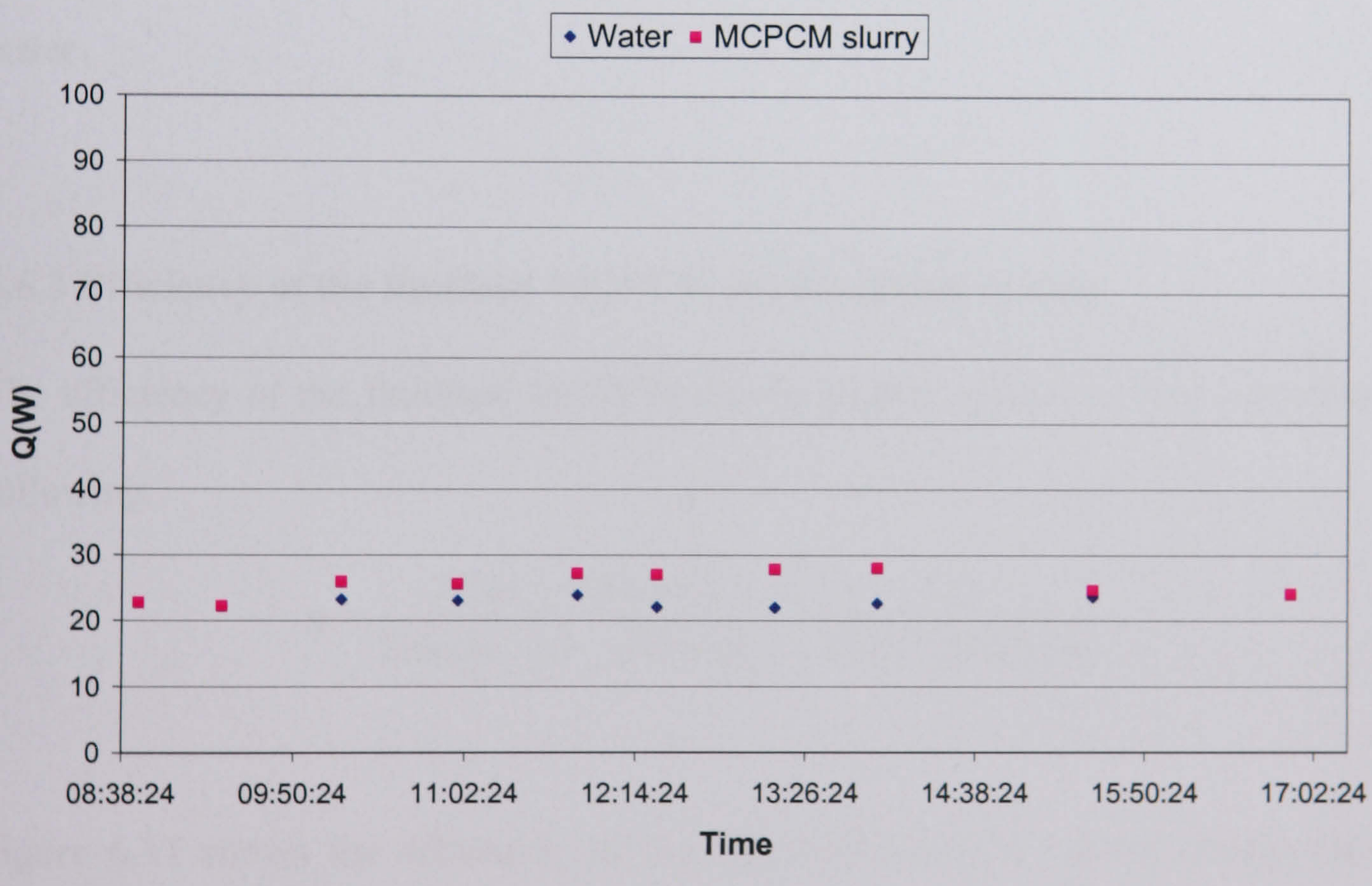

(d) I_{av} = 200 W/m^2

As seen in the above Figure, the rate of heat transfer of the MCPCM slurry started to increase and approached the peak during the initial state of melting process (the number of MCPCM particles in the working slurry began to melt). This phenomenon can be explained by Yamgishi (1999) that (1) the temperatures at the flow fields near the heated wall were higher than the melting temperature, while the slurry temperatures were lower; (2) the solid MCPCM particles migrating to the wall could melt when the temperature of the particles increased beyond the melting temperature; (3) the solid particles would have a greater possibility to melt as the slurry temperature approached the melting temperature. As a result, the number of solid particles melting near the wall increased with the measured temperature, resulting in an increase in the rate of heat transfer. Once all phase change particle completely melted, the figure started to drop and maintained slightly above the curve of pure water.

6.6.3 Efficiency of the fluidised MCPCM double glazed system

The efficiency of the fluidised MCPCM double glazed system, η, was calculated as following.

$$\eta = \frac{Heat\_collected}{Energy\_on\_absorber} = \frac{Q}{Area * Insolation}$$

Figure 6.17 shows the efficiency of the fluidised MCPCM glazed energy storage system as a function of the average fluid temperature, $(T_{in}+T_{out})/2$, using water and MCPCM slurry under insolation of (a) 806W/m^2, (b) 601W/m^2, (c) 399W/m^2 and (d) 200W/m^2. It was observed that the use of MCPCM slurry could significantly enhance the efficiency of the fluidised glazed energy storage system over the use of pure

water. For instance, at 399W/m^2, the efficiency of the system with the use of MCPCM slurry was seen at around 0.58 comparing to 0.5 of the pure water. The efficiency of the fluidised MCPCM double glazed system increased gradually and reached the maximum value at around the average fluid temperature of 33°C to 34°C due to the increased number of the melted MCPCM particles in a carrier fluid. After that, the efficiency of the system decreases and approaches the minimum value (all particles have completely melted). Thus, it is recommend maintaining the average slurry temperature of around 33°C to 34°C to maximise the benefit from this phase change slurry.

Figure 6.17: Efficiency of the fluidised MCPCM glazed energy storage system plotted against an average fluid temperature, $(T_{in}+T_{out})/2$, using MCPCM slurry and water at a) I_{av} = 806W/m^2 b) I_{av} = 601W/m^2 c) I_{av} = 399W/m^2 d) I_{av} = 200W/m^2

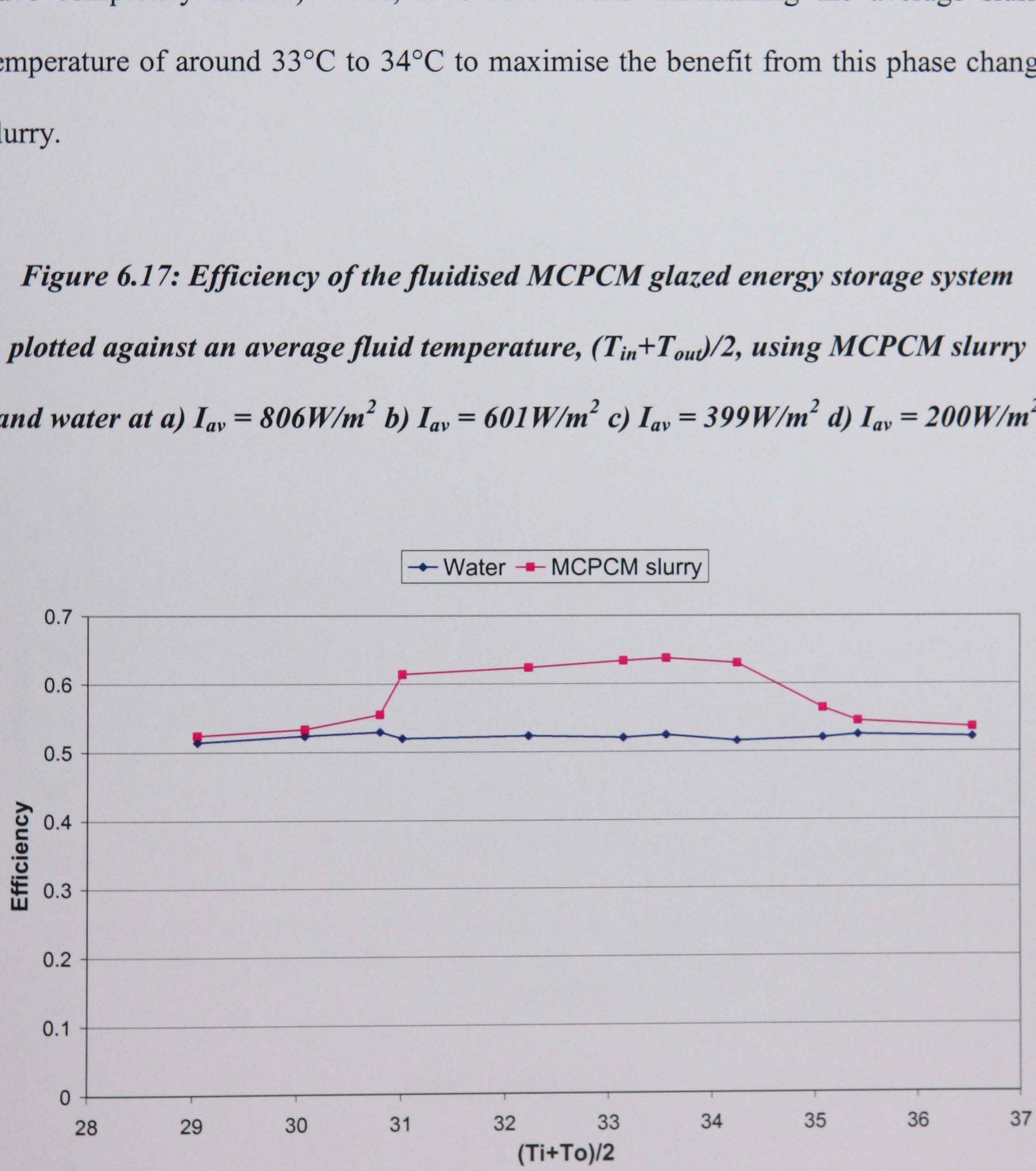

(a) I_{av} = 806 W/m^2

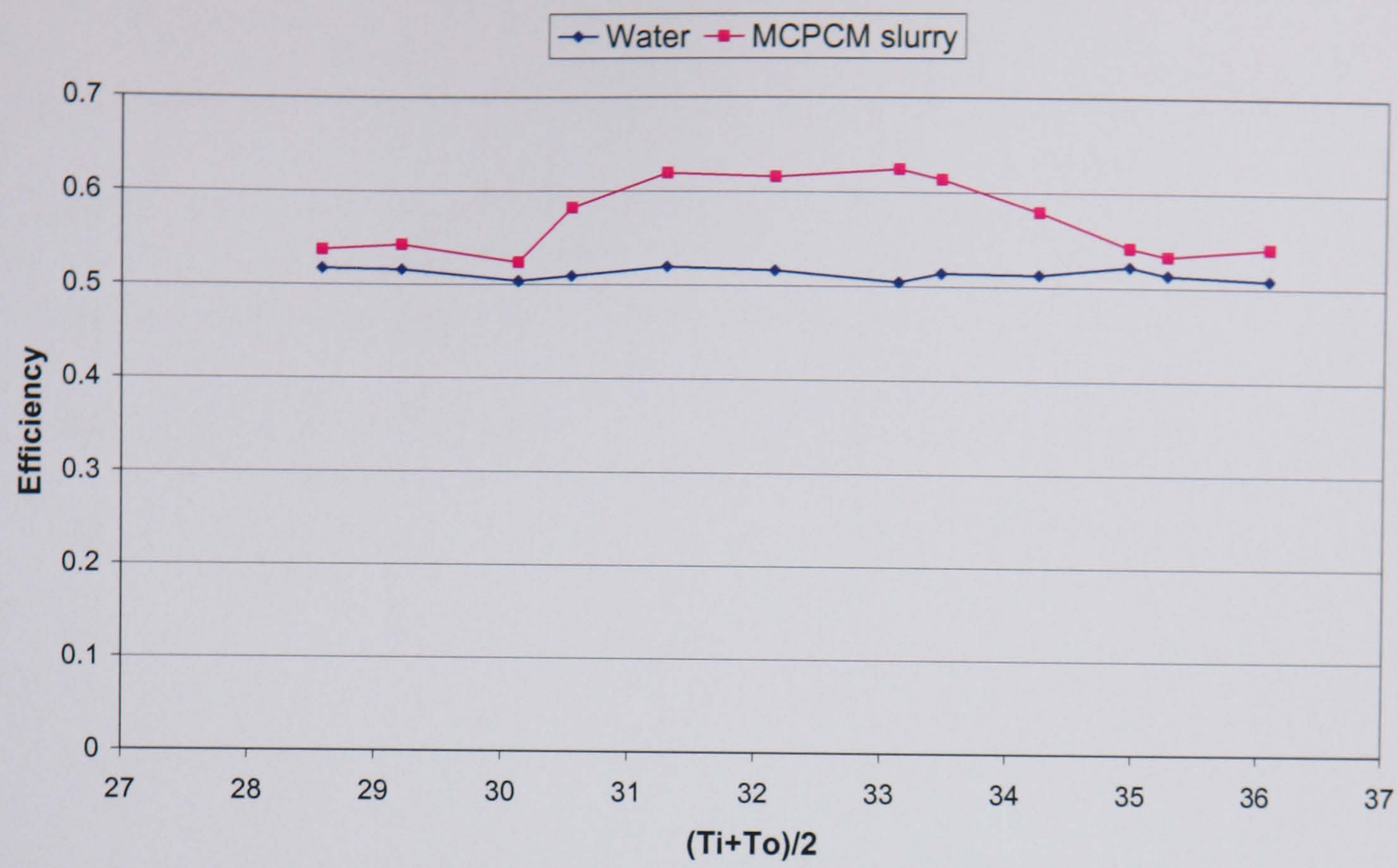

(b) I_{av} = 601 W/m^2

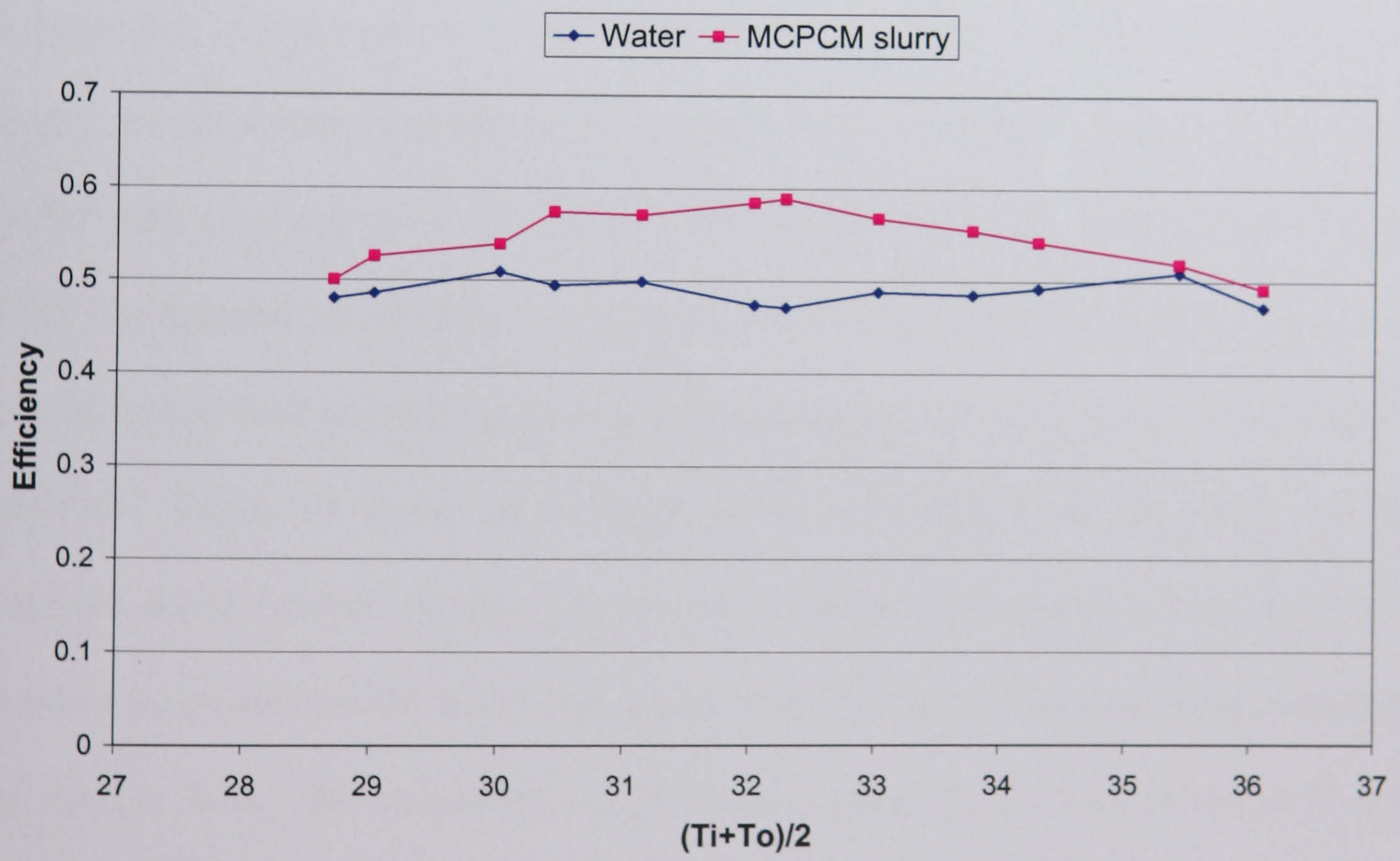

(c) I_{av} = 399 W/m^2

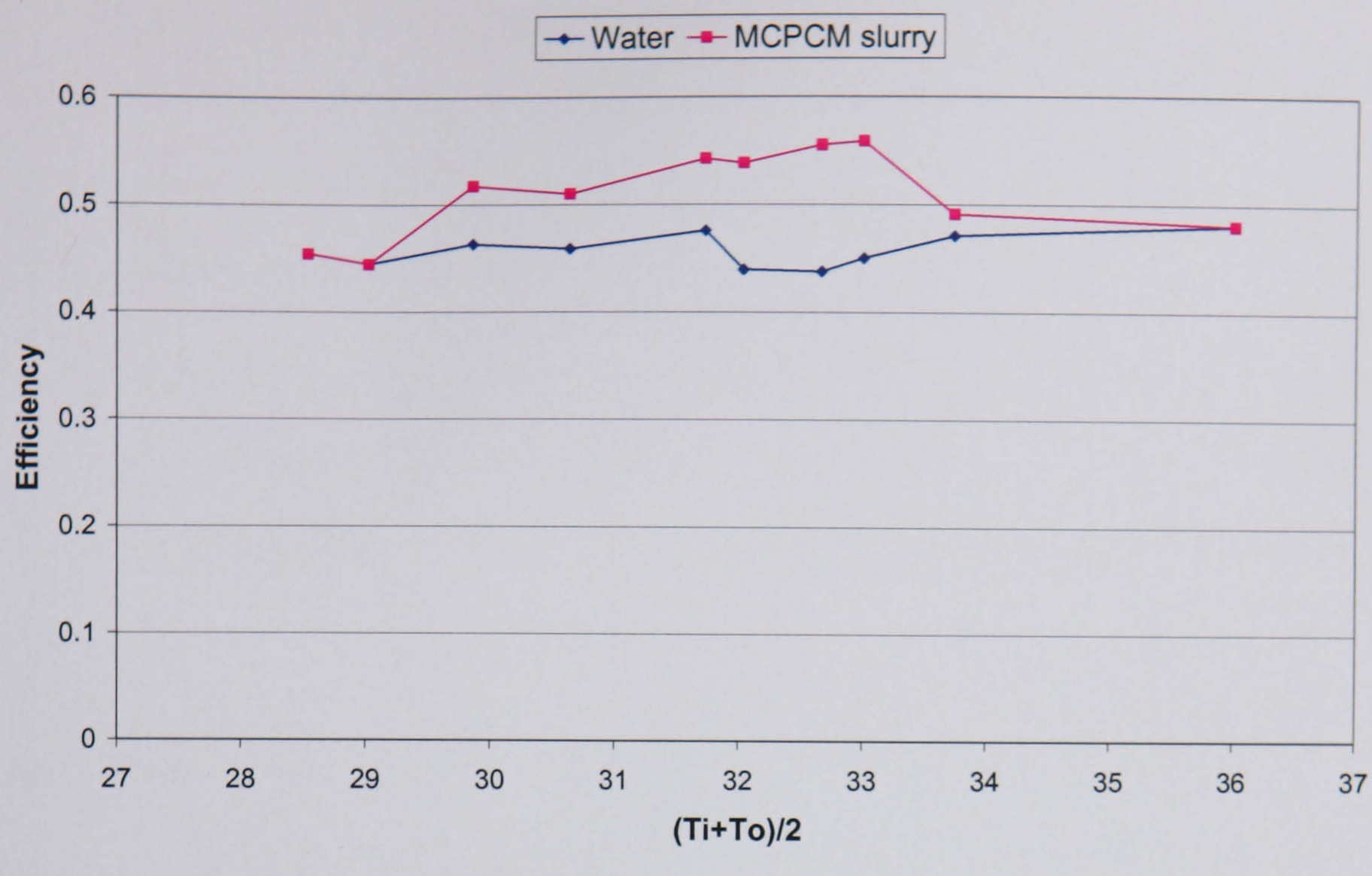

(d) I_{av} = 200 W/m^2

Furthermore, it was observed that the performance of the fluidised MCPCM glazed energy storage system was affected by the insolation of the light. The efficiency of the system with high insolation was greater than those of the low insolation (see Figure 6.18). For instance, at 806W/m^2 the efficiency of the system with MCPCM slurry was approximately 0.62 and the figure dropped significantly to 0.56 with the irradiance of 200W/m^2. Table 6.3 shows an average power consumption of the pump for the fluidised double glazed system. The average energy consumption of the pump was found to be around 44.2W which was higher than the rate of heat transfer provided by the system under the insolation of 200W/m^2. Thus, in the real situation it was recommended to switch off the pump once the solar radiation fail below 200W/m^2.

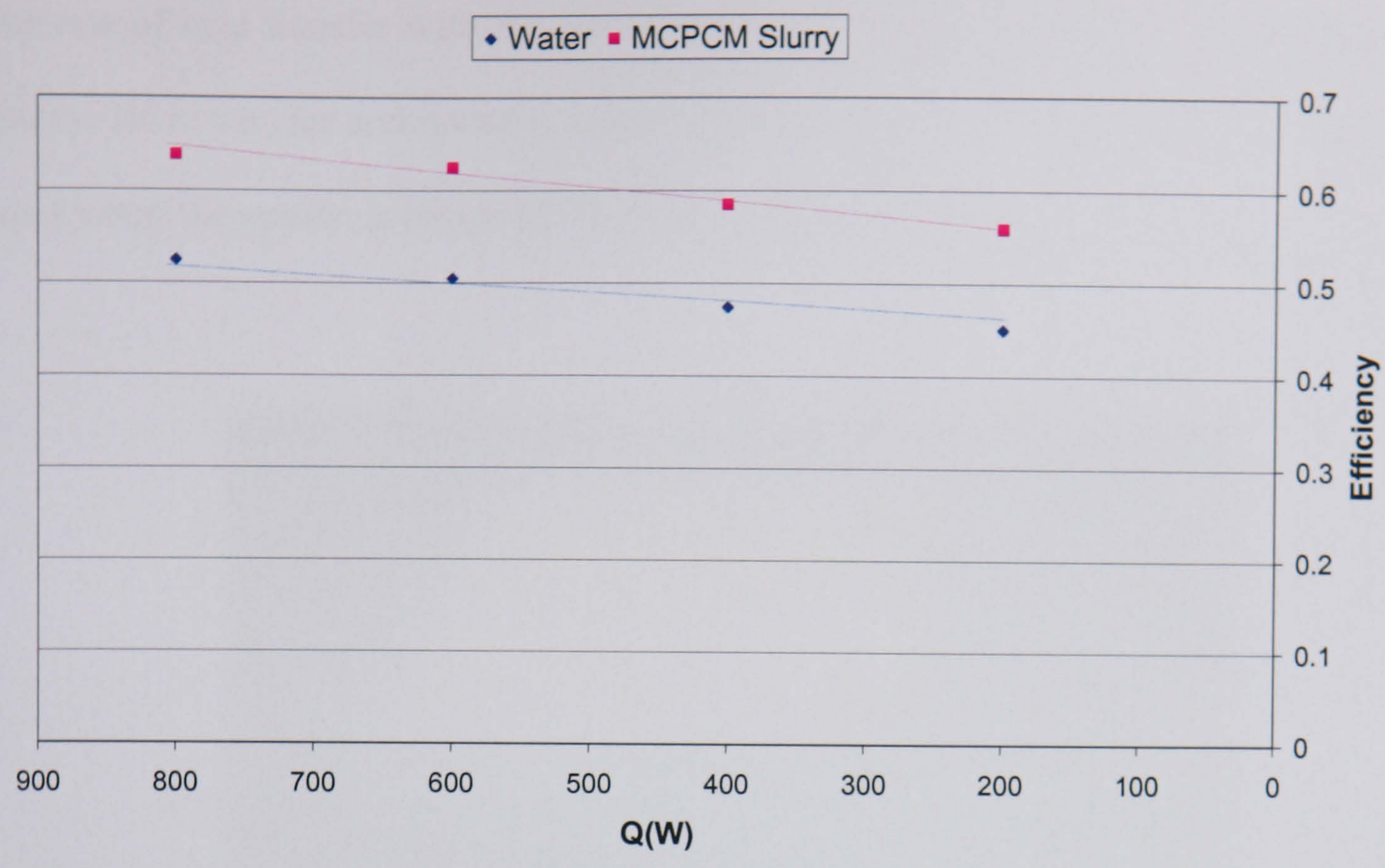

Figure 6.18: The efficiency of the fluidised MCPCM glazed energy storage system at difference insolation with the use of MCPCM slurry and water

Volt	Amp	Watts
249	0.190	47.31
246	0.141	34.686
247	0.202	49.894
248	0.181	44.888
	Average	**44.194**

Table 6.3: Pumping power requirement of the system

The further study is to investigate the performance of the fluidised glazed energy storage system with coloured MCPCM slurry. Water medium was coloured using a dye mixture to increase the absorptivity of water to solar radiation. Figure 6.19 illustrates a view of the fluidised double glazed energy storage system with yellow MCPCM slurry. Figure 6.20 shows the rate of heat transfer of the system with the yellow MCPCM slurry comparing with the original colour at the irradiance of 800W/m^2. Under the laboratory condition, there was no significant improvement in

the rate of heat transfer with the use of the yellow MCPCM slurry over the original slurry. However, for architectural reasons the coloured MCPCM slurry could then be used when the system is integrated into the building fabric.

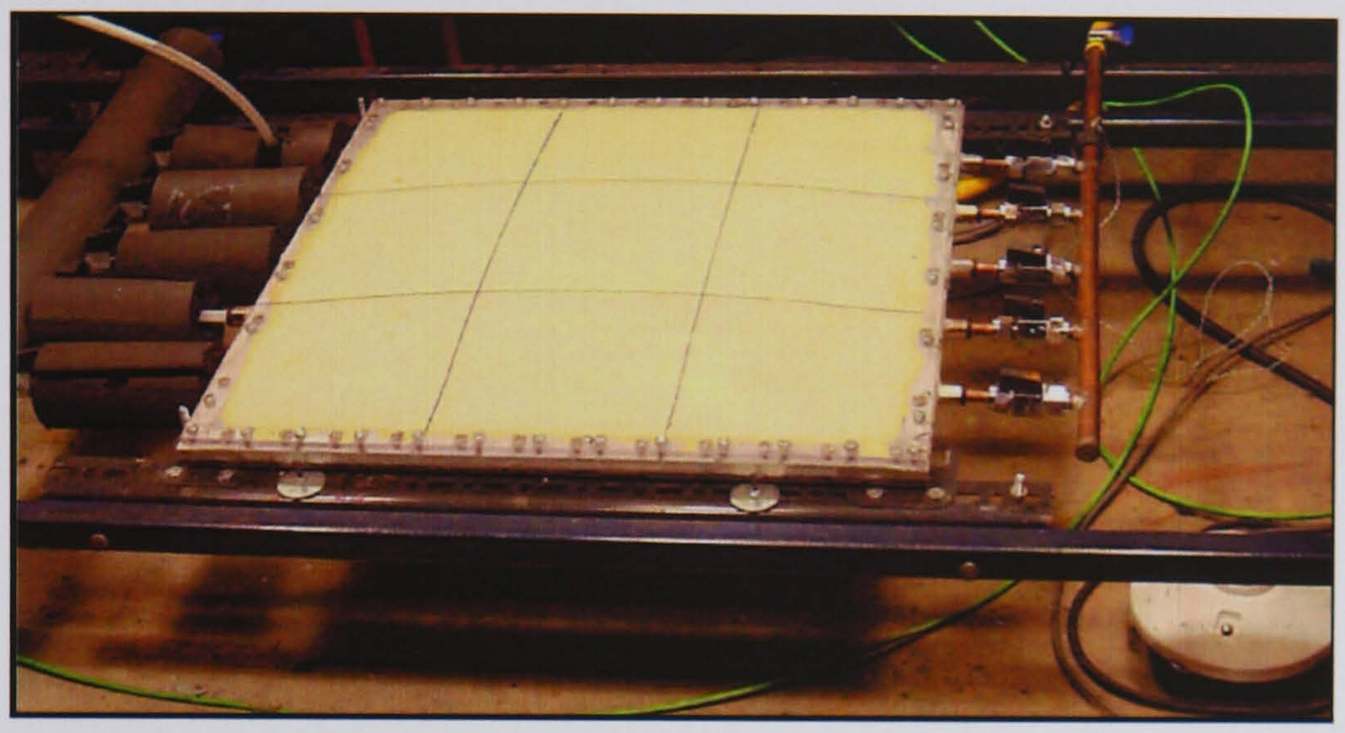

Figure 6.19: Fluidised glazed energy storage system with yellow MCPCM slurry

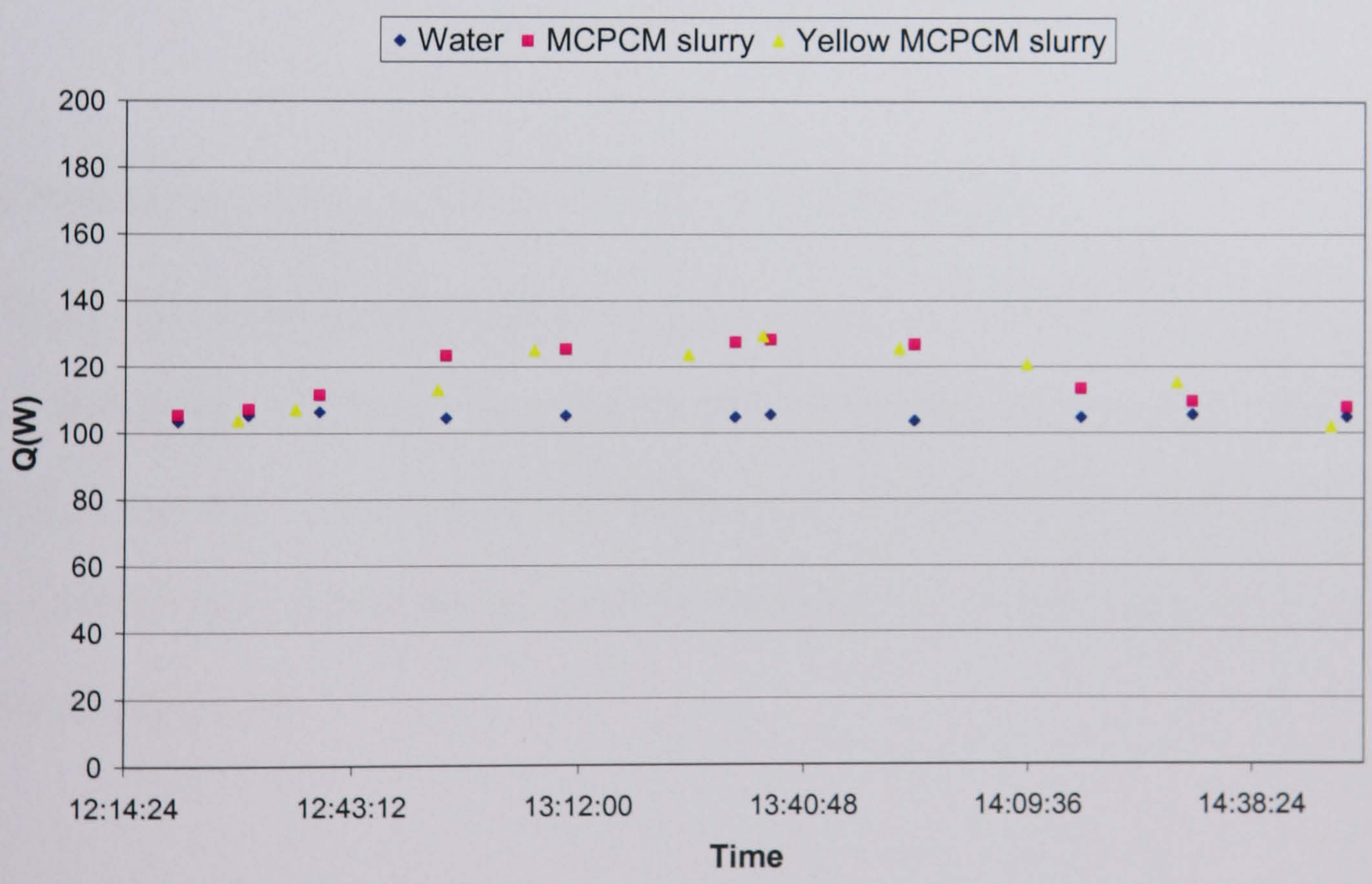

Figure 6.20: A comparison of the rate of heat transfer for 20% MCPCM slurry with yellow and original colour as the primary working fluid at I_{av} = 806 W/m^2

6.7 Energy and environmental effects: Simple analysis

An analysis to determine the energy and environmental benefits of the fluidised MCPCM glazed energy storage system was carried out by using a simple payback method. The number of glazed unit to be integrated into building fabrics was 1, 4, 8, and 80 units with the total surface area of 0.25m^2, 1m^2, 2m^2, and 20m^2, respectively. Three different locations were selected, namely, Tokyo (36°N), Bangkok (14°N) and Nottingham (54°N). The optimum configuration for the system is to face due south with an angle of inclination equivalent to the latitude angle. During the simulation, each module was assumed to provide the maximum efficiency based on the average slurry temperature of around 33°C to 34°C as illustrated in Figure 6.18. For instance, at 600W/m^2, the fluidised double glazed unit will provide the efficiency of around 0.62 with the rate of heat transfer of 93W (0.62x600W/m^{2}x0.25m^2).

6.7.1 Solar intensities in Bangkok, Tokyo and Nottingham

Figure 6.21 shows monthly available solar irradiance in (a) Bangkok, (b) Tokyo and (c) Nottingham. The available energy is lowest in January and December and highest in June and July. The overall annual solar energy in Bangkok, Tokyo and Nottingham is 2,491kWh/m^2, 2,095kWh/m^2 and 1,553kWh/m^2 for the due south-facing inclined plane, respectively.

Figure 6.21: Monthly available solar energy in (a) Bangkok, (b) Tokyo and (c) Nottingham (CIBSE guide, IHVE guide)

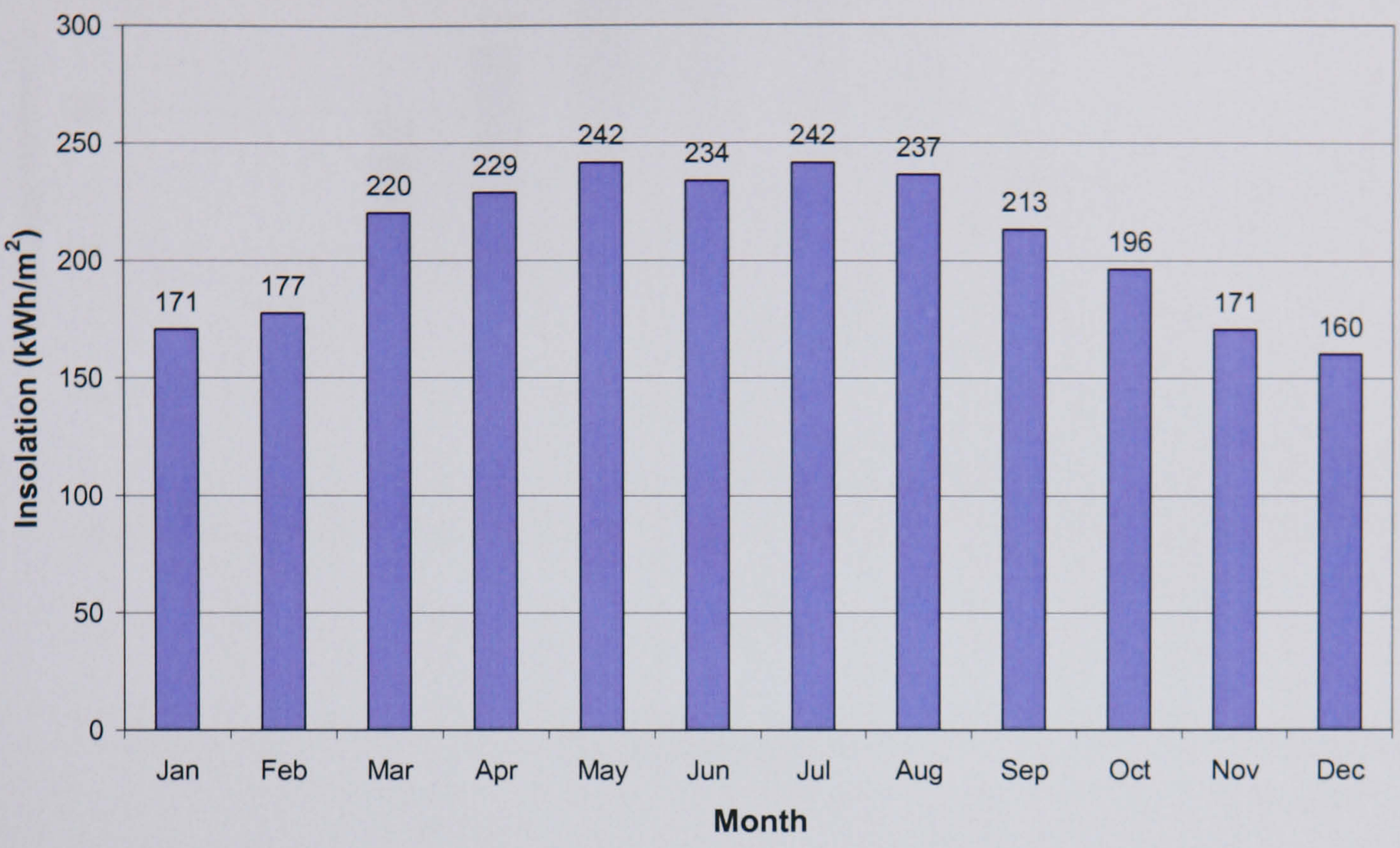

(a) Bangkok

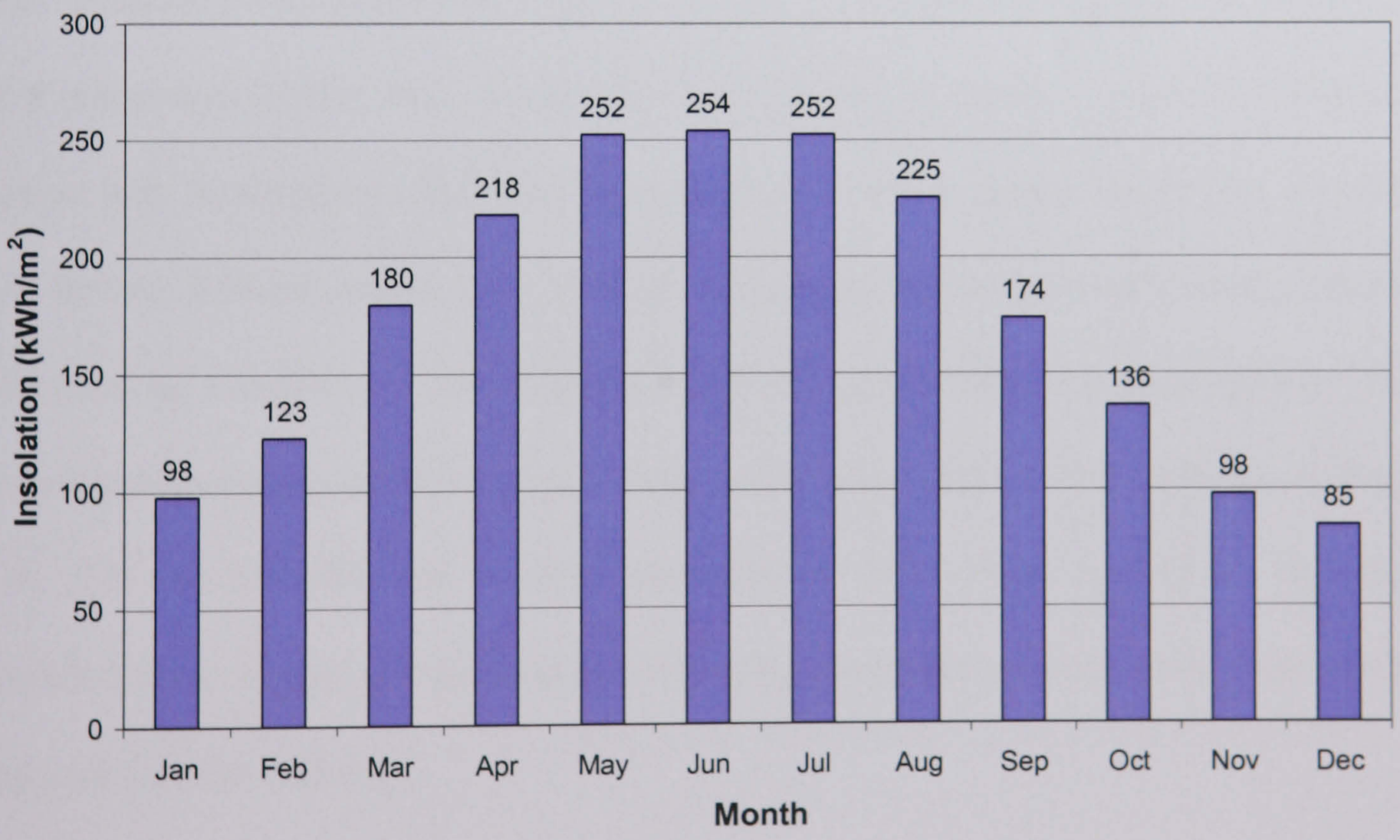

(b) Tokyo

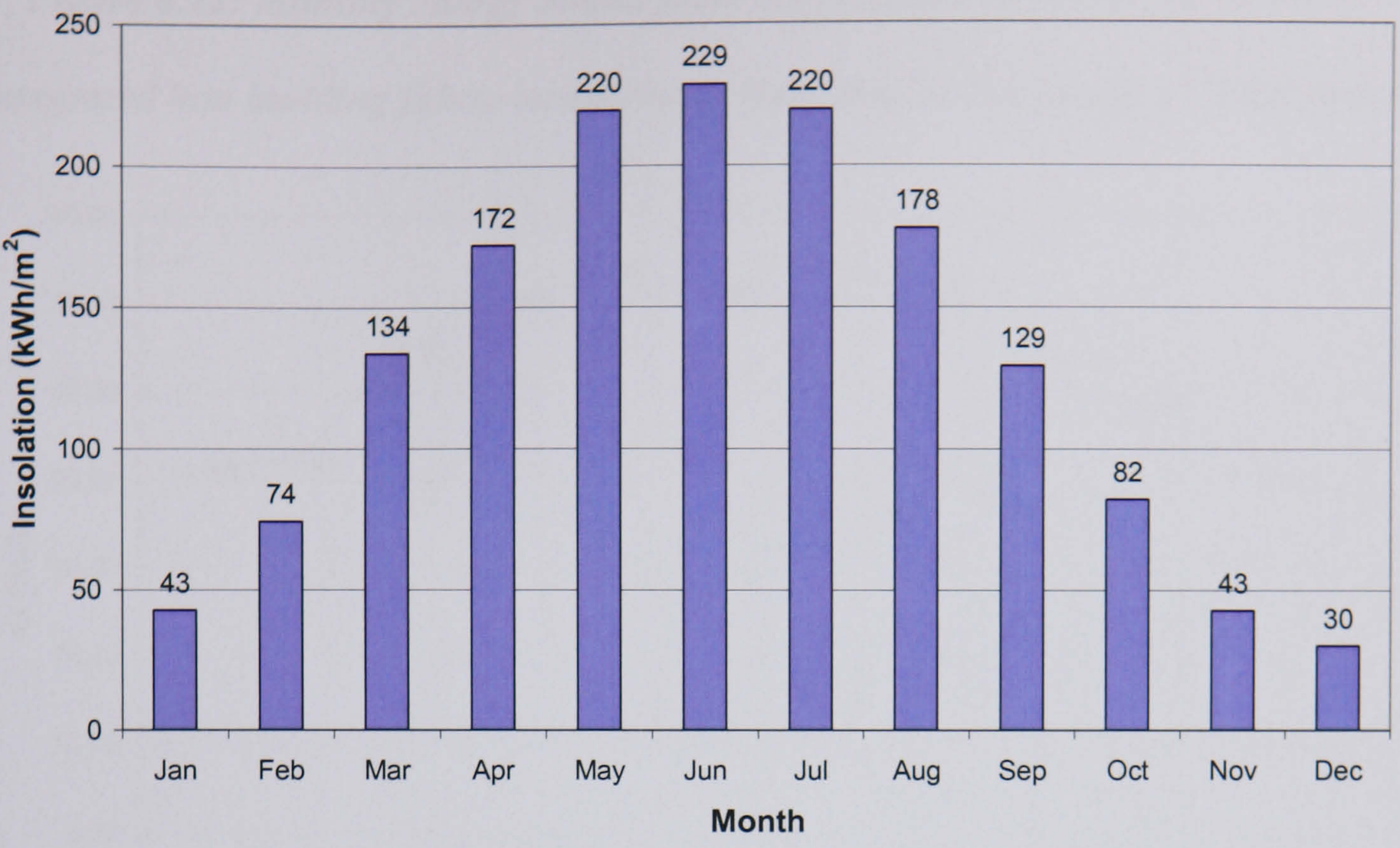

(c) Nottingham

The fluidised MCPCM glazed energy storage system would be switched off when the solar irradiance was lower than 200W/m^2. This was because the power consumption of a pump was higher than the energy received by the system. Thus, in Bangkok, Tokyo and Nottingham, the total operating time for a pump would be 3,600hr, 3,414hr and 2,922hr, respectively. Figure 6.22 shows the total monthly energy output generated by a module of the fluidised MCPCM glazed energy storage system. The annual energy output of the system located in Bangkok, Tokyo and Nottingham were 374, 310 and 220kWh per module, respectively. The system located in Bangkok provided more energy per module than the other areas because the solar intensity in this area was the highest.

Figure 6.22: Monthly energy output from the fluidised MCPCM glazed panel integrated into building fabric located in a) Bangkok, b) Tokyo and c) Nottingham

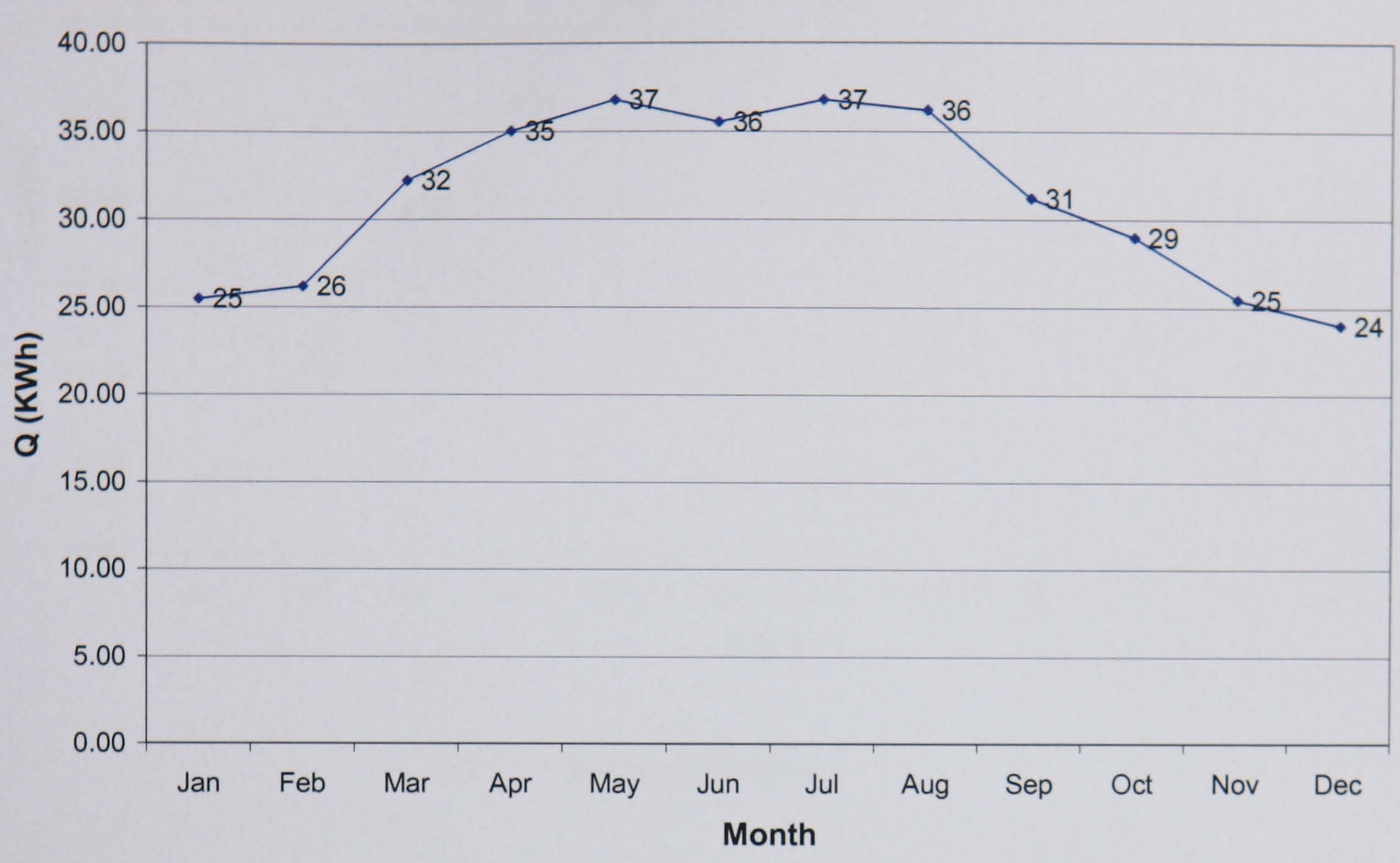

(a) Bangkok

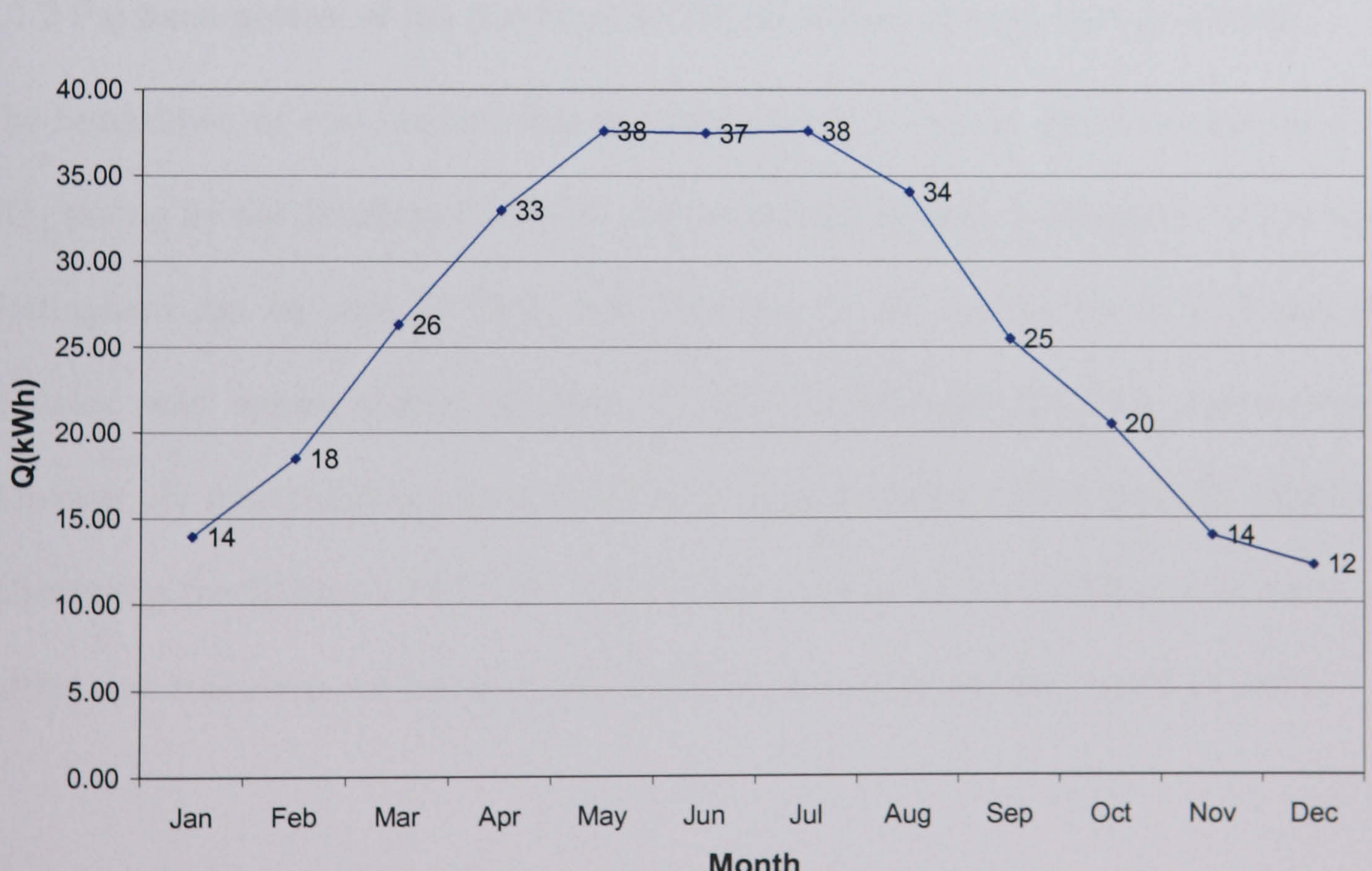

(b) Tokyo

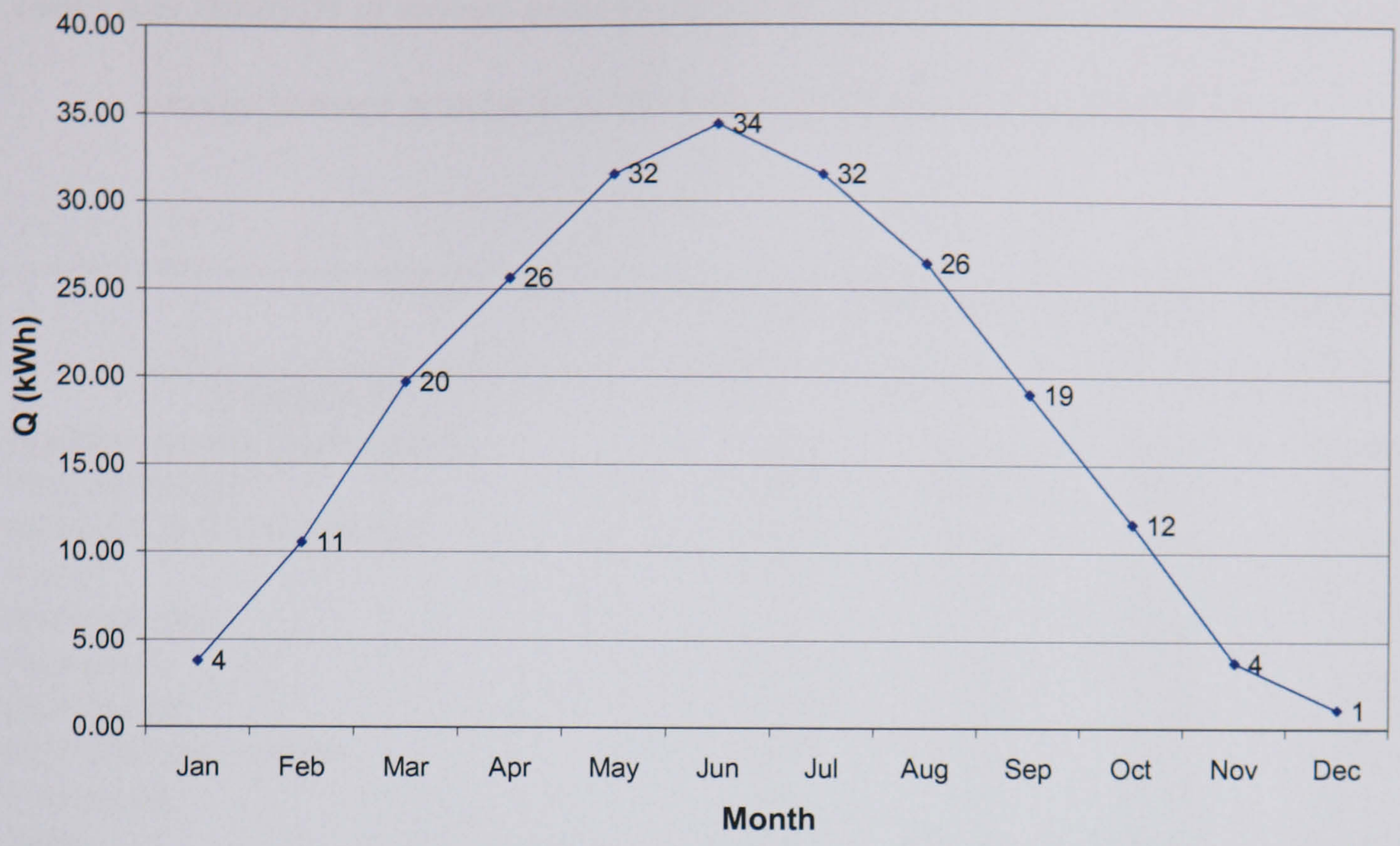

(c) Nottingham

6.7.2 Payback period of the fluidised MCPCM glazed energy storage system

The breakdown of cost, annual energy saving, payback period and total emission of CO_2 saving by the fluidised-MCPCM glazed system located in Bangkok, Tokyo and Nottingham can be seen in Table 6.4. The cost of the system for 1, 4, 8 and 80 modules was approximately £1,040, £1,340, £1,760 and £15,920, respectively. However, for new buildings the cost of the integrated system can be partially offset by substituting the fluidised-MCPCM glazed panel as part of the building's window. A further cost reduction can be obtained, which used to calculate the payback period.

Table 6.4: Analysis of energy and environment effect of fluidised-MCPCM glazed energy storage system in a) Bangkok, b) Tokyo and c) Nottingham

	1 Module $0.25m^2$	**4 Module** $1m^2$	**8 Module** $2m^2$	**80 Module** $20m^2$
Capital cost				
Fluidised double glazed panel	£80	£320	£640	£6,400
Heat exchanger	£220	£220	£220	£2,200
MCPCM (@ $13.65/pound)	£20	£40	£80	£1,600
Pump	£130	£130	£130	£1,300
Water storage	£140	£140	£140	£700
Flow meter	£120	£120	£120	£120
Piping work	£120	£140	£160	£1,600
MCPCM tank + Mixer	£150	£150	£150	£800
Framework	£60	£80	£120	£1,200
Total	**£1,040**	**£1,340**	**£1,760**	**£15,920**
Cost offset: Replacing window	£130	£187	£467	£4,670
Net capital cost	**£910**	**£1,153**	**£1,293**	**£11,250**
Annual saving				
Jan (kWh)	25.44	101.76	203.51	2035.12
Feb (kWh)	26.16	104.66	209.31	2093.14
Mar (kWh)	32.23	128.94	257.87	2578.71
Apr (kWh)	35.02	140.10	280.19	2801.93
May (kWh)	36.79	147.15	294.30	2943.01
Jun (kWh)	35.51	142.03	284.07	2840.69
Jul (kWh)	36.79	147.15	294.30	2943.01
Aug (kWh)	36.19	144.77	289.53	2895.33
Sep (kWh)	31.19	124.78	249.55	2495.53
Oct (kWh)	28.97	115.87	231.74	2317.41
Nov (kWh)	25.44	101.76	203.51	2035.12
Dec (kWh)	23.98	95.94	191.88	1918.77
Annual energy produce (kWh)	**373.72**	**1494.89**	**2989.78**	**29897.78**
Annual saving (@£0.0594/kWh)	**£22.20**	**£88.80**	**£177.59**	**£1,775.93**
Annual runing time of pump (hr)	3600	3600	3600	3600
Pumping power (kW)	0.044	0.176	0.352	3.520
Annual power requriment (kWh)	158.40	633.60	1267.20	12672.00
Running cost (@£0.0594/kWh)	**£9.41**	**£37.64**	**£75.27**	**£752.72**
Total annual cost saving	**£12.79**	**£51.16**	**£102.32**	**£1,023.21**
Simple payback time (Years)	**71**	**23**	**13**	**11**
Total emission of CO2 Saving (kg/year) (@ 0.180 kg/ KWh of heat)	**67**	**269**	**538**	**5382**

(a) Bangkok

	1 Module $0.25m^2$	4 Module $1m^2$	8 Module $2m^2$	80 Module $20m^2$
Capital cost				
Fluidised double glazed panel	£80	£320	£640	£6,400
Heat exchanger	£220	£220	£220	£2,200
MCPCM (@ $13.65/pound)	£20	£40	£80	£1,600
Pump	£130	£130	£130	£1,300
Water storage	£140	£140	£140	£700
Flow meter	£120	£120	£120	£120
Piping work	£120	£140	£160	£1,600
MCPCM tank + Mixer	£150	£150	£150	£800
Framework	£60	£80	£120	£1,200
Total	**£1,040**	**£1,340**	**£1,760**	**£15,920**
Cost offset: Replacing window	£130	£187	£467	£4,670
Net capital cost	**£910**	**£1,153**	**£1,293**	**£11,250**
Annual saving				
Jan (kWh)	13.92	55.69	111.39	1113.88
Feb (kWh)	18.48	73.91	147.81	1478.12
Mar (kWh)	26.30	105.19	210.38	2103.79
Apr (kWh)	32.95	131.79	263.58	2635.81
May (kWh)	37.60	150.39	300.79	3007.86
Jun (kWh)	37.45	149.79	299.57	2995.74
Jul (kWh)	37.60	150.39	300.79	3007.86
Aug (kWh)	34.05	136.18	272.37	2723.67
Sep (kWh)	25.45	101.80	203.59	2035.92
Oct (kWh)	20.46	81.82	163.65	1636.49
Nov (kWh)	13.92	55.69	111.39	1113.88
Dec (kWh)	12.21	48.83	97.66	976.55
Annual energy produce (kWh)	**310.37**	**1241.48**	**2482.96**	**24829.57**
Annual saving (@£0.0594/kWh)	**£18.44**	**£73.74**	**£147.49**	**£1,474.88**
Annual runing time of pump (hr)	3414	3414	3414	3414
Pumping power (kW)	0.044	0.176	0.352	3.520
Annual power requriment (kWh)	150.22	600.86	1201.73	12017.28
Running cost (@£0.0594/kWh)	**£8.92**	**£35.69**	**£71.38**	**£713.83**
Total annual cost saving	**£9.51**	**£38.05**	**£76.11**	**£761.05**
Simple payback time (Years)	**96**	**30**	**17**	**15**
Total emission of CO2 Saving (kg/year) (@ 0.180 kg/ KWh of heat)	**56**	**223**	**447**	**4469**

(b) Tokyo

	1 Module 0.25m^2	**4 Module** 1m^2	**8 Module** 2m^2	**80 Module** 20m^2
Capital cost				
Fluidised double glazed panel	£80	£320	£640	£6,400
Heat exchanger	£220	£220	£220	£2,200
MCPCM (@ $13.65/pound)	£20	£40	£80	£1,600
Pump	£130	£130	£130	£1,300
Water storage	£140	£140	£140	£700
Flow meter	£120	£120	£120	£120
Piping work	£120	£140	£160	£1,600
MCPCM tank + Mixer	£150	£150	£150	£800
Framework	£60	£80	£120	£1,200
Total	**£1,040**	**£1,340**	**£1,760**	**£15,920**
Cost offset: Replacing window	£130	£187	£467	£4,670
Net capital cost	**£910**	**£1,153**	**£1,293**	**£11,250**
Annual saving				
Jan (kWh)	3.74	14.97	29.95	299.45
Feb (kWh)	10.51	42.04	84.07	840.70
Mar (kWh)	19.67	78.68	157.35	1573.55
Apr (kWh)	25.63	102.53	205.07	2050.69
May (kWh)	31.54	126.17	252.34	2523.40
Jun (kWh)	34.38	137.51	275.02	2750.25
Jul (kWh)	31.54	126.17	252.34	2523.40
Aug (kWh)	26.49	105.95	211.90	2119.04
Sep (kWh)	19.03	76.14	152.28	1522.79
Oct (kWh)	11.63	46.54	93.08	930.78
Nov (kWh)	3.74	14.97	29.95	299.45
Dec (kWh)	1.05	4.20	8.39	83.92
Annual energy produce (kWh)	**218.97**	**875.87**	**1751.74**	**17517.42**
Annual saving (@£0.0594/kWh)	**£13.01**	**£52.03**	**£104.05**	**£1,040.53**
Annual running time of pump (hr)	2922	2922	2922	2922
Pumping power (kW)	0.044	0.176	0.352	3.520
Annual power requirement (kWh)	128.57	514.27	1028.54	10285.44
Running cost (@£0.0594/kWh)	**£7.64**	**£30.55**	**£61.10**	**£610.96**
Total annual cost saving	**£5.37**	**£21.48**	**£42.96**	**£429.58**
Simple payback time (Years)	**169**	**54**	**30**	**26**
Total emission of CO_2 Saving (kg/year) (@ 0.180 kg/ KWh of heat)	**39**	**158**	**315**	**3153**

(c) Nottingham

Figure 6.23 shows the payback period and annual CO_2 emission saving of the system integrated into building fabrics located in (a) Nottingham, (b) Tokyo and (c) Bangkok. The emissions of CO_2 saving from the system can be calculated from the annual energy output multiplied by amount of CO_2 emission. Natural gas emits 180gCO_2 for

each kWh of heat (DTI report, 1996). As seen in the Figure, the annual CO_2 emission savings with 80 modules of the system located in Nottingham, Tokyo and Bangkok were 3,153kg, 4,469kg and 5,382kg per year, respectively. In the UK the cost of electricity from national grid was assumed to be £0.0594/kWh (Scottish Hydro-Electric, 2003). In Japan, the cost of electricity was estimated to be +50% (£0.0891/kWh), +100% (£0.1188/kWh) and -50% (£0.0297/kWh) of the UK. In Bangkok, the cost of electricity was estimated to be -50% (£0.0297/kWh), -80% (£0.0118/kWh) and +50% (£0.0891/kWh) of the UK. This is to observe the sensitivity of the cost of electricity to the payback period.

Figure 6.23 Payback period and annual CO_2 emission saving for the system located in a) Nottingham, b) Tokyo and c) Bangkok

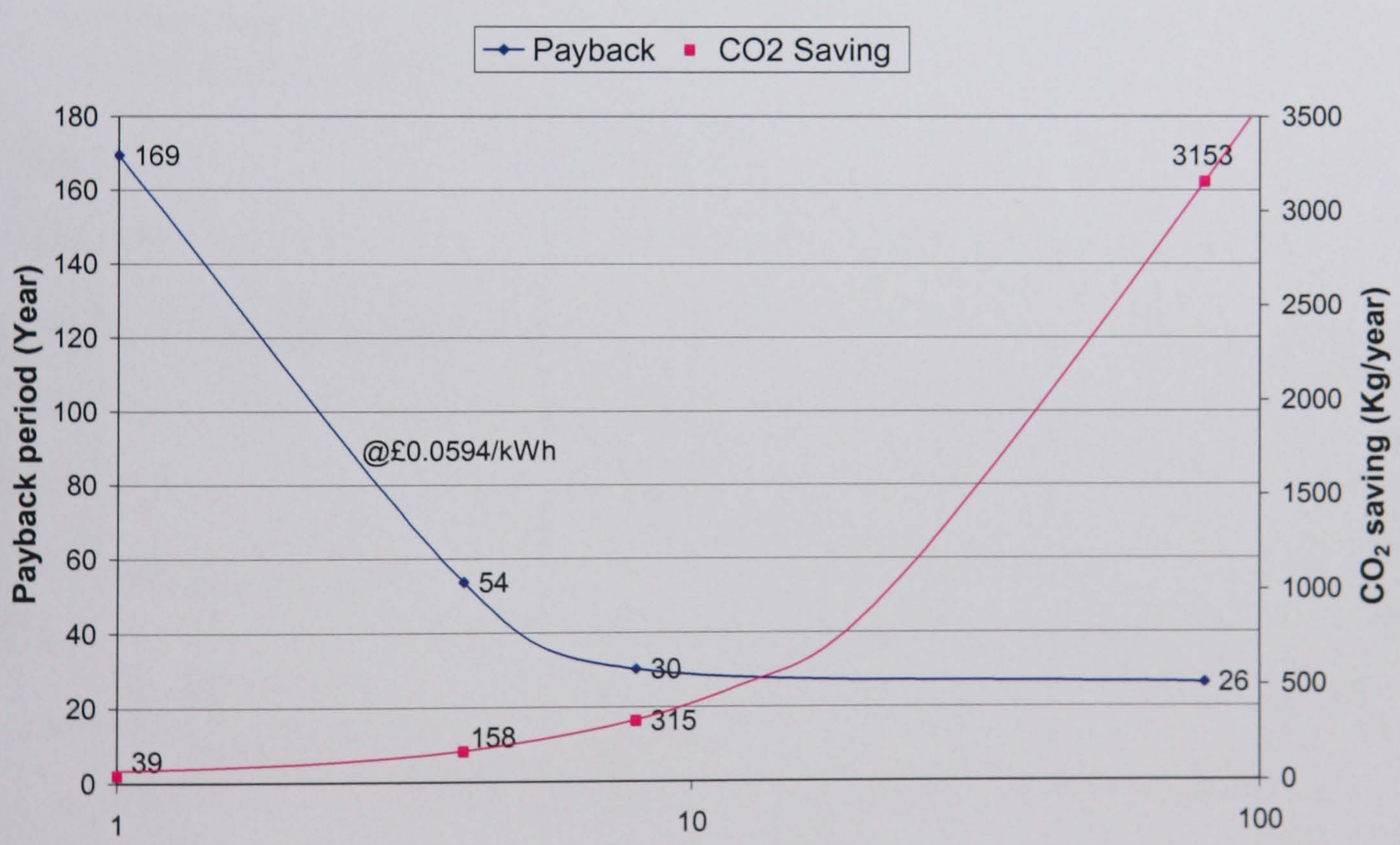

(a) Nottingham

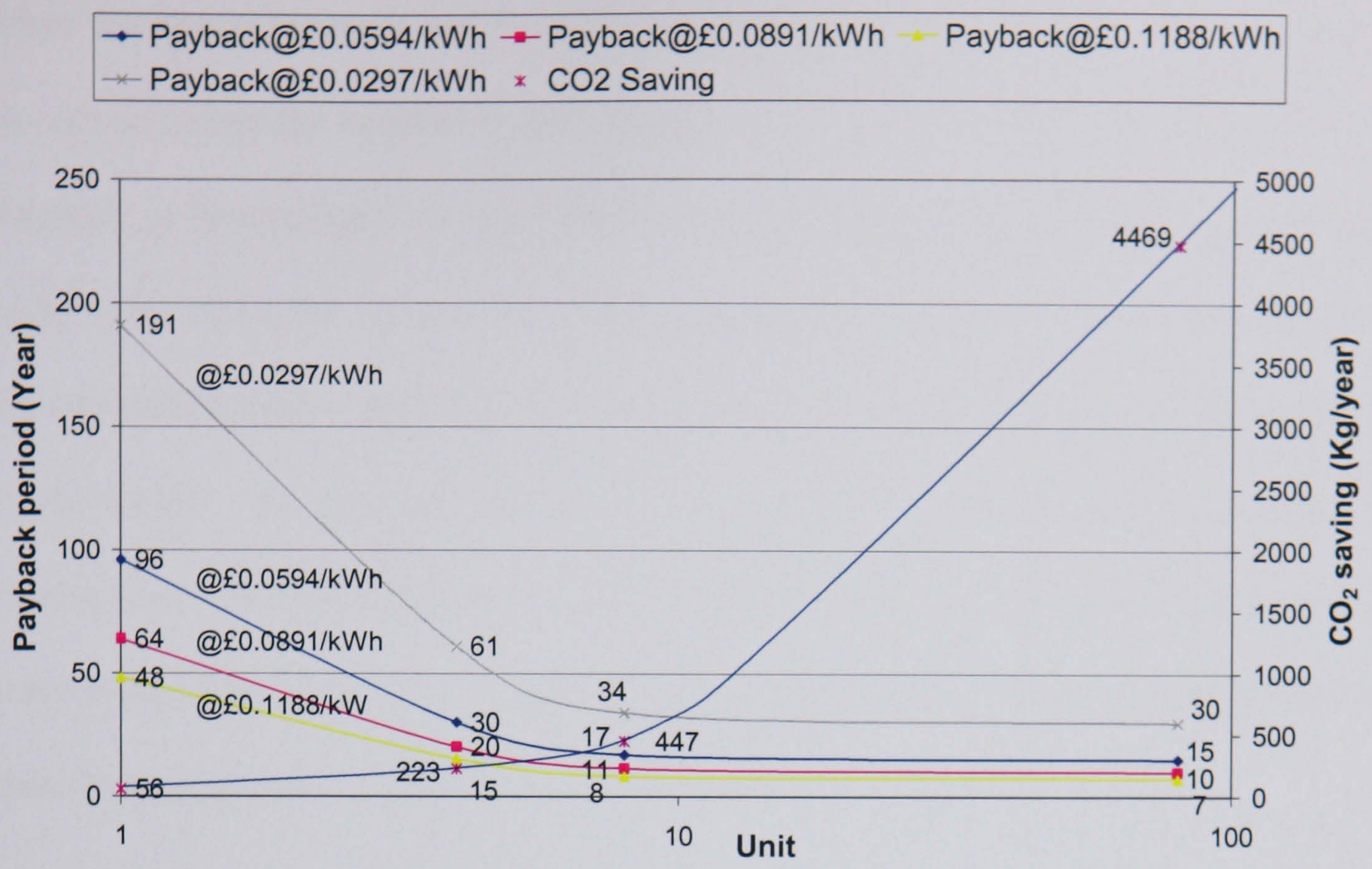

(b) Tokyo

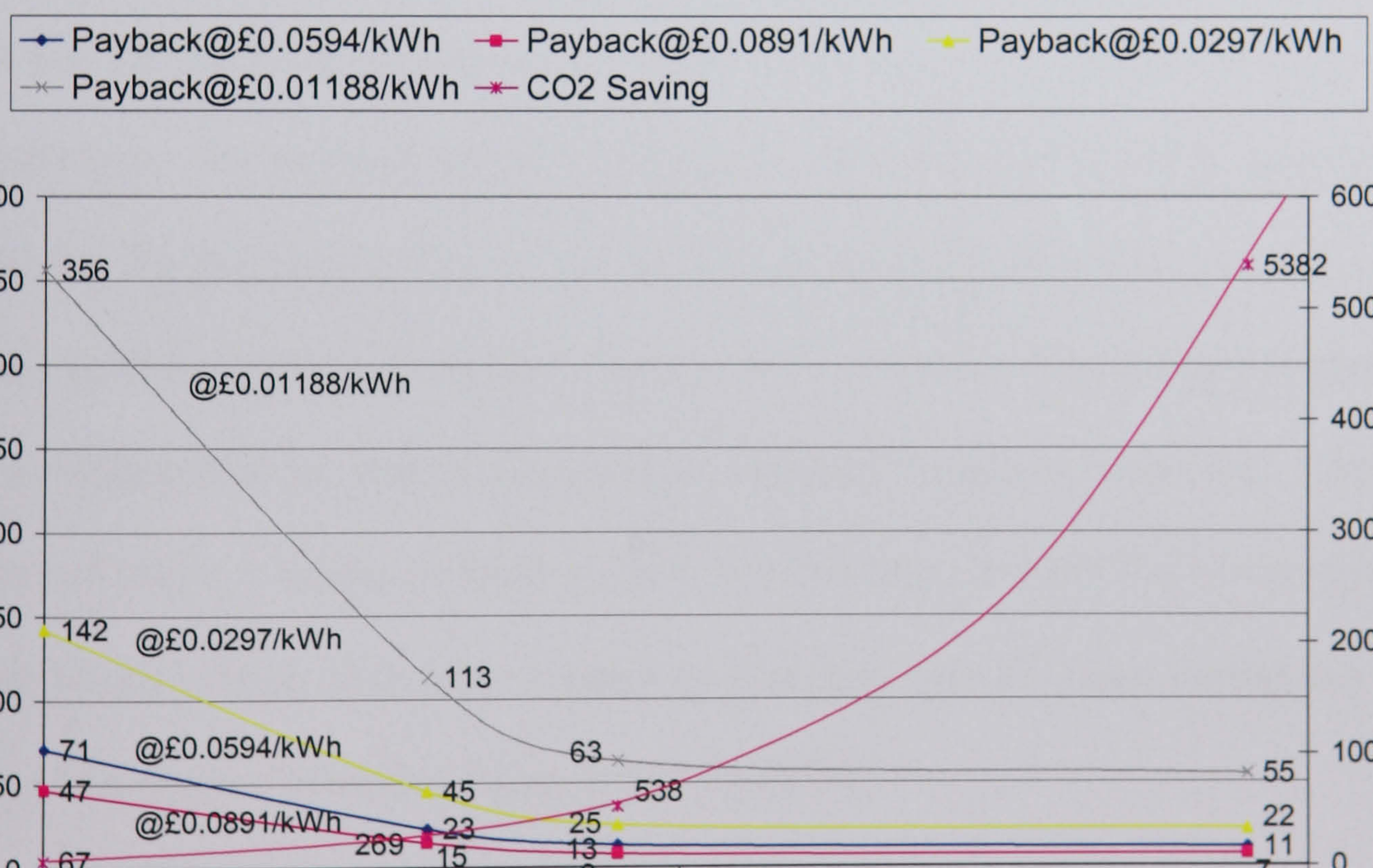

(C) Bangkok

From the above Figure it can be observed that the payback period of the system can be reduced when the number of units integrated into the building fabric increased. For instance, in Nottingham, the payback period was significantly reduced from 54 years to 30 years when the number of modules increased from 4 to 8 units. With 80 units, the payback period was decreased to 26 years. In Japan, at the cost of electricity of £0.0594/kWh, the payback period of the system was much lower than that of Nottingham. The payback period of the system with 8 units located in Japan was 17 years comparing to 30 years in Nottingham. This is because Japan is located in lower latitude and has more available solar irradiance.

Furthermore, when the cost of electricity increased the payback period was found to decrease. For example, in Japan, at the cost of electricity of £0.0891/kWh (+50% of the UK), the payback period of the system of 4 units was found to be 20 years comparing to the payback period of 30 years at £0.0594/kWh. At the same cost of electricity the payback period of the system in Bangkok was even lower than that located in Japan because Bangkok received more available solar energy. However, it was estimated that the cost of electricity in Bangkok would be lower than Japan and this could cause a longer payback period. For instance, at 0.0297/kWh the payback period of the system of 8 units located in Bangkok was 25 years comparing to 17 years of the system located in Japan at £0.0594/kWh.

The overall payback period of the proposed system seems to be long (more than 10 years). However, the system offers an advantage over other solar thermal applications by integrating a function of windows by letting in light meanwhile collecting and transferring the solar energy into buildings which could be stored for later use.

6.8 Conclusion

The present study investigated the performance of the solar collector system and the fluidised glazed energy storage system using the 20%MCPCM slurry employed phase change particles of 35°C *n*-eicosane as a heat transfer fluid. The rig was constructed and tested in a laboratory under artificial lighting conditions with the insolation between 200W/m^2 to 800W/m^2. Measurement of the heat transportation of the MCPCM slurry was determined from the calculation of the rate of heat transfer of the secondary fluid using the pure water.

Results indicated that with the use of MCPCM slurry as a working fluid the rate of heat transfer of the solar collector system was significantly improved by as mush as 20% over the use of pure water.

For fluidised MCPCM glazed energy storage system (with the collector area of 0.25m^2), the rate of heat transfer was found to be around 130W at the insolation of 806W/m^2. The figure reduced to around 28W when the irradiance decreased to 200W/m^2. The intensity of irradiance had a significant effect on the performance of the fluidised MCPCM energy storage system. At 200W/m^2, the energy output from the system was even lower than the power consumption of the pump and it is recommended turning off the pump when the solar radiation is too low. Furthermore, it was found that the rate of heat transfer of the fluidised glazed energy storage system could be enhanced by up to 18% with the use of MCPCM slurry over the pure water.

The heat transfer characteristic of both solar collector and fluidised glazed energy storage system using MCPCM slurry as a working fluid was found to be varied with

the fluid temperature. The rate of heat transfer started to increase when the average slurry temperature was around 30°C. The figure rose gradually and approached the peak at around 33 to 34°C. This was due to the increasing amount of the latent heat of fusion as the number of MCPCM suspension began to melt. After that, the rate of heat transfer began to drop and maintain slightly above the graph of pure water. To achieve best performance, all PCMs in the heat storage must change phase in one period. In this case, the best operating temperature of the phase change slurry (with 35°C *n*-eicosane) should be maintained at an average fluid temperature of around 33 to 34°C.

The present study also investigated an effect of using the yellow MCPCM slurry in fluidised double glazed panel. Results showed no significant enhancement in the rate of heat transfer over the use of the original MCPCM slurry. However, the coloured MCPCM slurry could be used with the fluidised glazed energy storage system when there is an architectural purpose, such as integrating the system into building fabrics.

A simple payback period was an analysis to determine the energy and environmental benefits of the fluidised-MCPCM glazed system integrated into building fabrics located in three different locations, Tokyo, Bangkok and Nottingham. The total annual energy outputs of the system for one module with the surface area of $0.25m^2$ based on the locations in Bangkok, Tokyo and Nottingham were found to be 374, 310 and 220kWh. These could save emissions of CO_2 for approximately 67kg, 56kg and 39kg per year.

The analysis indicated that the payback periods of the system located in Nottingham for 1, 4, 8 and 80 modules were 169, 54, 30 and 26 years, respectively. In Japan and Bangkok, the cost of electricity might vary from Nottingham with an assumption that the cost of electricity in Japan was higher and in Bangkok was lower than Nottingham. It was observed that the cost of electricity had a significant impact on the payback period. At high cost of electricity, the payback period of the system was shortened and vice versa for the cheaper electricity. In addition, the system integrated into building fabrics located in lower latitude had a lower payback period because there was more available solar irradiance. Furthermore, the payback period of the system can be decreased when the more units of the system was integrated into building fabrics.

Chapter 7 Conclusions and recommendations for further work

7.1 Conclusions

The wealth of nation is intimately linked with energy uses, which are central to industrial and economic activity. Most of the energy used in the World today comes from fossil fuels. Because of both rapid increase in population and economic development, the consumption of vast quantities of fossil fuels by mankind has increased dramatically. There are two main problems to be concerned. The first problem is that fossil fuels will inevitably have a finite lifetime and with current use fossil fuels will run out shortly. This may take a few decades as likely to be the case for gas and oil or many centuries as for coal. The second problem is that burning fossil fuels has had increasingly adverse impacts on the environment, especially to generate the excess CO_2 into the atmosphere. Travel up into the atmosphere of CO_2, which act as a screen to sunlight, is a cause of global warming. This problem has been recognized since the 1980's. By the end of the twenty-first century this effect could increase the earth's surface temperature to reach 2-3°C (Fay, 2002) Renewable energy sources, such as hydro, biomass, geothermal, wind, solar and ocean tidal energy, have lesser environmental effects than conventional energy sources and could satisfy the World's energy needs in future years.

In the UK buildings are largely responsible for the extraction and consumption of fossil fuels used in the construction and operation with the total annual energy consumption of 46% (DTI, 2000). These accounted for more than half of the UK's carbon dioxide emissions. Buildings can be seen as the main contributors to the greenhouse gases. At the Kyoto Summit, the UK has made a commitment to a 20%

CO_2 reduction below 1990 level by the year 2010. One sector where the use of renewable energy could benefit significantly is the building sector. With increased energy efficiency and the use of solar energy in buildings, a large proportion of the reduction of CO_2 emission could be achieved. The BRE (Building Research Establishment Ltd) estimated that technologies in use today could reduce CO_2 emissions by 7.4 million tonnes of carbon annually. The opportunities for conservation lie in an attempt to reduce energy consumed to provide heating and cooling for buildings. The inexhaustible supply of solar energy can provide the energy requirement of the buildings. Examples of developed technologies for making use of solar energy in buildings are active, passive solar heating and solar photovoltaic.

The nature of solar energy is inconsistency; not only night but clouds and seasonal changes, so the energy received from the sunlight could be fluctuated. The use of thermal energy storage, which is the temporary holding of energy for later use to correcting the mismatch between the supply and demand of energy, is essential for solar energy applications. The ability to store energy from solar radiation is important for effective use of thermal energy in buildings, for example, to provide hot water and space heating during the night and overcast periods. Basically, there are two types of thermal energy storage system, sensible (e.g. water, rock) and latent heat storage (e.g. paraffin wax, water/ice).

Storage of energy, which involves in increasing or decreasing in temperature of a storage substance, is known as sensible heat storage. It is desirable for the storage material to have high specific heat capacity, long term stability, compatibility with the containment and cheap. Solid sensible heat storage materials such as pebble rocks can

act as a storage medium and heat exchanger. This storage can be used for temperatures up to 100°C and for a temperature change of 50°C it will store heat around 36 kJ/kg. For liquid sensible heat storage, water is widely used because of its high specific heat and density, abundant, cheap and neither toxic nor combustible. For 50°C temperature change, water will store heat around 210 kJ/kg.

Another technique in thermal storage system is the use of phase change material, which recently has received a great deal of interest due to the high energy storage of phase change substances. For example, to melt 1kg of ice, 80 times as much energy is required as to raise the temperature of 1kg of water by 1°C. This technique involves the transition of phase from solid to liquid of a substance with no change in temperature, which is called latent heat storage. There are mainly two groups of phase change material (PCM), organic and inorganic compounds.

Organic group are such as paraffin waxes which is chemically stable and non-corrosive. They have high heat of fusion, low vapour pressure and are compatible with most building materials. However, their main disadvantages are, for instance, flammability, high changes in volume during phase transition and low thermal conductivity. Inorganic group are such as salt hydrates. The main advantage is that they exhibit a higher latent heat per unit volume and high thermal conductivity comparing with the organic compound. However, the major disadvantages are corrosion to most metals and suffering from supercooling and decomposition that can affect their phase change properties. The use of nucleating and thickening agents is recommended to reduce supercooling and phase segregation.

One major problem for latent heat storage systems is that most phase change mediums have low thermal conductivity. Thus, techniques to improve the rate of heat transfer are required. Several investigations are such as double pipe with finned tubes, direct contact heat transfer (between the aqueous crystallizing solution and an immiscible fluid) and a plate-fin heat exchanger with multi melting point of PCM. Extensive efforts have been made to apply the latent heat storage method to solar energy systems, where heat is required during the day for use at night. Some interesting applications to provide space heating or cooling and water heating using PCM as heat storage systems are, for example, heat pipes embedded PCM, PCM in greenhouses, PCM floor heating and wall PCM. Yet, many more applications can be discovered.

Another interesting technique is to use phase change slurry of PCM particle as the novel working fluid. Many conventional thermal-energy systems often operate with the use of a single phase working fluid (i.e. water or oil), which are likely to require high volumetric flowrate. Increasing the convective heat transfer coefficient by introducing the use of suspended particles of PCM in the carrier fluid would permit the use of smaller flowrate. As part of the research the feasibility of utilising microencapsulated phase change particles (MCPCM) slurry has been investigated. In the present study the paraffin waxes of *n*-eicosane were selected as phase change particles with the melting point of approximately 28°C, 35°C and 50°C to prepare the slurries with the concentration of 10% to 40%. Experimental investigations for thermal capacity, viscosity and pressure loss of the MCPCM slurries were conducted. Conclusions from the analysis are shown below;

- Results from the DSC (differential scanning calorimeter) measurement showed that the latent heat of fusion for phase change particles of 28°C, 35°C, and 50°C paraffin waxes were 183.42, 173.75 and 162.65kJ/kg, respectively. The supercooling phenomenon has also been observed and the crystallisation temperatures of the paraffin waxes were lower than the melting point of around 2°C to 4.6°C.
- Another technique to investigate the performance of a phase change slurry (in this approach, the PCM is microencapsulated and suspended in a heat transfer fluid) is by thermal analysis (TA). Results show that the temperature difference between the fluid and bath for the MCPCM slurries were higher than that of the pure water in both heating and cooling mode. Furthermore the slurry with high concentrations had the bigger temperature differences comparing to those of the small concentrations. This is because most of energy has been used during the transition of phase with no change in temperature. Thus, the suspension of MCPCM particles in a carrier fluid was found to increase the heat transportation of the working fluid.
- In the present study, the viscosity of the MCPCM slurry increased as the particle concentration increased. In addition, the viscosity of the slurry decreased with the increase temperature. Non-Newtonian behaviour has been observed whereas the viscosity of the slurries increased with decreasing shear rate. The investigation showed that adding 1% of an ionic surfactant could reduce the slurry viscosity and, thus, the slurries practically behaved as a Newtonian fluid.
- Results from the measurement of pressure drop show that the pressure loss of the phase change slurry increased with increasing flow rate. Furthermore, the

pressure drop of the slurry dramatically increased as the volumetric concentration increased.

In order to determine the most suitable concentration of MCPCM slurry between 5% and 40% concentration a small scale rig with a closed loop circuit was designed and constructed. The primary parameters for the investigation were volumetric concentrations and flow rates. The performance of the working fluid with phase change particles under repeated melting and solidification processes could be stuided. The following conclusions can be made.

- With the use of latent heat of fusion from the suspended particle, the heat transportation of a working fluid was significantly enhanced comparing with the use of a single phase working fluid. For instance, a 52% improvement in heat transportation can be achieved with the use of 30% MCPCM slurry at the flow rate of 2.7L/min. However, at 40% concentration, the heat transportation of the slurry was only 6% higher than the 30% MCPCM slurry. Although a high concentration of microcapsules signified large energy storage capability of the suspension, on the other hand, the drawback was that it led to increase viscosity of the suspension, which required more pumping power, and at high concentrations, non-Newtonian behaviour.

- In the present study, a concentration between 20% and 30% was found to be the most suitable percentage with its relatively high heat capacity and reasonable pressure drop. In term of energy saving, the use of 20% MCPCM slurry as a working fluid would allow to use the smaller flowrate, which could reduce the energy consumption for pumping by 12%.

- During the experimental investigation, one major problem was encountered, where was the phase separation between the suspended particles and carrier fluid. This caused the lighter particles to rise to the surface of water. This phenomenon was found to reduce a number of MCPCM particles going back into the system, which decreased the efficiency of latent energy from the phase change particles. This problem can be overcome by an introduction of a technique of using both an open and close system in which the operation was divided into three stages of open-close-open system.

The further work has been conducted to investigate the performance of the fluidised-MCPCM glazed energy storage system which could be integrated into building fabrics. The rig was constructed and tested in the IBT laboratory under artificial lighting system with the insolation between 200W/m^2 and 800W/m^2. Initially, the heat transportation of a flat plate solar collector system with the use of a phase change slurry was investigated. Then, the next investigation was for the fluidised-MCPCM glazed energy storage system. The working fluid used in the present study was the 20% MCPCM slurry with the phase change temperature of 35°C *n*-eicosane. The following conclusion was found.

- Results show that, for the solar collector system, the use of the MCPCM slurry as a working fluid was found to improve the heat transportation by as mush as 20%. Furthermore, the efficiency of the solar collector was significantly increased.
- For the fluidised-MCPCM glazed energy storage system (surface area of 0.25m^2), the maximum rate of heat transfer was found to be approximately

128W, 94W, 59W and 28W under the irradiance of 806W/m^2, 601W/m^2, 399W/m^2 and 200W/m^2, respectively. In addition, the performance of the system significantly reduced as the intensity of irradiance decreased. At 200W/m^2, the energy output from the system was lower than the pumping power of 44W. Thus, under real operation, it is recommended to turn off the pump when the solar radiation is smaller than 200W/m^2.

- With the use of MCPCM slurry as a working fluid the heat transportation of the fluidised glazed energy storage system could be enhanced by up to 18% comparing with the use of a single phase working fluid.
- The rate of heat transfer of a working fluid using the phase change slurry was found to be varied with the fluid temperature. The figure increased gradually and reached the peak at an average fluid temperature of around 33 to 34°C and after that the figure decreased. The fluctuation of the rate of heat transfer could relate to a number of solid PCM particles that migrated to the flow fields near the heated wall and melted. To achieve maximum benefit, all MCPCM particles in the heat storage must change phase in one period. In this case, the best operating fluid temperature for 20% MCPCM slurry of 35°C *n*-eicosane was found to be around 33 to 34°C.
- The performance of using the yellow MCPCM slurry as a working fluid for the fluidised glazed energy storage system was in equivalent with the original MCPCM slurry.
- An analysis to determine the environmental benefits of the fluidised MCPCM glazed energy storage system integrated into building fabrics located in Tokyo, Bangkok and Nottingham shows that the amount of CO_2 emission savings were 67kg, 56kg and 39kg per module per year, respectively.

- Furthermore, the total energy outputs of the fluidised MCPCM glazed energy storage system of one unit based on locations in Bangkok, Tokyo and Nottingham were 374, 310 and 220kWh per year, respectively.
- An analysis from the payback period method showed that the payback period of the system depended on a number of fluidised glazing panels integrated into building fabrics. The payback period decreased with an increasing number of the fluidised glazing panels. For instance, the payback periods of the system located in Nottingham of 1, 4, 8 and 80 modules were 169, 54, 30 and 26 years, respectively.
- Furthermore, it was observed that the cost of electricity had a significant impact on the payback period. At higher cost of electricity the payback period of the system was found to be lower than that of the cheaper electricity.
- Among the three different locations, the payback period of the fluidised MCPCM glazed energy storage system located in Bangkok was smaller than that of the rest because the annual solar energy was highest in Bangkok.

7.2 Recommendations for further work

Although substantial work has been carried out in this research, there are a number of potential avenues of further work to carry out in order to improve the system performance. These can be seen as following areas:

7.2.1 MCPCM slurry

- One of the main problem concerning on the use of MCPCM slurry was the phase separation between suspended particles and a carrier fluid due to the difference in density of the two substances. Further development of phase

change particles in an attempt to eliminate this problem would allow the wide use of the slurry and may yield good results.

- In many areas requiring heating and cooling there is a large difference between the daytime and night-time temperatures. Thus, for instance, the daytime temperature may be 30°C to 40°C and the night-time temperature is only 10°C to 20°C. To achieve best performance, a slurry contained two kinds of MCPCM with different melting points, e.g. the first has a melting point of 35°C and the second has a melting point of 15°C, may perform better than the slurry contained MCPCM of one melting point.

7.2.2 Double glazed panel

- It would be useful to continue the work on the types of glazing used in the system, including heat absorbing, light reflecting, infra-red reflection and infra red transmitting glazing to develop the model to perform better under small solar radiation. Materials used in the glazing may be glass, Perspex, plastic, or transparent fibres. Light weight materials are desirable because the system will be integrated into part of building fabrics. Further work should also aim to develop a large scale prototype. One interesting approach is to integrate the system with an intelligent window, which can be used to control the flow of light and heat into and out of a glazing. Examples of which are the electrically activated kinds, covering electrochromic, dispersed particle and dispersed liquid crystal glazing.
- In order to integrate a number of fluidised MCPCM glazed panels into building fabrics, two alternative schemes of connecting the units referred to as the series and the parallel set up should be investigated.

7.2.3 System design

- It would be useful to develop a theoretical model to determine the local bulk mean temperature of the MCPCM slurry flowing through a heat exchanger. This is important because to achieve best performance all phase change particles must change phase in one period.

7.2.4 Novel application with the use of MCPCM

- Another interesting approach to use the MCPCM is to incorporate them into building materials for passive solar heating applications or insulation materials. They can be impeded into a variety of building materials, including wallboard insolation.
- The use of MCPCM suspensions as heat transfer fluids can improve the effective specific heat, which includes the effect of latent heat, and can lead to an increase in the heat transfer coefficient. Many applications can benefit from the use of this novel slurry such as fuel cells, CHP, heat pumps, chillier, etc.

References

Abhat, A., Performance studies of a finned heat pipe latent heat thermal energy storage system. *Mankind's Future Source of Energy*, 1978, 1, 541-546.

Abhat, A., Low temperature latent heat thermal energy storage: Heat storage materials, *Solar Energy*, 1982, 30 (4), 313-332.

Adamson, B. *Swedish Council for Building Research*. 1989, (Document No. D18)

AES, *solar collector* (online), Available at http://www.aessolar.co.uk/product.htm, November 2003.

Alexander, Gary. *Renewable energy, Overview: the context of renewable energy technologies*, Oxford: Oxford University Press, 1998

Ali, Mohamed E. Laminar natural convection from constant heat flux helical coiled tubes. *International Journal of Heat and Mass Transfer*, 1998, 41 (14), 2175-2182

Amar, M. Khudhair., et al. A review on energy conservation in building applications with thermal storage by latent heat using phase change materials, Energy Conversion and Management, 2003, 45(2), 263-275

Amaya, M., et al. *Materials Science and Engineering, High temperature corrosion performance of FeAl intermetallic alloys in molten salts*. 2003, Vol. 349 (1-2), pp. 12-19

Austen, Richard, Soon-in floor PCM, *Presentation: TSG Conference*, 1990, 1-4

Baker, Roger C. *Flow Measurement Handbook: industrial designs, operation, performance and applications*. Cambridge: Cambridge University Press, 2000

Barba, A. and Spiga, M. *Solar Energy, Discharge mode for encapsulated PCMs in storage tanks*. 2003. Vol. 74 (2), pp. 141-148

Benita, S. *Microencapsulation: methods and industrial applications*, New York: Marcel Dekker Inc.,1996

Berger, John. *Charging Ahead.* USA, University of California: Berkeley. 1997.

Biswas, DR. *Solar Energy, Thermal energy storage using sodium sulphate decahydrate and water.* 1977, Vol. 19, pp 99–100

Blawzdziewicz, J. Structure and transport properties of colloidal suspensions in stationary shear flow. *CISM Courses and Lectures: Flow of Particles in Suspensions*, Italy: Springer Wien New York, 1996, 1-39.

Birtles, B., et al, Night cooling and ventilation design for office-type buildings. *Renewable Energy: Proceedings of the World Renewable Energy Congress*, Denver, USA, 15-21 June 1996, 259-263.

BRE, *Energy, Heating and Thermal Comfort Volume 4*, England: The Construction Press Ltd, 1978.

Brooke, Bob. *Solar Energy*. New York: Chelsea House, 1992

Burns, P., Survey of thermal storage systems relevant to solar air heating: A review, *BHRA Project RP 21666*, 1981, 35.

Carter, C., Phase change storage in passive solar home heating. *Passive Solar Conference Proc*, 1981, 3, 1920-1928.

Cartsson, B. and Stymre H. *Storage of Heat-A Survey of Efforts and Possibilities*. Stockholm: Swedish Council for Building Research, 1979, (Document D2)

CDIAC. *Carbon Dioxide Information Analysis Centre, Trends online: A compendium of data on global change*. Oak Ridge: Oak Ridge National Laboratory, 2000

Charunyakorn, P. Forced convection heat transfer in microencapsulated phase change material slurries: flow in circular ducts. *International Journal of Heat and Mass Transfer*, 1991, 34 (3), 819-833

Chen, Kuan. An analytical and experimental investigation of the convective heat transfer of phase change slurry flows. *Int. Symp. Multiphase Flow (II)*, 1987, 496, 496-501

Chen, Xuejun and Guo, Liejin. Flow patterns and pressure drop in oil-air-water three phase flow through helically coiled tubes. *International Journal of Multiphase Flow*, 1999, 25, 1053-1072

Chhabra, R. P. and Richardson, J. F. *Non-newtonian Flow in the Process Industries* Oxford: Butterworth Heinemann, 1999

Choi, Eunsoo., et al. Forced convection heat transfer with phase-change-material slurries: turbulent flow in a circular tube. *International Journal of Heat and Mass Transfer*, 1994, 37 (2), 207-215

Choi, J. C., et al. *Korean J. of Chem. Eng., Heat transfer characteristics in low-temperature latent heat storage systems using salt hydrates*. 1995, Vol. 12 (2), pp.258-263

CIBSE, *Energy efficiency in buildings*, London, 1998.

Cleary, C., et al. Hydraulic characteristics of ice slurry and chilled water flows, *IEA District Heating: Advanced Energy Transmission Fluid-Final Report of Research*, Novem BV, Sittard, Netherlands, 1990

Colvin, D. P., et al. Enhanced heat transport in environmental systems using microencapsulated phase change materials. *Int. Conf. Environmental Systems*, 1992, 717-725

Conti, M. and CH Charach. Thermodynamics of heat storage in a PCM shell-and-tube heat exchanger in parallel or in series with a heat engine. *Solar Energy*, 1996, 57 (1), 59-68.

Costa, M., et al. *Energy Convers Mgmt, Numerical simulation of a latent heat thermal energy storage system with enhanced heat conduction.* 1998, Vol. 39, pp. 319–330

DTI, *UK Energy in brief 2000* (online), Available at http://www.dti.gov.uk, July 2003

Dincer, I. and Rosen, M., *Thermal energy storage: Systems and applications*, John Wiley and Sons Ltd, 2002.

Drake, Frances. *Global warming: The science of climate change*. New York: Oxford University Press Inc, 2000

Dubois, P. and Berthet M. Heat storage by paraffin wax fusion for space heating. *Proceedings of the International Seminar*, 1983, Nov, 704-718.

Duffie, A. John and William A. Beckman. *Solar Energy of Thermal Processes*. New York: John Wiley & Sons, 1989

Duffie, A. John and William A. Beckman. *Solar Energy of Thermal Processes*. New York: John Wiley & Sons, 1991

Edie, D.D., et al. Latent heat energy storage using direct contact heat transfer. *Proceedings of the International Solar Energy Society Conference*, 1982, 8,640-644

Elliott, David. *Energy, society and environment: Technology for a sustainable future*, London: Routledge, 1998

ENERDATA, *The world energy consumption in 2002, Statistical Yearbook* (online). Available at

http://www.enerdata.fr/enerdata_UK/Produits/exemples/pressannu_A.pdf , January 2003

Encyclopedia of Polymer Science and Technology (EPST), Wiley, New York, 1971, Vol .14.

EPS, *Plus-Ice Thermal Energy Storage Design Guide*, UK, 1996

Everett, B., Integration, *in* Boyle, Godfrey, *ed.*, *Renewable Energy Power for a Sustainable Future*, Oxford: Oxford University Press, 1998, 393-434

Eveson, G F. The rheological properties of stable suspensions of very small spheres at low rates of shear. *J Oil Colour Chem Assoc*, 1957, 40, 456.

Fay, James. *Energy and the environment*. New York: Oxford University Press Inc, 2002

Feldman, D., et al. Obtaining an energy storing building material by direct incorporation of an organic phase change material in gypsum wallboard. *Solar Energy Materials*, 1991, 22 (2-3), 231-242

Ferrier, J.P. The world energy outlook: implications for economies in transition. *IAEE Newsletter*, 5, 8-11

Fossa, M. A simple model to evaluate direct contact heat transfer and flow characteristics in annular two-phase flow. *International Journal of Heat and Fluid Flow*, 1995, 16 (4), 272-279.

Frisby, *Microencapsulated phase change materials* (online), Available at http://www.frisby.com, October 2002.

Gibbs B. and Hasnain S. DSC study of technical grade phase change heat storage materials for solar heating applications. *Proceedings of the 1995 ASME/JSME/JSEJ International Solar Energy Conference*, 1995, Part 2.

Goel, Manish. Laminar forced convection heat transfer in microencapsulated phase change material suspensions. *International Journal of Heat and Mass Transfer*, 1994, 37 (4), 593-604

Green, K. B. *Carbonless paper production*. Ohio: NCR Corporation, 1953

Groll, M. et al., Corrosion of steels in contact with salt eutectics as latent heat storage materials: Influence of water and other impurities. *Heat Recovery Systems and CHP*, 1990, 10 (5-6), 567-572

Guyer, E.C. and Brownell, D.L. *Handbook of Apply Thermal Design*. New York: McGraw-Hill Inc., 1988

Hale, D.V., et al. *Phase Change Materials Handbook*. 1971, USA: (NASA CR-61363)

Hariri, A.S. and Ward, I.C. A review of thermal storage systems used in building applications. *Building and Environment*, 1988, 2 (1), 1-11

Hart, R. and Thornton, F. *Microencapsulation of phase change materials*. Ohio: Ohio Department of Energy, 1982 (Final Report Contract NO. 82-80)

Harvey, Danny. *Global warming: The hard science*. Singapore: Pearson Education Ltd, 2000

Hasan A. and Sayigh A A. Some fatty acids as phase change thermal energy storage materials. *Renewable Energy*, 1994, 4, 69–76

Hasan, A.S., et al. Cyclic melting and freezing. *Chemical Engineering Science*, 1991, 46 (7), 1573-1587

Hasnain, S.M. Review on sustainable thermal energy storage technologies, Part I: Heat storage materials and techniques. *Energy Convers Mgmt*, 1998, 39 (11), 1127-1138

Hasnain. S.M. King Abdulaziz City of Science and Technology (KACST). *Journal of Science and Technology,* 1995, 34 (34)

Hassan, E.S. Fath, Heat exchanger performance for latent heat thermal energy storage system. *Energy Conversion and Management*, 1991, 31 (2), 149-155

Hawlader, M. N. A, M. S. Uddin and Mya Mya Khin, Microencapsulated PCM thermal-energy storage system, *Applied Energy* 2003, Vol. 74(1-2), pp. 195-202.

Hayashi, Y., et al. Charging and discharging characteristics. *Trans. Japan Society of Mechanical Engineers*, 1986, 52 (477-B), 2187-2194

Heine, D. The chemical compatibility of construction materials with latent heat storage materials. *Proc Int. Conf. on Energy Storage, Brighton,* 1981, pp. 185-192

Heine, D. and Abhat, A. *In SUN: Mankind's Future Source of Energy, Investigation of physical and chemical properties of phase change materials for space heating/cooling applications*. New York: Pergamon Press, 1978, Vol. 1, pp. 500-506.

Hepp, P.S. Sun Oil Company of Pennsylvania, Philadelphia, USA. *System for collecting and storing solar energy*. 14 Dec 1976 , 3996919

Hirech, K., et al. Microencapsulation of an insecticide by interfacial polymerization. *Powder Technology,* 2003, 130(1-3), *324-330*

Hoagland, William. *Solar Energy: Key Technologies for the 21st Century*, New York: Freeman, 1996

International Energy Agency (IEA). *World energy outlook 2000*. France: OECD, 2000

Ismail, K.A.R and Castro J.N. PCM thermal insulation in buildings. *International Journal of Energy Research,* 1997, 21(14), 1281-1296

Jackson, T., Renewable energy: summary paper for the renewable series, *Energy Policy*, 1992, Vol. 20 (9), pp. 861-883.

Jaffrin, A., et al. La Baronne solar greenhouse of CREAT-CNRS. In: Zabeltitz, C. Von, ed. *REUR technical series I – Greenhouse heating with solar energy*. 1987, 192-194.

Kaasinen, H. The absorption of phase change substances into commonly used building materials. *Solar Energy Materials and Solar Cells*, 1992, 27, 173-179

Kadoshin, Shiro., et al. *Applied Energy, The trend in current and near future energy consumption from a statistical perspective*, 2000, Vol. 67, pp. 407-417

Kai J. Phase change stability of $CaCl_26H_2O$. *Solar Energy*, 1984, 33, 557–563

Kamimoto, M., et al. Trans. Am. Soc. Mech. *Engrs*, 1986, 108, 282

Kasza, E and Chen, M.M. Improvement of the performance of solar energy or waste heat utilisation systems by using phase change slurry as an enhanced heat transfer storage fluid. *Journal of Solar Energy Engineering*, 1985, 107, 229-236

Kessel, G. Dagobert. Global warming-facts, assessment, countermeasures. *Journal of petroleum science & engineering,* 2000, 26, 157-168.

Kiatsiriroat, T., et al. Performance analysis of a direct-contact thermal energy storage-solidification. *Renewable Energy*, 2000, 20 (2), 195-206

King, R. and AP. Burns., in *Proc. Inti Cong. On Energy Storage*, Brighton, UK, 1981, 231.

Kurklu, Ahmet. Energy storage applications in greenhouses by means of phase change materials (PCMs): a review. *Renewable Energy*, 1998, 13 (1), l 89-103

Lodhi, M.A.K. Solar ponds in alkaline lake and oil well regions. *Energy Convers Mgmt*, 1996, 37 (12), 1677-1694

Lunde, J. Peter. *Solar Thermal Engineering*. New York: John Wiley & Sons, 1980.

Malkina-Pykh, I.G. and Pykh, Y.A. *Sustainable Energy: Resources, technology and planning*. Russia: WIT Press, 2002

Manley, B.J.W. and Smith, I.E. Thermal energy storage using encapsulated phase change materials. *Energy Storage for Energy Management*, 1983, May, 151-160

Marks, S. An investigation of Glauber's salt with respect to thermal cycling. *Solar Energy*, 1980, 25, 255-258

Markvart, Thomas. *Solar Electricity*. New York: John Wiley & Sons, 1994

Maxwell, J.C.A. *Treatise on Electricity and Magnetic*. New York: Dover, 1954. Vol. 1, pp. 440-441

Mehalick, E.M. and Tweedie, A.T. *Two component thermal energy storage material program phase I final report*. 1979, (DOE EY-76-02-2845)

Melbourne, B. *A comparison of energy consumption in MEDCs and LEDCs: A World Overview* (online). Available at http://geography.wincoll.ac.uk/geofiles/gf447.pdf (March 2003)

Miller, R.W. *Flow Measurement Engineering Handbook*. New York: McGraw-Hill Inc., 1989

Monegon Report. *Phase Change Thermal Storage: A comprehensive look at developments and prospects*, Maryland, 1980, (M105)

Morcos VH. Investigation of a latent heat thermal energy storage system. Solar Wind Technology, 1990, 7, 197–202

Mulligan, J.C., et al. *Use of two-component fluids of microencapsulated phase change materials for heat transfer in spacecraft thermal systems*, 1994, pp. 2004, (AIAA Paper No. 94)

Necati, M. Ozisik. *Heat Transfer A Basic Approach*. Singapore: McGraw-Hill Inc., 1987

Okada, J. Characteristics of plate-fin heat exchanger with phase change material. *Trans. Japanese Assoc. of Refrigeration*, 1988, 5 (2), 125-132

Okada, J. Characteristics of a plate-fin heat exchanger with phase change materials. *Journal of Enhanced Heat Transfer*, 1995, 2 (4), 273-281

Peck, S. and Jacobson D. Performance analysis of phase change thermal energy storage/heat pipe systems. *AIAA 14th Thermophysics Conference*. Orlando, 1979

Perry, H. Robert. *Perry's Chemical Engineers' Handbook*. USA: McGraw-Hill Inc, 1997

Porisini, Fernanda Coen. Salt hydrates used for latent heat storage: Corrosion of metals and reliability of thermal performance. *Solar Energy*, 1988, 41 (2), 193-197

Roberts, S. *SOLAR electricity: A Practical Guide to Designing and Installing Small Photovoltaic Systems*. London: Prentice Hall, 1991

Roy, S.K. An evaluation of phase change microcapsules for use in enhanced heat transfer fluids. *International Journal of Heat and Mass Transfer*, 1991, 18, 495-507

Roy, S.K. Laminar forced convection heat transfer with phase change material emulsions. *Int. Comm. Heat Mass Transfer*, 1997, 24 (5), 653-662

Royon, L., et al. Forced convection heat transfer in a slurry of phase change material in an agitated tank. *Int. Comn. Heat Mass Transfer*, 2000, 27 (8), 1057-1065

Ryu, W. Hee., et al. Prevention of supercooling and stabilization of inorganic salt hydrates as latent heat storage materials. *Solar Energy Materials and Solar Cells*, 1992, 27 (2), 161-172

Sadasuke, I. and Naokatsu, M. Heat transfer enhancement by fins in latent heat thermal energy devices. *Solar Eng ASME*, 1991, 223–228

Saito, T. and Hirose, K. Phase change thermal energy storage/heat pump system. *Trans. Japanese Society of Mechanical Engineers*, 1985, 51 (462-B), 705-711

Samuels, Robert and Prasad, D.E. *Global warming and the built environment.* London: E & FN Spon, 1994

Sar, A. and Kaygusuz, K. Some fatty acids used for latent heat storage: thermal stability and corrosion of metals with respect to thermal cycling. Renewable Energy, 2003, 28 (6), 939-948.

Schobert, H. Harold. *Energy and society: An introduction*. New York: Taylor & Francis, 2002.

Schroder, J. R. Seminar New Ways to Save Energy, R. and D systems for thermal energy storeage in the temperature range from -25°C to 150°C. In: Strub, A.S., ed. *Proceeding of the International Seminar held in Brussels*. London, 1980, 495-504

Shahidi, M. K. T. A. Özbelge. Direct contact heat transfer between two immiscible liquids flowing in a horizontal concentric annulus. *International Journal of Multiphase Flow*, 1995, 21(6), 1025-1036

Sheffield, John. The role of energy efficiency and renewable energies in the future world energy market, *Renewable Energy,* 1997, Vol. 10 (2/3), pp. 315-318

Sideman, S. Direct contact heat transfer with change of phase: Bubble growth in three-phase systems. *Desalination,* 1967, 2, 207-214

Sleigh A. An introduction to fluid mechanics: Notes for the 1st year lecture. School of Civil Engineering, University of Leeds, *CIVE1400 Fluid Mechanics*, May 2001.

Sorour, M. Performance of a small sensible heat energy storage unit. *Energy Conversion and Management.* 1988, 28 (3), 211-217

Stritih, U. and Novak, P. Solar heat storage wall for building ventilation. *Renewable Energy*, 1996, 8 (1-4), 268-271

Swearingen, Corte. *High viscosity flowmeters: Solution to a sticky problem* (online). Available at

http://www.coleparmer.com/techinfo/Techart/default.asp?art=flowcontrol, (May 2002)

Swearingen, Corte. *Choosing the best flow meter* (online). Available at http://www.coleparmer.com/techinfo/Techart/default.asp?art=bestflow. (July, 2003)

- Thaicham, Pruitipong. An investigation of an economiser for use with a ground-coupled heat pump. *MSc Dissertation*, The University of Nottingham, 1999.

Toyoda, N., et al. Heat transfer in solidification process to fined tube. *Trans. Japanese Assoc. of Refrigeration*, 1984, 1, 13-19

- Turnpenny, J.R., et al. Novel ventilation cooling system for reducing air conditioning in building 1: Testing and theoretical modelling. *PhD Thesis*, University of Nottingham, 1998.

Turrent, D. and Barlex, M. The queens building for Anglia Polytechnic University, *Proceedings of PLEA 1997 conference*, 1997, Vol.2 (January), pp 145-152

Vand, V. Theory of viscosity of concentrated suspensions. *Nature*, 1945, 155, 364-365

Velraj R., et al. Heat transfer enhancement in a latent heat storage system, *Solar energy*, 1999, 65, 171–180

White, M. Frank. *Heat and Mass Transfer*. USA: Addison-Wesley Publishing Company, 1991.

World Resources Institute. *World Resources 1998-1999, 1998*. Washington DC, 1999

Yamagishi, Y. An evaluation of microencapsulated PCM for use in cold energy transportation medium. *Proc. IECEC*, Washington DC, 1996, pp. 2077

Yamagishi, Y. Characteristics of microencapsulated PCM slurry as a heat-transfer fluid. *AIChE Journal*, April 1999, 45 (4), 696-707

Yamaguchi, M. and Sayama Sogo. Heat storage-type floor heating system with heat pump driven by nighttime electric power. *Kagaku Kogaku Ronbunshu*, 1997, 26 (2), 122-130

Yoneda, N. and Takanashi, S. Eutectic mixtures for solar heat storage. *Solar Energy*, 1978, 21, 61-63

Yunus, A. Cengel. *Heat Transfer A Practical Approach*, USA: McGraw-Hill Inc., 1998

Yunus, A. and Michael A. Boles. *Thermodynamics: An engineering approach*. Singapore: McGraw-Hill Inc., 1989

Zalba B., Marin J., Cabeza L. and Mehling H. Review on thermal energy storage with phase change: materials, heat transfer analysis and applications. *Appl Therm Eng*, 2003, 23, 251–283

Zhen-Xiang, Gong and Arun S. Mujumdar. Cyclic heat transfer in a novel storage unit of multiple phase change materials. *Applied Thermal Engineering*, 1995, 16 (10), 807-815

Appendix

Table A.1: Viscosity of MCPCM slurries (see Figure 4.3)

MCPCM slurry (% concentration)	Fluid Temperature (°C)	Viscosity (g/sec cm)
2.5%	21	4.1
	33.5	4
	40	4
3.5%	20.5	5.1
	32	5.1
	41	5
10%	20.5	3.8
	31	3.8
	40.5	3.7
20%	21	4.3
	31	4.3
	40	4.1
30%	21	5.5
	30	5.4
	40	5.4
40%	20	6.8
	30.5	6.8
	40	6.6
0% (water)	20	3.1
	30.5	3.1
	40	3.1

Table A.2: Apparent viscosity of 10-40% MCPCM slurry and shear rate for the paraffin wax with the melting point of 28°C (see Figure 4.4a)

MCPCM slurry (% concentration)	Shear rate (1/s)	Viscosity (Pas)	
		Temp=20°C	Temp=60°C
(0%) Water	1.09E+01	2.26E-03	2.06E-03
	1.98E+01	1.57E-03	1.32E-03
	2.74E+01	1.44E-03	1.16E-03
	3.55E+01	1.41E-03	1.13E-03
	4.47E+01	1.41E-03	1.14E-03
	5.60E+01	1.43E-03	1.24E-03
	6.96E+01	1.46E-03	1.36E-03
	8.55E+01	1.50E-03	1.49E-03
	9.77E+01	1.67E-03	1.62E-03
	1.15E+02	1.80E-03	1.78E-03
	1.19E+02	2.20E-03	2.19E-03
	1.51E+02	2.19E-03	2.20E-03
	1.57E+02	2.66E-03	2.69E-03
10%	7.70439E+00	3.40176E-03	2.15E-03
	1.40812E+01	3.21468E-03	1.55E-03

Table A.2 (Continued)

	2.04636E+01	1.90842E-03	1.37E-03
	2.77037E+01	1.70438E-03	1.22E-03
	3.58306E+01	1.76536E-03	1.20E-03
	4.52108E+01	1.77354E-03	1.28E-03
	5.70506E+01	1.77667E-03	1.35E-03
	7.21148E+01	1.78120E-03	1.47E-03
	9.08859E+01	1.79006E-03	1.50E-03
	1.08578E+02	1.99780E-03	1.61E-03
	1.11497E+02	2.53734E-03	2.09E-03
	1.41410E+02	2.63526E-03	2.27E-03
	1.46910E+02	2.84345E-03	2.52E-03
20%	4.30795E+00	5.42606E-03	2.64E-03
	7.66062E+00	4.07087E-03	1.97E-03
	1.21989E+01	3.23493E-03	1.74E-03
	1.82793E+01	2.73467E-03	1.56E-03
	2.60920E+01	2.42427E-03	1.42E-03
	3.50821E+01	2.28559E-03	1.41E-03
	4.56960E+01	2.21815E-03	1.46E-03
	5.92038E+01	2.18964E-03	1.56E-03
	7.66083E+01	2.16367E-03	1.71E-03
	9.77379E+01	2.14828E-03	1.86E-03
	1.19449E+02	2.18173E-03	2.21E-03
	1.22496E+02	2.69584E-03	2.49E-03
	1.56434E+02	2.67034E-03	2.44E-03
30%	2.70756E+00	8.81063E-03	2.76E-03
	4.78132E+00	6.52234E-03	1.85E-03
	7.02335E+00	5.61876E-03	1.62E-03
	1.03747E+01	4.81826E-03	1.54E-03
	1.48610E+01	4.25637E-03	1.52E-03
	2.08145E+01	3.85227E-03	1.59E-03
	2.85726E+01	3.54747E-03	1.61E-03
	3.90743E+01	3.08736E-03	1.65E-03
	5.32059E+01	3.05776E-03	1.79E-03
	7.22010E+01	2.85397E-03	1.93E-03
	9.53319E+01	2.73366E-03	2.07E-03
	1.21136E+02	2.72609E-03	2.55E-03
	1.48638E+02	2.81041E-03	2.59E-03
40%	5.55664E-01	4.63930E-02	8.23E-03
	2.05694E+00	1.91611E-02	6.29E-03
	4.19348E+00	9.41045E-03	4.85E-03
	7.27625E+00	6.87000E-03	4.04E-03
	1.17660E+01	5.37601E-03	3.60E-03
	1.78192E+01	4.49983E-03	3.34E-03
	2.56688E+01	3.94877E-03	3.13E-03
	3.68722E+01	3.48368E-03	2.88E-03
	5.13503E+01	3.16826E-03	2.69E-03
	6.80270E+01	3.02908E-03	2.55E-03
	8.91962E+01	2.92171E-03	2.52E-03
	1.15259E+02	3.16511E-03	2.67E-03
	1.47161E+02	3.23861E-03	3.30E-03

Table A.3 Apparent viscosity of 10-40% MCPCM slurry and shear rate for the paraffin wax with the melting point of 35°C (see Figure 4.4b)

MCPCM slurry (% concentration)	**Shear rate** (1/s)	**Viscosity** (Pas)	
		T=20°C	T=60°C
0% (Water)	1.09E+01	2.26E-03	2.06E-03
	1.98E+01	1.57E-03	1.32E-03
	2.74E+01	1.44E-03	1.16E-03
	3.55E+01	1.41E-03	1.13E-03
	4.47E+01	1.41E-03	1.14E-03
	5.60E+01	1.43E-03	1.24E-03
	6.96E+01	1.46E-03	1.36E-03
	8.55E+01	1.50E-03	1.49E-03
	9.77E+01	1.67E-03	1.62E-03
	1.15E+02	1.80E-03	1.78E-03
	1.19E+02	2.20E-03	2.19E-03
	1.51E+02	2.19E-03	2.20E-03
	1.57E+02	2.66E-03	2.69E-03
10%	7.70439E+00	3.20176E-03	2.25E-03
	1.40812E+01	2.21468E-03	1.45E-03
	2.04636E+01	1.92842E-03	1.27E-03
	2.77037E+01	1.80438E-03	1.22E-03
	3.58306E+01	1.76536E-03	1.22E-03
	4.52108E+01	1.77354E-03	1.28E-03
	5.70506E+01	1.77667E-03	1.35E-03
	7.21148E+01	1.78120E-03	1.47E-03
	9.08859E+01	1.79006E-03	1.60E-03
	1.08578E+02	1.89780E-03	1.71E-03
	1.11497E+02	2.33734E-03	2.09E-03
	1.41410E+02	2.33526E-03	2.07E-03
	1.46910E+02	2.84345E-03	2.52E-03
20%	4.30795E+00	5.72606E-03	2.64E-03
	7.66062E+00	4.07087E-03	1.77E-03
	1.21989E+01	3.23493E-03	1.54E-03
	1.82793E+01	2.73467E-03	1.46E-03
	2.60920E+01	2.42427E-03	1.42E-03
	3.50821E+01	2.28559E-03	1.41E-03
	4.56960E+01	2.21815E-03	1.46E-03
	5.92038E+01	2.16964E-03	1.56E-03
	7.66083E+01	2.12367E-03	1.71E-03
	9.77379E+01	2.10828E-03	1.86E-03
	1.19449E+02	2.18173E-03	2.01E-03
	1.22496E+02	2.69584E-03	2.49E-03
	1.56434E+02	2.67034E-03	2.44E-03
30%	2.70756E+00	9.11063E-03	2.86E-03
	4.78132E+00	6.52234E-03	1.85E-03
	7.02335E+00	5.61876E-03	1.62E-03
	1.03747E+01	4.81826E-03	1.54E-03
	1.48610E+01	4.25637E-03	1.52E-03
	2.08145E+01	3.85227E-03	1.59E-03
	2.85726E+01	3.54747E-03	1.61E-03

Table A.3 (Continued)

	3.90743E+01	3.28736E-03	1.65E-03
	5.32059E+01	3.05776E-03	1.79E-03
	7.22010E+01	2.85397E-03	1.93E-03
	9.53319E+01	2.73366E-03	2.07E-03
	1.21136E+02	2.72609E-03	2.55E-03
	1.48638E+02	2.81041E-03	2.49E-03
40%	5.55664E-01	4.43930E-02	7.93E-03
	2.05694E+00	1.51611E-02	6.29E-03
	4.19348E+00	9.41045E-03	4.85E-03
	7.27625E+00	6.87000E-03	4.04E-03
	1.17660E+01	5.37601E-03	3.60E-03
	1.78192E+01	4.49983E-03	3.34E-03
	2.56688E+01	3.94877E-03	3.13E-03
	3.68722E+01	3.48368E-03	2.88E-03
	5.13503E+01	3.16826E-03	2.69E-03
	6.80270E+01	3.02908E-03	2.55E-03
	8.91962E+01	2.92171E-03	2.52E-03
	1.15259E+02	2.86511E-03	2.67E-03
	1.47161E+02	2.83861E-03	3.30E-03

Table A.4: Apparent viscosity of 10-40% MCPCM slurry and shear rate for the paraffin wax with the melting point of 50°C (see Figure 4.4c)

MCPCM slurry (% concentration)	**Shear rate** (1/s)	**Viscosity** (Pas)	
		T=20°C	T=60°C
(0%) Water	1.09E+01	2.26E-03	2.06E-03
	1.98E+01	1.57E-03	1.32E-03
	2.74E+01	1.44E-03	1.16E-03
	3.55E+01	1.41E-03	1.13E-03
	4.47E+01	1.41E-03	1.14E-03
	5.60E+01	1.43E-03	1.24E-03
	6.96E+01	1.46E-03	1.36E-03
	8.55E+01	1.50E-03	1.49E-03
	9.77E+01	1.67E-03	1.62E-03
	1.15E+02	1.80E-03	1.78E-03
	1.19E+02	2.20E-03	2.19E-03
	1.51E+02	2.19E-03	2.20E-03
	1.57E+02	2.66E-03	2.69E-03
10%	7.70439E+00	3.40176E-03	2.05E-03
	1.40812E+01	3.01468E-03	1.55E-03
	2.04636E+01	2.50842E-03	1.37E-03
	2.77037E+01	1.90438E-03	1.22E-03
	3.58306E+01	1.76536E-03	1.20E-03
	4.52108E+01	1.77354E-03	1.28E-03
	5.70506E+01	1.77667E-03	1.35E-03
	7.21148E+01	1.78120E-03	1.47E-03
	9.08859E+01	1.79006E-03	1.50E-03
	1.08578E+02	1.99780E-03	1.81E-03
	1.11497E+02	2.33734E-03	2.09E-03
	1.41410E+02	2.63526E-03	2.27E-03

Table A.4 (Continued)

	1.46910E+02	2.74345E-03	2.52E-03
20%	4.30795E+00	6.42606E-03	3.24E-03
	7.66062E+00	4.07087E-03	1.97E-03
	1.21989E+01	3.23493E-03	1.74E-03
	1.82793E+01	2.73467E-03	1.56E-03
	2.60920E+01	2.42427E-03	1.42E-03
	3.50821E+01	2.28559E-03	1.46E-03
	4.56960E+01	2.21815E-03	1.46E-03
	5.92038E+01	2.18964E-03	1.56E-03
	7.66083E+01	2.16367E-03	1.71E-03
	9.77379E+01	2.14828E-03	1.86E-03
	1.19449E+02	2.48173E-03	2.21E-03
	1.22496E+02	2.69584E-03	2.39E-03
	1.56434E+02	2.77034E-03	2.44E-03
30%	2.70756E+00	9.81063E-03	2.56E-03
	4.78132E+00	7.52234E-03	1.85E-03
	7.02335E+00	5.61876E-03	1.62E-03
	1.03747E+01	4.81826E-03	1.54E-03
	1.48610E+01	4.25637E-03	1.52E-03
	2.08145E+01	3.85227E-03	1.59E-03
	2.85726E+01	3.54747E-03	1.61E-03
	3.90743E+01	3.08736E-03	1.65E-03
	5.32059E+01	3.05776E-03	1.79E-03
	7.22010E+01	2.85397E-03	1.93E-03
	9.53319E+01	2.73366E-03	2.47E-03
	1.21136E+02	2.72609E-03	2.55E-03
	1.48638E+02	2.81041E-03	2.59E-03
40%	5.55664E-01	4.63930E-02	9.03E-03
	2.05694E+00	1.91611E-02	6.29E-03
	4.19348E+00	9.41045E-03	4.85E-03
	7.27625E+00	7.87000E-03	4.04E-03
	1.17660E+01	5.37601E-03	3.60E-03
	1.78192E+01	4.49983E-03	3.34E-03
	2.56688E+01	3.94877E-03	3.13E-03
	3.68722E+01	3.48368E-03	2.88E-03
	5.13503E+01	3.16826E-03	2.69E-03
	6.80270E+01	3.02908E-03	2.55E-03
	8.91962E+01	2.92171E-03	2.72E-03
	1.15259E+02	3.16511E-03	3.00E-03
	1.47161E+02	3.23861E-03	3.30E-03

Table A.5: Apparent viscosity for 20% and 40% MCPCM slurry with 35°C n-eicosane of with and without additive at the slurry temperature of 25 °C (see Figure 4.5)

MCPCM slurry (% concentration)	**Shear rate** (1/s)	**Viscosity** (Pas) T=25°C
20%	4.30795E+00	5.72606E-03
	7.66062E+00	4.07087E-03
	1.21989E+01	3.23493E-03
	1.82793E+01	2.73467E-03
	2.60920E+01	2.42427E-03
	3.50821E+01	2.28559E-03
	4.56960E+01	2.21815E-03
	5.92038E+01	2.16964E-03
	7.66083E+01	2.12367E-03
	9.77379E+01	2.10828E-03
	1.19449E+02	2.18173E-03
	1.22496E+02	2.69584E-03
	1.56434E+02	2.67034E-03
20% with 1% additive	9.83E+00	2.51E-03
	1.67E+01	1.87E-03
	2.22E+01	1.78E-03
	2.79E+01	1.79E-03
	3.50E+01	1.80E-03
	4.40E+01	1.82E-03
	5.51E+01	1.84E-03
	6.91E+01	1.86E-03
	8.66E+01	1.88E-03
	1.07E+02	1.92E-03
	1.25E+02	2.09E-03
	1.27E+02	2.60E-03
	1.62E+02	2.57E-03
40%	5.55664E-01	4.43930E-02
	2.05694E+00	1.51611E-02
	4.19348E+00	9.41045E-03
	7.27625E+00	6.87000E-03
	1.17660E+01	5.37601E-03
	1.78192E+01	4.49983E-03
	2.56688E+01	3.94877E-03
	3.68722E+01	3.48368E-03
	5.13503E+01	3.16826E-03
	6.80270E+01	3.02908E-03
	8.91962E+01	2.92171E-03
	1.15259E+02	2.86511E-03
	1.47161E+02	2.83861E-03
40% with 1% additive	9.10E+00	2.71E-03
	1.49E+01	2.09E-03
	1.96E+01	2.01E-03
	2.50E+01	2.00E-03
	3.13E+01	2.02E-03

Table A.5 (Continued)

	3.89E+01	2.06E-03
	4.83E+01	2.10E-03
	6.00E+01	2.14E-03
	7.49E+01	2.17E-03
	9.30E+01	2.22E-03
	1.15E+02	2.26E-03
	1.41E+02	2.35E-03
	1.44E+02	2.90E-03
40%	8.44E+00	2.92E-03
with	1.41E+01	2.21E-03
2% additive	1.88E+01	2.10E-03
	2.43E+01	2.06E-03
	3.06E+01	2.07E-03
	3.83E+01	2.09E-03
	4.74E+01	2.14E-03
	5.89E+01	2.18E-03
	7.34E+01	2.22E-03
	9.12E+01	2.26E-03
	1.13E+02	2.30E-03
	1.39E+02	2.38E-03
	1.43E+02	2.93E-03

Table A.6: Pressure drop and volumetric flow rate for water and 5-40% MCPCM slurry at 25 ℃ (see Figure 4.7)

Flowrate (L/min)	**Pressure drop** (mm H_2O/m)					
	Water	**5%Slurry**	**10%Slurry**	**20%Slurry**	**30%Slurry**	**40%Slurry**
2.05	0.51	0.75	1.04	1.27	1.35	1.61
2.11	0.55	0.80	1.09	1.31	1.39	1.65
2.2	0.60	0.84	1.13	1.35	1.43	1.69
2.27	0.64	0.89	1.18	1.39	1.47	1.73
2.39	0.69	0.93	1.22	1.43	1.51	1.77
2.51	0.73	0.98	1.27	1.47	1.54	1.81
2.63	0.78	1.02	1.31	1.51	1.58	1.85
2.71	0.82	1.06	1.36	1.55	1.62	1.89
2.78	0.87	1.11	1.40	1.59	1.66	1.93
2.9	0.91	1.15	1.45	1.63	1.70	1.97
3.02	0.96	1.20	1.50	1.67	1.74	2.01
3.11	1.00	1.24	1.54	1.71	1.77	2.05
3.22	1.05	1.29	1.59	1.75	1.81	2.09
3.3	1.10	1.33	1.63	1.79	1.85	2.13
3.41	1.14	1.37	1.68	1.83	1.89	2.17
3.5	1.19	1.42	1.72	1.87	1.93	2.21
3.59	1.23	1.46	1.77	1.91	1.97	2.25
3.69	1.28	1.51	1.82	1.95	2.00	2.29
3.81	1.32	1.55	1.86	1.99	2.04	2.33
3.92	1.37	1.60	1.91	2.03	2.08	2.37
4.02	1.41	1.64	1.95	2.07	2.12	2.45
4.11	1.48	1.70	2.00	2.12	2.17	2.49
4.19	1.55	1.76	2.05	2.17	2.22	2.53
4.3	1.62	1.81	2.09	2.22	2.28	2.57

Table A.6 (Continued)

4.41	1.69	1.87	2.14	2.27	2.33	2.60
4.49	1.76	1.93	2.19	2.32	2.38	2.64
4.62	1.83	1.98	2.24	2.37	2.43	2.68
4.68	1.90	2.04	2.28	2.42	2.48	2.72
4.8	1.97	2.10	2.33	2.47	2.54	2.76
4.93	2.04	2.16	2.38	2.52	2.59	2.80
5.02	2.11	2.21	2.42	2.57	2.64	2.84
5.13	2.18	2.27	2.47	2.62	2.69	2.87
5.19	2.24	2.33	2.52	2.67	2.74	2.91
5.3	2.31	2.38	2.56	2.72	2.80	2.95
5.41	2.38	2.44	2.61	2.77	2.85	2.99
5.52	2.45	2.50	2.66	2.82	2.90	3.03
5.62	2.52	2.55	2.71	2.87	2.95	3.07
5.7	2.59	2.61	2.75	2.92	3.00	3.11
5.78	2.66	2.67	2.80	2.97	3.06	3.14
5.9	2.73	2.73	2.85	3.02	3.11	3.18
6.05	2.80	2.80	2.91	3.09	3.16	3.23

Table A.7: Friction factor and Reynolds number for pure water and 10%-40% MCPCM slurry at 25°C (see Figure 4.8)

Flowrate	Water		10%Slurry		20%Slurry		30%Slurry		40%Slurry	
L/min	F factor	Re no.	F factor	Re no.	F factor	Re no.	F factor	Re no.	F factor	Re no.
2.05	0.069717	2803.299	0.139104	1375.57	0.1703023	878.675	0.181013	634.5168	0.214906	490.2982
2.11	0.071692	2885.347	0.1370625	1415.831	0.165766576	904.3924	0.175701	653.088	0.209461	504.6484
2.2	0.071359	3008.418	0.1313735	1476.222	0.157091598	942.9683	0.166067	680.9448	0.198748	526.1737
2.27	0.072109	3104.141	0.1283704	1523.192	0.15188288	972.9719	0.160161	702.6113	0.192385	542.9156
2.39	0.069636	3268.236	0.1202905	1603.713	0.140920371	1024.407	0.148251	739.7537	0.178698	571.616
2.51	0.067294	3432.332	0.1131321	1684.235	0.131309854	1075.841	0.137831	776.8962	0.166686	600.3164
2.63	0.065081	3596.427	0.1067494	1764.756	0.12282658	1127.276	0.128653	814.0386	0.156072	629.0168
2.71	0.064862	3705.824	0.10403	1818.437	0.118720215	1161.566	0.124101	838.8002	0.150997	648.1503
2.78	0.065026	3801.547	0.1021736	1865.407	0.115704038	1191.569	0.120715	860.4667	0.147292	664.8922
2.9	0.062871	3965.642	0.0969406	1945.928	0.10897991	1243.004	0.113492	897.6091	0.138851	693.5926
3.02	0.060846	4129.738	0.0922001	2026.45	0.10293792	1294.438	0.107012	934.7516	0.131259	722.293
3.11	0.060083	4252.809	0.0895911	2086.84	0.099373349	1333.014	0.103134	962.6084	0.126811	743.8183
3.22	0.058575	4403.23	0.0860466	2160.651	0.094851947	1380.163	0.098284	996.6556	0.121131	770.127
3.3	0.058175	4512.627	0.0842789	2214.332	0.092357841	1414.453	0.095554	1021.417	0.118028	789.2606
3.41	0.056735	4663.048	0.0811336	2288.143	0.088414345	1461.601	0.09134	1055.464	0.113065	815.5693
3.5	0.055993	4786.12	0.079107	2348.534	0.085747331	1500.177	0.08846	1083.321	0.109725	837.0945
3.59	0.055253	4909.192	0.0771792	2408.925	0.083233274	1538.753	0.085751	1111.178	0.106573	858.6198
3.69	0.054223	5045.938	0.0749352	2476.026	0.080421906	1581.615	0.082747	1142.13	0.103034	882.5368
3.81	0.052666	5210.033	0.0720549	2556.547	0.076972925	1633.05	0.0791	1179.273	0.098671	911.2372
3.92	0.051456	5360.454	0.0697358	2630.358	0.074165754	1680.198	0.076124	1213.32	0.095125	937.5459
4.02	0.050573	5497.201	0.067942	2697.459	0.071958711	1723.06	0.073739	1244.272	0.092293	961.4629
4.11	0.050754	5620.272	0.066563	2757.85	0.07050543	1761.636	0.072275	1272.129	0.089247	982.9882
4.19	0.051117	5729.669	0.0655503	2811.531	0.069439568	1795.926	0.071207	1296.89	0.086787	1002.122
4.3	0.050703	5880.09	0.0636682	2885.342	0.067452202	1843.074	0.069191	1330.938	0.083273	1028.43
4.41	0.050266	6030.511	0.0618901	2959.153	0.065574243	1890.223	0.067285	1364.985	0.079998	1054.739
4.49	0.050478	6139.908	0.0610147	3012.834	0.064652341	1924.513	0.066359	1389.747	0.07797	1073.873
4.62	0.049555	6317.678	0.058867	3100.065	0.062381744	1980.234	0.064046	1429.984	0.074397	1104.965

Table A.7 (Continued)

4.68	0.050122	6399.726	0.0585735	3140.326	0.062075577	2005.951	0.063749	1448.555	0.073235	1119.315
4.8	0.049386	6563.822	0.0568281	3220.847	0.060230353	2057.385	0.06187	1485.698	0.070317	1148.015
4.93	0.048465	6741.592	0.0549576	3308.078	0.058252063	2113.106	0.059853	1525.935	0.067319	1179.107
5.02	0.048333	6864.663	0.054053	3368.469	0.057297256	2151.682	0.058886	1553.792	0.065565	1200.633
5.13	0.047805	7015.084	0.0527636	3442.28	0.055934286	2198.831	0.057498	1587.84	0.063394	1226.941
5.19	0.048194	7097.132	0.0525315	3482.541	0.055691812	2224.548	0.057262	1606.411	0.062534	1241.292
5.3	0.047641	7247.553	0.0513141	3556.352	0.054404537	2271.696	0.05595	1640.458	0.060537	1267.6
5.41	0.047092	7397.974	0.0501512	3630.163	0.053174845	2318.845	0.054696	1674.505	0.05865	1293.909
5.52	0.046549	7548.395	0.0490394	3703.974	0.051998986	2365.993	0.053497	1708.553	0.056863	1320.218
5.62	0.046176	7685.141	0.0481462	3771.075	0.051054733	2408.855	0.052536	1739.505	0.055367	1344.135
5.7	0.046123	7794.538	0.0476173	3824.756	0.050496656	2443.145	0.051971	1764.266	0.054318	1363.268
5.78	0.046054	7903.935	0.0470991	3878.437	0.0499497	2477.435	0.051418	1789.028	0.053306	1382.402
5.9	0.045351	8068.031	0.0459616	3958.958	0.048745843	2528.87	0.050187	1826.17	0.051622	1411.102
6.05	0.044177	8278.62	0.0445784	4062.293	0.047335942	2594.877	0.04853	1873.836	0.049488	1447.934

Table A.8: Reynolds number and volumetric flow rate for water and 10%-40% MCPCM slurry at 25 ℃ (see Figure 4.9)

Flowrate	**Reynolds number**				
(L/min)	**Water**	**10%Slurry**	**20%Slurry**	**30%Slurry**	**40%Slurry**
2.05	2602	1344	858	620	496
4.02	4078	2688	1717	1240	992
6.05	6218	4032	2576	1860	1488

Table A.9: Temperature variations of MCPCM slurries (10% to 40%) in heating mode with 28°C melting point (see Figure 4.13a)

Time	Temperature (°C)				
	Water	20% Slurry	30% slurry	40% Slurry	Bath
12:13:40	14.371	14.658	14.447	15.177	45.264
12:13:50	14.373	14.69	14.479	15.089	45.237
12:14:00	14.432	14.691	14.48	15.179	45.096
12:14:10	16.974	15.319	16.366	16.887	45.239
12:14:20	21.425	19.97	20.587	21.05	45.041
12:14:30	24.504	23.396	23.609	23.928	45.015
12:14:40	26.805	25.442	25.509	25.743	44.988
12:14:50	28.698	26.65	26.544	26.329	44.962
12:15:00	30.215	27.97	27.32	27.048	44.935
12:15:10	31.502	29.23	28.379	27.478	44.793
12:15:20	32.648	30.161	29.153	28.052	44.767
12:15:30	33.564	31.105	30.268	28.798	44.768
12:15:40	34.364	32.165	30.813	29.77	44.741
12:15:50	35.048	32.852	31.644	30.6	44.684
12:16:00	35.619	33.596	32.503	31.374	44.657
12:16:10	36.133	34.196	33.261	31.861	44.545
12:16:20	36.56	34.767	33.433	32.291	44.545
12:16:30	36.903	35.224	33.834	33.228	44.405
12:16:40	37.217	35.624	34.428	33.686	44.492
12:16:50	37.531	35.853	34.8	34.144	44.436
12:17:00	37.729	36.138	35.228	34.544	44.437
12:17:10	37.9	36.394	35.598	34.942	44.609
12:17:20	38.043	36.622	35.94	35.342	44.581
12:17:30	38.216	36.879	36.255	35.6	44.412
12:17:40	38.36	37.08	36.513	35.971	44.556
12:17:50	38.474	37.28	36.684	36.228	44.471
12:18:00	38.532	37.449	36.884	36.656	44.387
12:18:10	38.591	37.565	37.084	36.885	44.388
12:18:20	38.649	37.709	37.256	37.114	44.361
12:18:34	38.765	37.882	37.514	37.429	44.307

Table A.10: Temperature variations of MCPCM slurries (10% to 40%) in heating mode with 35°C melting point (see Figure 4.13b)

Time	Temperature (°C)				
	Water	20% Slurry	30% slurry	40% Slurry	Bath
11:04:40	22.371	22.758	22.997	23.177	48.264
11:04:50	22.373	22.79	23.029	23.089	48.237
11:05:00	22.432	22.791	23.03	23.179	48.096
11:05:10	24.974	23.419	24.916	24.887	48.239
11:05:20	29.425	28.07	29.137	29.05	48.041
11:05:30	32.504	31.496	32.159	31.928	48.015
11:05:40	34.805	33.542	34.059	33.743	47.988
11:05:50	36.698	34.75	35.094	34.979	47.962
11:06:00	38.215	36.07	35.87	35.698	47.935

Table A.10 (Continued)

11:06:10	39.502	37.33	36.929	36.128	47.793
11:06:20	40.648	38.161	37.703	36.702	47.767
11:06:30	41.564	39.105	38.818	37.448	47.768
11:06:40	42.364	40.165	39.363	38.42	47.741
11:06:50	43.048	40.852	40.194	39.25	47.684
11:07:00	43.619	41.596	41.053	40.024	47.657
11:07:10	44.133	42.196	41.511	40.511	47.545
11:07:20	44.56	42.767	41.683	40.941	47.545
11:07:30	44.903	43.224	42.084	41.428	47.405
11:07:40	45.217	43.624	42.428	41.886	47.492
11:07:50	45.531	44.053	42.8	42.344	47.436
11:08:00	45.729	44.338	43.228	42.744	47.437
11:08:10	45.9	44.594	43.598	43.142	47.409
11:08:20	46.043	44.822	43.94	43.542	47.381
11:08:30	46.216	45.079	44.255	43.8	47.212
11:08:40	46.36	45.28	44.513	44.171	47.356
11:08:50	46.474	45.48	44.684	44.428	47.271
11:09:00	46.532	45.649	44.884	44.656	47.187
11:09:10	46.591	45.765	45.084	44.885	47.188
11:09:20	46.649	45.909	45.256	45.114	47.161
11:09:34	46.765	46.082	45.514	45.429	47.107

Table A.11: Temperature variations of MCPCM slurries (10% to 40%) in heating mode with 50°C melting point (see Figure 4.13c)

Time	Temperature (°C)				
	Water	20% Slurry	30% slurry	40% Slurry	Bath
10:58:40	36.371	36.758	36.997	37.177	65.264
10:58:50	36.373	36.79	37.029	37.089	65.237
10:59:00	36.432	36.791	37.03	37.179	65.096
10:59:10	38.974	37.419	38.916	38.887	65.239
10:59:20	43.425	41.57	42.137	43.05	65.041
10:59:30	46.504	44.996	45.159	45.928	65.015
10:59:40	48.805	47.042	47.059	46.743	64.988
10:59:50	50.698	48.25	48.094	47.979	64.962
11:00:00	52.215	49.57	48.87	48.698	64.935
11:00:10	53.502	50.83	49.929	49.128	64.793
11:00:20	54.648	51.661	50.703	49.702	64.767
11:00:30	55.564	52.605	51.818	50.448	64.768
11:00:40	56.364	54.165	52.363	51.42	64.741
11:00:50	57.048	54.852	53.194	52.25	64.684
11:01:00	57.619	55.596	54.053	53.024	64.657
11:01:10	58.133	56.196	55.511	53.511	64.545
11:01:20	58.56	56.767	55.683	53.941	64.545
11:01:30	58.903	57.224	56.084	55.428	64.405
11:01:40	59.217	57.624	56.428	55.886	64.492
11:01:50	59.531	58.053	56.8	56.344	64.436
11:02:00	59.729	58.338	57.228	56.744	64.437
11:02:10	59.9	58.594	57.598	57.142	64.409
11:02:20	60.043	58.822	57.94	57.542	64.381
11:02:30	60.216	59.079	58.255	57.8	64.712

Table A.11 (Continued)

11:02:40	60.36	59.28	58.513	58.171	64.856
11:02:50	60.474	59.48	58.684	58.428	64.771
11:03:00	60.532	59.649	58.884	58.656	64.687
11:03:10	60.591	59.765	59.084	58.885	64.688
11:03:20	60.649	59.909	59.256	59.114	64.661
11:03:34	60.765	60.082	59.514	59.429	64.607

Table A.12: Temperature variations of MCPCM slurries (10% to 40%) in cooling mode with 28°C melting point (see Figure 4.14a)

Time	Temperature (°C)				
	Water	20% Slurry	30% slurry	40% Slurry	Bath
12:51:40	45.462	45.446	45.006	45.656	9.098
12:51:50	45.406	45.362	45.95	45.515	9.07
12:52:00	45.293	45.305	45.978	45.572	8.98
12:52:10	40.67	44.11	44.312	43.305	9.101
12:52:20	36.716	39.819	40.505	40.178	9.101
12:52:30	33.319	35.924	36.982	37.135	9.225
12:52:40	30.748	31.867	33.869	34.42	9.315
12:52:50	28.542	29.177	30.955	32.263	9.347
12:53:00	26.674	27.802	29.179	30.63	9.378
12:53:10	25.065	26.996	27.946	29.023	9.38
12:53:20	23.686	25.73	26.97	27.845	9.411
12:53:30	22.478	24.526	25.935	26.783	9.412
12:53:40	21.441	23.25	24.817	25.405	9.475
12:53:50	20.546	22.543	23.984	24.889	9.506
12:54:00	19.68	21.621	22.949	24.256	9.478
12:54:10	19.014	20.871	21.969	23.738	9.539
12:54:20	18.321	20.149	21.162	22.931	9.511
12:54:30	17.772	19.541	20.757	22.382	9.571
12:54:40	17.26	19.136	19.979	21.48	9.544
12:54:50	17.11	18.82	19.776	21.422	9.574
12:55:00	16.813	18.503	19.199	21.106	9.576
12:55:10	16.397	18.071	18.592	20.499	9.607
12:55:20	16.039	17.609	17.957	20.152	9.578
12:55:30	15.741	18.085	17.296	19.806	9.61
12:55:40	15.415	16.795	16.701	19.404	9.612
12:55:50	15.147	16.466	16.581	18.97	9.612
12:56:00	14.908	16.109	16.433	18.623	9.613
12:56:10	14.73	15.812	16.286	18.252	9.645
12:56:20	14.582	15.603	16.196	17.953	9.645

Table A.13: Temperature variations of MCPCM slurries (10% to 40%) in cooling mode with 35°C melting point (see Figure 4.14b)

Time	Temperature (°C)				
	Water	20% Slurry	30% slurry	40% Slurry	Bath
12:40:40	51.562	50.571	51.986	50.656	18.098
12:40:50	51.506	50.487	51.93	50.515	18.07
12:41:00	51.393	50.43	51.958	50.572	17.98
12:41:10	46.77	50.235	50.292	48.305	18.101
12:41:20	42.816	45.944	46.485	45.178	18.101
12:41:30	39.419	42.049	42.962	42.135	18.225
12:41:40	36.848	37.992	39.849	39.42	18.315
12:41:50	34.642	35.302	36.935	36.763	18.347
12:42:00	32.774	34.327	35.159	35.13	18.378
12:42:10	31.165	33.121	33.926	33.523	18.38
12:42:20	29.786	31.855	32.95	32.345	18.411
12:42:30	28.578	30.651	31.915	31.283	18.412
12:42:40	27.541	29.675	30.797	29.905	18.475
12:42:50	26.646	28.668	29.964	29.389	18.506
12:43:00	25.78	27.746	28.929	28.756	18.478
12:43:10	25.114	26.996	27.949	28.238	18.539
12:43:20	24.421	26.274	27.142	27.431	18.511
12:43:30	23.872	25.666	26.737	26.882	18.571
12:43:40	23.36	25.061	25.959	26.48	18.544
12:43:43	23.21	24.945	25.756	26.422	18.574
12:43:50	22.913	24.628	25.179	26.106	18.576
12:44:00	22.497	24.196	24.572	25.499	18.607
12:44:10	22.139	23.734	23.937	25.152	18.578
12:44:20	21.841	23.335	23.276	24.806	18.61
12:44:30	21.515	22.92	22.681	24.404	18.612
12:44:40	21.247	22.591	22.561	23.97	18.612
12:44:50	21.008	22.234	22.413	23.623	18.613
12:45:00	20.83	21.937	22.266	23.252	18.645
12:45:08	20.682	21.728	22.176	22.953	18.645

Table A.14: Temperature variations of MCPCM slurries (10% to 40%) in cooling mode with 50°C melting point (see Figure 4.14c)

Time	Temperature (°C)				
	Water	20% Slurry	30% slurry	40% Slurry	Bath
13:02:20	68.062	67.571	68.986	68.156	29.598
13:02:30	68.006	67.987	68.93	68.015	29.57
13:02:40	67.893	67.93	68.958	68.072	29.48
13:02:50	62.77	66.735	67.292	65.805	29.601
13:03:00	58.816	62.444	63.485	62.678	29.601
13:03:10	55.419	58.549	59.962	59.635	29.725
13:03:20	52.848	54.492	56.349	56.92	29.815
13:03:30	50.642	51.802	53.435	53.263	29.847
13:03:40	49.274	50.827	51.659	51.63	29.878
13:03:50	47.665	49.621	50.426	52.023	29.88

Table A.14 (Continued)

13:04:00	46.286	48.355	50.45	50.845	29.911
13:04:10	45.078	47.151	49.415	49.783	29.912
13:04:20	44.041	46.175	48.297	48.405	29.975
13:04:30	43.646	45.168	47.464	47.889	30.006
13:04:40	42.78	44.246	46.429	47.256	29.978
13:04:50	42.114	43.496	45.449	46.738	30.039
13:05:00	41.421	42.774	44.642	45.931	30.011
13:05:10	40.872	42.166	44.237	45.382	30.071
13:05:20	40.36	41.561	43.459	44.98	30.044
13:05:30	40.21	41.445	42.256	43.922	30.074
13:05:40	39.413	41.128	41.679	43.606	30.076
13:05:50	38.997	40.696	41.072	42.999	30.107
13:06:00	38.639	40.234	40.437	42.652	30.078
13:06:10	38.341	39.835	39.776	42.306	30.11
13:06:20	38.015	39.42	39.181	41.404	30.112
13:06:30	37.747	39.091	39.061	40.97	30.112
13:06:40	37.508	38.734	38.913	40.623	30.113
13:06:50	37.33	38.437	38.766	40.252	30.145
13:07:00	37.182	38.228	38.676	39.953	30.145

Table A.15: Temperature differences between the fluid and bath for 20%-40%MCPCM slurry with 35°C n-eicosane and water in cooling mode (see Figure 4.15a)

Time	Temperature (°C)			
	Tw-Tb	Ts@20%-Tb	Ts@30%-Tb	Ts@40%-Tb
12:40:40	33.464	32.473	33.888	32.558
12:40:50	33.436	32.417	33.86	32.445
12:41:00	33.413	32.45	33.978	32.592
12:41:10	28.669	32.134	32.191	30.204
12:41:20	24.715	27.843	28.384	27.077
12:41:30	21.194	23.824	24.737	23.91
12:41:40	18.533	19.677	21.534	21.105
12:41:50	16.295	16.955	18.588	18.416
12:42:00	14.396	15.949	16.781	16.752
12:42:10	12.785	14.741	15.546	15.143
12:42:20	11.375	13.444	14.539	13.934
12:42:30	10.166	12.239	13.503	12.871
12:42:40	9.066	11.2	12.322	11.43
12:42:50	8.14	10.162	11.458	10.883
12:43:00	7.302	9.268	10.451	10.278
12:43:10	6.575	8.457	9.41	9.699
12:43:20	5.91	7.763	8.631	8.92
12:43:30	5.301	7.095	8.166	8.311
12:43:40	4.816	6.517	7.415	7.936
12:43:43	4.636	6.371	7.182	7.848
12:43:50	4.337	6.052	6.603	7.53
12:44:00	3.89	5.589	5.965	6.892
12:44:10	3.561	5.156	5.359	6.574
12:44:20	3.231	4.725	4.666	6.196

Table A.15 (Continued)

12:44:30	2.903	4.308	4.069	5.792
12:44:40	2.635	3.979	3.949	5.358
12:44:50	2.395	3.621	3.8	5.01
12:45:00	2.185	3.292	3.621	4.607
12:45:08	2.037	3.083	3.531	4.308

Table A.16: Temperature differences between the fluid and bath for 20%-40%MCPCM slurry with 35°C n-eicosane and water in heating mode (see Figure 4.15b)

Time	Temperature (°C)			
	Tb-Tw	Tb-Ts@20%	Tb-Ts@30%	Tb-Ts@40%
11:04:40	25.893	25.506	25.267	25.087
11:04:50	25.864	25.447	25.208	25.148
11:05:00	25.664	25.305	25.066	24.917
11:05:10	23.265	24.82	23.323	23.352
11:05:20	18.616	19.971	18.904	18.991
11:05:30	15.511	16.519	15.856	16.087
11:05:40	13.183	14.446	13.929	14.245
11:05:50	11.264	13.212	12.868	12.983
11:06:00	9.72	11.865	12.065	12.237
11:06:10	8.291	10.463	10.864	11.665
11:06:20	7.119	9.606	10.064	11.065
11:06:30	6.204	8.663	8.95	10.32
11:06:40	5.377	7.576	8.378	9.321
11:06:50	4.636	6.832	7.49	8.434
11:07:00	4.038	6.061	6.604	7.633
11:07:10	3.412	5.349	6.034	7.034
11:07:20	2.985	4.778	5.862	6.604
11:07:30	2.502	4.181	5.321	5.977
11:07:40	2.275	3.868	5.064	5.606
11:07:50	1.905	3.383	4.636	5.092
11:08:00	1.708	3.099	4.209	4.693
11:08:10	1.509	2.815	3.811	4.267
11:08:20	1.338	2.559	3.441	3.839
11:08:30	0.996	2.133	2.957	3.412
11:08:40	0.996	2.076	2.843	3.185
11:08:50	0.797	1.791	2.587	2.843
11:09:00	0.655	1.538	2.303	2.531
11:09:10	0.597	1.423	2.104	2.303
11:09:20	0.512	1.252	1.905	2.047
11:09:34	0.342	1.025	1.593	1.678

Table A.17: Temperature difference between the outlet and inlet of the test section for water and 5% to 40% MCPCM slurry with 28°C melting point (see Figure 5.13a)

Flowrate (L/min)	Temperature (°C)					
	Water	**5% Slurry**	**10% Slurry**	**20% Slurry**	**30% Slurry**	**40% Slurry**
2.05	13.34	13.25	12.77	12.20	11.11	9.34
2.11	13.16	13.15	12.58	12.01	10.99	9.25
2.2	12.99	12.99	12.39	11.82	10.87	9.16
2.27	12.81	12.83	12.20	11.63	10.70	9.07
2.39	12.63	12.65	12.01	11.44	10.53	8.98
2.51	12.46	12.47	11.82	11.25	10.36	8.89
2.63	12.28	12.29	11.67	11.06	10.19	8.80
2.71	12.11	12.13	11.48	10.87	10.02	8.71
2.78	11.93	11.94	11.29	10.68	9.85	8.62
2.9	11.75	11.75	11.10	10.49	9.68	8.53
3.02	11.58	11.56	10.95	10.30	9.51	8.44
3.11	11.40	11.37	10.76	10.11	9.34	8.35
3.22	11.23	11.18	10.57	9.92	9.19	8.26
3.3	11.05	10.99	10.42	9.73	9.09	8.17
3.41	10.87	10.80	10.27	9.58	8.99	8.08
3.5	10.70	10.61	10.12	9.43	8.89	7.99
3.59	10.52	10.42	9.93	9.28	8.79	7.90
3.69	10.35	10.23	9.74	9.13	8.69	7.81
3.81	10.17	10.04	9.55	8.98	8.59	7.72
3.92	9.99	9.85	9.43	8.83	8.49	7.63
4.02	9.82	9.78	9.40	8.60	8.41	7.59
4.11	9.72	9.68	9.30	8.53	8.34	7.55
4.19	9.62	9.58	9.20	8.46	8.27	7.50
4.3	9.52	9.48	9.10	8.39	8.20	7.45
4.41	9.42	9.38	9.00	8.32	8.13	7.40
4.49	9.32	9.28	8.90	8.25	8.06	7.35
4.62	9.23	9.18	8.80	8.18	7.99	7.31
4.68	9.13	9.08	8.70	8.11	7.92	7.26
4.8	9.03	8.98	8.60	8.04	7.85	7.21
4.93	8.93	8.88	8.50	7.97	7.78	7.16
5.02	8.83	8.78	8.40	7.90	7.71	7.11
5.13	8.73	8.68	8.30	7.83	7.64	7.07
5.19	8.63	8.58	8.20	7.76	7.57	7.02
5.3	8.53	8.48	8.10	7.69	7.50	6.97
5.41	8.43	8.38	8.00	7.62	7.43	6.92
5.52	8.33	8.28	7.90	7.55	7.36	6.87
5.62	8.24	8.18	7.80	7.48	7.30	6.83
5.7	8.14	8.08	7.70	7.41	7.23	6.78
5.78	8.04	7.98	7.60	7.34	7.16	6.73
5.9	7.94	7.88	7.50	7.27	7.09	6.68
6.05	7.76	7.77	7.42	7.19	7.08	6.57

Table A.18: Temperature difference between the outlet and inlet of the test section for water and 5% to 40% MCPCM slurry with 35°C melting point (see Figure 5.13b)

Flowrate (L/min)	Temperature (°C)					
	Water	**5% Slurry**	**10% Slurry**	**20% Slurry**	**30% Slurry**	**40% Slurry**
2.05	13.34	13.15	12.37	12.24	11.01	9.24
2.11	13.16	12.97	12.18	12.05	10.89	9.15
2.2	12.99	12.79	11.99	11.86	10.77	9.06
2.27	12.81	12.61	11.80	11.67	10.65	8.97
2.39	12.63	12.43	11.61	11.48	10.53	8.88
2.51	12.46	12.25	11.42	11.29	10.41	8.79
2.63	12.28	12.07	11.27	11.10	10.29	8.70
2.71	12.11	11.89	11.08	10.91	10.17	8.61
2.78	11.93	11.71	10.89	10.72	10.05	8.52
2.9	11.75	11.53	10.70	10.53	9.93	8.43
3.02	11.58	11.35	10.55	10.34	9.81	8.34
3.11	11.4	11.17	10.36	10.15	9.69	8.25
3.22	11.23	10.99	10.17	9.96	9.57	8.16
3.3	11.05	10.81	10.02	9.77	9.45	8.07
3.41	10.87	10.63	9.87	9.58	9.33	7.98
3.5	10.7	10.45	9.72	9.43	9.21	7.89
3.59	10.52	10.27	9.53	9.28	9.06	7.80
3.69	10.35	10.09	9.34	9.13	8.91	7.71
3.81	10.17	9.91	9.15	8.98	8.76	7.62
3.92	9.993	9.91	9.03	8.83	8.58	7.53
4.02	9.819	9.78	8.80	8.65	8.41	7.49
4.11	9.72	9.65	8.72	8.57	8.34	7.45
4.19	9.621	9.54	8.67	8.49	8.27	7.40
4.3	9.522	9.43	8.59	8.41	8.20	7.35
4.41	9.423	9.32	8.51	8.33	8.13	7.30
4.49	9.324	9.21	8.43	8.25	8.06	7.25
4.62	9.225	9.10	8.35	8.17	7.99	7.21
4.68	9.126	8.99	8.27	8.09	7.92	7.16
4.8	9.027	8.88	8.19	8.01	7.85	7.11
4.93	8.928	8.77	8.11	7.93	7.78	7.06
5.02	8.829	8.66	8.03	7.85	7.71	7.01
5.13	8.73	8.55	7.95	7.77	7.64	6.97
5.19	8.631	8.44	7.87	7.69	7.57	6.92
5.3	8.532	8.33	7.79	7.61	7.50	6.87
5.41	8.433	8.22	7.71	7.53	7.43	6.82
5.52	8.334	8.11	7.63	7.45	7.36	6.77
5.62	8.235	8.00	7.55	7.37	7.29	6.73
5.7	8.136	7.89	7.47	7.29	7.22	6.68
5.78	8.037	7.78	7.39	7.21	7.15	6.63
5.9	7.938	7.67	7.31	7.13	7.08	6.58
6.054	7.76	7.56	7.23	7.05	7.08	6.57

Table A.19: Temperature difference between the outlet and inlet of the test section for water and 5% to 40% MCPCM slurry with 50°C melting point (see Figure 5.13c)

Flowrate (L/min)	Temperature (°C)					
	Water	5% Slurry	10% Slurry	20% Slurry	30% Slurry	40% Slurry
2.05	13.34	13.33	12.37	12.14	10.81	9.84
2.11	13.16	13.18	12.22	11.95	10.69	9.75
2.2	12.99	12.99	12.07	11.76	10.57	9.66
2.27	12.81	12.80	11.92	11.57	10.45	9.57
2.39	12.63	12.61	11.77	11.38	10.33	9.48
2.51	12.46	12.42	11.62	11.19	10.21	9.39
2.63	12.28	12.17	11.47	11.00	10.09	9.30
2.71	12.11	11.92	11.32	10.81	9.97	9.21
2.78	11.93	11.67	11.17	10.62	9.85	9.12
2.9	11.75	11.42	11.02	10.43	9.73	9.03
3.02	11.58	11.17	10.87	10.24	9.61	8.94
3.11	11.40	11.07	10.72	10.09	9.49	8.85
3.22	11.23	10.97	10.57	9.94	9.37	8.76
3.3	11.05	10.87	10.42	9.79	9.25	8.67
3.41	10.87	10.71	10.27	9.64	9.13	8.58
3.5	10.70	10.56	10.12	9.49	9.01	8.49
3.59	10.52	10.40	9.97	9.34	8.89	8.40
3.69	10.35	10.25	9.82	9.19	8.75	8.31
3.81	10.17	10.10	9.67	9.04	8.61	8.22
3.92	9.99	9.84	9.52	8.89	8.49	8.13
4.02	9.82	9.78	9.37	8.65	8.41	8.04
4.11	9.72	9.63	9.30	8.64	8.34	8.00
4.19	9.62	9.52	9.23	8.57	8.27	7.95
4.3	9.52	9.41	9.16	8.50	8.20	7.90
4.41	9.42	9.30	9.09	8.43	8.13	7.85
4.49	9.32	9.19	9.02	8.36	8.06	7.80
4.62	9.23	9.08	8.95	8.29	7.99	7.76
4.68	9.13	8.97	8.88	8.22	7.92	7.71
4.8	9.03	8.87	8.81	8.15	7.85	7.66
4.93	8.93	8.77	8.74	8.08	7.78	7.61
5.02	8.83	8.67	8.63	8.01	7.71	7.56
5.13	8.73	8.57	8.52	7.94	7.64	7.52
5.19	8.63	8.47	8.41	7.87	7.57	7.47
5.3	8.53	8.37	8.30	7.80	7.50	7.42
5.41	8.43	8.27	8.19	7.73	7.43	7.37
5.52	8.33	8.16	8.08	7.66	7.36	7.32
5.62	8.24	8.05	7.97	7.59	7.29	7.28
5.7	8.14	7.94	7.86	7.52	7.22	7.23
5.78	8.04	7.83	7.75	7.45	7.15	7.18
5.9	7.94	7.72	7.64	7.38	7.08	7.13
6.054	7.76	7.61	7.56	7.30	7.08	7.08

Table A.20: Measured heat transportation of water and 5-40% MCPCM slurry as a function of flow rate with n-eicosane melting point of 28°C (see Figure 5.14a)

Flowrate (L/min)	Heat transportation (W)					
	Water	5% Slurry	10% Slurry	20% Slurry	30% Slurry	40% Slurry
2.05	2178.92	2275.91	2673.75	3359.54	3800.41	3914.62
2.11	2225.92	2318.91	2710.75	3385.54	3813.91	3925.62
2.2	2272.92	2361.91	2747.75	3411.54	3827.41	3936.62
2.27	2319.92	2404.91	2784.75	3437.54	3840.91	3947.62
2.39	2366.92	2447.91	2821.75	3463.54	3854.41	3958.62
2.51	2413.92	2490.91	2858.75	3489.54	3867.91	3969.62
2.63	2460.92	2533.91	2895.75	3515.54	3881.41	3980.62
2.71	2507.92	2576.91	2932.75	3541.54	3894.91	3991.62
2.78	2554.92	2619.91	2969.75	3567.54	3908.41	4002.62
2.9	2601.92	2662.91	3006.75	3593.54	3921.91	4013.62
3.02	2648.92	2705.91	3043.75	3619.54	3935.41	4024.62
3.11	2695.92	2748.91	3080.75	3645.54	3948.91	4035.62
3.22	2742.92	2791.91	3117.75	3671.54	3962.41	4046.62
3.3	2789.92	2834.91	3154.75	3697.54	3975.91	4057.62
3.41	2836.92	2877.91	3191.75	3723.54	3989.41	4068.62
3.5	2883.92	2920.91	3228.75	3749.54	4002.91	4079.62
3.59	2930.92	2963.91	3265.75	3775.54	4016.41	4090.62
3.69	2977.92	3006.91	3302.75	3801.54	4029.91	4101.62
3.81	3024.92	3049.91	3339.75	3827.54	4043.41	4112.62
3.92	3071.92	3092.91	3376.75	3853.54	4056.91	4123.62
4.02	3116.72	3135.91	3413.75	3879.54	4070.41	4134.62
4.11	3139.99	3157.80	3434.85	3897.68	4085.82	4150.94
4.19	3163.26	3179.69	3455.95	3915.82	4101.23	4167.26
4.3	3186.53	3201.58	3477.05	3933.96	4116.64	4183.58
4.41	3209.80	3223.47	3498.15	3952.10	4132.05	4199.90
4.49	3233.07	3245.36	3519.25	3970.24	4147.46	4216.22
4.62	3256.34	3267.25	3540.35	3988.38	4162.87	4232.54
4.68	3279.61	3289.14	3561.45	4006.52	4178.28	4248.86
4.8	3302.88	3311.03	3582.55	4024.66	4193.69	4265.18
4.93	3326.15	3332.92	3603.65	4042.80	4209.10	4281.50
5.02	3349.42	3354.81	3624.75	4060.94	4224.51	4297.82
5.13	3372.69	3376.70	3645.85	4079.08	4239.92	4314.14
5.19	3395.96	3398.59	3666.95	4097.22	4255.33	4330.46
5.3	3419.23	3420.48	3688.05	4115.36	4270.74	4346.78
5.41	3442.50	3442.37	3709.15	4133.50	4286.15	4363.10
5.52	3465.77	3464.26	3730.25	4151.64	4301.56	4379.42
5.62	3489.04	3486.15	3751.35	4169.78	4316.97	4395.74
5.7	3512.31	3508.04	3772.45	4187.92	4332.38	4412.06
5.78	3535.58	3529.93	3793.55	4206.06	4347.79	4428.38
5.9	3558.85	3551.82	3814.65	4224.20	4363.20	4444.70
6.05	3582.21	3635.20	3927.61	4230.16	4421.34	4517.79

Table A.21: Measured heat transportation of water and 5-40% MCPCM slurry as a function of flow rate with n-eicosane melting point of 35°C (see Figure 5.14b)

Flowrate (L/min)	Heat transportation (W)					
	Water	5% Slurry	10% Slurry	20% Slurry	30% Slurry	40% Slurry
2.05	2178.92	2305.91	2873.75	3339.54	3844.41	3978.62
2.11	2225.92	2348.91	2910.75	3365.54	3857.91	3989.62
2.20	2272.92	2391.91	2947.75	3391.54	3871.41	4000.62
2.27	2319.92	2434.91	2984.75	3417.54	3884.91	4011.62
2.39	2366.92	2477.91	3021.75	3443.54	3898.41	4022.62
2.51	2413.92	2520.91	3058.75	3469.54	3911.91	4033.62
2.63	2460.92	2563.91	3095.75	3495.54	3925.41	4044.62
2.71	2507.92	2606.91	3132.75	3521.54	3938.91	4055.62
2.78	2554.92	2649.91	3169.75	3547.54	3952.41	4066.62
2.90	2601.92	2692.91	3206.75	3573.54	3965.91	4077.62
3.02	2648.92	2735.91	3243.75	3599.54	3979.41	4088.62
3.11	2695.92	2778.91	3280.75	3625.54	3992.91	4099.62
3.22	2742.92	2821.91	3317.75	3651.54	4006.41	4110.62
3.30	2789.92	2864.91	3354.75	3677.54	4019.91	4121.62
3.41	2836.92	2907.91	3391.75	3703.54	4033.41	4132.62
3.50	2883.92	2950.91	3428.75	3729.54	4046.91	4143.62
3.59	2930.92	2993.91	3465.75	3755.54	4060.41	4154.62
3.69	2977.92	3036.91	3502.75	3781.54	4073.91	4165.62
3.81	3024.92	3079.91	3539.75	3807.54	4087.41	4176.62
3.92	3071.92	3122.91	3576.75	3833.54	4100.91	4187.62
4.02	3116.72	3165.91	3605.32	3867.16	4113.02	4191.23
4.11	3139.99	3187.80	3626.42	3885.30	4128.43	4207.55
4.19	3163.26	3209.69	3647.52	3903.44	4143.84	4223.87
4.30	3186.53	3231.58	3668.62	3921.58	4159.25	4240.19
4.41	3209.80	3253.47	3689.72	3939.72	4174.66	4256.51
4.49	3233.07	3275.36	3710.82	3957.86	4190.07	4272.83
4.62	3256.34	3297.25	3731.92	3976.00	4205.48	4289.15
4.68	3279.61	3319.14	3753.02	3994.14	4220.89	4305.47
4.80	3302.88	3341.03	3774.12	4012.28	4236.30	4321.79
4.93	3326.15	3362.92	3795.22	4030.42	4251.71	4338.11
5.02	3349.42	3384.81	3816.32	4048.56	4267.12	4354.43
5.13	3372.69	3406.70	3837.42	4066.70	4282.53	4370.75
5.19	3395.96	3428.59	3858.52	4084.84	4297.94	4387.07
5.30	3419.23	3450.48	3879.62	4102.98	4313.35	4403.39
5.41	3442.50	3472.37	3900.72	4121.12	4328.76	4419.71
5.52	3465.77	3494.26	3921.82	4139.26	4344.17	4436.03
5.62	3489.04	3516.15	3942.92	4157.40	4359.58	4452.35
5.70	3512.31	3538.04	3964.02	4175.54	4374.99	4468.67
5.78	3535.58	3559.93	3985.12	4193.68	4390.40	4484.99
5.90	3558.85	3581.82	4006.22	4211.82	4405.81	4501.31
6.05	3582.21	3635.20	4027.61	4230.16	4421.34	4517.79

Table A.22: Measured heat transportation of water and 5-40% MCPCM slurry as a function of flow rate with n-eicosane melting point of 50°C (see Figure 5.14c)

Flowrate (L/min)	Heat transportation (W)					
	Water	5% Slurry	10% Slurry	20% Slurry	30% Slurry	40% Slurry
2.05	2178.92	2195.91	2603.75	3300.54	3650.41	3814.62
2.11	2225.92	2238.91	2640.75	3326.54	3663.91	3825.62
2.2	2272.92	2281.91	2677.75	3352.54	3677.41	3836.62
2.27	2319.92	2324.91	2714.75	3372.54	3690.91	3846.62
2.39	2366.92	2367.91	2751.75	3392.54	3704.41	3856.62
2.51	2413.92	2410.91	2788.75	3412.54	3717.91	3866.62
2.63	2460.92	2453.91	2825.75	3432.54	3731.41	3876.62
2.71	2507.92	2496.91	2862.75	3458.54	3744.91	3886.62
2.78	2554.92	2539.91	2899.75	3484.54	3758.41	3896.62
2.9	2601.92	2582.91	2936.75	3510.54	3771.91	3906.62
3.02	2648.92	2625.91	2973.75	3538.54	3785.41	3916.62
3.11	2695.92	2668.91	3010.75	3566.54	3798.91	3926.62
3.22	2742.92	2711.91	3047.75	3594.54	3812.41	3939.62
3.3	2789.92	2754.91	3084.75	3622.54	3825.91	3952.62
3.41	2836.92	2797.91	3121.75	3650.54	3839.41	3965.62
3.5	2883.92	2840.91	3158.75	3678.54	3852.91	3978.62
3.59	2930.92	2903.91	3195.75	3706.54	3866.41	3991.62
3.69	2977.92	2966.91	3232.75	3732.54	3879.91	4004.62
3.81	3024.92	3029.91	3269.75	3758.54	3893.41	4017.62
3.92	3071.92	3092.91	3306.75	3784.54	3906.91	4030.62
4.02	3116.72	3155.91	3343.75	3810.54	3920.41	4041.62
4.11	3139.99	3177.80	3364.85	3825.68	3935.82	4057.94
4.19	3163.26	3199.69	3385.95	3840.82	3951.23	4074.26
4.3	3186.53	3221.58	3407.05	3855.96	3966.64	4090.58
4.41	3209.80	3243.47	3428.15	3871.10	3982.05	4106.90
4.49	3233.07	3265.36	3449.25	3886.24	3997.46	4123.22
4.62	3256.34	3287.25	3470.35	3901.38	4012.87	4139.54
4.68	3279.61	3309.14	3491.45	3916.52	4028.28	4155.86
4.8	3302.88	3331.03	3512.55	3931.66	4043.69	4172.18
4.93	3326.15	3352.92	3533.65	3946.80	4059.10	4188.50
5.02	3349.42	3374.81	3554.75	3961.94	4074.51	4204.82
5.13	3372.69	3396.70	3575.85	3977.08	4089.92	4221.14
5.19	3395.96	3418.59	3596.95	3992.22	4105.33	4237.46
5.3	3419.23	3440.48	3618.05	4007.36	4120.74	4250.78
5.41	3442.50	3462.37	3639.15	4022.50	4136.15	4264.10
5.52	3465.77	3484.26	3660.25	4037.64	4151.56	4277.42
5.62	3489.04	3506.15	3681.35	4052.78	4166.97	4290.74
5.7	3512.31	3528.04	3702.45	4067.92	4182.38	4304.06
5.78	3535.58	3549.93	3723.55	4083.06	4197.79	4317.38
5.9	3558.85	3571.82	3744.65	4098.20	4213.20	4330.70
6.05	3582.21	3635.20	3827.61	4113.34	4261.34	4344.02

Table A.23: Insulation map for the solar collector at I_{av} = 779W/m^2

(see Figure 6.8a)

Insulation (W/m^2)

	1	2	3	4	5	6
S5	762	818	780	811	840	776
S4	750	808	766	827	888	810
S3	776	803	762	787	823	761
S2	755	817	793	803	833	740
S1	720	750	710	722	733	666

Table A.24: Insulation map for the solar collector at I_{av} = 599W/m^2

(see Figure 6.8b)

Insulation (W/m^2)

	1	2	3	4	5	6
S5	611	660	637	607	611	546
S4	566	628	605	620	640	560
S3	578	625	612	610	620	549
S2	564	654	629	615	645	555
S1	537	610	563	574	608	547

Table A.25: Insulation map for the solar collector at I_{av} = 396W/m^2

(see Figure 6.8c)

Insulation (W/m^2)

	1	2	3	4	5	6
S5	380	414	392	400	403	409
S4	351	394	388	424	443	396
S3	365	408	397	397	399	360
S2	369	428	415	425	432	383
S1	373	410	392	394	403	362

Table A.26: Insulation map for the solar collector at I_{av} = 217W/m^2

(see Figure 6.8d)

Insulation (W/m^2)

	1	2	3	4	5	6
S5	217	238	233	233	234	202
S4	206	232	220	222	218	188
S3	209	222	213	208	207	180
S2	208	237	226	233	242	217
S1	199	222	213	218	228	210

Table A.27: Temperature difference between the inlet and outlet of the solar collector using water and 20%MCPCM slurry with the irradiance between 200W and 800W/m^2(see Figure 6.9)

Q (W/m^2)	Temperature (°C)	
	Water	MCPCM Slurry
800	4.091	2.631
600	3.18	2.269
400	2.053	1.428
200	1.04	0.756

Table A.28: A comparison of the rate of heat transfer of the primary working fluid (Q_2) using water and 20% MCPCM slurry at I_{av} = 779W/m^2 (see Figure 6.10a)

Time	Q (w)	
	MCPCM slurry	Water
15:36:35	522	517
15:39:40	526	521
15:42:25	577	512
15:47:15	591	514
15:52:10	591	528
15:58:15	609	528
16:00:30	626	521
16:08:15	637	523
16:14:15	569	523
16:18:30	566	526
16:27:25	544	522

Table A.29: A comparison of the rate of heat transfer of the primary working fluid (Q_2) using water and 20% MCPCM slurry at I_{av} = 599W/m^2 (see Figure 6.10b)

Time	Q (w)	
	MCPCM slurry	Water
13:15:50	405	394
13:20:25	421	396
13:25:15	430	398
13:28:25	424	397
13:32:40	434	394
13:41:00	436	400
13:47:05	438	392
13:48:45	448	387
13:56:30	460	387
14:04:25	448	396
14:22:35	415	398

Table A.30: A comparison of the rate of heat transfer of the primary working fluid (Q_2) using water and 20% MCPCM slurry at $I_{av} = 396W/m^2$ (see Figure 6.10c)

Time	Q (w)	
	MCPCM slurry	Water
12:48:45	257	252
13:03:35	258	254
13:10:50	260	258
13:18:20	267	261
13:21:40	270	252
13:37:40	274	257
13:51:25	277	254
13:53:20	278	256
14:09:10	284	256
14:15:40	287	254
14:26:05	275	252
14:49:30	274	257
15:02:20	253	249

Table A.31: A comparison of the rate of heat transfer of the primary working fluid (Q_2) using water and 20% MCPCM slurry at $I_{av} = 217W/m^2$ (see Figure 6.10d)

Time	Q (w)	
	MCPCM slurry	Water
13:50:25	124	126
14:02:55	125	125
14:20:50	126	122
14:38:20	128	125
14:56:20	130	121
15:08:20	136	126
15:26:10	140	126
15:41:40	141	123
16:14:20	142	124
16:44:25	138	125
17:04:25	128	124

Table A.32: Solar collector efficiency with an average fluid temperature, $(T_{in}+T_{out})/2$, for MCPCM slurry and water for at $I_{av} = 779W/m^2$ (see Figure 6.11a)

Temperature	Efficiency	
(°C)	MCPCM slurry	Water
27.69	0.55	0.55
28.76	0.55	0.56
29.45	0.54	0.61
29.65	0.55	0.63
30.65	0.56	0.63
31.65	0.56	0.65

Table A.32 (Continued)

32.17	0.55	0.66
32.65	0.55	0.68
33.65	0.55	0.60
34.21	0.56	0.60
34.65	0.55	0.58

Table A.33: Solar collector efficiency with an average fluid temperature, $(T_{in}+T_{out})/2$, for MCPCM slurry and water for at $I_{av} = 599W/m^2$ (see Figure 6.11b)

Temperature (°C)	Efficiency MCPCM slurry	Water
27.31	0.54	0.55
27.95	0.54	0.57
28.95	0.54	0.59
29.49	0.54	0.58
30.24	0.54	0.59
30.95	0.55	0.60
31.95	0.54	0.60
32.34	0.53	0.61
32.95	0.53	0.63
33.93	0.54	0.61
35.30	0.54	0.57

Table A.34: Solar collector efficiency with an average fluid temperature, $(T_{in}+T_{out})/2$, for MCPCM slurry and water for at $I_{av} = 396W/m^2$ (see Figure 6.11c)

Temperature (°C)	Efficiency MCPCM slurry	Water
27.38	0.53	0.54
28.28	0.53	0.54
28.52	0.54	0.54
29.58	0.54	0.56
30.00	0.53	0.56
30.63	0.54	0.57
31.57	0.53	0.58
31.83	0.53	0.58
32.58	0.53	0.59
33.08	0.53	0.60
33.61	0.53	0.57
34.87	0.54	0.57
35.52	0.52	0.53

Table A.35: Solar collector efficiency with an average fluid temperature, $(T_{in}+T_{out})/2$, for MCPCM slurry and water for at $I_{av} = 217W/m^2$ (see Figure 6.11d)

Temperature (°C)	Efficiency	
	MCPCM slurry	Water
28.15	0.51	0.50
28.56	0.51	0.51
29.45	0.50	0.51
30.22	0.51	0.52
31.24	0.49	0.53
31.64	0.51	0.55
32.26	0.51	0.57
32.59	0.50	0.57
33.33	0.50	0.58
34.65	0.51	0.56
35.65	0.50	0.52

Table A.36: The efficiency of the solar collector at difference insolation with the use of MCPCM slurry and water (see Figure 6.12)

Q (W/m^2)	Efficiency	
	Water	MCPCM Slurry
800	0.55	0.68
600	0.53	0.63
400	0.53	0.60
200	0.50	0.58

Table A.37: Insulation map for the double glazed panel with $I_{av} = 806W/m^2$ (see Figure 6.15a)

	Insulation (W/m^2)		
	1	2	3
S3	796	793	800
S2	822	837	831
S1	800	784	795

Table A.38: Insulation map for the double glazed panel with $I_{av} = 601W/m^2$ (see Figure 6.15b)

	Insulation (W/m^2)		
	1	2	3
S3	602	601	595
S2	627	630	614
S1	584	583	581

Table A.39: Insulation map for the double glazed panel with I_{av} = 399W/m^2

(see Figure 6.15c)

	Insulation (W/m^2)		
	1	2	3
S3	395	396	398
S2	406	420	409
S1	397	389	387

Table A.40: Insulation map for the double glazed panel with I_{av} = 200W/m^2

(see Figure 6.15d)

	Insulation (W/m^2)		
	1	2	3
S3	200	192	200
S2	204	201	203
S1	207	202	196

Table A.41: A comparison of the rate of heat transfer of the primary working fluid (Q_2) using water and 20% MCPCM slurry at I_{av} = 806 W/m^2 (see Figure 6.16a)

Time	**Q** (w)	
	MCPCM slurry	**Water**
09:15:20	103	105
09:24:17	105	107
09:32:15	106	112
09:46:16	104	123
10:00:31	105	125
10:18:10	105	127
10:30:41	105	128
10:47:10	104	127
11:04:34	105	113
11:16:53	105	110
11:42:45	105	108

Table A.42: A comparison of the rate of heat transfer of the primary working fluid (Q_2) using water and 20% MCPCM slurry at I_{av} = 601 W/m^2 (see Figure 6.16b)

Time	**Q** (w)	
	MCPCM slurry	**Water**
10:12:25	78	81
10:24:23	78	82
10:37:00	76	79
10:45:16	77	88

Table A.42 (Continued)

10:56:21	78	93
11:18:06	78	93
11:33:59	76	94
11:38:20	77	92
11:58:33	77	87
12:19:13	79	82
12:42:43	77	80
13:06:38	77	82

Table A.43: A comparison of the rate of heat transfer of the primary working fluid (Q_2) using water and 20% MCPCM slurry at I_{av} = 399 W/m^2 (see Figure 6.16c)

Time	Q (w)	
	MCPCM slurry	Water
09:27:32	48	50
09:46:19	49	53
10:05:44	51	54
10:14:22	49	57
10:55:49	50	57
11:31:25	47	58
11:36:23	47	59
12:17:24	49	57
12:34:14	48	55
13:01:12	49	54
14:01:51	51	52
14:35:06	47	49

Table A.44: A comparison of the rate of heat transfer of the primary working fluid (Q_2) using water and 20% MCPCM slurry at I_{av} = 200 W/m^2 (see Figure 6.16d)

Time	Q (w)	
	MCPCM slurry	Water
08:45:20	23	23
09:20:20	22	22
10:10:30	23	26
10:59:30	23	26
11:49:54	24	27
12:23:30	22	27
13:13:26	22	28
13:56:50	23	28
15:28:18	24	25
16:52:32	24	24

Table A.45: Efficiency of the fluidised MCPCM glazed energy storage system with an average fluid temperature, $(T_{in}+T_{out})/2$, using MCPCM slurry and water at I_{av} = 806W/m^2 (see Figure 6.17a)

Temperature (°C)	Efficiency	
	MCPCM slurry	Water
29.05	0.51	0.52
30.08	0.52	0.53
30.80	0.53	0.56
31.02	0.52	0.61
32.23	0.52	0.62
33.15	0.52	0.63
33.56	0.52	0.64
34.25	0.52	0.63
35.08	0.52	0.56
35.42	0.52	0.54
36.54	0.52	0.54

Table A.46: Efficiency of the fluidised MCPCM glazed energy storage system with an average fluid temperature, (Tin+Tout)/2, using MCPCM slurry and water at I_{av}= 601W/m2 (see Figure 6.17b)

Temperature (°C)	Efficiency	
	MCPCM slurry	Water
28.57	0.52	0.54
29.20	0.52	0.54
30.13	0.50	0.52
30.55	0.51	0.58
31.30	0.52	0.62
32.15	0.52	0.62
33.13	0.50	0.62
33.46	0.51	0.61
34.24	0.51	0.58
34.95	0.52	0.54
35.25	0.51	0.53
36.07	0.51	0.54

Table A.47: Efficiency of the fluidised MCPCM glazed energy storage system with an average fluid temperature, $(T_{in}+T_{out})/2$, using MCPCM slurry and water at I_{av} = 399W/m^2 (see Figure 6.17c)

Temperature (°C)	Efficiency	
	MCPCM slurry	Water
28.71	0.48	0.50
29.02	0.49	0.53
30.01	0.51	0.54
30.45	0.49	0.57
31.14	0.50	0.57
32.03	0.47	0.58
32.28	0.47	0.59
33.02	0.49	0.57
33.77	0.48	0.56
34.30	0.49	0.54
35.42	0.51	0.52
36.10	0.47	0.49

Table A.48: Efficiency of the fluidised MCPCM glazed energy storage system with an average fluid temperature, $(T_{in}+T_{out})/2$, using MCPCM slurry and water at I_{av} = 200W/m^2 (see Figure 6.17d)

Temperature (C)	Efficiency	
	MCPCM slurry	Water
28.53	0.45	0.45
29.02	0.44	0.44
29.86	0.46	0.52
30.64	0.46	0.51
31.73	0.48	0.54
32.04	0.44	0.54
32.66	0.44	0.56
33.00	0.45	0.56
33.73	0.47	0.49
36.00	0.48	0.48

Table A.49: The efficiency of the fluidised MCPCM glazed energy storage system at difference insolation with the use of MCPCM slurry and water (see Figure 6.18)

Q (W/m^2)	Efficiency	
	Water	MCPCM Slurry
800	0.52	0.64
600	0.50	0.62
400	0.47	0.58
200	0.45	0.56

Table A.50: A comparison of the rate of heat transfer for 20% MCPCM slurry with yellow and original colour as the primary working fluid at I_{av} = 806 W/m^2 (see Figure 6.20)

Time	Q(W)		Time	Q(W)
	Water	MCPCM slurry		Yellow MCPCM slurry
12:21:05	103	105	12:28:42	103
12:30:02	105	107	12:36:00	106
12:39:00	106	111	12:54:01	112
12:55:01	104	123	13:06:16	124
13:10:16	105	125	13:25:55	123
13:31:55	104	127	13:35:26	129
13:36:26	105	128	13:52:55	125
13:54:55	103	126	14:09:19	120
14:16:19	104	113	14:28:38	115
14:30:38	105	109	14:48:30	101
14:50:30	104	107		